Cell Journal (Yakhteh)

Guide for Authors

Aims and Scope: The "Cell Journal (Yakhteh)" is a peer review and monthly English publication of Royan Institute of Iran. The aim of the journal is to disseminate information through publishing the most recent scientific research studies on exclusively Cellular, Molecular and other related topics. **Cell J**, has been certified by the Ministry of Culture and Islamic Guidance since 1999 and also accredited as a scientific and research journal by HBI (Health and Biomedical Information) Journal Accreditation Commission since 2000 which is an open access journal. **This journal holds the membership of the Committee on Publication Ethics (COPE).**

1. Types of articles

The articles in the field of Cellular and Molecular can be considered for publications in **Cell J.** These articles are as below:

A. Original articles

Original articles are scientific reports of the original research studies. The article consists of English Abstract (structured), Introduction, Materials and Methods, Results, Discussion, Conclusion, Acknowledgements, Author's Contributions, and References **(Up to 40).**

B. Review articles

Review articles are the articles written by well experienced authors and those who have excellence in the related fields. The corresponding author of the review article must be one of the authors of at least three published articles appearing in the references. The review article consists of English Abstract (unstructured), Introduction, Conclusion, Author's Contributions, and References **(Up to 70).**

C. Systematic Reviews

Systematic reviews are a type of literature review that collect and critically analyzes multiple research studies or papers. The Systematic reviews consist of English Abstract (unstructured), Introduction, Materials and Methods, Results, Discussion, Conclusion, Acknowledgements, Author's Contributions, and References **(Up to 70).**

D. Short communications

Short communications are articles containing new findings. Submissions should be brief reports of ongoing researches. The short communication consists of English Abstract (unstructured), the body of the manuscript (should not hold heading or subheading), Acknowledgements, Author's Contributions, and References **(Up to 30).**

E. Case reports

Case reports are short discussions of a case or case series with unique features not previously described which make an important teaching point or scientific observation. They may describe novel techniques or use equipment, or new information on diseases of importance. It consists of English Abstracts (Unstructured), Introduction, Case Report, Discussion, Acknowledgements, Author's Contributions, and References **(Up to 30).**

F. Editorial

Editorials are articles should be written in relevant and new data of journals' filed by either the editor in chief or the editorial board.

G. Imaging in biology

Images in biology should focus on a single case with an interesting illustration such as a photograph, histological specimen or investigation. Color images are welcomed. The text should be brief and informative.

H. Letter to the editors

Letter to the editors are in response to previously published **Cell J** articles, and may also include interesting cases that do not meet the requirement of being truly exceptional, as well as other brief technical or clinical notes of general interest.

I. Debate

Debates are articles which show a discussion of the positive and negative view of the author concerning all aspect of the issue relevant to scientific research.

2. Submission process

It is recommended to see the guidelines for reporting different kinds of manuscripts. This guide explains how to prepare the

manuscript for submission. Before submitting, we suggest authors to familiarize themselves with **Cell J** format and content by reading the journal via the website (www.celljournal.com). The corresponding author ensures that all authors are included in the author list and agree with its order, and they must be aware of the manuscript submission.

A. Author contributions statements

It is essential for authors to include a statement of responsibility in the manuscript that specifies the contribution of every one of them. This participation must include conception and design of the manuscript, data acquisition or data analysis and interpretation, drafting of the manuscript and/or revising it for critically important intellectual content, revision and final approval of the manuscript and statistical analysis, obtaining funding, administrative, technical, or material support, or supervision. Authors who do not meet the above criteria should be acknowledged in the **Acknowledgments section.**

B. Cover letter and copyright

Each manuscript should be accompanied by a cover letter, signed by all authors specifying the following statement: "The manuscript has been seen and approved by all authors and is not under active consideration for publication. It has neither been accepted for publication nor published in another journal fully or partially (except in abstract form). **Also, no manuscript would be accepted in case it has been pre-printed or submitted to other websites.** I hereby assign the copyright of the enclosed manuscript to **Cell J.**" Corresponding author must confirm the proof of the manuscript before online publishing. Also, it is needed to suggest three peer reviewers in the field of their manuscript.

C. Manuscript preparation

Authors whose first language is not English encouraged to consult a native English speaker in order to confirm his manuscripts to American or British (not a mixture) English usage and grammar. It is necessary to mention that we will check the plagiarism of your manuscript by iThenticate Software. The manuscript should be prepared in accordance with the "International Committee of Medical Journal Editors (ICMJE)". Please send your manuscript in two formats word and PDF (including: title, name of all the authors with their degree, abstract, full text, references, tables and figures) and also send tables and figures separately in the site. The abstract and text pages should have consecutive line numbers in the left margin beginning with the title page and continuing through the last page of the written text. Each abbreviation must be defined in the abstract and text when they are mentioned for the first time. Avoid using abbreviation in the title. Please use the international and standard abbreviations and symbols

It should be added that an essential step toward the integration and linking of scientific information reported in published literature is using standardized nomenclature in all fields of science and medicine. Species names must be italicized (*e.g., Homo sapiens*) and also the full genus and species written out in full, both in the title of the manuscript and at the first mention of an organism in a paper.

It is necessary to mention that genes, mutations, genotypes, and alleles must be indicated in italics. Please use the recommended name by consulting the appropriate genetic nomenclature database, e.g., HUGO for human genes. In another words; if it is a human gene, you must write all the letters in capital and italic (*e.g., OCT4, c-MYC*). If not, only write the first letter in capital and italic (*e.g., Oct4, c-Myc*). **In addition, protein designations are the same as the gene symbol but are not italicized.**

Of note, Cell J will only consider publishing genetic association study papers that are novel and statistically robust. Authors are advised to adhere to the recommendations outlined in the STREGA statement (http://www.strega-statement.org). The following criteria must be met for all submissions:

1. Hardy-Weinberg Equilibrium (HWE) calculations must be carried out and reported along with the P-values if applicable [see Namipashaki et al. 2015 (Cell J, Vol 17, N 2, Pages: 187-192) for a discussion].

2. Linkage disequilibrium (LD) structure between SNPs (if multiple SNPs are reported) must be presented.

3. Appropriate multiple testing correction (if multiple independent SNPs are reported) must be included.

Submissions that fail to meet the above criteria will be rejected before being sent out for review.

Each of the following manuscript components should begin in the following sequence:

Authors' names and order of them must be carefully considered (full name(s), highest awarded academic degree(s), email(s), and institutional affiliation(s) of all the authors in English. Also, you must send mobile number and full postal address of the corresponding author).

Changes to Authorship such as addition, deletion or rearrangement of author names must be made only before the manuscript has been accepted in the case of approving by the journal editor. In this case, the corresponding author must explain the reason of changing and confirm them (which has been signed by all authors of the manuscript). If the manuscript has already been published in an online issue, an erratum is needed.

Title is providing the full title of the research (do not use abbreviations in title).

Running title is providing a maximum of 7 words (no more than 50 characters).

Abstract must include Objective, Materials and Methods, Results, and Conclusion (no more than 300 words).

Keywords, three to five, must be supplied by the authors at the foot of the abstract chosen from the Medical Subject Heading (MeSH). Therefore; they must be specific and relevant to the paper.

The following components should be identified after the abstract:

Introduction: The Introduction should provide a brief background to the subject of the paper, explain the importance of the study, and state a precise study question or purpose.

Materials and Methods: It includes the exact methods or observations of experiments. If an apparatus is used, its manufacturer's name and address should be stipulated in parenthesis. If the method is established, give reference but if the method is new, give enough information so that another author can perform it. If a drug is used, its generic name, dose, and route of administration must be given. Standard units of measurements and chemical symbols of elements do not need to be defined.

Statistical analysis: Type of study and statistical methods should be mentioned and specified by any general computer program used.

Ethical considerations*:* Please state that informed consent was obtained from all human adult participants and from the parents or legal guardians of minors and include the name of the appropriate institutional review board that approved the project. It is necessary to indicate in the text that the maintenance and care of experimental animals complies with National Institutes of Health guidelines for the humane use of laboratory animals, or those of your Institute or agency.

Clinical trial registration: All of the Clinical Trials performing in Iran must be registered in Iranian Registry of Clinical Trials (www.irct.ir). The clinical trials performed abroad, could be considered for publication if they register in a registration site approved by WHO or www.clinicaltrials.gov. If you are reporting phase II or phase III randomized controlled trials, you must refer to the CONSORT Statement for recommendations to facilitate the complete and transparent reporting of trial findings. Reports that do not conform to the CONSORT guidelines may need to be revised before peer-reviewing.

Results: They must be presented in the form of text, tables, and figures. Take care that the text does not repeat data that are presented in tables and/or figures. Only emphasize and summarize the essential features of the main results. Tables and figures must be numbered consecutively as appeared in the text and should be organized in separate pages at the end of the manuscript while their location should be mentioned in the main text.

Tables and figures: If the result of your manuscript is too short, it is better to use the text instead of tables & figures. Tables should have a short descriptive heading above them and also any footnotes. Figure's caption should contain a brief title for the whole figure and continue with a short explanation of each part and also the symbols used (no more than 100 words). All figures must be prepared based on cell journal's guideline in color (no more than 6 Figures and Tables) and also in GIF or JPEG format.

Of Note: Please put the tables & figures of the result in the results section not any other section of the manuscript.

Supplementary materials would be published on the online version of the journal. This material is important to the understanding and interpretation of the report and should not repeat material within the print article. The amount of supplementary material should be limited. Supplementary material should be original and not previously published and will undergo editorial and peer review with the main manuscript. Also, they must be cited in the manuscript text in parentheses, in a similar way as when citing a figure or a table. Provide a caption for each supplementary material submitted.

Discussion: It should emphasize the present findings and the variations or similarities with other researches done by other researchers. The detailed results should not be repeated in the discussion again. It must emphasize the new and important aspects of the study.

Conclusion: It emphasizes the new and important aspects of the study. All conclusions are justified by the results of the study.

Acknowledgements: This part includes a statement thanking those who contributed substantially with work relevant to the study but does not have authorship criteria. It includes those who provided technical help, writing assistance and name of departments that provided only general support. You must mention financial support in the study. Otherwise; write this sentence "There is no financial support in this study".

Conflict of interest: Any conflict of interest (financial or otherwise) and sources of financial support must be listed in the Acknowledgements. It includes providers of supplies and services from a commercial organization. Any commercial affiliation must be disclosed, regardless of providing the funding or not.

References: The references must be written based on the Vancouver style. Thus the references are cited numerically in the text and listed in the bibliography by the order of their appearance. The titles of journals must be abbreviated according to the style

used in the list of Journals Indexed in PubMed. Write surname and initials of all authors when there are six or less. In the case of seven or more authors, the names of the first six authors followed by "et al." must be listed. You can download Endnote file for Journal references style: endnote file

The reference of information must be based on the following order:

Article:

Surname(s) and first letter of name &middle name(s) of author(s) .Manuscript title. Journal title (abbr).publication date (year); Volume & Issue: Page number.

Example: Manicardi GC, Bianchi PG, Pantano S, Azzoni P, Bizzaro D, Bianchi U, et al. Presence of endogenous nicks in DNA of ejaculated human spermatozoa and its relationship to chromomycin A3 accessibility. Biol Reprod. 1995; 52(4): 864-867.

Book:

Surname(s) and first letter of name & middle name(s) of author(s).Book title. Edition. Publication place: publisher name; publication date (year); Page number.

Example: Edelman CL, Mandle CL. Health promotion throughout the lifespan. 2nd ed. ST Louis: Mosby; 1998; 145-163.

Chapter of book:

Surname(s) and first letter of name & middle name(s) of author(s).Chapter title. In: Surname(s) and first letter of name & middle name(s) of editor(s), editors. Book title. Edition. Publication place: publisher name; publication date (year); Page number.

Example: Phillips SJ, Whisnant JP. Hypertension and stroke. In: Laragh JH, Brenner BM, editors. Hypertension: pathophysiology, diagnosis, and management. 2nd ed. New York: Raven Press; 1995; 465-478.

Abstract book:

Example: Amini rad O.The antioxidant effect of pomegranate juice on sperm parameters and fertility potential in mice. Cell J. 2008;10 Suppl 1:38.

Thesis:

Name of author. Thesis title. Degree. City name. University. Publication date (year).

Example: Eftekhari Yazdi P. Comparison of fragment removal and co-culture with Vero cell monolayers on development of human fragmented embryos. Presented for the Ph.D., Tehran. Tarbiyat Modarres University. 2004.

Internet references

Article:

Example: Jahanshahi A, Mirnajafi-Zadeh J, Javan M, Mohammad-Zadeh M, Rohani M. Effect of low-frequency stimulation on adenosineA1 and A2A receptors gene expression in dentate gyrus of perforant path kindled rats. Cell J. 2008; 10 (2): 87-92. Available from: http://www.celljournal.org. (20 Oct 2008).

Book:

Example: Anderson SC, Poulsen KB. Anderson's electronic atlas of hematology.[CD-ROM]. Philadelphia: Lippincott Williams & Wilkins; 2002.

D. Proofs are sent by email as PDF files and should be checked and returned within 72 hours of receipt. It is the authors' responsibility to check that all the text and data as contained in the page proofs are correct and suitable for publication. **We are requested to pay particular attention to author's names and affiliations as it is essential that these details be accurate when the article is published.**

E. Pay for publication: Publishing an article in **Cell J** requires Article Processing Charges (APC) that will be billed to the submitting author following the acceptance of an article for publication. For more information please see www.celljournal.org.

F. Ethics of scientific publication: Manuscripts that have been published elsewhere with the same intellectual material will refer to duplicate publication. If authors have used their own previously published work or work that is currently under review, as the basis for a submitted manuscript, they are required to cite the previous work and indicate how their submitted manuscript offers novel contributions beyond those of the previous work. Research and publication misconduct is considered a serious breach of ethics.

The Journal systematically employs iThenticate, plagiarism detection and prevention software designed to ensure the originality of written work before publication. Plagiarism of text from a previously published manuscript by the same or

another author is a serious publication offence. Some parts of text may be used, only where the source of the quoted material is clearly acknowledged.

3. General information

A. You can send your manuscript via online submission system which is available on our website. If the manuscript is not prepared according to the format of **Cell J**, it will be returned to authors.

B. The order of article appearance in the Journal is not demonstrating the scientific characters of the authors.

C. Cell J has authority to accept or reject the manuscript.

D. The received manuscript will be evaluated by associate editor. **Cell J** uses a single-blind peer review system and if the manuscript suits the journal criteria, we select the reviewers. If three reviewers pass their judgments on the manuscript, it will be presented to the editorial board of **Cell J.** If the editorial board has a positive judgment about the manuscript, reviewers' comments will be presented to the corresponding author (the identification of the reviewers will not be revealed). The executive member of journal will contact the corresponding author directly within 3-4 weeks by email. If authors do not receive any reply from journal office after the specified time, they can contact journal office. Finally, executive manager will respond promptly to authors' request.

The Final Checklist

The authors must ensure that before submitting the manuscript for publication, they have to consider the following parts:

1. The first page of manuscript should contain title, name of the author/coauthors, their academic qualifications, designation & institutions they are affiliated with, mailing address for future correspondence, email address, phone, and fax number.

2. Text of manuscript and References prepared as stated in the "guide for authors" section.

3. Tables should be on a separate page. Figures must be sent in color and also in JPEG (Jpg) format.

4. Cover Letter should be uploaded with the signature of all authors.

5. An ethical committee letter should be inserted at the end of the cover letter.

The Editor-in-Chief: Ahmad Hosseini, Ph.D.

Cell Journal *(Yakhteh)*

P.O. Box: 16635-148, Iran

Tel/Fax: + 98-21-22510895

Emails: Celljournal@royaninstitute.org

info@celljournal.org

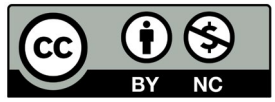

Dr. Saeed Kazemi Ashtiani

IN THE NAME OF GOD

Gone But not Forgotten

In the memory of the late Director of Royan Institute, Founder of Stem Cells Research in Iran and Chairman of ***Cell Journal*** *(Yakhteh)*. May he rest in peace.

PUBLISHED & SPONSORED BY:
Publication of Royan Institute (ACECR)

Indexed in:
1. Thomson Reuters (ISI)
2. PubMed
3. PubMed Central (PMC)
4. National Library Medicine (NLM)
5. Biosis Preview
6. Index Medicus for the Eastern Mediterranean Region (IMEMR)
7. Regional Information Center for Sciences and Technology (RICeST)
8. Index Copernicus International
9. Cambridge Scientific Abstract (CSA)
10. EMBASE
11. Scopus
12. Cinahl Database
13. Google Scholar
14. Chemical Abstract Service (CAS)
15. Proquest
16. Directory of Open Access Journals (DOAJ)
17. Open Academic Journals Index (OAJI)
18. Directory of Research Journals Indexing (DRJI)
19. Scientific Information Database (SID)
20. Iranmedex
21. Islamic World Science Citation Center (ISC)
22. Magiran
23. Science Library Index
24. Biological Abstracts
25. Essential Science Indicators
26. EuroPub

ACECR

Editorial Office Address (Dr. Ahmad Hosseini):
Royan Institute, P.O.Box: 16635-148,
Tehran, Iran
Tel & Fax: (+9821)22510895
Website: www.celljournal.org
Emails: info@celljournal.org
celljournal@royaninstitute.org

Printing Company:
Naghshe e Johar Co.
No. 103, Fajr alley, Tehranpars Street,
Tehran, Iran.

Cell Journal(Yakhteh), Vol 23, No 5, October 2021, Serial Number: 93, Pages: 495-602

CONTENTS

Review Article

Original Articles

Case Reports

Review Article

Sperm Associated Antigens: Vigorous Influencers in Life

Samaneh Faraji, M.Sc.[1, 2], Mohsen Sharafi, Ph.D.[2], Abdolhossein Shahverdi, Ph.D.[2, 3*], Rouhollah Fathi, Ph.D.[2*]

1. Department of Molecular and Cellular Biology, Faculty of Basic Science and Advanced Technologies in Biology, University of Science and Culture, ACECR, Tehran, Iran
2. Department of Embryology, Reproductive Biomedicine Research Center, Royan Institute for Reproductive Biomedicine, ACECR, Tehran, Iran
3. Reproductive Epidemiology Research Center, Royan Institute for Reproductive Biomedicine, ACECR, Tehran, Iran

Corresponding Address: P.O.Box: 16635-148: Department of Embryology, Reproductive Biomedicine Research Center, Royan Institute for Reproductive Biomedicine, ACECR, Tehran, Iran
Emails: shahverdi@royaninstitute.org, rfathi79@royaninstitute.org

Received: 05/January/2020, Accepted: 27/June/2020

Abstract

Sperm associated antigens (SPAGs) are specific proteins in terms of performance and evolution, that have common expressions in the testes or sperm cells. Moreover, the humoral immune response against some of SPAGs can result in immunological infertilities. On the other hand, recent studies have explored several new properties of SPAGs and shed light on sperm's function, the impact of anti-sperm antibodies (ASA) in immunological infertility, and some tumors related to SPAGs. This article presents an exhaustive review of SPAGs and their roles in the cell cycle, signaling pathways, fertility, sperm-oocyte cross-talk as well as their unfavorable positions as prognostic factors in many types of cancers.

Keywords: Antigen, Cancer, Fertility, Human, Sperm

Cell Journal(Yakhteh), Vol 23, No 5, October 2021, Pages: 495-502

Citation: **Faraji S, Sharafi M, Shahverdi AH, Fathi R. Sperm associated antigens: vigorous influencers in life. Cell J. 2021; 23(5): 495-502. doi: 10.22074/cellj.2021.7377.**

Introduction

Sperm associated antigens (SPAGs) family comprises 18 proteins, first described as sperm membrane proteins, which could stimulate immune responses as immunogens. The molecular weight of these antigens is considered between 24-71 kDa and each protein-coding gen is located on a particular chromosome (Table 1). The role of SPAGs in the structural integrity of sperm tail, sperm motility, evaluation, fertility, cell adhesion, and cell signaling of spermatozoa has been revealed in a study by Bohring et al. (1). Silina et al. (2); also showed SPAGs 1, 2, 8, 9, 12, 13, and 15 may play roles in male infertility. About 13% of the general reproductive-age population are suffered from fertility problems, and malefactors are estimated to up to 30% of them (3). More than 90% of male infertilities are due to low count or low quality of sperm cells (4) and various factors could influence this process. Moreover, these antigens play a vigorous role in sperm and egg cross-talk and subsequent development of derived embryos. In 2017, Cui et al. (5) study showed that during sperm evolution, the level of expression for some proteins such as SPAGs 6 and 16 that impact the processes of spermatogenesis, cellular motility, energy metabolism, and oxidative phosphorylation has been increased. Since protein synthesis has been ceased throughout spermiogenesis, so most of the changes occurring at the sperm surface are a result of the sperm's interaction with the surrounding environment (6). Any modification of these proteins may result in a change in sperm function and capabilities (7). The other factors that affect male fertility are anti-sperm antibodies. These antibodies can disrupt the power of sperm fertility and produce types of immunological infertility. Mainly one of the causes of male infertility could be due to the interaction between anti-sperm antibodies and SPAGs (8). In addition, this research has several practical applications. The most important case points out to cryopreservation and of molecular importance of healthy sperms. Using frozen healthy sperms in infertility clinics in order to artificial insemination is a case in point. The purpose of this study is to present a comprehensive review of databases and many pieces of research on SPAGs and also the result of our study on the cryopreservation of human sperm.

Overview of SPAGs expression status and function

SPAG proteins present in many tissues and cells such as sperm cells. According to their particular functions in sperm, any deficiency of them may lead to infertility due to sperm dysfunction. The expression of SPAGs in various organs or cells is summarised in Table 2.

The performance of these momentous proteins separately has been investigated in different studies and comprehensively compiled in this study. So far the introduction has focused on general information about SPAGs. The following section will discuss the function of each SPAG.

Table 1: A summary overview of the main characteristics of all sperm associated antigen (SPAG) genes

Gene name (Aliases)	Chromosome	Location	Exon count	Source (UniProt ID)
SPAG1	8	8q22.2	21	Q07617
SPAG2 (UAP1)	1	1q23.3	13	Q16222
SPAG3 (HSPA2)	14	14q23.3	1	P54652
SPAG4	20	20q11.22	13	Q9NPE6
SPAG5	17	17q11.2	24	Q96R06
SPAG6	10	10p12.2	15	O75602
SPAG7	17	17p13.2	8	O75391
SPAG8	9	9p13.3	9	Q99932
SPAG9	17	17q21.33	34	O60271
SPAG10 (MFGE8)	15	15q26.1	12	Q08431
SPAG11B	8	8p23.1	7	Q08648
SPAG12 (SNU13/NHP2L1)	22	22q13.2	6	P55769
SPAG13 (SSFA2/KRAP)	2	2q31.3	22	P28290
SPAG15 (SPAM1/PH20)	7	7q31.32	9	P38567
SPAG16	2	2q34	33	Q8N0X2
SPAG17	1	1p12	56	Q6Q759
SPAG18 (PSMA5)	1	1p13.3	9	P28066

The function of SPAG1 is attributed to the cytoplasmic assembly of the ciliary dynein arms, nucleotide guanosine triphosphate binding (GTP), and GTPase activity. Recent evidence suggests that the GTPase activity of SPAG1 plays a role in mammalian gametogenesis and fertility. This protein plays an important role in the oocyte via its potential association in adenosine monophosphate-activated protein kinase (AMPK) and mitogen-activated protein kinase (MAPK) signaling pathways (9). Besides, findings indicated this protein could be involved in female infertility through anti-sperm antibodies too. *SPAG1* gene indirectly inactivates phosphoinositide 3-kinase/ RAC-alpha serine/threonine-protein kinase pathway (PI3K/ AKT) which can result in inhibition of immature Sertoli cell growth via microRNA 638 (miR-638) and can lead to apoptosis (10).

SPAG2 is part of the sperm axoneme structural element in the outer dense fiber (11). The practical roles of this protein in the cells can be attributed to the biosynthesis pathway of UDP-N-Acetyl-Alpha-D-glucosamine which is itself part of nucleotide-sugar biosynthesis. It could be noted that SPAG2 has a nucleotidyltransferase role in the cytoplasm (GeneCard ID GC01P162561).

Based on a study by Bohring et al. (1), which first described SPAG3 function as heat shock protein family A member 2 (HSPA2) according to identification by two-dimensional polyacrylamide gel electrophoresis (2D-PAGE) and matrix-assisted laser desorption/ ionization mass spectrometry (MALDI-MS); SPAG3 was assumed as HSPA2. The functional role of HSPA2 in cells can be ascribed to molecular chaperone, in a wide variety of cellular processes (UniProt ID P54652). Research by Ayaz et al. (12) has argued that induced HSPA2 by oxidative stress (ROS) has a role in male factor infertility, and any damage in sperm function can result in the reduction of *HSPA2* expression level, mitochondrial dysfunction, and induced oxidative stress in varicocele patients (13). In a study conducted by Bromfield et al. (14), it was shown that alkylation of HSPA2 with an attendant decrease in zona pellucida-receptor arylsulphatase A (ARSA) occurs during capacitation due to oxidative stress. This can destroy the zona pellucida receptor complex on sperm surface and consequently have an effect on sperm-egg cross talk. Subsequent study has unveiled that Protein Disulfide Isomerase A6 (PDIA6) is a potential HSPA2-adhering protein that is located in sperm head peri-acrosomal region and very fragile to oxidative stress (15).

SPAG4 is involved in spermatogenesis and protein localization in the sperm axoneme. The quoted protein may assist in the organization and assembly of outer dense fiber, and sperm tail-specific structure (16). It also plays a role in nuclear envelope integrity and preservation (UniProt ID Q9NPE6). Pairing performance of nucleus-cytoskeleton in spermatozoa and establishment of strength in head-tail junction complex are other functions that are clarified on SPAG4 in sperm cells (17).

Table 2: An overview of tissues in which sperm associated antigens (SPAGs) are expressed

SPAGs	Organs/cells	Cellular status
SPAG1	Lungs, Large intestine, Kidneys, Brain[i], Testicles, Neck, and midpiece of pachytene primary Spermatocytes (UniProt ID Q07617)	Part of the cytoskeleton microtubules in the Cytoplasm
SPAG2/UAP1	Testicle, Somatic tissues[ii], Low expression level in Placenta, Muscle, and Liver (UniProt ID Q16222)	Cytoplasm
SPAG3/ HSPA2	Ubiquitous, Globus pallidus[i] (UniProt ID P54652; GeneCard ID GC14P064535)	Cytoskeleton and mitotic cell cycle
SPAG4	Testicle, Sperm cells (UniProt ID Q9NPE6)	Cytoplasmic membrane, Cytoplasm, Nucleus membrane
SPAG5	Testis, Placenta, Liver, Pancreas, Thymus, Colon[iii] (UniProt ID Q96R06)	Cytoskeleton, Cytoplasm
SPAG6	Testis[iv] (UniProt ID O75602)	Cytoskeleton, Flagellum
SPAG7	Fetal brain (UniProt ID O75391)	Nucleus
SPAG8	Testis germ cells[v] (UniProt ID Q99932)	Nucleus, Cytoplasm
SPAG9	Testis[i] (UniProt ID O60271)	Cytoplasm
SPAG10/ MFGE8	Mammary epithelial cell surfaces[i], Aortic media (UniProt ID Q08431)	External side of the plasma membrane, Endoplasmic reticulum lumen, can be secreted as extracellular exosome
SPAG11B	Caput and proximal corpus of the epididymis, Epididymal epithelium, Sperm head (UniProt ID Q08648; GeneCard ID GC08M007442)	Secretory protein[vi]
SPAG12/ SNU13/ NHP2L1	Ubiquitous (UniProt ID P55769)	Dense fibrillar component of the nucleolus
SPAG13/ KRAP/SSFA2	Pancreas, Testis (UniProt ID P28290)[i]	Plasma membrane, membrane bound arrangement with extracellular regions
SPAG15/ SPAM1	Testis[i] (UniProt ID P38567)	Human sperm surface, Inner acrosomal membrane
SPAG16	Testis, Brain, Liver, Pancreas, Adrenal gland, Spinal cord, Heart, Thyroid, Trachea, Ovary, Kidney[vii] (UniProt ID Q8N0X2)	Axoneme of the tail in sperm cells, Nucleus of post-meiotic germ cells
SPAG17	Testis[i] (UniProt ID Q6Q759)	Axonemal central apparatus, Cilia-bearing cells consist of Lung, Brain, Uterus, Oviduct, Bronchial, Tracheal epithelial cells
SPAG18/ PSMA5	Ubiquitous (UniProt ID P28066; GeneCard ID GC01M109399)	Cytoplasm, Nucleus

[i]; High expression level, [ii]; There are two isoforms of alanine--glyoxylate aminotransferase 1 (*AGX1*) and *AGX2* for *SPAG2*, which former is numerous in testicle while the latter is more numerous than isoform one in somatic tissues, [iii]; *SPAG5* is highly expressed in testis. By contrast, it is detected at a low level in the placenta, liver, pancreas, thymus, and colon, [iv]; *SPAG6* is highly expressed in the testis; however, it is not detected in the prostate, ovary, spleen, thymus, small intestine, colon, and peripheral blood leukocytes, [v]; Although it is widely expressed in testis (germ cells), there is no expression in the liver, kidney, prostate, and small intestine, [vi]; *SPAG11* gene encodes several androgen-dependent and epididymis-specific secretory proteins, and [vii]; It appears to be 5 isoforms for *SPAG16*, which isoform1 is detected in testis while isoform four has been detected in also testis and brain. Also, it is stated that isoform 4 has a low expression level in the liver, pancreas, adrenal gland, spinal cord, heart, thyroid, trachea, ovary, and kidney.

SPAG5 is an essential component of the mitotic spindle required for normal chromosome separation entry into anaphase. Moreover, it correlates with the duration of sister chromatid segregation, mitotic progression, maintenance of spindle pole architecture and may contribute to the regulation of separase activity (UniProt ID Q96R06). This protein interacts with sperm axoneme and outer dense fiber structural proteins (18), the integrity of centrosome (19), and has a role in embryonic development of testis (20).

SPAG6 is important for the structural integrity of sperm tail central apparatus and flagellar motility. In addition, it contributes to ciliogenesis in bronchial epithelium cells (21). Recent evidence suggests that SPAG6 is involved in proliferation, differentiation, a function of brain neurons (22), and the formation of the immunological synapses (23). Li et al. (22) have identified the regulation role of SPAG6 in

cell apoptosis through the tumor necrosis factor-related apoptosis-inducing ligand (TRAIL) signaling pathway and fibroblast cell growth. Moreover, SPAG6 contributes to proliferation, migration, and cell morphology modulation (24). In a study by Huo et al. (25), one of the important causes of asthenospermia appears to lie in SPAG6, due to reduced expressions of solute carrier family 22 member 14 (*SLC22A14*) and *SPAG6* in spermatozoa.

SPAG7 has a molecular function of nucleic-acid binding protein (UniProt ID O75391). This protein may be a possible structural element of sperm acrosome (26). Furthermore, The quoted gene contributes to periodic fever, aphthous stomatitis, pharyngitis, and adenopathy (PFAPA) syndrome (27).

SPAG8 is one of the testis-specific proteins that is expressed during germ cell differentiation. The functional role of SPAG8 in the cell can be attributed to its role in spermatogenesis, fertility, and microtubule formation through interaction with Ran-binding protein 9 (RANBP9) (UniProt ID Q99932). According to Li et al. (28), G2/M phase regulation in the cell cycle is related to SPAG8 (possibly due to a delay in activation of Cyclin-dependent kinase 1 (CDK1) required for entry into mitosis). As highlighted by Wu et al. (29), it has been stated that this protein is involved in the acrosome reaction and sperm-zona pellucida interaction that is a vital prerequisite for successful fertilization. Besides, SPAG8 contributes to increasing actin-like protein (ACT) related transcriptional cyclic adenosine monophosphate responsive element modulator (CREM) activity during spermatogenesis. In addition, it has been declared that sperm-associated antigen 8 reacts with sera from melanoma patients (UniProt ID Q99932).

SPAG9 is contributes to the positive regulation of the cell cycle, muscle cell, and neuron differentiation. It also involves in activation of JUN kinase activity (Jun proto-oncogene) and spermatogenesis (UniProt ID O60271). SPAG9 has been identified as a scaffold protein that ties Jun N-terminal kinase (JNK) and p38 mitogen-activated protein kinase (MAPK) transcription factors and signaling modules (30). The relationship between SPAG9 and endometrial stem cell differentiation, development of male germ cells, and also fertility has been widely investigated by Kashef, 2006 and Iwanaga, 2008 (31, 32). A recent study by Li et al. (33) has highlighted the role of SPAG9 in preventing cancer cells from reactive oxygen species (ROS) induced cell death. Furthermore, it has control over cell motility, invasion, and angiogenesis besides activating host immune responses (34).

SPAG10 has a role in apoptotic cell clearance, sperm-egg adhesion, mammary gland development, maintenance of epididymal and intestinal epithelium, promotion of vascularization, exocytosis, and also it facilitates antigen presentation (35). The quoted protein may act as cell adhesion protein to conjoin involuntary muscle to elastic fiber in arteries and contains a phosphatidylserine (PS) binding domain as well as an (ARG-GLY- ASP) motif, which enables the binding to integrin (35). SPAG10 attenuates acute renal injury caused by sepsis, inhibits neointima formation after arterial damage, and also transfers fatty acids to the placenta and it can facilitate angiogenesis and induce recovery from ischemia (36-38). The studies presented thus far provide evidence that SPAG10 promotes phagocytosis and inhibits inflammation. Besides, this protein responds to cerebral infarction by endogenous protective factors. Above and beyond, the quoted protein has a role in Alzheimer's disease, subarachnoid hemorrhage, and prion disease (39). An overexpression of SPAG10 is correlated with several carcinomas (40).

The specific functions of SPAG11 have not been specified yet (UniProt ID Q08648). Nevertheless, it is thought that this protein is involved in the adhesion, maturation, storage, and protection of sperm. The most attractive aspect of this protein is that some of the isoforms are consist of regions that present resemblance to beta-defensin, a family of antimicrobial peptides (41). The functional role of SPAG11 in the cell can be attributed to spermatogenesis and inhibition of inflammatory parameters in rheumatoid arthritis (42).

It can be noted that SPAG12 was originally titled non-histone chromosome protein 2-like1 (NHP2L1)**,** because of the similarities between the *SPAG12* sequence and Saccharomyces cerevisiae non-histone protein 2 (NHP2). This protein seems to be a highly conserved nuclear protein that is a component of the [U4/U6. U5] tri-snRNP that binds to the 5′ stem-loop of U4 snRNA. Another name of this protein is small nuclear ribonucleoprotein 13 (SNU13) involved in pre-mRNA splicing as part of the spliceosome. Moreover, it binds to the 5′ stem-loop of U4 snRNA and contributes to spliceosome assembly through that (UniProt ID P55769). SPAG12 has a role in fertilization and also functions in elements of the sperm tail, midpiece, and post-acrosomal region (43). Adjustment disorder in this gene has been seen in some cancers (44, 45).

SPAG13 is involved in signaling receptor and actin filament bindings. The most interesting finding of this protein is that sperm-associated antigen 13 is actively involved in energy equilibrium and obesity (46).

SPAG15 is a receptor that contributes to sperm-zona pellucida interaction. Moreover, it is a hyaluronidase that enables sperm cells to interpenetrate via hyaluronic acid-rich mass cell layer that surrounds the egg cell (UniProt ID P38567). SPAG15 is involved in sperm maturation, intracellular signaling (47), fluid reabsorption, and urine condensation in the kidney (48).

SPAG16 is appearing to lie in sperm flagella function

and plays a role in motile ciliogenesis as well (UniProt ID Q8N0X2). *SPAG16* encodes 2 major proteins that associate with the axoneme of the tail in sperm cells and the nucleus of post-meiotic germ cells respectively (49). Knevel et al. (50) has demonstrated that SPAG16 protects against joint demolition in autoantibody-positive rheumatoid arthritis. The quoted protein exerts structure, stability, motility, survival, and stress-induced reaction in astrocytes and neurons of the brain. Furthermore, with the accentuate increasing expression of this protein, it is identified as the goal of autoantibodies in humoral immune responses against multiple sclerosis (MS) autoimmune disease (51).

SPAG17 is involved in axonemal central apparatus construction and epithelial cilium beating. Additionally, it may have a role in endochondral bone formation, most likely because of the primary cilia performance of chondrocytes and osteoblasts. Findings corroborate that it is localized in the central pair of the sperm flagellar axoneme and interacts with SPAG6 via the C-terminus so thereby the interaction occurs on polymerized microtubules. The quoted protein is identified in the cytoplasm of globular spermatid cells and the condensing spermatids (UniProt ID Q6Q759). Asthenozoospermia (AZS) is a prevalent cause of male infertility which is determined by abnormal reduction in motility of ejaculated spermatozoa. A recent study has pointed out a homozygous mutation in *SPAG17* through exome sequencing. Consequently, due to the fact that SPAG17 is localized in the axonemal central apparatus, it may be a new pathogenic gene-associated AZS (52). Moreover, SPAG17 has an effect on the fertility and differentiation of male germ cells (53). A report by Teves et al. (54) 2015 pointed out that deficiency of SPAG17 may result in skeletal malformations and bone deformation.

Table 3: A summary overview of cancers in which sperm associated antigens (SPAGs) are involved

SPAG	Cancer type
*SPAG*1	Pancreatic tumorigenesis (55), Renal cancer, Seminoma, Colon cancer, Breast cancer (2)
*SPAG*2/*UAP*1	Prostate cancer (56), Lymphoma, Renal cancers (2)
*SPAG*3/*HSPA*2	Pancreatic tumorigenesis (57)
*SPAG*4	Lung cancer, Kidney cancer (58), Prostate cancer, Liver cancer, Breast cancer (2)
*SPAG*5	Urothelial cancer (59), Breast cancer (2, 60), Lung cancer (61, 62), Gastric cancer (61), Hepatocellular carcinoma (63), Bladder cancer (2)
*SPAG*6	Myelodysplastic syndrome (24), Spinal cord neoplasm, Prostate cancer, Colon cancer (2)
*SPAG*7	Brain cancer, Synovial sarcoma, Prostate cancers (2)
*SPAG*8	Lung cancer, Breast cancer, Cervical carcinoma (2)
*SPAG*9	Thyroid cancer, Hepatocellular carcinoma, Renal cell carcinoma, Gastric cancer, Endometrial carcinoma, Lung cancer, Osteosarcoma, Breast cancer, Cervical cancers, Acute myeloid leukemia, Ovarian cancer (34), Brain cancer (2)
*SPAG*10/*MFGE*8	Breast cancer, Colorectal cancer (40)
*SPAG*11*B*	Testicular seminoma, Breast cancer (2)
*SPAG*12/*SNU*13/ *NHP*2*L*1	Bladder cancer, Renal carcinoma (2)
*SPAG*13/*KRAP*/*SSFA*2	Brain cancer, Colorectal cancer, Esophagus cancer (2), Lung adenocarcinoma (64), Oral squamous cell carcinoma (65)
*SPAG*15/*SPAM*1	Breast cancer (66), Laryngeal carcinoma, Brain cancer, Colon cancer, Lung carcinoma, Melanoma (2)
*SPAG*16	Urothelial cancer, Breast cancer (2)
*SPAG*17	Pancreatic cancer, Brain cancer (2)
*SPAG*18/*PSMA*5	Colorectal cancer cell lines, Chromophobe renal cell adenocarcinoma, Gastric cancer, Bladder cancer, Lung carcinoma, Head and neck cancer, Melanoma, Pulmonary neuroendocrine tumor (67)

Based on Bohring et al. (1), that defined SPAG18 functions as proteasome subunit alpha type-5 (PSMA5) according to identification by two-dimensional polyacrylamide gel electrophoresis (2D-PAGE) and matrix-assisted laser desorption/ionization mass spectrometry (MALDI-MS); SPAG18 was assumed as PSMA5. Proteasome zeta chain is another name of the protein which encodes by this gene. The quoted protein is involved in the cell cycle progression, mitosis, and proto-oncogene tyrosine-protein kinase receptor (RET) signaling pathway. Moreover, it is essential for endopeptidase activity and threonine-type endopeptidase activity. The 26S proteasome is a multi-catalytic proteinase complex that is composed of a ring-shaped 20S proteasome core and two 19S regulatory subunits. 20S core proteasome complex is associated with proteolysis of most intracellular proteins. The structure of the core is barrel-shaped, that is consists of 4 rings of 28 different subunits; two outer loops are composed of seven alpha subunits and the two inner loops are composed of seven beta subunits. The protease activity is imposed by three beta-subunits PSMB5, PSMB6, and PSMB7. PSMA5 directly interacts with the proteasome assembly chaperone PSMG1-PSMG2 heterodimer, which contributes to 20S proteasome assembly. Proteasomes are spread throughout eukaryotic cells with high concentrations, and this complex plays numerous essential roles within the cell by linking with diverse regulatory particles. It is related to two 19S regulatory particles and forms the 26S proteasome component. Nevertheless, it participates in peptides cleavage in an ATP/Ubiquitin-dependent process through a non-lysosomal pathway deterioration of ubiquitinated proteins. The 26S proteasome is essential for the maintenance of protein equilibrium through removing misfolded or damaged proteins. SPAG18 is correlated with the proteasome activator PA200 or PA28, which is 20S proteasome mediates ubiquitin-independent protein deterioration. This type of protease activity is required in several pathways consist of spermatogenesis (20S-PA200 complex) and the major histocompatibility complex (MHC) class I peptides loading (20S-PA28 complex), which is an essential function of a modified proteasome (immunoproteasome). *PSMA5* encodes part of the peptidase T1-Alpha (T1A) family, which is a 20S core alpha subunit (UniProt ID P28066; GeneCard ID GC01M109399).

To date, Scientists have come to understand the role of SPAGs in the process of various cancers, and different studies have proven it. In this regard, scientists have been interested in SPAGs and their contribution to tumorigenesis and angiogenesis by directly studying these genes. Table 3 presents the role of all SPAGs in various cancers. According to these data, *SPAGs 9* and *5* have the highest impact on carcinogenesis, respectively.

Hitherto, a horde of studies has revealed that various factors can have an impact on gene expression likewise sperm functions. In the past years, some evidence has been provided to explain the unfavorable influence of cryopreservation procedures on human spermatozoa. Most papers written on sperm cryopreservation include a section relating to DNA damage and epigenetic changes as a consequence of ROS (68, 69) and the detrimental impact of freezing on momentous macromolecules in particular transcriptome and proteins (70). To the best of the authors' knowledge, no report has been found so far studying the role of the freezing procedure on these consequential proteins. Thereby, due to the importance of these proteins in the fertility process and the plentiful application of freezing in clinical methods such as fertility preservation, the effect of freezing on the expression of SPAG genes, analysis of the freezing consequences on all of SPAGs gene expression was first carried out by Faraji et al. in Royan institute (unpublished data). Refer to the study above, decreased expression of some SPAGs genes is considered as a consequence of cryopreservation. Thereby, this could be a momentous issue in the research process. However, further studies are needed to confirm this finding.

Conclusion

Given their biological significance and roles, SPAGs appear to be a promising research vision for the future. The current approaches in literature have indicated that SPAG 2, 3, 5, 6, 9, 10, and 18 are currently the most popular sperm-associated antigens for investigating among scholars. Specifically, any changes that may occur in the sperm cells, may play a remarkable role in the development and future of the fetus. From a cautionary perspective, it could be pointed out that any alteration in these proteins may affect infant diseases and likely some diseases appear later on. Sperm-associated antigens have the ability to be changed during the freezing process. Although gene activity and expression are restricted in mature spermatozoa, they could still be altered during the freezing procedure. Cryopreservation can alter the gene expression of *SPAGs*, and it is an important issue to be concerned about, for the reason that these changes could be sustained in the future and even have repercussions on the next generation.

Acknowledgements

The authors would like to assert that there is no conflicting financial interests and also no funding was received for this article.

Authors' Contributions

S.F.; Contributed to explicit literature search, data collection, and classification as well as summarizing papers and writing the manuscript. M.Sh.; Contributed to manuscript writing and revision. R.F.; Contributed to structuring the review study as well as being responsible for overall supervision. A.Sh.; Supervised the study and contributed to design the mian study background to this review paper. All authors performed editing and approving

the final version of this manuscript for submission, also approved the final draft.

References

1. Bohring C, Krause E, Habermann B, Krause W. Isolation and identification of sperm membrane antigens recognized by antisperm antibodies, and their possible role in immunological infertility disease. Mol Hum Reprod. 2001; 7(2): 113-118.
2. Silina K, Zayakin P, Kalnina Z, Ivanova L, Meistere I, Endzelinš E, et al. Sperm-associated antigens as targets for cancer immunotherapy: expression pattern and humoral immune response in cancer patients. J Immunother. 2011; 34(1): 28-44.
3. Sandlow JI. Shattering the myths about male infertility. Treatment of male factors may be more successful and cost-effective than you think. Postgrad Med. 2000; 107(2): 235-239, 242, 245.
4. Leaver RB. Male infertility: an overview of causes and treatment options. Br J Nurs. 2016; 25(18): S35-S40.
5. Cui Z, Sharma R, Agarwal A. Proteomic analysis of mature and immature ejaculated spermatozoa from fertile men. Asian J Androl. 2017; 18(5): 735-746.
6. Myles DG, Koppel DE, Cowan AE, Phelps BM, Primakoff P. Rearrangement of sperm surface antigens prior to fertilization. Ann N Y Acad Sci. 1987; 513(1): 262-273.
7. Moore HD. Contribution of epididymal factors to sperm maturation and storage. Andrologia. 1998; 30(4-5): 233-239.
8. Vazquez-Levin MH, Marin-Briggiler CI, Veaute C. Antisperm antibodies: invaluable tools toward the identification of sperm proteins involved in fertilization. Am J Reprod Immunol. 2014; 72(2): 206-218.
9. Huang C, Wu D, Khan FA, Jiao X, Guan K, Huo L. The GTPase SPAG-1 orchestrates meiotic program by dictating meiotic resumption and cytoskeleton architecture in mouse oocytes. Mol Biol Cell. 2016; 27(11): 1776-1785.
10. Hu P, Guan K, Feng Y, Ma C, Song H, Li Y, et al. miR-638 Inhibits immature Sertoli cell growth by indirectly inactivating PI3K/AKT pathway via SPAG1 gene. Cell Cycle. 2017; 16(23): 2290-2300.
11. Diekman AB, Olson G, Goldberg E. Expression of the human antigen SPAG2 in the testis and localization to the outer dense fibers in spermatozoa. Mol Reprod Dev. 1998; 50(3): 284-293.
12. Ayaz A, Agarwal A, Sharma R, Kothandaraman N, Cakar Z, Sikka S. Proteomic analysis of sperm proteins in infertile men with high levels of reactive oxygen species. Andrologia. 2018; 50(6): e13015.
13. Samanta L, Agarwal A, Swain N, Sharma R, Gopalan B, Esteves S C, et al. Proteomic signatures of sperm mitochondria in varicocele: clinical utility as biomarkers of varicocele associated infertility. J Urol. 2018; 200(2): 414-422.
14. Bromfield EG, Aitken RJ, Anderson AL, McLaughlin EA, Nixon B. The impact of oxidative stress on chaperone-mediated human sperm–egg interaction. Hum Reprod. 2015; 30(11): 2597-2613.
15. Bromfield EG, McLaughlin EA, Aitken RJ,Nixon B. Heat shock protein member A2 forms a stable complex with angiotensin converting enzyme and protein disulfide isomerase A6 in human spermatozoa. Mol Hum Reprod. 2016; 22(2): 93-109.
16. Shao X, Tarnasky HA, Lee JP, Oko R, van der Hoorn FA. Spag4, a novel sperm protein, binds outer dense-fiber protein Odf1 and localizes to microtubules of manchette and axoneme. Dev Biol. 1999; 211(1): 109-123.
17. Yang K, Adham IM, Meinhardt A, Hoyer-Fender S. Ultra-structure of the sperm head-to-tail linkage complex in the absence of the spermatid-specific LINC component SPAG4. Histochem Cell Biol. 2018; 150(1): 49-59.
18. Shao X, Xue J, van der Hoorn FA. Testicular protein Spag5 has similarity to mitotic spindle protein Deepest and binds outer dense fiber protein Odf1. Mol Reprod Dev. 2001; 59(4): 410-416.
19. Thein KH, Kleylein-Sohn J, Nigg EA,Gruneberg U. Astrin is required for the maintenance of sister chromatid cohesion and centrosome integrity. J Cell Biol. 2007; 178(3): 345-354.
20. Suzuki H, Yagi M, Suzuki K. Duplicated insertion mutation in the microtubule-associated protein Spag5 (astrin/MAP126) and defective proliferation of immature Sertoli cells in rat hypogonadic (hgn/hgn) testes. Reproduction. 2006; 132(1): 79-93.
21. Lonergan KM, Chari R, Deleeuw RJ, Shadeo A, Chi B, Tsao MS, et al. Identification of novel lung genes in bronchial epithelium by serial analysis of gene expression. Am J Respir Cell Mol Biol. 2006; 35(6): 651-661.
22. Li X, Xu L, Sun G, Wu X, Bai X, Li J, et al. Spag6 mutant mice have defects in development and function of spiral ganglion neurons, apoptosis, and higher sensitivity to paclitaxel. Sci Rep. 2017; 7(1): 8638.
23. Cooley LF, El Shikh ME, Li W, Keim RC, Zhang Z, Strauss JF, et al. Impaired immunological synapse in sperm associated antigen 6 (SPAG6) deficient mice. Sci Rep. 2016; 6: 25840.
24. Jiang M, Chen Y, Deng L, Luo X, Wang L, Liu L. Upregulation of SPAG6 in myelodysplastic syndrome: knockdown inhibits cell proliferation via AKT/FOXO signaling pathway. DNA Cell Biol. 2019; 38(5): 476-484.
25. Huo FY, Li YS, Yang XY, Wang QX, Liu JJ, Wang LK, et al. Expressions of SLC22A14 and SPAG6 proteins in the ejaculated sperm of idiopathic asthenozoospermia patients. Zhonghua Nan Ke Xue. 2017; 23(8): 703-707.
26. Beaton S, Cleary A, ten Have J, Bradley MP. Cloning and characterization of a fox sperm protein FSA-1. Reprod Fertil Dev. 1994; 6(6): 761-770.
27. Bens S, Zichner T, Stütz AM, Caliebe A, Wagener R, Hoff K, et al. SPAG7 is a candidate gene for the periodic fever, aphthous stomatitis, pharyngitis and adenopathy (PFAPA) syndrome. Genes Immun. 2014; 15(3): 190-194.
28. Li R, Tang XL, Miao SY, Zong SD, Wang LF. Regulation of the G2/M phase of the cell cycle by sperm associated antigen 8 (SPAG8) protein. Cell Biochem Funct. 2009; 27(5): 264-268.
29. Wu H, Chen Y, Miao S, Zhang C, Zong S, Koide SS, et al. Sperm associated antigen 8 (SPAG8), a novel regulator of activator of CREM in testis during spermatogenesis. FEBS Lett. 2010; 584(13): 2807-2815.
30. Lee CM, Onésime D, Reddy CD, Dhanasekaran N, Reddy EP. JLP: a scaffolding protein that tethers JNK/p38MAPK signaling modules and transcription factors. Proc Natl Acad Sci USA. 2002; 99(22): 14189-14194.
31. Iwanaga A, Wang G, Gantulga D, Sato T, Baljinnyam T, Shimizu K, et al. Ablation of the scaffold protein JLP causes reduced fertility in male mice. Transgenic Res. 2008; 17(6): 1045-1058.
32. Kashef K, Xu H, Reddy EP, Dhanasekaran DN. Endodermal differentiation of murine embryonic carcinoma cells by retinoic acid requires JLP, a JNK-scaffolding protein. J Cell Biochem. 2006; 98(4): 715-722.
33. Li R, Gunarta IK, Suzuki R, Boldbaatar J, Nakazato R, Yuliana D, et al. JLP-JNK signaling protects cancer cells from reactive oxygen species-induced cell death. Biochem Biophys Res Commun. 2018; 501(3): 724-730.
34. Pan J, Yu H, Guo Z, Liu Q, Ding M, Xu K, et al. Emerging role of sperm-associated antigen 9 in tumorigenesis. Biomed Pharmacother. 2018; 103: 1212-1216.
35. Raymond A, Ensslin MA, Shur BD. SED1/MFG-E8: a bi-motif protein that orchestrates diverse cellular interactions. J Cell Biochem. 2009; 106(6): 957-966.
36. Barua S, Macedo A, Kolb DS, Wynne-Edwards KE, Klein C. Milk-fat globule epidermal growth factor 8 (MFGE8) is expressed at the embryo–and fetal–maternal interface in equine pregnancy. Reprod Fertil Dev. 2018; 30(4): 585-590.
37. Cen C, Aziz M, Yang WL, Zhou M, Nicastro JM, Coppa GF, et al. Milk fat globule-epidermal growth factor-factor VIII attenuates sepsis-induced acute kidney injury. J Surg Res. 2017; 213: 281-289.
38. Viola JR, Lemnitzer P, Paulin N, Drechsler M, Nazari-Jahantigh M, Maas S, et al. Deletion of MFGE8 inhibits neointima formation upon arterial damage. Thromb Haemost. 2018; 118(7): 1340-1342.
39. Xiao Y, Li G, Chen Y, Zuo Y, Rashid K, He T, et al. Milk fat globule-epidermal growth factor-8 pretreatment attenuates apoptosis and inflammation via the integrin-β3 pathway after surgical brain injury in rats. Front Neurol. 2018; 9: 96.
40. Jia M, Yao H, Chen C, Wang Y, Wang H, Cui T, et al. Prognostic correlation between MFG-E8 expression level and colorectal cancer. Arch Med Res. 2017; 48(3): 270-275.
41. Narmadha G, Yenugu S. Molecular modeling of the human sperm associated antigen 11 B (SPAG11B) proteins. Syst Biol Reprod Med. 2015; 61(2): 78-88.
42. Denadai-Souza A, Ribeiro CM, Rolland C, Thouard A, Deraison C, Scavone C, et al. Effect of tryptase inhibition on joint inflammation: a pharmacological and lentivirus-mediated gene transfer study. Arthritis Res Ther. 2017; 19(1): 124.
43. Naz RK. Effects of sperm-reactive antibodies present in human infertile sera on fertility of female rabbits. J Reprod Immunol. 1990; 18(2): 161-177.
44. Chen C, Wang B. Brucea javanica oil emulsion alleviates cachexia induced by Lewis lung cancer cells in mice. J Drug Target. 2018; 26(3): 222-230.
45. Tusup M, Kundig T, Pascolo S. Epitranscriptomics of cancer. World

J Clin Oncol. 2018; 9(3): 42-55.
46. Fujimoto T, Miyasaka K, Koyanagi M, Tsunoda T, Baba I, Doi K, et al. Altered energy homeostasis and resistance to diet-induced obesity in KRAP-deficient mice. PLoS One. 2009; 4(1): e4240.
47. Zhang H, Martin-Deleon PA. Mouse epididymal Spam1 (pH-20) is released in the luminal fluid with its lipid anchor. J Androl. 2003; 24(1): 51-58.
48. Grigorieva A, Griffiths GS, Zhang H, Laverty G, Shao M, Taylor L, et al. Expression of SPAM1 (PH-20) in the murine kidney is not accompanied by hyaluronidase activity: evidence for potential roles in fluid and water reabsorption. Kidney Blood Press Res. 2007; 30(3): 145-155.
49. Zhang Z, Zariwala MA, Mahadevan MM, Caballero-Campo P, Shen X, Escudier E, et al. A heterozygous mutation disrupting the SPAG16 gene results in biochemical instability of central apparatus components of the human sperm axoneme. Biol Reprod. 2007; 77(5): 864-871.
50. Knevel R, Klein K, Somers K, Ospelt C, Houwing-Duistermaat JJ, van Nies JAB, et al. Identification of a genetic variant for joint damage progression in autoantibody-positive rheumatoid arthritis. Ann Rheum Dis. 2014; 73(11): 2038-2046.
51. Fraussen J, de Bock L,Somers V. B cells and antibodies in progressive multiple sclerosis: Contribution to neurodegeneration and progression. Autoimmun Rev. 2016; 15(9): 896-899.
52. Xu X, Sha YW, Mei LB, Ji ZY, Qiu PP, Ji H, et al. A familial study of twins with severe asthenozoospermia identified a homozygous SPAG17 mutation by whole-exome sequencing. Clin Genet. 2018; 93(2): 345-349.
53. Kazarian E, Son H, Sapao P, Li W, Zhang Z, Strauss JF, et al. SPAG17 Is required for male germ cell differentiation and fertility. Int J Mol Sci. 2018; 19(4): 1252.
54. Teves ME, Sundaresan G, Cohen DJ, Hyzy SL, Kajan I, Maczis M, et al. Spag17 deficiency results in skeletal malformations and bone abnormalities. PLoS One. 2015; 10(5): e0125936.
55. Neesse A, Gangeswaran R, Luettges J, Feakins R, Weeks ME, Lemoine NR, et al. Sperm-associated antigen 1 is expressed early in pancreatic tumorigenesis and promotes motility of cancer cells. Oncogene. 2007; 26(11): 1533-1545.
56. Itkonen HM, Engedal N, Babaie E, Luhr M, Guldvik IJ, Minner S, et al. UAP1 is overexpressed in prostate cancer and is protective against inhibitors of N-linked glycosylation. Oncogene. 2015; 34(28): 3744-3750.
57. Zhai LL, Xie Q, Zhou CH, Huang DW, Tang ZG, Ju TF. Overexpressed HSPA2 correlates with tumor angiogenesis and unfavorable prognosis in pancreatic carcinoma. Pancreatology. 2017; 17(3): 457-463.
58. Ji Y, Jiang J, Huang L, Feng W, Zhang Z, Jin L, et al. Sperm-associated antigen 4 (SPAG4) as a new cancer marker interacts with Nesprin3 to regulate cell migration in lung carcinoma. Oncol Rep. 2018; 40(2): 783-792.
59. Liu JY, Zeng QH, Cao PG, Xie D, Yang F, He LY, et al. SPAG5 promotes proliferation and suppresses apoptosis in bladder urothelial carcinoma by upregulating Wnt3 via activating the AKT/mTOR pathway and predicts poorer survival. Oncogene. 2018; 37(29): 3937-3952.
60. Li M, Li A, Zhou S, Lv H, Yang W. SPAG5 upregulation contributes to enhanced c-MYC transcriptional activity via interaction with c-MYC binding protein in triple-negative breast cancer. J Hematol Oncol. 2019; 12(1): 14.
61. Liu G, Liu S, Cao G, Luo W, Li P, Wang S, et al. SPAG5 contributes to the progression of gastric cancer by upregulation of Survivin depend on activating the wnt/β-catenin pathway. Exp Cell Res. 2019; 379(1): 83-91.
62. Song L, Dai Z, Zhang S, Zhang H, Liu C, Ma X, et al. MicroRNA-1179 suppresses cell growth and invasion by targeting sperm-associated antigen 5-mediated Akt signaling in human non-small cell lung cancer. Biochem Biophys Res Commun. 2018; 504(1): 164-170.
63. Yang YF, Zhang MF, Tian QH, Fu J, Yang X, Zhang CZ, et al. SPAG5 interacts with CEP55 and exerts oncogenic activities via PI3K/AKT pathway in hepatocellular carcinoma. Mol Cancer. 2018; 17(1): 117.
64. Okayama A, Kimura Y, Miyagi Y, Oshima T, Oshita F, Ito H, et al. Relationship between phosphorylation of sperm-specific antigen and prognosis of lung adenocarcinoma. J Proteomics. 2016; 139: 60-66.
65. Khowal S, Naqvi SH, Monga S, Jain SK, Wajid S. Assessment of cellular and serum proteome from tongue squamous cell carcinoma patient lacking addictive proclivities for tobacco, betel nut, and alcohol: case study. J Cell Biochem. 2018; 119(7): 5186-5221.
66. Beech DJ, Madan AK, Deng N. Expression of PH-20 in normal and neoplastic breast tissue. J Surg Res. 2002; 103(2): 203-207.
67. Li Y, Huang J, Sun J, Xiang S, Yang D, Ying X, et al. The transcription levels and prognostic values of seven proteasome alpha subunits in human cancers. Oncotarget. 2017; 8(3): 4501-4519.
68. Hezavehei M, Mohseni Kouchesfahani H, Shahverdi A, Sharafi M, Hosseini Salekdeh G , Eftekhari-Yazdi P. Preconditioning of sperm with sublethal nitrosative stress: a novel approach to improve frozen–thawed sperm function. Reprod Biomed Online. 2019; 38(3): 413-425.
69. Salehi M, Mahdavi AH, Sharafi M, Shahverdi A. Cryopreservation of rooster semen: Evidence for the epigenetic modifications of thawed sperm. Theriogenology. 2020; 142: 15-25.
70. Gholami D, Ghaffari SM, Shahverdi A, Sharafi M, Riazi G, Fathi R, et al. Proteomic analysis and microtubule dynamicity of human sperm in electromagnetic cryopreservation. J Cell Biochem. 2018; 119(11): 9483-9497.

Original Article

AntagomiR-19a Induced Better Responsiveness to Bortezomib in Myeloma Cell Lines

Azam Kazemi, Ph.D., Saeid Abroun, Ph.D.*, Masoud Soleimani, Ph.D.

Department of Haematology and Blood Banking, Faculty of Medical Sciences, Tarbiat Modares University, Tehran, Iran

**Corresponding Address: P.O.Box: 14115-111, Department of Haematology and Blood Banking, Faculty of Medical Sciences, Tarbiat Modares University, Tehran, Iran*
Email: abroun@modares.ac.ir

Received: 04/December/2019, Accepted: 19/April/2020

Abstract

Objective: Multiple myeloma (MM) is the clonal proliferation of neoplastic plasma cells in the bone marrow. Although bortezomib (BTZ) is a crucial drug for the treatment of MM, drug resistance is a major problem. OncomiR-19a plays an oncogenic role in many cancers, including MM; however, the function of miR-19a in the pathogenesis of MM and drug resistance has not been completely identified. The present research aims to investigate the inhibition of miR-19a by an antagomir to determine BTZ responsiveness, and determine if miR-19a can be a prognostic biomarker for MM.

Materials and Methods: In this experimental study, viability and apoptosis of myeloma cells were analysed by the colorimetric 3-(4, 5-Dimethylthiazol-2-yl)-2, 5-Diphenyltetrazolium Bromide (MTT) and Annexin V/propidium iodide (PI) flow cytometry assays. Quantitative real-time polymerase chain reaction (qRT-PCR) was implemented to evaluate the expression levels of miR-19a, its targets *SOCS3, STAT3*, B-cell lymphoma 2 *(BCL-2), PTEN* and *CDKN1A* (anti-apoptotic and cell cycle related genes) at the mRNA level.

Results: miR-19a was downregulated and exacerbated in transfected cells treated with BTZ. The rate of apoptosis in the myeloma cells after BTZ treatment considerably increased, which indicated an increase in the mRNA of *SOCS3, PTEN, BCL-2,* and *CDKN1*. A decrease in *STAT3* was also observed.

Conclusion: OncomiR-19a, as a biomarker, may induce better responsiveness to BTZ in myeloma cell lines through its targets *SOCS3, STAT3* and *PTEN*. In the future, this biomarker may provide new therapeutic targets for MM.

Keywords: Antagomir-19a, Bortezomib, Multiple Myeloma, *SOCS3*

Cell Journal(Yakhteh), Vol 23, No 5, October 2021, Pages: 503-509

Citation: Kazemi A, Abroun S, Soleimani M. AntagomiR-19a induced better responsiveness to bortezomib in myeloma cell lines. Cell J. 2021; 23(5): 503-509. doi: 10.22074/cellj.2021.7302.

Introduction

Multiple myeloma (MM) is a tumour of differentiated B cells from the germinal centre, plasma cells, within 10% of all haematologic neoplasms and is considered the second most commonly occurring non-Hodgkin lymphoma (1, 2). Over the last two decades, advancements in available treatments have increased the median survival time of patients with MM from three to six years. MM accounts for 2% of total cancer deaths and more than 20% of deaths due to malignancies (3). Although tremendous advancements have been made in new healthcare strategies in the past decade, to a great extent, this tumour is incurable and new therapies are required (4, 5). Despite the innovation and benefits of a new therapeutic strategy such as proteasome inhibitors, the clinical outcome of the patients aggravates and most patients with MM eventually relapse and engenders drug resistance (1).

The proteasome inhibitor, bortezomib (BTZ), is a crucial Food and Drug Adminisration (FDA)-approved drug for the treatment of MM, especially in patients diagnosed with relapsed and refractory MM (6). Although BTZ has a significant impact on MM treatment (5), drug resistance or relapse are two major challenges and patients with BTZ resistance have a poor prognosis (7, 8). Therefore, new therapeutic methods are urgently required to prevent BTZ resistance. In addition, a more profound molecular grasp of this cancer's pathogenesis is required to recognize new molecular targets and present therapeutic agents suitable for patients (9). There is developing evidence that MM stems from the deregulation of noncoding RNAs (ncRNAs), which include microRNAs (miRNAs) (1). Recent studies show that MM is caused by interruptions in many different signalling pathways driven by miRNAs that are a class of ncRNAs about 18-22 nucleotides (nt) in length. These miRNAs act as master regulators of gene expression at the post-transcriptional level via RNA interference pathways (6). miRNAs are involved in many biological processes that include differentiation, senescence, survival and apoptosis (3, 6). Disturbances in miRNA regulation are accompanied by the pathogenesis of diseases such as cancer, and miRNA expression profiles have prognostic implications in numerous types of cancer (6). Altogether, miRNAs play a fundamental role as an oncogene and they operate as 'oncomiRs' if their targets are tumour suppressor genes (1). Therefore, controlling oncomiRs may be an effective treatment strategy.

The miR-17-92 clusters located in chromosome 13q31.3, including miR-19a, were the first oncomiRs discovered. Disturbances in the expression levels of miR-

17-92 clusters result in malignant progression of MM (4, 5). miR-19a, a crucial component of the miR-17-92 cluster, is directly involved in myeloma pathogenesis and progression of MM (9). In addition, target genes of miR-19a are considered potential biomarkers of this disease (10). Compared with normal plasma cells, miR-19a is upregulated in patients with MM and in MM cell lines.

miR-19a can adjust the expressions of proteins essential for myeloma pathogenesis and include suppressors of cytokine signalling (*SOCSs*). miR-19a targets *SOCS3*, a potent regulator of the JAK-STAT pathway, which is followed by a considerable reduction in *SOCS3* mRNA together with enhanced activation of the *SOCS3* target, *STAT3* (9). Based on these findings, a strategy that can be developed to regulate aberrant expressions of miRNAs in cancer is the inhibition of upregulated miRNAs (1). Therefore, we assume that the use of mir-19a inhibitors (antagomir) could be a new treatment approach for MM.

B-cell lymphoma 2 (*BCL-2*) is one of the anti-apoptotic members of the *BCL-2* family that interacts with these proteins and in response to drug therapy, it determines cellular fate decisions and represents an attractive target for therapy (11, 12). *In vitro* studies indicated that *CDKN1A* might be an oncogene in lymphomas and plasma cell disorders, and these studies indicate that *CDKN1A* can act as a molecular target for drug developments (13). Although BTZ is used to treat MM, 60% of patients treated with BTZ experience resistance. Therefore, we intend to investigate the impact of antagomiR-19a on improving responsiveness to BTZ. The findings may show that miR-19a can be an effective biomarker for treatment response (9, 14).

Materials and Methods

Cell lines and cultures

In this experimental study, we purchased the RPM I8226 and U266 cell lines from Pasteur Institute of Iran (IPI), Tehran, Iran. The cells were grown in suspension in RPMI 1640 medium (Bio-Idea, Bio Idea Group, Iran) supplemented with 10% foetal bovine serum (FBS, Gibco-BRL, Germany), 100 mg/mL penicillin, 100 mg/mL streptomycin, and 2 mM L-glutamine (Bio-Idea, Bio Idea Group, Iran). The cells were maintained at 37˚C in an environment of 5% CO_2 and 95% air, and were passaged twice per week.

The present study was conducted with the approval of the Ethical Committee of the Tarbiat Modares University (IR.TMU.REC.1394.290).

Reagents

BTZ (PS-341, Selleckchem.com, cat. no. S1013) was dissolved in 0.2603 mL DMSO to prepare a 50 mM stock solution and stored at -20˚C. The LentimiRa-off-has-miR-19a-3p vector (Applied Biological Materials, Inc., cat. no. mh30299) that included a green fluorescent protein (GFP) promoter, miRNA insert and kanamycin resistance gene was transformed in a DH5α E. coli strain, then isolated with a Qiagen plus Midi Plasmid Purification kit. The final product was stored at -20˚C until further use.

In vitro cell culture and drug treatment

The human myeloma cell lines RPMI 8226 and U266 were cultured in RPMI 1640 and the stock solution of BTZ was diluted in RPMI 1640 medium prior to use. RPMI 8226 and U266 cells were cultured in RPMI 1640 medium, then seeded at a density of 5×10^3 cells in 96-well plates. These cells were treated with various working concentrations of BTZ, which was obtained from a 50 mM stock solution, in order to determine the half maximal inhibitory concentration (IC_{50}) for each cell line.The concentrations of BTZ were based on approximate concentrations noted in the cell assay part of the BTZ datasheet, which were 0.5, 5, and 50 μM for U266 and 150, 450, 750, and 1050 nM for RPMI 8226. The BTZ concentrations and cells were mixed well in RPMI 1640 medium and 10% FBS, and incubated for 48 hours.

3-(4, 5-dimethylthiazol-2-yl)-2, 5-diphenyltetrazolium bromide colorimetric assay

We used a standard protocol to assess the inhibitory impact of BTZ on cell growth by the 3-(4, 5-dimethylthiazol-2-yl)-2, 5-diphenyltetrazolium bromide (MTT) assay. Briefly, cells from the 48-hour cultures were pulsed with 10 μL of 5 mg/mL MTT in each well for at least four hours of the 48-hour cultures, followed by 100 μL of isopropanol that contained 0.04 N HCl. Absorbance was measured at 570 nm using a spectrophotometer and the results were expressed as the mean of three replicates, as a percentage of the control (100%). The extent of cytotoxicity was defined as the relative reduction in optical density, which correlated to the number of viable cells in relation to the control (100%). In order to decide the optimum dosage of the drugs for further studies, the cell viability was plotted in a graph and we calculated the IC_{50}.

Cell viability analysis

The effect of transfection on cellular viability was assessed by flow cytometry using propidium iodide (PI). PI can only pass through disordered areas of the membranes of nonviable cells and intercalate with DNA of the nuclei, emitting a red fluorescence light. PI solution was used with 1 mg/mL concetration by dissolving PI (Sigma, P 4170, Germany) in dH_2O. The PI solution was added in a final concentration of 2 μg/mL to 1×10^6 cells in suspension, incubated in the dark for five minutes, then analysed by flow cytometry with an Attune NXT flow cytometer.

Analysis of apoptosis

We assessed the level of apoptosis by annexin V/PI staining and flow cytometry with an Attune NXT flow cytometer in transfected cells that were treated with BTZ and in the untreated cells. The cells were washed in PBS and then in 1X binding buffer before they were resuspended in 1X binding buffer at 1×10^6 cells/mL. Then, we added 5 μL of FITC-conjugated annexin V to 100 μL of the cell suspension and incubated this suspension for 10-15 minutes in the dark at room temperature. The incubated cells were washed with binding buffer and resuspended in it. Next, we added 5 μL PI staining solution (Sigma, P 4170, Germany) and analysed the cells with flow cytometry.

Prediction of *SOCS3* as a target of miR-19a

TargetScan (version 5) and PicTar were used to confirm that *SOCS3* is a target of miR-19a at its 3´UTR. TargetScan predicted the biological targets of miRNA by searching for the presence of conserved 7 and 8 base sites that match its seed region.

Cell transfection

The cells were grown in RPMI 1640 medium without antibiotics prior to transfection. The U266 and RPMI 8226 cell lines were transfected by a final concentration of 2 µg of the pLenti-III-miR-Off-has-miR-19a-3p vector that contained GFP (Applied Biological Materials, Inc., Canada). Transfection of cells was performed using UltraCruz® Transfection Reagent (Santa Cruz Biotechnology, Inc., Germany). Briefly, before transfection, we prepared transfection reagent and the vector in Opti-MEM I reduced serum medium (Gibco, Germany) in accordance with the manufacturer's protocol. The transfection reagent and plasmid were prepared in OPTI-MEM I medium and incubated at room temperature. Next, we added the plasmid reagent to the transfection reagent, vortexed it vigorously, and incubated the mixture for 20 minutes. A total of 6×10^3 cells were added to the Eppendorf tube and were poured above mix dropwise to the cells, then the solution was incubated in the incubator for two hours. Each 30 minutes the tube was flicked by a fingertip. After the incubation, the cells were transferred to a six-well plate and incubated for 24-72 hours, followed by evaluation of GFP expression by an Attune NXT flow cytometer.

Quantitative real-time polymerase chain reaction assessment of miR-19a expression

Total RNA was isolated from the untransfected, transfected, and BTZ-treated RPMI 8226 and U266 cells according to the TRIzol manufacturer's protocol (Invitrogen™, USA). A total of 2000 ng of RNA was reverse transcribed using specific miRNA stem-loop primers from Qiagen for miR-19a to generate cDNA using a Hyperscript Reverse Transcriptase First-strand Synthesis kit (GeneAll Biotechnology Co., Ltd., Korea). Snord47 was used as the internal control for normalization of miRNA expression. Quantitative real-time polymerase chain reaction (qRT-PCR) was performed with a SYBR® Premix Ex Taq™ miRNA RT-qPCR Detection Kit (Takara, USA, cat. no. RR820Q) using a Qiagen Rotor-Gene Q 5PLEX HRM Real-Time PCR. Table 1 shows the primer sequences used in this experiment. The PCR program cycling parameters were: 95˚C for 15 seconds, 58˚C for 30 seconds, and 72˚C for 30 seconds for 45 cycles. Data analysis was done by $2^{-\Delta\Delta CT}$ to calculate the fold change for relative miR-19a expression compared to the untreated control.

Quantitative real-time polymerase chain reaction analysis for the *SOCS3*, *STAT3*, *PTEN*, *BCL-2* and *CDKN1A* genes

Total RNA was isolated from the untransfected, transfected, and BTZ-treated RPMI 8226 and U266 cells according to the TRIzol manufacturer's protocol (Invitrogen™, USA). A total of 2 µg of total RNA was reverse transcribed into cDNA using a Hyperscript Reverse Transcriptase First-strand Synthesis kit with oligo-dT primers in accordance with the manufacturer's instructions (GeneAll Biotechnology Co., Ltd., Korea) for evaluation of the *SOCS3, STAT3, BCL-2, CDKN1A* and *PTEN* genes. *β-Actin* was used as the internal control. qRT-PCR was performed with the SYBR® Premix Ex Taq™ miRNA RT-qPCR Detection Kit (Takara, USA, cat. no. RR820Q) using a Qiagen Rotor-Gene Q 5PLEX HRM Real-Time PCR. The PCR program cycling parameters were: 95˚C for 15 seconds, 58˚C for 30 seconds, and 72˚C for 30 seconds for 45 cycles. Data analysis was performed by $2^{-\Delta\Delta CT}$ to calculate the fold changes for the relative expressions of the above genes compared to the untreated control.

Statistical analysis

Data was presented as mean ± standard deviation. The statistical analysis was performed with the Graphpad prism 8.4.0 software The mean values of two groups or multiple groups were compared by one-way analysis of variance (ANOVA). $P<0.05$ was considered statistically significant. Flow cytometric assays were analyzed with flowjo version 7.6.1.

Results

Determination of the IC_{50} for bortezomib in the U266 and RPMI 8226 multiple myeloma cell lines

We treated the RPMI 8226 and U266 cell lines with different concentrations of BTZ to determine the optimal IC_{50} to treat the cell lines with proper concentrations of BTZ throughout the analysis. The MTT assay and viability test with PI by flow cytometry showed that the optimized concentration of BTZ for the U266 cell line was 5 µM and it was 150 nM for the RPMI 8226 cell line (Fig.1A-D).

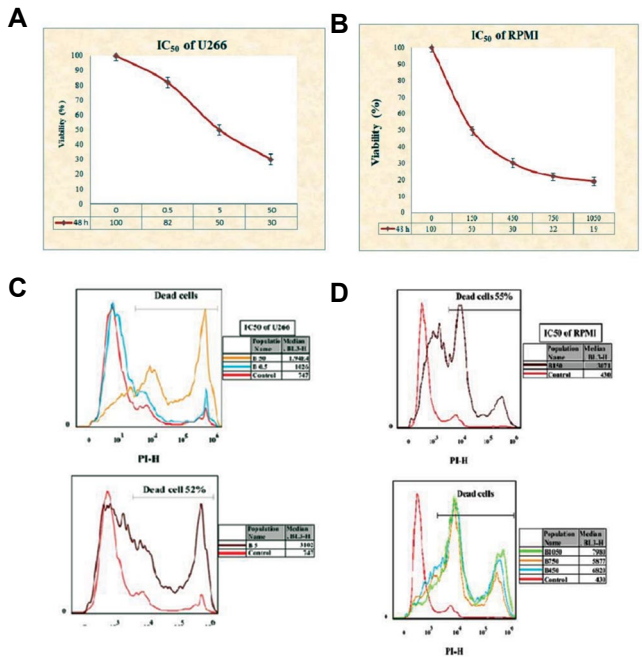

Fig.1: IC_{50} evaluation of the U266 and RPMI 8226 cell lines to optimize the concentration of bortezomib (BTZ). **A, B.** The U266 and RPMI 8226 cell lines were incubated with increasing concentrations of BTZ (0 to 50 µM) and (0 to 1050 nM), respectively, for 48 hours. Cell viability was assessed by the 3-(4, 5-Dimethylthiazol-2-yl)-2, 5-Diphenyltetrazolium Bromide (MTT) colorimetric assay. **C, D.** Treated U266 and RPMI 8226 cells were incubated with propidium iodide (PI) and the percentage of nonviable cells was assessed by flow cytometry.

Downregulation of miR-19a decreased cell viability and prevented proliferation of the myeloma cell lines

We first evaluated the expression levels of miR-19a in the non-transfected (control) RPMI 8226 and U266 myeloma cell lines. After transfection of these cell lines with the LentimiRa-off-has-miR-19a-3p vector, the efficiency of transfection was monitored by GFP fluorescence as observed by fluorescent microscopy (Fig.2A, 3A) and flow cytometry (Fig.2B, 3B). The expression levels of miR-19a were determined in the transfected RPMI 8226 and U266 myeloma cell lines by qRT-PCR. As shown in Figures 2C and 3C, the expression level of miR-19a significantly decreased in the transfected group compared with the un-transfected myeloma cell line. The data showed that the antagomir-19a downregulated expression of miR-19a, a previously-known oncomiR. After transfection of the RPMI 8226 and U266 myeloma cell lines with the LentimiRa-off-has-miR-19a-3p vector, we evaluated cell viability after 72 hours with PI and the rate of viability was detected by flow cytometry (Fig.2D, 3D). The data confirmed the possibility of the analyses of the cell lines within 72 hours after transfection, and indicated a decrease in cell viability because of miR-19a downregulation. When compared with the negative control group, this finding suggested that miR19a suppression decreased cell proliferation.

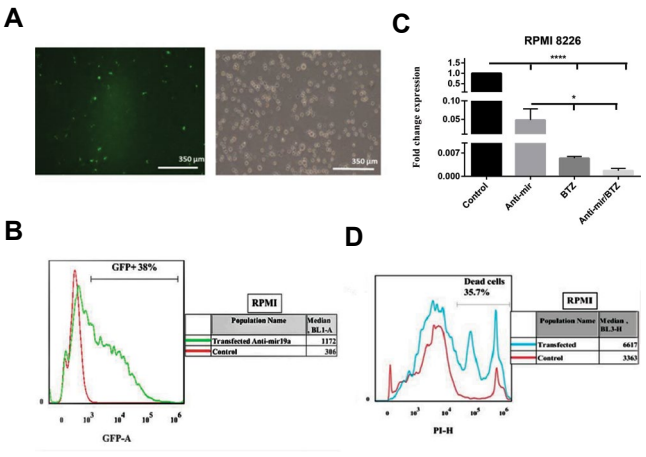

Fig.2: RPMI 8226 cells were transfected with the LentimiRa-off-has-mir-19a-3p vector. **A, B**. The transfection efficiency was assessed by fluorescence microscopy and flow cytometry through GFP fluorescence. **C.** miR-19a expression was assessed by quantitative real-time polymerase chain reaction (qRT-PCR) in the non-transfected RPMI cell line (control), transfected RPMI cell line with the LentimiRa-off-has-mir-19a-3p vector, treated RPMI cell line with bortezomib (BTZ) and treated RPMI cell lines with BTZ after transfection with the LentimiRa-off-has-mir-19a-3p vector The ratios of miR-19a were calculated relative to Snord47. Values are expressed as the mean ± standard deviation of three independent experiments. **D.** Evaluation of RPMI 8226 myeloma cell line viability at 72 hours after transfection. RPMI 8226 cells were transfected with the LentimiRa-off-has-mir-19a-3p vector, then incubated with propidium iodide (PI). Cell viability was assessed by flowcytometry. *; P<0.05 vs. the control and ****; P<0.001.

Reduction in miR-19a expression in the myeloma cell lines after bortezomib treatment

We used qRT-PCR to evaluate the expression level of miR-19a after treatment with BTZ. Our data showed a reduction in its expression in the treated cells compared to the non-treated cells. miR-19a expression was also evaluated in cells transfected by the LentimiRa-off-has-miR-19a-3p vector. The data showed a substantial reduction in miR-19a expression after BTZ treatment compared to the non-treated and non-transfected controls (Fig.2C, 3C). Cell viability evaluation after 72 hours with PI using flow cytometry showed that it was possible to evaluate every analysis on the transfected cell lines 72 hours after transfection. On the other hand, viability of the cell lines decreased due to downregulation of miR-19a (Fig.2D, 3D).

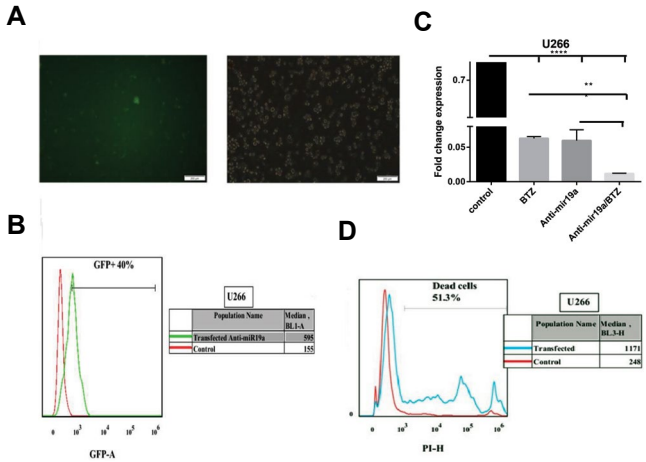

Fig.3: U266 cells were transfected with the LentimiRa-off-has-mir-19a-3p vector. **A, B.** The transfection efficiency was assessed by fluorescence microscopy and flow cytometry through GFP green fluorescence. **C.** Expression of miR-19a was assessed by quantitative real-time polymerase chain reaction (qRT-PCR) in the non-transfected U266 cell line (control), U266 cell line transfected with the LentimiRa-off-has-mir-19a-3p vector, U266 cell line treated with bortezomib (BTZ) and U266 cell line treated with BTZ after transfection with the LentimiRa-off-has-mir-19a-3p vector. The ratios of miR-19a were calculated relative to snord47. Values are expressed as the mean ± standard deviation of three independent experiments. **D.** Evaluation of U266 myeloma cell viability 72 hours after transfection. U266 cells were transfected with the LentimiRa-off-has-mir-19a-3p vector then the cells were incubated with propidium iodide (PI) and cell viability was assessed by flow cytometry after 72 hours. **; P<0.001 vs. the control and ****; P<0.0001.

Anti-miR-19a increased susceptibility to bortezomib-induced apoptosis

We investigated the effect of antagomir-19a on BTZ-induced apoptosis on the myeloma cell lines. The LentimiRa-off-has-miR-19a-3p transfected myeloma cells were incubated for 48 hours with BTZ (5 µM for U266 and 150 nM for RPMI 8226) followed by annexin V/PI staining and flow cytometry analysis to determine the percentage of apoptosis. The percentage of cells that underwent apoptosis increased after transfection in the RPMI 8226 (23.5% vs. 68.2%, P=0.0038) and U266 (25.2% vs. 96.4%, P=0.0006) cell lines compared with the non-transfected cell lines and the negative control (Fig.4A-D). The data showed that antagomir-19a could increase myeloma cell susceptibility to drug-induced apoptosis.

SOCS3 and *STAT3* mRNA expression levels after transfection of myeloma cell lines with the LentimiRa-off-has-miR-19a-3p vector

SOCS3 is a target of miR-19a. Therefore, we evaluated mRNA levels of *SOCS3* and its target, *STAT3,* in the myeloma cell lines after transfection with the Lentini-off-has-mir-19a-3p vector. There was an increase in mRNA expression of *SOCS3* and a decrease in *STAT3* mRNA

expression compared with the non-transfected cell lines (negative control) (Fig.5A-D).

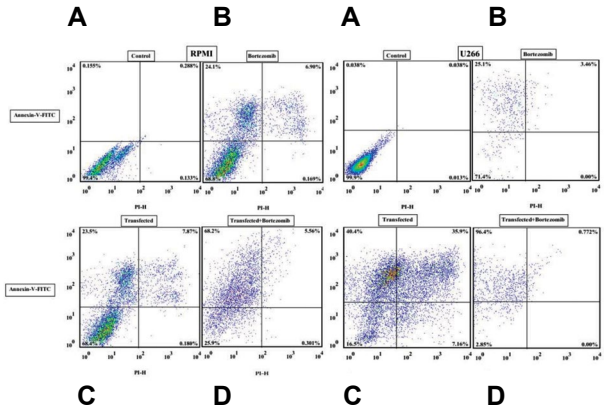

Fig.4: Evaluation of apoptosis by annexin V-FITC/propidium iodide (PI) staining and analysis by flow cytometry in RPMI 8226 and U266 myeloma cell lines. **A.** Untreated and nontransfected cell lines are the negative controls. **B.** After bortezomib (BTZ) treatment. **C.** After transfection with the LentimiRa-off-has-mir-19a-3p vector. **D.** After treatment of the transfected RPMI cell line with BTZ.

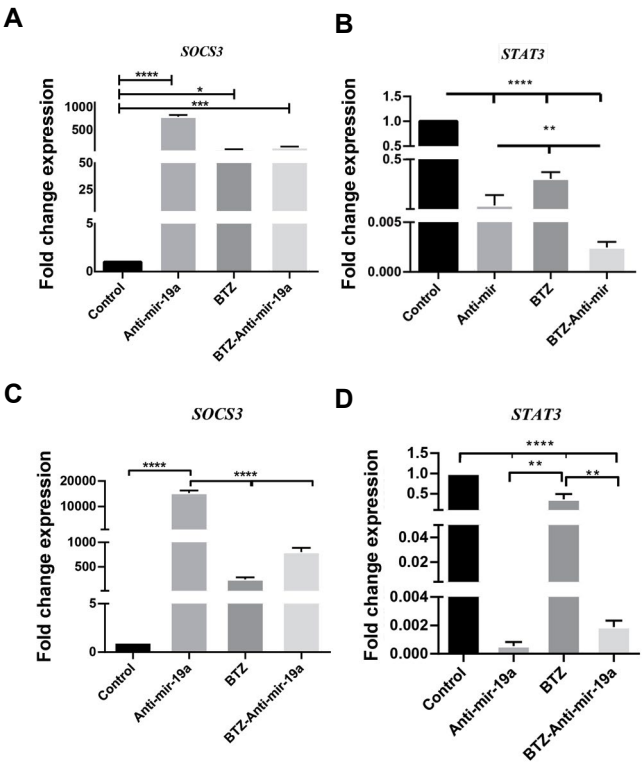

Fig.5: *SOCS3* and *STAT3* gene expression analyses at the mRNA level in RPMI 8226 and U266 cell lines by quantitative real-time polymerase chain reaction (qRT-PCR). The RPMI 8226 and U266 cells were cultured and treated with bortezomib (BTZ) (150 nM for RPMI 8226 and 5 µM for U266), transfected with the LentimiRa-off-has-mir-19a-3p vector and treated with BTZ (150 nM and 5 µM, respectively) after transfection. **A, B.** Expressions of *SOCS3* and *STAT3* were examined in RPMI 8226 cells after 48 hours of BTZ treatment and transfection with the LentimiRa-off-has-mir-19a-3p vector and after 48 hours of BTZ treatment in the transfected cells. **C, D.** *SOCS3* and *STAT3* expressions were examined in U266 cells after 48 hours of BTZ treatment and transfection with the LentimiRa-off-has-mir-19a-3p vector and after 48 hours of BTZ treatment in the transfected cells. Untreated RPMI 8226 and U266 cells were used as the controls to evaluate the relative gene expressions. The data are presented as mean ± SD of three independent experiments. *β-Actin* was the control in the qRT-PCR assessment. *; P<0.05, **; P<0.01, ***; P<0.001, and ****; P<0.0001 vs. the control.

Anti-miR-19a induced downregulation of *PTEN*, *BCL-2*, and *CDKN1A* in the bortezomib-treated myeloma cell lines

Transfection of the LentiviRal-off-has-miR-19a-3p vector caused a decrease in *PTEN*, *BCL-2* and *CDKN1A* mRNA expressions in the BTZ-treated cell lines, which was consistent with downregulation of miR-19a after transfection compared to the BTZ-treated non-transfected cell lines (Fig.6).

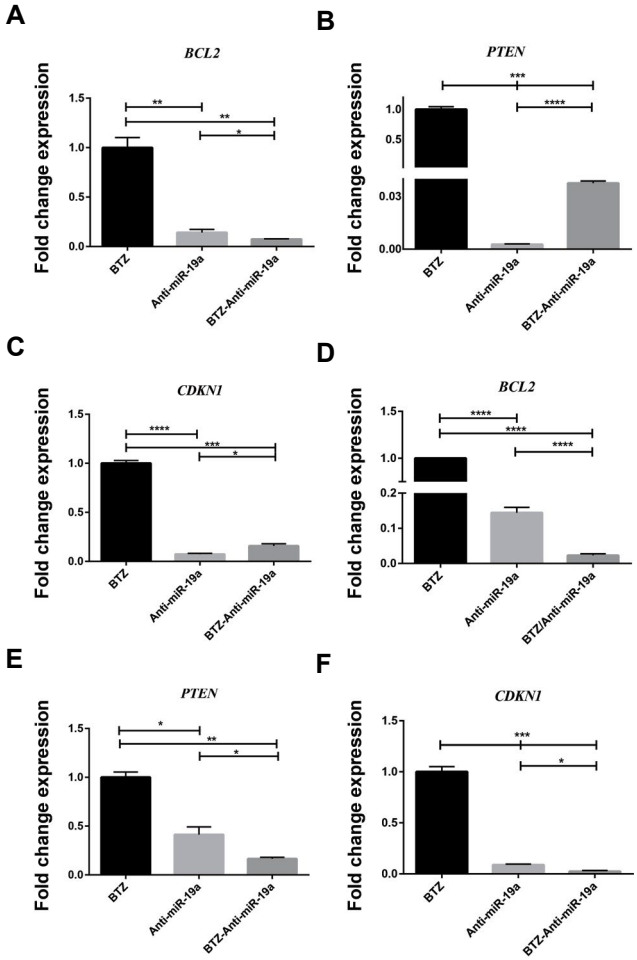

Fig.6: B-cell lymphoma 2 (*BCL-2*), *PTEN* and *CDKN1* expressions at the mRNA level in the U266 and RPMI 8226 cell lines according to quantitative real-time polymerase chian reaction (qRT-PCR) analysis. The U266 and RPMI 8226 cells were cultured and treated with bortezomib (BTZ), 5 µM and 150 nM, respectively, transfected with the LentimiRa-off-has-mir-19a-3p vector and treated with BTZ (5 µM and 150 nM, respectively) after transfection. **A-C.** Expressions of *BCL-2*, *PTEN* and *CDKN1* were examined in U266 cells after 48 hours of BTZ treatment and transfection with LentimiRa-off-has-mir-19a-3p vector, and after 48 hours of BTZ treatment in the transfected cells. **D-F.** Expressions of *BCL-2*, *PTEN* and *CDKN1* were examined in RPMI 8226 cells after 48 hours of BTZ treatment and transfection with LentimiRa-off-has-mir-19a-3p vector, and after 48 hours of BTZ treatment in the transfected cells. The U266 and RPMI 8226 cells treated with BTZ were used as the controls to evaluate the relative gene expressions. The data are presented as mean ± SD of three independent experiments. *β-Actin* served as the control for the qRT-PCR assessment. *; P<0.05, **; P<0.01, ***; P<0.001, and ****; P<0.0001 vs. the control.

Discussion

Based on findings of previous studies (15), the first

outcome of deregulated miRNA expression in MM was reported by Löffler et al. (16) when they reported that miR-21 ectopic expression made MM cells independent from IL-6 growth stimulus. Pichiorri et al. (17) identified a miRNA signature associated with transformation of normal PCs to clinical MM via monoclonal gammopathy of undetermined significance (MGUS) and demonstrated that miR-32, miR-21, miR-17-92, the miR-106b-25 cluster, and miR-181a/b upregulated in both MM cell lines and primary tumours versus normal PCs. Among these, the miR-17-92 cluster was only highly expressed in patients with MM. OncomiR-19a, one of the members of the miR-17-92 cluster, plays a role in promotion of cell proliferation, migration, and induction of apoptosis, and it is suggested to have a critical role in myeloma pathogenesis (10). Patients with low levels of miR-19a in their sera have a better response and shortened progression-free with downregulation of it obtained from others studies (18). Here, we evaluated the response of two MM cell lines to BTZ in the presence of antagomiR-19a in an attempt to avoid resistance to MM through targets of miR-19a. The results of recent studies have shown that *SOCS3* is a target of miR-19a and a negative regulator of *SOCS3* (19, 20), and showed that the molecule beneath it, *STAT3* is a significant promoter of cancers such as MM when activated (5, 21, 22). *STAT3*, one of the components of the *JAK/STAT* pathway, acts as an oncogene in human cancers (22, 23). Some miRNAs have close relativity with drug resistance; for example, it has been shown that miR-181a expression is in consistence with MM tumour load and could be a biomarker for treatment monitoring, as much as miR-20a, which is a potential diagnostic biomarker (4, 6). BTZ is a proteasome inhibitor and an effective treatment for MM in some patients; however, drug resistance is a major problem for 60% of these patients (8, 24). Our data primarily showed that antagomir-19a downregulated miR-19a expression. BTZ inhibited miR-19a in a concentration-dependent manner and, in the presence of antagomir-19a and BTZ, miR-19a efficiently downregulated in parallel with an increase in the proportion of apoptotic cells following treatment with BTZ. On the other hand, our viability studies showed that the ratio of proliferation of myeloma cell lines decreased after transfection with the antagomiR-19a vector. The data supported the results of other studies where miR-181a and miR-20a were inhibited by BTZ (6).

We observed downregulation of *STAT3* and upregulation of *SOCS3* at the mRNA level, which confirmed that miR-19a is a negative regulator of *SOCS3*. This finding supported data from previous studies (19, 20). The oncogenic function of *STAT3* has been previously reported (21, 22); therefore, we could conclude that inhibition of miR-19a caused suppression of *STAT3*. Our results showed that the expression level of *STAT3* in BTZ-treated cells highly decreased when used in parallel with anatago-miR-19a. Thus, inhibition of miR-19a could be used to improve BTZ responsiveness in myeloma cells. The results of another study showed that *PTEN* plays critical roles in regulating cell proliferation, differentiation and apoptosis, and a molecular study identified *PTEN* as a downstream target of miR-19a, which was inversely correlated with miR-19a expression in ovarian cancer tissues (10). We also assessed *BCL-2,* which is an attractive target for therapy. In this context, there is a drug that targets *BCL-2* in *BCL-2*-dependent haematologic malignancies, such as chronic lymphoid leukaemia and mantle cell lymphoma (11, 25). In a recent study, miR-19a promoted drug resistance of myeloma cells to chemotherapeutic agents by upregulation of *BCL-2* (11). A previous study indicated that *CDKN1* is an oncotarget in Burkitt lymphoma and MM. Currently, *CDKN1* is more broadly considered to be a regulator of fundamental cell-fate decisions such as proliferation, differentiation, and senescence (13).

In accordance with these studies, our data showed that inhibition of miR-19a by the antagomiR-19a and BTZ treatment of cells increased the expression levels of *PTEN*, *BCL-2*, and *CDKN1*. However, their expressions decreased in myeloma cell lines treated with BTZ after induction of antagomiR-19a. The results supplement the findings that miRNAs are differentially expressed in BTZ-resistant myeloma cells. miR-19a could be a possible prognostic biomarker for responsiveness to BTZ in MM patients. In order to overcome resistance and improve the level of responsiveness to BTZ, miR-19a targets such as *SOCS3* and *STAT3* could be tracked. We faced some restrictions in our studies that must be adverted. They include the use of other MM cell lines and myeloma cells obtained from MM patients, and evaluation of targets at the protein level expression and downstream molecules, which could have helped us to generalize our results.

Conclusion

Overall, our data indicated that induction of antagomir-19a in myeloma cell lines resulted in downregulation of mir-19a and enhanced responsiveness to BTZ treatment. On the other hand, the ratio of apoptosis in the BTZ-treated cell lines was drastically more effective in the presence of mir-19a inhibition. Thus, mir-19a could be a potential prognostic biomarker in MM treatment. Downregulation of the *PTEN* and *CDKN1* oncogenes due to inhibition of oncomiR-19a following BTZ treatment would most likely lead to a better treatment response.

Acknowledgments

We express our appreciation to Tarbiat Modares University for technical assistance and financial support. The research was financially supported by Tarbiat Modares University, Tehran, Iran. There is no conflict of interest in this study.

Authors' Contributions

S.A., A.K., M.S.; Participated in study design, data

collection and evaluation, drafting and statistical analysis. S.A.; Conceived the presented idea. A.K.; Conducted all the experiments from cellular and molecular experiments, trasfection part, flowcytometry and RT-qPCR analysis and wrote the manuscript. M.S.; Advised the project. All authors performed editing and approving the final version of this manuscript for submission, also approved the final draft.

References

1. Caracciolo D, Montesano M, Altomare E, Scionti F, Di Martino MT, Tagliaferri P, et al. The potential role of miRNAs in multiple myeloma therapy. Expert Rev Hematol. 2018; 11(10): 793-803.
2. Szymczyk A, Macheta A, Podhorecka M. Abnormal microRNA expression in the course of hematological malignancies. Cancer Manag Res. 2018; 10: 4267-4277.
3. Spicka I. Advances in multiple myeloma therapy during two past decades. Comput Struct Biotechnol J. 2014; 10(16): 38-40.
4. Zhang X, Chen Y, Zhao P, Zang L, Zhang Z, Wang X. MicroRNA-19a functions as an oncogene by regulating PTEN/AKT/pAKT pathway in myeloma. Leuk Lymphoma. 2017; 58(4): 932-940.
5. Yin Z, Yang J, Ning R, Liu Y, Feng M, Gu C, et al. Signal pathways, diseases, and functions associated with the miR-19a/92a cluster and the use of berberine to modulate the expression of this cluster in multiple myeloma cells. J Biochem Mol Toxicol. 2018; 32(6): e22057.
6. Peng J, Thakur A, Zhang S, Dong Y, Wang X, Yuan R, et al. Expressions of miR-181a and miR-20a in RPMI8226 cell line and their potential as biomarkers for multiple myeloma. Tumor Biol. 2015; 36(11): 8545-8552.
7. Richardson PG, Barlogie B, Berenson J, Singhal S, Jagannath S, Irwin D, et al. A phase 2 study of bortezomib in relapsed, refractory myeloma. N Engl J Med. 2003; 348(26): 2609-2617.
8. Niewerth D, Jansen G, Assaraf YG, Zweegman S, Kaspers GJL, Cloos J. Molecular basis of resistance to proteasome inhibitors in hematological malignancies. Drug Resist Updat. 2015; 18: 18-35.
9. Lv H, Wu X, Ma G, Sun L, Meng J, Song X, et al. An integrated bioinformatical analysis of miR-19a target genes in multiple myeloma. Exp Ther Med. 2017; 14(5): 4711-4720.
10. Wang Y, Zhao S, Zhu L, Zhang Q, Ren Y. MiR-19a negatively regulated the expression of PTEN and promoted the growth of ovarian cancer cells. Gene. 2018; 670: 166-173.
11. Touzeau C, Maciag P, Amiot M, Moreau P. Targeting Bcl-2 for the treatment of multiple myeloma. Leukemia. 2018; 32(9): 1899-1907.
12. Letai AG. Diagnosing and exploiting cancer's addiction to blocks in apoptosis. Nat Rev Cancer. 2008; 8(2): 121-132.
13. Han SS, Tompkins VS, Son DJ, Han S, Yun H, Kamberos NL, et al. CDKN1A and FANCD2 are potential oncotargets in Burkitt lymphoma and multiple myeloma. Exp Hematol Oncol. 2015; 4: 9.
14. Zhu B, Ju S, Chu H, Shen X, Zhang Y, Luo X, et al. The potential function of microRNAs as biomarkers and therapeutic targets in multiple myeloma. Oncol Lett. 2018; 15(5): 6094-6106.
15. Peng Y, Croce CM. The role of MicroRNAs in human cancer. Signal Transduct Target Ther. 2016; 1: 15004.
16. Löffler D, Brocke-Heidrich K, Pfeifer G, Stocsits C, Hackermuller J, Kretzschmar AK, et al. Interleukin-6 dependent survival of multiple myeloma cells involves the Stat3-mediated induction of microRNA-21 through a highly conserved enhancer. Blood. 2007; 110(4): 1330-1333.
17. Pichiorri F, Suh SS, Ladetto M, Kuehl M, Palumbo T, Drandi D, et al. MicroRNAs regulate critical genes associated with multiple myeloma pathogenesis. Proc Natl Acad Sci USA. 2008; 105(35): 12885-12890.
18. Federico C, Sacco A, Belotti A, Ribolla R, Cancelli V, Giacomini A, et all. Circulating microRNAs and their role in multiple myeloma. Noncoding RNA. 2019; 5(2): 37.
19. Collins AS, McCoy CE, Lloyd AT, O'Farrelly C, Stevenson NJ. miR-19a: an effective regulator of SOCS3 and enhancer of JAK-STAT signaling. PLoS One. 2013; 8(7): e69090.
20. Mahony R, Ahmed S, Diskin C, Stevenson NJ. SOCS3 revisited: a broad regulator of disease, now ready for therapeutic use? Cell Mol Life Sci. 2016; 73(17): 3323-3336.
21. He G, Karin M. NF-κB and STAT3 - key players in liver inflammation and cancer. Cell Res. 2011; 21(1): 159-168.
22. Bromberg J. Stat proteins and oncogenesis. J Clin Invest. 2002; 109(9): 1139-1142.
23. Selvi N, Kaymaz BT, Gunduz C, Aktan C, Kiper HD, Sahin F, et al. Bortezomib induces apoptosis by interacting with the JAK/STAT pathway in K562 leukemic cells. Tumour Biol. 2014; 35(8): 7861-7870.
24. Rastgoo N, Abdi J, Hou J, Chang H. Role of epigenetics-microRNA axis in drug resistance of multiple myeloma. J Hematol Oncol. 2017; 10(1): 121.
25. Roberts AW, Davids MS, Pagel JM, Kahl BS, Puvvada SD, Gerecitano JF, et al. Targeting BCL2 with Venetoclax in relapsed chronic lymphocytic leukemia. N Engl J Med. 2016; 374(4): 311-322.

Original Article

EGF Receptor Transactivation by Endothelin-1 Increased CHSY-1 Mediated by NADPH Oxidase and Phosphorylation of ERK1/2

Hossein Babaahmadi-Rezaei, Ph.D.[1], Alireza Kheirollah, Ph.D.[2], Mojtaba Rashidi, Ph.D.[2], Faezeh Seif, Ph.D.[3], Zahra Niknam, M.Sc.[1], Masoumeh Zamanpour, M.Sc.[1]*

1. Hyperlipidemia Research Center, Department of Clinical Biochemistry, Faculty of Medicine, Ahvaz Jundishapur University of Medical Sciences, Ahvaz, Iran
2. Cellular and Molecular Research Center, Department of Clinical Biochemistry, Faculty of Medicine, Ahvaz Jundishapur University of Medical Sciences, Ahvaz, Iran.
3. Shoushtar Faculty of Medical Sciences, Shoushtar, Iran

**Corresponding Address: Hyperlipidemia Research Center, Department of Clinical Biochemistry, Faculty of Medicine, Ahvaz Jundishapur University of Medical Sciences, Ahvaz, Iran*
Email: zamanpour.m.bio@gmail.com

Received: 12/January/2020, Accepted: 14/September/2020

Abstract

Objective: Growth factors [transforming growth factor-β (TGF-β), epidermal growth factor (EGF), endothelin-1 (ET-1)] stimulate proteoglycan synthesis resulting in retention and accumulation of low density lipoprotein (LDL) in vessel intima and leading to atherosclerosis development. This study investigated the role of ET-1 on the expression of CHSY1, proteoglycan synthesizing enzyme, through both EGF and TGF-β receptor transactivation in human vascular smooth muscle cells (VSMCs). Also, we explored the involvement of NADPH oxidase (NOX), an important intermediate of redox signaling, in ET-1 transactivated EGF receptor (EGFR) through endothelin receptors.

Materials and Methods: In this experimental study, phosphorylated ERK1/2 and CHSY1 protein levels in the human VSMCs were measured by Western blot analysis using anti phospho-ERK1/2 (Thr202/Tyr204) and anti CHSY1 antibodies.

Results: ET-1 (100 nM) and EGF (100 ng/ml) stimulated ERK1/2 phosphorylation and inhibited in the presence of bosentan (ET receptor inhibitor), AG1478 (EGFR inhibitor), and DPI (NOX antagonist). Also, ET-1 treatment increased CHSY1 enzyme level; this response was suppressed by bosentan, AG1478, DPI, and SB431542, TGF-β receptor antagonist. This study revealed that ET-1 increases expression of CHSY1 through transactivation of EGF and TGF-β receptors.

Conclusion: Transactivation through the EGF receptor mediated by phospho-ERK1/2 leads to expression of CHSY1 protein. EGF receptor transactivation by ET-1 is shown for the first time, to be dependent on NOX enzymes.

Keywords: CHSY1 Enzyme, Endothelin-1, Epidermal Growth Factor, NADPH Oxidase

Cell Journal(Yakhteh), Vol 23, No 5, October 2021, Pages: 510-515

Citation: Babaahamdi-Rezaei H, Kheirollah A, Rashidi M, Seif F, Niknam Z, Zamanpour M. EGF receptor transactivation by endothelin-1 increased CHSY-1 mediated by NADPH oxidase and phosphorylation of ERK1/2. Cell J. 2021; 23(5): 510-515. doi: 10.22074/cellj.2021.7392.

Introduction

Based on the "response to retention hypothesis" stating, atherosclerosis is commenced by atherogenic lipoprotein entrapment by proteoglycan in the vessel wall. This is one of the crucial causes of atherosclerosis early stage. Proteoglycans are highly glycosylated proteins, consisting of core protein, which is covalently linked to glycosaminoglycan (GAG) chain. GAG chain is negatively charged due to the sulfate and carboxylic acid groups of chondroitin/dermatan sulfate (CS/DS) chains. Therefore low density lipoprotein (LDL) particle (apo B100 has positively charged amino acid residues) interact with negative GAG chain results in retention of LDL in intima space of artery wall. Due to interactions with extracellular matrix (ECM) proteoglycan, LDL retention in the extracellular space of the arterial increases the chance of its oxidation and accumulation, promoting atherosclerosis (1, 2). Studies have shown that an increasing GAG chain length association with lipid binding affinity results in LDL retention in vascular wall and atherosclerosis development (3, 4).

Chondroitin sulfate synthase 1 (CHSY1) is one of the family of GAG synthesizing enzymes involved in hyper elongation of GAG chain (5, 6). Previous atherosclerosis mouse model studies have demonstrated that GAG synthesizing enzymes genes elevated expression is correlated with increase in the GAG chain length and lipid deposition in vascular wall (3, 7).

Several growth factors have been shown to mediate alteration and modification (hyper-elongation) of proteoglycan structure via regulated expression of GAG bio-synthesis enzymes in the vascular smooth muscle cells (VSMCs) (8, 9). Endothelin-1 (ET-1) is a novel vasoconstrictor peptide, a 21 amino acid peptide that was produced by endothelial cells in the vascular wall (10, 11). Studies have revealed that ET-1 level increases

in cardiovascular diseases such as atherosclerosis (12). Ballinger et al. (13) reported that ET-1 mediated elevation in radiosulfate incorporation secreted proteoglycan and induced proteoglycan synthesis in the VSMCs. ET-1 receptors (type A and type B) belong to G protein coupled receptors (GPCRs) family. GPCRs are seven transmembrane cell surface receptors which mediate pathophysiological cellular response through three signaling pathways. First, in classical pathway, GPCR agonists cause conformational changes in receptor that leads to downstream signaling activation. Second is β-arrestin scaffold pathway (14, 15) and third is transactivation pathway; transactivation signaling pathway was initially described by Daub et al. (16) who reported that GPCR agonists such as angiotensin II (Ang II) lead to activation and phosphorylation of epidermal growth factor receptor (EGFR) resulting in phosphorylation of downstream signaling mediators such as extracellular signal-regulated kinases (ERKs). GPCR agonists such as ET-1 and thrombin mediated TGF-β receptor type I (TβRI) activation by C-terminal phosphorylation of smad2 (pSmad2) induction, which is immediately TβRI downstream regulation that also, followed by increasing proteoglycan synthesis (14, 17, 18).

Chen et al. (19) reported that ET-1 mediated EGFR transactivation stimulated NADPH Oxidase (NOX), which produced reactive oxygen species (ROS) in different cell types such as cardiac fibroblasts. ROS generation is one of the critical components of the ET-1 signaling pathway. ROS activates and regulates numerous signal transduction cascades and gene expression in VSMC stimulated by ET-1, Thrombin, and Ang II. NOX enzymes especially produce ROS through acting as an electron donor to oxygen molecule in the superoxide anion formation. NOX1 is important in atherosclerosis pathogenesis. And, it is expressed in endothelial cells and VSMCs (20-22).

In this study, we tested hypothesis that ET-1 could increase CHSY1 enzyme level through transactivation of EGF receptor and whether NOX is involved in this transactivation signaling pathway. The results revealed that ET-1 mediated p-ERK1/2 via EGFR transactivation. ET-1 from transactivation of two receptors (EGFR and TGFR) increased the expression of CHSY1 protein and NOX as an important mediator involved in this signaling pathway.

Material and Methods

This study was approved by the Research Committee and The Ethical Committee of The Ahvaz Jundishapur University of Medical Sciences (IR.AJUMS.REC.1395.575).

Methods and Materials

In this experimental study, Dulbecco's Modified Eagle Medium (DMEM F12), trypsin EDTA 0.025%, penicillin streptomycin, and fetal bovine serum (FBS) were purchased from Gibco (Invitrogen, Carlsbad, USA). SB431542, Tyrphostin AG 1478, bosentan, transforming growth factor β (TGF-β), ET-1 (Sigma, USA, cat no: E7764), EGF, Tween 20, bovine serum albumin (BSA), and dimethyl sulfoxide (DMSO) were from Sigma Alderich (USA). Bicinchoninic acid (BCA) protein assay kit was purchased from Pars Tous (Iran). Polivinilydene difluoride (PVDF) membrane was purchased from Roche Diagnostic (Mannheim, Germany). Tris, Glysine, SDS, TEMED, and acrylamide were from Merck (Germany). Phospho p44/42 MAPK (ERK1/2) (Thr202/Tyr204) Rabbit monoclonal antibody (Cell signaling: 4370S) and HRP- anti-rabbit IgG- peroxidase were from Cell Signaling Technology (Beverly, MA, USA). Anti GAPDH antibody and anti CHSY1 antibody (Abcam, USA, cat no: 153813) were purchased from Abcam (Cambridge, MA, USA). Chemiluminesence ECL detection kit was from BIO-RAD (Hercules, CA, cat no: 1705061).

Cell culture

Human VSMCs were grown in DMEM-F12 supplemented with 10% FBS and 1% Penicillin-Streptomycin at 37˚C in 5% CO_2 followed by 24 hours starvation in DMEM-F12 with 0.1% FBS before treatments.

Western blotting

After treatment with various agents, the cells were washed twice with cold PBS and lysed in 75 µl RIPA buffer), and all cell lysates were collected. Protein concentration was measured by BCA assay. Equal amounts of protein (50 µg) were loaded and resolved on 10% SDS-polyacrylamide gel electrophoresis, transferred to PVDF membrane, and then incubated overnight at 4˚C with anti p-ERK1/2 (Thr202/Tyr204) antibody (1:2000) and anti CHSY1 antibody (1:1000), followed by HRP-anti rabbit IgG (1:10000), secondary antibody, for 1 hour at room temperature, and protein band visualized by ECL. To determine equal loading of proteins, the membrane was striped and re-incubated with GAPDH polyclonal antibody (1:2500) followed by a secondary HRP-conjugated antibody (1:10000) followed by development with enhanced chemiluminescence ECL clarity (Bio-Rad, Hercules, CA) and bands were visualized with BioRad ChemiDoc. Image J software was used to describe the intensity of protein bands (23).

Statistical analysis

Results are presented as the mean ± standard error of the mean (SEM) of three independent experiments. Statistical analysis was performed by one way ANOVA test, and $P<0.05$ and $P<0.01$ were considered significant.

Results

EGF-mediated phosphorylation of ERK1/2 (Thr202/Tyr204) in VSMCs

In order to verify whether ERK1/2 is phosphorylated by EGF through its receptor (EGFR), VSMCs were treated with increasing dose of EGF, respectively, 10, 50, 100 ng/ml. We observed EGF at 100 ng/ml dose stimulates phosphorylation of ERK1/2 significantly ($P<0.05$) at 5 minutes. Also, AG1478

(5 μM), the antagonist of EGFR, inhibited EGF-stimulated ERK1/2 phosphorylation (P<0.05, Fig.1) which showed EGF through its receptor induced ERK1/2.

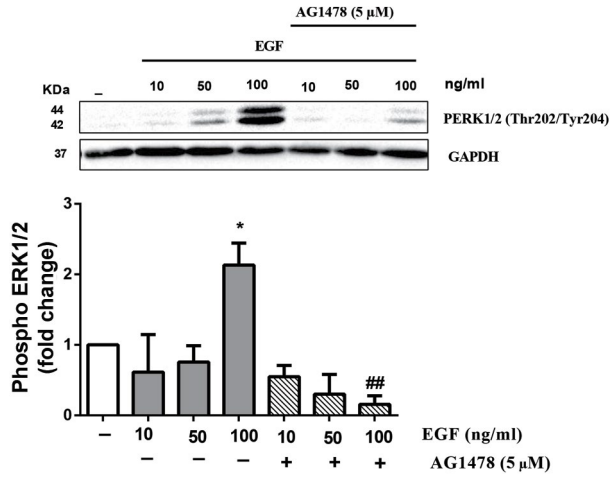

Fig.1: EGF induced ERK1/2 (Thr202/Tyr204) phosphorylation via EGFR. VSMCs were treated with AG1478 (5 μM) for 30 minutes before adding EGF. After 5 minutes, stimulation with EGF cell lysates were immuneblotted with anti ERK1/2 (Thr202/Tyr204) followed by HRP-conjugated rabbit IgG secondary antibody. The band intensity of three independent blots were measured by densitometric quantitation. *; P<0.05 control vs. EGF, ##; P<0.05 antagonist vs. EGF, EGFR; Epidermal growth factor recptor, ERK; The extracellular signal-regulated kinases, VSMCs; Vascular smooth muscle cell, and HRP; Horseradish peroxidase.

ET-1 caused phosphorylation of ERK1/2 (Thr202/Tyr204) in VSMCs

To examine whether ET-1 induced ERK1/2, VSMCs were treated with ET-1 (100 nM) at different time points respectively, 5, 15, 30 minutes and 1, 2, 4, 6 hours. Our results showed that maximum ERK1/2 phosphorylation was at minute 5 (P<0.01, Fig.2).

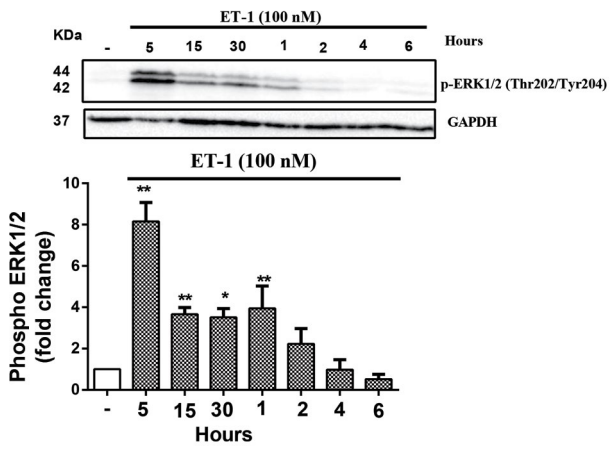

Fig.2: ET-1 mediated phosphotylation of ERK1/2 (Thr202/Tyr204) in the VSMCs. VSMCs were treated with ET-1 (100 nM) for 6 hours. Cell lysates were immunoblotted with anti ERK1/2 (Thr202/Tyr204) followed by HRP-conjugated rabbit IgG secondary antibody. The band intensity of three independent blots were measured by densitometric quantitation. *; P<0.05, **; P<0.01 control vs. ET-1 treated group, ET-1; Endothelin-1, ERK; The extracellular signal-regulated kinases, VSMC; Vascular smooth muscle cell, and HRP; Horseradish peroxidase.

ET-1 mediated ERK1/2 (Thr202/Tyr204) phosphorylation increase via both of ET receptors and EGFR transactivation

To investigate ET-1 mediated increase in p-ERK1/2 via its receptor, the cells were treated in the presence and absence of bosentan (10 μM), the antagonist of ET-1 receptors (ETA and ETB receptors), for 30 minutes prior to treatment with ET-1 (100 nM). ET-1 had about 2-fold increase in the ERK1/2 phosphorylation (P<0.01) at minute 5. Bosentan completely inhibited the stimulatory effect of ET-1 on p-ERK1/2 (P<0.01). To explore the EGFR role on ERK1/2 phosphorylation by ET-1, ET-1 and EGF were stimulated in the presence of AG1478. AG1478 (P<0.01) abolished ET-1 stimulated phosphorylation of ERK1/2 (Fig.3).

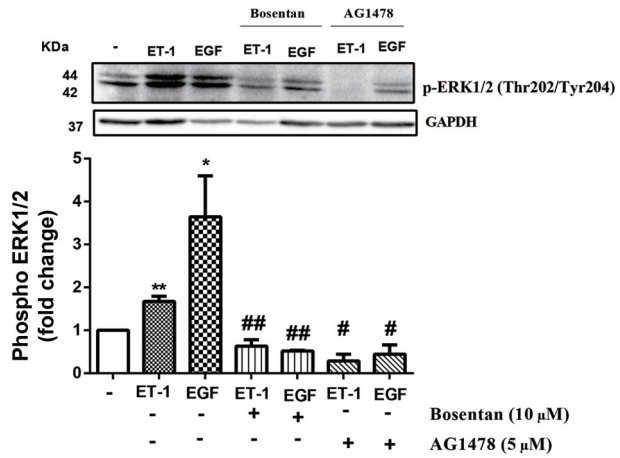

Fig.3: ET-1 stimulation increased phosphorylation of ERK1/2 (Thr202/Tyr204) via its receptor and receptor tyrosine kinase EGF (EGFR) Transactivation. VSMCs were treated with bosentan (10 μM) and AG1478 (5 μM) for 30 minutes before stimulation with EGF (100 ng/ml) or ET-1 (100 nM) for 5 minutes. Cell lysates were immunoblotted with anti ERK1/2 (Thr202/Tyr204) followed by HRP-conjugated rabbit IgG secondary antibody. The band intensity of three independent blots were measured by densitometric quantitation. *; P<0.05, **; P<0.01 control vs. growth factor treated group, #; P<0.05, ##; P<0.01 antagonist vs. growth factor treated group, ET-1; Endothelin-1, ERK; The extracellular signal-regulated kinases, EGF; Epidermal growth factor, VSMC; Vascular smooth muscle cell, and HRP; Horseradish peroxidase.

NOX acted as a mediator of ET-1 stimulated of p-ERK1/2 (Thr202/Tyr204) through EGFR

To evaluate the implication of NOX in phosphorylation of ERK1/2 caused by ET-1 or EGF, DPI (5 μM), the inhibitor of NOX, was used for 2 hours prior to the treatment with ET-1 or EGF. DPI completely attenuated the stimulatory effect of ET-1 and EGF (P<0.01) on p-ERK1/2 (Fig.4).

ET-1, TGF-β, and EGF stimulation invoked an increase in the level of CHSY1 protein

To confirm the stimulatory effect of ET-1, TGF-β, and EGF on the CHSY1 protein level, VSMCs were exposed to ET-1 (100 nM), EGF (100 ng/ml), and TGF-β (2 ng/ml) for 24 hours. About 2-fold increase was observed on

the level of CHSY1protein following of ET-1 addition (P<0.01). Also, VSMCs treated with EGF and TGF-β showed an increase on the level of this protein (P<0.05, Fig.5A).

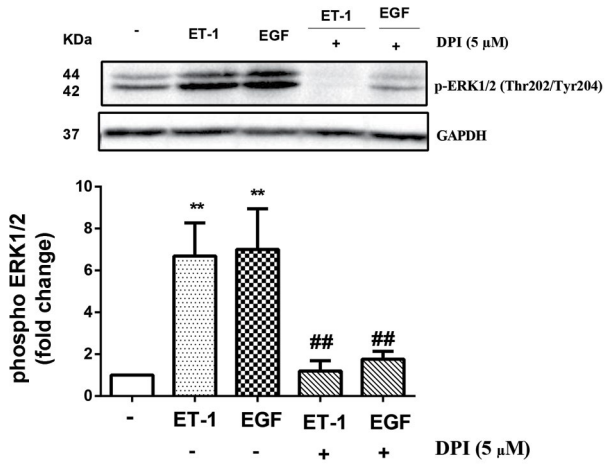

Fig.4: ET-1 and EGF induced phosphorylation of ERK1/2 (Thr202/Tyr204) involving NOX. VSMCs were pre-treated with DPI (5 μM) for 2 hours before treatment with EGF (100 ng/ml) or ET-1 (100 nM). Cell lysates were immunoblotted with anti ERK1/2 (Thr202/Tyr204) followed by HRP-conjugated rabbit IgG secondary antibody. The band intensity of three independent blots were measured by densitometric quantitation. **; P<0.01 control vs. growth factor treated group, ##; P<0.01 antagonist vs. growth factor treated group, ET-1; Endothelin-1, ERK; The extracellular signal-regulated kinase, NOX; NADPH oxidase, VSMC; Vascular smooth muscle cell, DPI; Diphenyleneiodonium, and EGF; Epidermal growth factor.

ET-1 induced increase level of CHSY1 protein via transactivation of EGFR and TβRI, a process that also mediated by NOX

It is important to show that which receptors or pathways are involved in ET-1 induced CHSY1 protein synthesis. Also, the CHSY1 protein level was upregulated following ET-1 stimulation (100 nM, for 24 hours), and this response was blocked in the presence of bosentan (P<0.05), indicating the specific role of ET-1 receptors which mediated increase in CHSY1 protein.

SB431542 (TβRI inhibitor) was used to assess ET-1 as well through transactivation of TβRI, increasing the level of CHSY1 protein. Our result showed that SB431542 (10 μM) reduces the CHSY1 protein induced by ET-1 (P<0.05).

To confirm EGFR transactivation by ET-1 increased CHSY1 protein level as a target protein; the role of EGFR was also examined in this transactivation pathway by utilization of AG1478. We obseved ET-1 induced increase in CHSY1 protein level is attenuated in the presence of AG1478 (P<0.01).

ET-1 exerts its effect to induce expression of gene such as CHSY1 protein through transactivation of both EGFR and TβRI. To evaluate the role of NOX as a mediator in this pathway, we used DPI (5 μM) for 2 hours before treatment with ET-1. DPI significantly reduced ET-1 stimulatory effect on the level of CHSY1protein (P<0.01, Fig.5B).

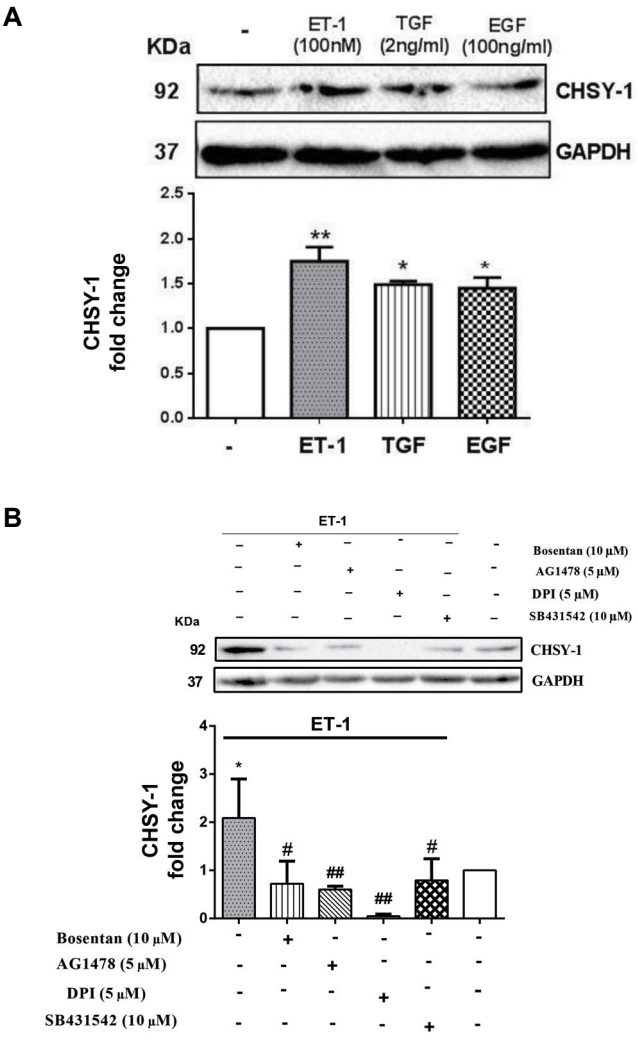

Fig.5: ET-1, TGF-β, and EGF increased CHSY-1 mediated by NOX. **A.** ET-1, TGF-β, and EGF mediated increase CHSY1 protein level. VSMCs were treated with ET-1 (100 nM), TGF-β (2 ng/ml), and EGF (100 ng/ml) for 24 hours. Cell lysates were immunoblotted with anti CHSY1 antibody followed by HRP-conjugated rabbit IgG secondary antibody. The band intensity of three independent blots were measured by densitometrics quantitation. *; P<0.05 and **; P< 0.01 control vs. growth factor treated group. **B.** ET-1 mediated increases CHSY1 protein level by transactivation of EGFR and TβRI, and NOX is a mediator of this signaling pathway. VSMCs were treated with ET-1 (100 nM) in the presence of each of the following inhibitors: Bosentan (10 μM), SB431542 (10 μM), and AG1478 (5 μM) for 30 minutes; DPI (5 μM) for 2 hours before treatment with ET-1 (100 nM) for 24 hours. Cell lysates were immunoblotted with anti CHSY1 antibody followed by HRP-conjugated rabbit IgG secondary antibody. The band intensity of three independent blots were measured by densitometrics quantitation. *; P<0.05 control vs. ET-1, #; P<0.05, ##; P<0.01 antagonist vs. growth factor treated group, ET-1; Endothelin-1, TGF-β; Transforming growth factor-β, EGF; Epidermal growth factor, VSMC; Vascular smooth muscle cell, DPI; Diphenyleneiodonium, and HRP; Horseradish peroxidase.

Discussion

The role of ET-1 transactivation of EGFR and TβRI was studied on phosphorylation of ERK1/2 and production of GAG synthesizing enzyme, CHSY1. ET-1 stimulates phosphorylation of ERK1/2 and increases the level of CHSY1 protein via EGFR and TβRI, and NOX has a crucial role in this pathway.

EGF induced p-ERK1/2 and also stimulated VSMC by ET-1, that resulted in the ERK1/2 phosphorylation,

which is consistent with the data observed by Yogi in VSMCs (24). Bosentan, a specific antagonist of ET receptors, attenuated ERK1/2 phosphorylation, that verified the specific role of ET-1 receptors in ERK1/2 phosphorylation. Daub et al. (16) presented the first evidence of GPCR transactivation on protein tyrosine kinase receptor (PTKR) in rat fibroblasts. They proved that transactivation of PTKR such as EGFR by GPCR agonists like ET-1, thrombin, and lysophosphatidic acid mediated ERK1/2 phosphorylation and activation of downstream signaling pathways. ERK1/2 plays an important role in the GAG hyper-elongation in VSMCs (3). We found that AG1478 (EGFR antagonist) reduced the ET-1 effect on p-ERK1/2, suggesting that p-ERK1/2 level increase by ET-1 mediation is dependent on EGFR transactivation. GPCRs transactivated EGFR through two major mechanisms: ligand dependent and ligand independent pathways. In ligand dependent EGFR transactivation pathway, activation of EGFR depends on the binding of active ligands such as heparin binding EGF like growth factor (HB-EGF) which comes from the cleavage. This cleavage is mediated by a disinterring and a metalloproteinase (ADAM), a group of matrix metalloproteinase (MMP). Activated MMPs cleavage HB-EGF ligand and release EGF into extracellular space that resulted in exposure to the EGF receptor. And, this causes the dimerization and stimulation of EGFR. Further, the activated receptor is able to stimulate ERK MAP kinase pathway, the downstream signaling cascade. In the ligand independent mechanism, EGFR transactivation via GPCR agonists occurs through activation of several second messengers such as Ca^{2+}, ROS, and Src tyrosine kinase (15, 25, 26). ET-1 has been shown to be associated with the elevation of NOX activity and consequently the production of ROS generation in the human VSMCs (22), which has a main role in the majority of GPCR signaling pathways (19). Similarly, assessing the NOX role in EGFR transactivation mediated by ET-1, we observed that it causes ERK1/2 phosphorylation in VSMCs. It was found that DPI decreased apparently p-ERK1/2 induction by ET-1 and EGF, confirming that NOX has an important role in ET-1 transactivation of EGFR which brings about ERK1/2 phosphorylation. This is also consistent with previous studies, reporting that GPCR agonists, including Ang II and thrombin mediated EGFR transactivation are dependent on NOX in VSMCs (27, 28).

Based on studies, retention of LDL on hyper-elongated GAG chains on proteoglycans such as biglycan results in increased foam cell formation and progression of arterial wall atherosclerosis (1). CSs are widely prevalent sulfated carbohydrates on cell surfaces and in the ECM. CS belongs to the GAG family that consists of disaccharide units containing glucuronic acid and N-acetylgalactosamine residues. It is synthesized as a CS proteoglycan by attaching linear CSs to Ser residue in the core protein. Also, CHSY1, glycosyltransferases enzyme, is responsible for biosynthesis of chondroitin and dermatan sulfate GAG. It is shown that increased sulfated GAG, mainly CSc, enhances CHSY1 transcriptional activity (29). Anggraeni et al. (7) showed that 8 weeks high fat diet feeding increased plaque development and markedly elevated level of CHSY1 mRNA expression in a mouse model. The current results demonstrated that ET-1 enhanced CHSY1 level expression in VSMCs. Also, EGF and TGF-β, both which are known to be involved in the atherosclerosis development, up-regulates CHSY1 level. Recent studies demonstrated that TGF-β mediated proteoglycan synthesis and up-regulated mRNA expression of CHSY1 in retinal choroidal endothelial cell and VSMCs (8, 30). Also Kamato et al. (31) demonstrated that EGF treatment of VSMCs increased GAG length and induced mRNA expression of CHSY1 through downstream intermediate ERK1/2 which is blocked by AG1478. Rostam et al. (30) reported that increased protein level of CHSY1 and other GAG synthesizing enzymes were associated with elevated induction of their mRNA expression. It has been previously reported that thrombin transactivated EGFR and TβRI that both of them are involved in phosphorylation of Smad2 linker region and increase of CHSY1 enzyme mRNA expression (23, 31). It was found that ET-1, stimulated increased level of CHSY1 protein that were inhibited by the ET-1 receptors antagonist. This issue suggested that the response is mediated through ET-1 receptors. Also, ET-1 was reported to cause enhanced proteoglycan synthesis and GAG chain hyper-elongation (11-13). In addition, CHSY1 is induced by ET-1 and also, decreased by SB431542 and AG1478. It is suggested that the ET-1 stimulation of CHSY1 is mediated by transactivation of EGFR and TβR1. To address the role of NOX on mediating the transactivation of EGFR and TβRI, we investigated the level of CHSY1 protein in the presence of DPI, NOX antagonist,; it was confirmed that NOX is involved in ET-1 transactivation of EGFR, and TβR1 mediated the elevation of CHSY1 expression.

The strength of the current study is the involvement of NOX in ET-1 transactivation of both EGFR and TβRI that mediated elevation on CHSY1 protein level.

Conclusion

It was demonstrated that ET-1 increased the level of p-ERK1/2, and this response was attenuated by AG1478, suggesting that ET-1 causes ERK1/2 phosphorylation, mediated through transactivation of EGFR. Also, this mechanism is dependent on NOX signaling. It was indicated that ET-1 mediated the elevated level of CHSY1 protein, which is implicated in hyperelongation of GAG chain through transactivation of EGFR and TβRI. Moreover, TGF-β and EGF mediated the elevation of CHSY1protein level, which was inhibited by NOX antagonist.

Acknowledgments

This research financially supported by Ahvaz Jundishapur University of Medical Sciences (Grant no. HLRC-9508). The authors declare that there is no conflicts

of interest in this study.

Authors' Contributions

H.B.-R.; Experiments design and performance, manuscript finalization. M.Z.; Experiment performance and manuscript drafting. A.Kh.; Experiments design. F.S.; Manuscript editing and statistical analysis. M.R.; Statistical analysis. Z.N.; Data collection and manuscript drafting. All authors read and approved the final manuscript.

References

1. Boren J, Williams KJ. The central role of arterial retention of cholesterol-rich apolipoprotein-B-containing lipoproteins in the pathogenesis of atherosclerosis: a triumph of simplicity. Curr Opin Lipidol. 2016; 27(5): 473-483.
2. Delgado-Roche L. The response-to-retention hypothesis: from theory to the potential therapeutic approaches. Biomed Aging Pathol. 2014; 4(4): 291-295.
3. Getachew R, Ballinger ML, Burch ML, Reid JJ, Khachigian LM, Wight TN, et al. PDGF beta-receptor kinase activity and ERK1/2 mediate glycosaminoglycan elongation on biglycan and increases binding to LDL. Endocrinology. 2010; 151(9): 4356-4367.
4. Skålén K, Gustafsson M, Rydberg EK, Hultén LM, Wiklund O, Innerarity TL, et al. Subendothelial retention of atherogenic lipoproteins in early atherosclerosis. Nature. 2002; 417(6890): 750-754.
5. Izumikawa T, Koike T, Shiozawa S, Sugahara K, Tamura J, Kitagawa H. Identification of chondroitin sulfate glucuronyltransferase as chondroitin synthase-3 involved in chondroitin polymerization: chondroitin polymerization is achieved by multiple enzyme complexes consisting of chondroitin synthase family members. J Biol Chem. 2008; 283(17): 11396-11406.
6. Izumikawa T, Saigoh K, Shimizu J, Tsuji S, Kusunoki S, Kitagawa H. A chondroitin synthase-1 (ChSy-1) missense mutation in a patient with neuropathy impairs the elongation of chondroitin sulfate chains initiated by chondroitin N-acetylgalactosaminyltransferase-1. Biochim Biophys Acta. 2013; 1830(10): 4806-4812.
7. Anggraeni VY, Emoto N, Yagi K, Mayasari DS, Nakayama K, Izumikawa T, et al. Correlation of C4ST-1 and ChGn-2 expression with chondroitin sulfate chain elongation in atherosclerosis. Biochem Biophys Res Commun. 2011; 406(1): 36-41.
8. Al Gwairi O, Osman N, Getachew R, Zheng W, Liang XL, Kamato D, et al. Multiple growth factors, but not VEGF, stimulate glycosaminoglycan hyperelongation in retinal choroidal endothelial cells. Int J Biol Sci. 2016; 12(9): 1041-1051.
9. Mehr RNM, Kheirollah A, Seif F, Dayati PM, Babaahmadi-Rezaei H. Reactive oxygen species and p38MAPK Have a role in the Smad2 linker region phosphorylation induced by TGF-β. Iran J Med Sci. 2018; 43(4): 401-408.
10. Seif F, Little PJ, Niayesh-Mehr R, Zamanpour M, Babaahmadi-Rezaei H. Endothelin-1 increases CHSY-1 expression in aortic endothelial cells via transactivation of transforming growth factor β type I receptor induced by type B receptor endothelin-1. J Pharm Pharmacol. 2019; 71(6): 988-995.
11. Little PJ, Burch ML, Getachew R, Al-aryahi S, Osman N. Endothelin-1 stimulation of proteoglycan synthesis in vascular smooth muscle is mediated by endothelin receptor transactivation of the transforming growth factor-[beta] type I receptor. J Cardiovasc Pharmacol. 2010; 56(4): 360-368.
12. Shraga-Levine Z,Sokolovsky M. Functional coupling of G proteins to endothelin receptors is ligand and receptor subtype specific. Cell Mol Neurobiol. 2000; 20(3): 305-317.
13. Ballinger ML, Ivey ME, Osman N, Thomas WG, Little PJ. Endothelin-1 activates ETA receptors on human vascular smooth muscle cells to yield proteoglycans with increased binding to LDL. Atherosclerosis. 2009; 205(2): 451-457.
14. Little PJ. GPCR responses in vascular smooth muscle can occur predominantly through dual transactivation of kinase receptors and not classical Galphaq protein signalling pathways. Life Sci. 2013; 92(20-21): 951-956.
15. Cattaneo F, Guerra G, Parisi M, De Marinis M, Tafuri D, Cinelli M, et al. Cell-surface receptors transactivation mediated by g protein-coupled receptors. Int J Mol Sci. 2014; 15(11): 19700-19728.
16. Daub H, Weiss FU, Wallasck C, Ullrich A. role of transactivation of the EGF receptor in signalling by G- protein- coupled receptors. Nature. 1996; 379(6565): 557-560.
17. Burch ML, Ballinger ML, Yang SNY, Getachew R, Itman C, Loveland K, et al. Thrombin stimulation of proteoglycan synthesis in vascular smooth muscle is mediated by protease-activated receptor-1 transactivation of the transforming growth factor βtype I receptor. J Biol Chem. 2010; 285(35): 26798-26805.
18. Sharifat N, Mohammad Zadeh G, Ghaffari MA, Dayati P, Kamato D, Little PJ, et al. Endothelin-1 (ET-1) stimulates carboxy terminal Smad2 phosphorylation in vascular endothelial cells by a mechanism dependent on ET receptors and de novo protein synthesis. J Pharm Pharmacol. 2017; 69(1): 66-72.
19. Chen CH, Cheng TH, Lin H, Shih NL, Chen YL, Chen YS, et al. Reactive oxygen species generation is involved in epidermal growth factor receptor transactivation through the transient oxidization of Src homology 2-containing tyrosine phosphatase in endothelin-1 signaling pathway in rat cardiac fibroblasts. Mol Pharmacol. 2006; 69(4): 1347-1355.
20. Gimenez M, Schickling BM, Lopes LR, Miller FJ. Nox1 in cardiovascular diseases: regulation and pathophysiology. Clin Sci (Lond). 2016; 130(3): 151-165.
21. Santillo M, Colantuoni A, Mondola P, Guida B, Damiano S. NOX signaling in molecular cardiovascular mechanisms involved in the blood pressure homeostasis. Front Physiol. 2015; 6: 194.
22. Todirita A, Manea A, Manea SA. Endothelin type A receptor mediates endothelin-1-induced upregulation of NADPH oxidase activity in human aortic smooth muscle cells. Annals of the Romanian Society for Cell Biology. 2013; 18(1): 44-50.
23. Kamato D, Thach L, Getachew R, Burch M, Hollenberg MD, Zheng W, et al. Protease activated receptor-1 mediated dual kinase receptor transactivation stimulates the expression of glycosaminoglycan synthesizing genes. Cell Signal. 2016; 28(1): 110-119.
24. Yogi A, Callera GE, Montezano AC, Aranha AB, Tostes RC, Schiffrin EL, et al. Endothelin-1, but not Ang II, activates MAP kinases through c-Src independent Ras-Raf dependent pathways in vascular smooth muscle cells. Arterioscler Thromb Vasc Biol. 2007; 27(9): 1960-1967.
25. Dayati P, Babahmadi Rezaei H, Sharifat N, Kamato D, Little PJ. G protein coupled receptors can transduce signals through carboxy terminal and linker region phosphorylation of Smad transcription factors. Life Sci. 2018; 199: 10-15.
26. Little PJ, Burch ML, Al-aryahi S, Zheng W. The paradigm of G protein receptor transactivation: a mechanistic definition and novel example. ScientificWorldJournal. 2011; 11: 709-714.
27. Frank GD, Eguchi S, Inagami T, Motley ED. N-acetylcysteine inhibits angiotensin ii-mediated activation of extracellular signal-regulated kinase and epidermal growth factor receptor. Biochem Biophys Res Commun. 2001; 280(4): 1116-1119.
28. Seshiah PN, Weber DS, Rocic P, Valppu L, Taniyama Y, Griendling KK. Angiotensin II stimulation of NAD (P) H oxidase activity: upstream mediators. Circ Res. 2002; 91(5): 406-413.
29. Susarla BT, Laing ED, Yu P, Katagiri Y, Geller H M, Symes AJ. Smad proteins differentially regulate transforming growth factor-β-mediated induction of chondroitin sulfate proteoglycans. J Neurochem. 2011; 119(4): 868-878.
30. Rostam MA, Kamato D, Piva TJ, Zheng W, Little PJ, Osman N. The role of specific Smad linker region phosphorylation in TGF-β mediated expression of glycosaminoglycan synthesizing enzymes in vascular smooth muscle. Cell Signal. 2016; 28(8): 956-966.
31. Kamato D, Rostam MA, Bernard R, Piva TJ, Mantri N, Guidone D, et al. The expansion of GPCR transactivation-dependent signalling to include serine/threonine kinase receptors represents a new cell signalling frontier. Cell Mol Life Sci. 2015; 72(4): 799-808.

Original Article

Toll-Like Receptor 4: A Macrophage Cell Surface Receptor Is Activated by Trimethylamine-N-Oxide

Mohammad Saeed Hakhamaneshi, Ph.D.[1], Alina Abdolahi, M.Sc.[2], Zakaria Vahabzadeh, Ph.D.[1, 3*], Mohammad Abdi, Ph.D.[4], Pedram Andalibi, M.D.[1]

1. Department of Biochemistry, Faculty of Medicine, Kurdistan University of Medical Sciences, Sanandaj, Iran
2. Department of Molecular Medicine and Genetics, Faculty of Medicine, Kurdistan University of Medical Sciences, Sanandaj, Iran
3. Liver and Digestive Research Center, Research Institute for Health Development, Kurdistan University of Medical Sciences, Sanandaj, Iran
4. Cellular and Molecular Research Centre, Research Institute for Health Development, Kurdistan University of Medical Sciences, Sanandaj, Iran

**Corresponding Address: P.O.Box: 6617713446, Department of Biochemistry, Faculty of Medicine, Kurdistan University of Medical Sciences, Sanandaj, Iran*
Email: zakariav@yahoo.com

Received: 25/October/2020, Accepted: 03/February2021

Abstract

Objective: Trimethylamine-N-Oxide (TMAO) is considered as a risk factor for atherosclerosis which further leads to inflammation during atherosclerosis. The exact mechanism(s) by which TMAO induces the inflammatory reactions remains to be determined. TMAO can cause the endoplasmic reticulum (ER) stress that triggers activation of Toll-Like Receptors (TLRs). In macrophages, this process stimulates the production of proinflammatory cytokines. This study designed to evaluate the expression level of *TLR4* in TMAO-treated macrophages.

Materials and Methods: In this experimental study, different concentrations of TMAO (37.5, 75, 150, and 300 μM) were exposed to murine macrophage (J774A.1 cell line) for 8, 18, 24, and 48 hours. The cells were also treated with 2.5 mM of 4-phenyl butyric acid as well as 2μg/ml of tunicamycin respectively as negative and positive controls for inducing ER-stress. We measured the viability of treated cells by the MTT test. Besides, the expression levels of *TLR4* gene and protein were evaluated using western blotting and reverse transcription- quantitative polymerase chain reaction (RT-qPCR) analysis. One-Way ANOVA was used for statistical analysis.

Results: No cell death was observed in treated cells. The cells treated with 150 and 300 μM doses of TMAO for 24 hours showed a significant elevation in the protein and/or mRNA levels of *TLR4* when compared to normal control or tunicamycin-treated cells.

Conclusion: Our results may in part elucidate the mechanism by which TMAO induces the macrophage inflammatory reactions in response to the induction of ER stress, similar to what happens during atherosclerosis. It also provides documentation to support the direct contribution of *TLR4* in TMAO-induced inflammation.

Keywords: Macrophage, Toll-Like Receptor 4, Trimethylamine-N-Oxide

Cell Journal(Yakhteh), Vol 23, No 5, October 2021, Pages: 516-522

Citation: Hakhamaneshi MS, Abdolahi A, Vahabzadeh Z, Abdi M, Andalibi P. Toll-Like receptor 4: a macrophage cell surface receptor is activated by trimethylamine-N-Oxide. Cell J. 2021; 23(5): 516-522. doi: 10.22074/cellj.2021.7849.

Introduction

Trimethylamine N-Oxide (TMAO) is a common metabolite in humans and other species (1) mainly produced from the oxidation of Trimethylamine (TMA) by hepatic flavin-containing monooxygenase 3 (FMO3) (2). The bacterial flora of gastrointestinal tract converts choline, phosphatidylcholine, and carnitine to TMA, known as TMA/FMO3/TMAO metaorganismal pathway. Recently, TMAO has been extensively reconsidered for its role in development of several diseases including atherosclerosis and other cardiovascular diseases, non-alcoholic fatty liver (3), Alzheimer (4), type 2 diabetes mellitus (5), chronic kidney disease (6), insulin resistance (7), and gastrointestinal cancers (8).

Nowadays, TMAO is certainly known as a new risk factor for atherosclerosis (2, 9). Atherosclerosis is a multifactorial and gradual disease that is also known as an inflammatory disorder. Macrophages are one of the main cells involved in the inflammation. The role of inflammation has been identified in all stages of diseases including onset, progression and the rupture of atherosclerotic plaques. Risk factors for atherosclerosis can lead to inflammation or exacerbation of symptoms from the beginning of life. Various risk factors for atherosclerosis including both biochemical and environmental stressor are associated with atherosclerosis pathology through a common fundamental mechanism. They all cause endoplasmic reticulum (ER) stress which in turn disrupts the proper folding of newly synthesized proteins (10). Aggregation of misfolded proteins starts the Unfolded Protein Response (UPR) pathway. UPR increases the expression of heat shock proteins (HSPs) to correct or degrade the misfolded protein (11). Prolonged stimulation of HSPs, as a danger signal, induces humoral and cellular immune responses and exacerbates inflammation of various vascular cells including macrophages (12). HSPs bind to toll like receptors (including *TLR4*) to stimulate production of inflammatory cytokines (13). TMAO has a potential to induce ER stress and activation of UPR pathway (14). It also induces the inflammatory reactions in macrophages (2,

15). Furthermore, TMA/FMO3/TMAO pathway has been documented to induce the inflammatory reactions in other cells (15-17). The detailed mechanism by which TMAO induces the inflammatory reactions in macrophages is still unclear.

TLRs are known as cell surface receptors that is highly expressed in macrophages, T and B lymphocytes, and other cells. These molecules recognize the pathogen-associated microbial patterns (PAMPs) presented by microbial pathogens, and/or danger-associated molecular patterns (DAMPs) which have been released from dead cells. TLRs are known as a part of our innate immune system and their activation stimulates the expression of proinflammatory cytokines which consequently triggers the inflammatory reactions as well as other metabolic regulations (18-20). *TLR4* is a member of this big family that can initiate a signaling pathway resulting in production of pro-inflammatory cytokines (19). Considering the role of TMAO in activation of ER stress-induced inflammation of macrophages as well as the possible contribution of *TLR4* in this pathway, this study was designed to evaluate the amount of *TLR4* in macrophages treated with different concentrations of TMAO.

Material and Methods

Cell culture

This experimental study was approved by Kurdistan University of Medical Sciences under a project number of IR.MUK.REC.1395.90. J774A.1 cell line which is a murine macrophage cell was purchased from Pasture Institute (Tehran, Iran). Cells were cultured in high glucose DMEM containing 10% fetal bovine serum, 1% penicillin-streptomycin and 4 mM L-glutamine (all from Sigma-Aldrich, USA). Cells were maintained in a cell culture incubator with sufficient humidity, at 37˚C temperature and 5% CO_2. Cells were treated in three separate replicates with different concentrations of TMAO including 37.5, 75, 150, and 300 µM for 8, 18, 24, and 48 hours. Another group of cells were treated with 4-phenyl butyric acid (4-PBA) at 2.5 mM concentration for 8 hours as negative control for suppressing ER stress. To provide a positive group for inducing ER stress, the same numbers of macrophages were treated with tunicamycin with a concentration of 2 µg/ml for 18 hours. Macrophages which did not receive any treatment were used as normal control group. MTT assay was applied to check the viability of the studied groups.

MTT Test

MTT test was performed as previously described (14, 21). Briefly, in a 96-well plate, approximately 5,000 cells were seeded in each well. Different concentrations of TMAO, 4-PBA, or tunicamycin were then added to the wells in six replications for each group. Subsequently, each well was incubated with 20 ul of 3-(4, 5-Dimethylthiazol-2-yl)-2, 5-diphenyltetrazolium bromide solution for 3.5 hours. Formation of crystals was then confirmed by microscopic assessment and then each well was incubated with 100 µl of MTT solvent for 4 hours at room temperature in the dark. A microplate reader instrument (Synergy HTX, BioTek, USA) was used to measure the absorbance of each well at 570 nm. Corrected absorbance was used to calculate the viability of treated and untreated cells using the following equation: % cell viability=(mean of sample absorbance /mean of control absorbance)×100

Western blotting

Total protein was extracted from 2.5×10^6 cells of each group (three replicates) using cold Radio-Immunoprecipitation Assay (RIPA) lysis buffer (Sigma-Aldrich, USA). A complete protease inhibitor cocktail (at final concentration of 1 µg/ml, Santa Cruz Biotechnology, California) and PMSF (Phenyl Methyl Sulfonyl Fluoride, at final concentration of 1 mM, Sigma-Aldrich, USA) was added to lysis buffer to inhibit any protease activity. Total protein concentration was measured using bicinchoninic acid (BCA) assay. For electrophoresis, 100 µg of total protein was loaded on 12% polyacrylamide gel containing sodium dodecyl sulfate (SDS-PAGE). A semi-dry blotting for 1.5 hours at 80 mA was applied to transfer the separated proteins to a preconditioned PVDF membrane (0.2 µm, BIO-RAD, USA). To avoid a non-specific binding of antibodies, the protein-free sites of membranes were blocked by 5% skim milk. Specific primary antibodies against TLR4 (ab13867, 1:2000, Abcam, USA), and GAPDH (NB300-328, 1: 10000, Novus Biological, UK) were exposed to membranes for 60 minutes. After three times washing with TBST solution, the membranes were incubated with the appropriate secondary antibody (HAF007, R&D, USA) for 1 hour. The chemiluminescence signals were then exposed to the X-ray film and visualized using developing and fixing solutions. The density of each band was analyzed using Image J 1.48V software. In each sample, the relative amount of TLR4 protein was normalized to the GAPDH protein. Finally, the fold change was calculated for each group relative to the control group.

Reverse transcription- quantitative polymerase chain reaction

To extract total RNA, approximately 2.5×10^6 cells were applied according to manufacturer instruction (Jena Bioscience, Germany). The quality and quantity of the extracted RNA were assessed spectrophotometrically using a Picodrop-Take3 instrument (Synergy HTX, BioTek, USA). Genomic DNA was eliminated using DNase I treatment (Scientific Inc, USA). For cDNA synthesis, a PrimeScript™ RT reagent Kit (RR037A, Takara, Japan) was applied in one cycle of three-step reactions (step 1: 15 minutes at 37˚C, step 2: 5 seconds at 85˚C, step 3: 5 minutes at 4˚C) using an Eppendorf thermal cycler (Germany). Reverse transcription-quantitative polymerase chain reaction (RT-qPCR) analysis was performed by a SYBR GREEN kit (SYBR Premix Ex Taq II kit, Tli Plus, Takara, Japan) for quantification of *TLR4* (NM_010477) and *GAPDH* (NM_008084.2) using a Corbett RG-6000 machine (Australia). For this purpose, about 50 ng of cDNA and 0.5 µl of gene-specific primers (10 pmol/µl, Table 1) were used in 40 cycles of two-step reactions (step 1: 5 seconds at 95˚C, step 2: 30 seconds at 60˚C).

The entity of RT-qPCR assay was controlled by analysis of melting curves and gel electrophoresis of related products. LinRegPCR software (version 2013.x) was used to calculate the mRNA levels of *TLR4* and *GAPDH* (22). In each run, the relative amount of *TLR4* mRNA was normalized to *GAPDH* mRNA.

Statistical analysis

The relative amounts (fold change) of protein and mRNA were provided as mean ± standard error of three replication of separate measurements (n=3). SPSS software, version 20 (IBM® SPSS Inc Chicago), was used for statistical analysis. To evaluate the mean difference between the groups, One-Way ANOVA was performed. Dunnett's test was utilized as a post-hoc test to compare the mean values of each group to the control group. P<0.05 was considered as statistically significant value.

Results

To evaluate whether treatments of cells has any effects on cell viability, MTT assay was performed. The viabilities of treated and untreated cells were more than 96% suggesting no treatment-dependent cell death had occurred in macrophages. Figures 1 to 4 show the western blotting bands and the relative amounts of TLR4 at protein and mRNA levels in groups treated with TMAO, PBA and TUN for different time intervals (8, 18, 24 and 48 hours). One-Way ANOVA showed a significant difference in protein amount of TLR4 after 8 hours among TMAO-treated cells (P<0.05). Post-hoc Dunnett's test showed that only 150 µM of TMAO significantly increased the relative amount of TLR4 protein in comparison with tunicamycin treated cells (P=0.046, Fig.1B).

When cells were treated with TMAO for 18 hours, the relative amount of TLR4 protein was elevated. A dose of 37.5 µM TMAO significantly increased TLR4 protein amount when compared with normal control (P=0.020, Fig.2B). Besides, TMAO significantly increased the protein amount of TLR4 compared to tunicamycin treated cells at 37.5 and 75 µM concentrations (P<0.05, Fig.2B). However, *TLR4* mRNA levels were not significantly different from control group (P> 0.05, Fig.2C).

Table 1: Characteristics of specific primers used for reverse transcription- quantitative polymerase chain reaction (RT-qPCR)

Genes	Oligonucleotide sequences (5´-3´)	PCR product size (bp)	Tm (˚C)	Accession number
TLR4	F: ACCTGGCTGGTTTACACGTC	201	60	NM_010477
	R: CTGCCAGAGACATTGCAGAA			
GAPDH	F: CCATCCGGGTTCCTATAAAT	198	54	NM_008084
	R: AATCTCCACTTTGCCACTG			

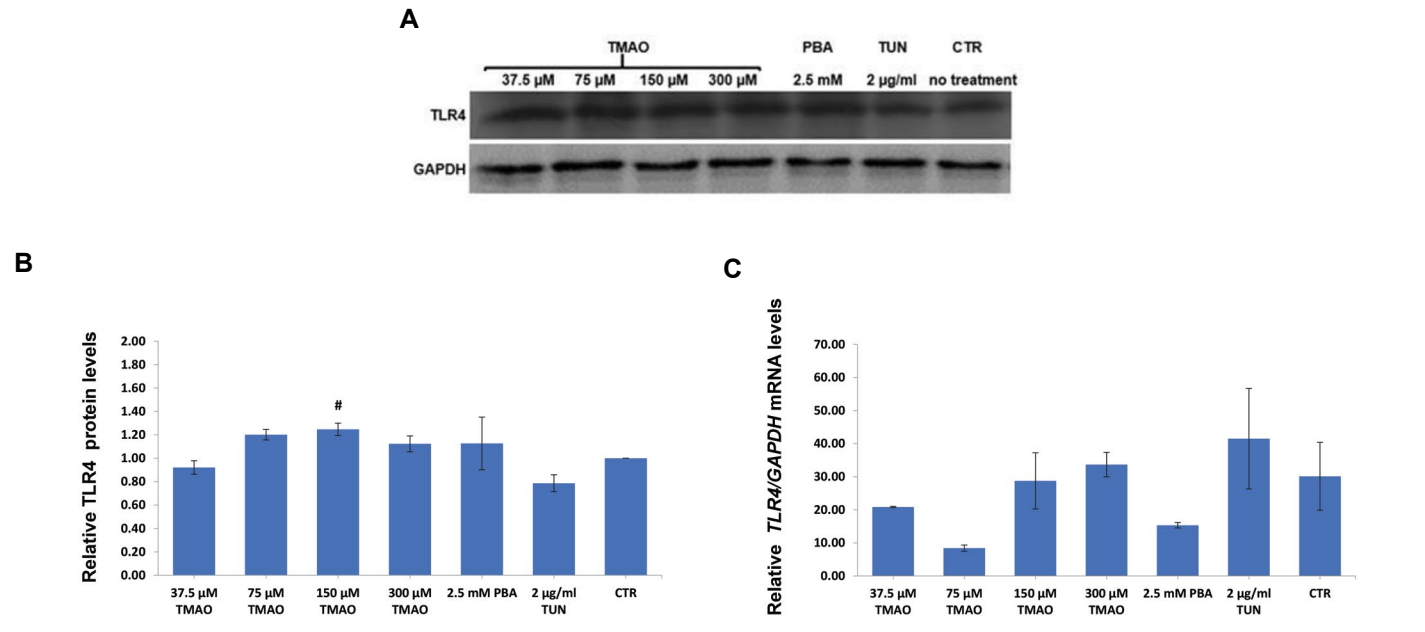

Fig.1: Protein and mRNA levels of TLR4 in macrophages (J774A.1 cell line) treated with TMAO and PBA (for 8 hours), and TUN (for 18 hours). **A.** Western blotting bands. **B.** Relative TLR4 protein levels. **C.** Relative *TLR4* mRNA levels. Only 150 µM of TMAO significantly increased the protein levels of TLR4. Values are mean ± standard error of three or four separate measurements. P<0.05 were considered significant. #; P<0.05 in comparison with the tunicamycin group, TMAO; Trimethylamine-N-Oxide, PBA; 4-Phenylbutyric acid, TUN; Tunicamycin, and CTR; Control.

After 24 hours of incubation, 150 and 300 µM of TMAO significantly increased the relative amount of TLR4 at both protein and mRNA levels compared to CTR and/or TUN groups (P<0.05, Fig.3B, C).

TMAO-treated cells for 48 hours showed no significant difference in the relative amount of TLR4 at protein level compared to the control or tunicamycin treated cells (P>0.05, Fig.4B). Only 37.5 µM TMAO significantly increased the mRNA level of *TLR4* when compared to the control (P=0.026, Fig.4C).

These findings suggest in macrophages the expression level of *TLR4* changed in altered in a concentration and time-dependent manner when treated with TMAO (P<0.05, Figs.S1, 2, See Supplementary Online Information at celljournal.org).

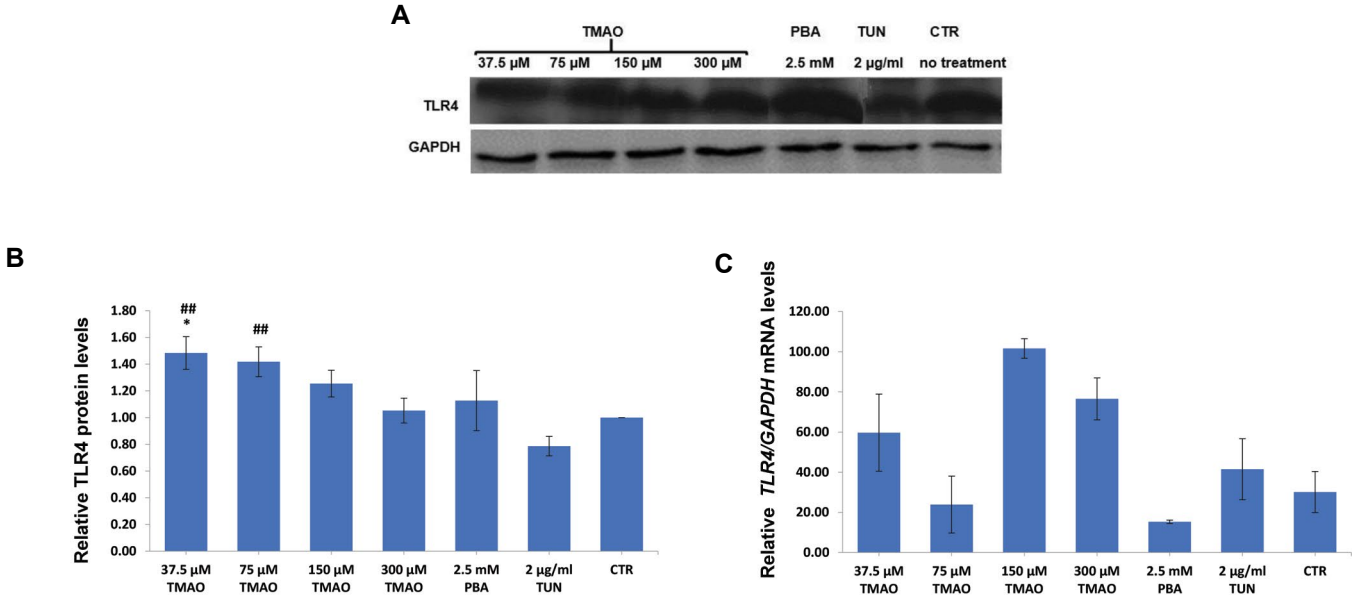

Fig.2: Protein and mRNA levels of TLR4 in macrophages (J774A.1 cell line) treated with TMAO and TUN (for 18 hours), and PBA (for 8 hours). **A.** Western blotting bands. **B.** Relative TLR4 levels. **C.** Relative *TLR4* mRNA levels. Only low concentrations of TMAO significantly increased the protein levels of TLR4. Values are mean ± standard error of three or four separate measurements. P<0.05 were considered significant. *; P<0.05 in comparison with control, ##; P<0.01 compared to the TUN group, TMAO; Trimethylamine-N-Oxide, PBA; 4-Phenylbutyric acid, TUN; Tunicamycin, and CTR; Control.

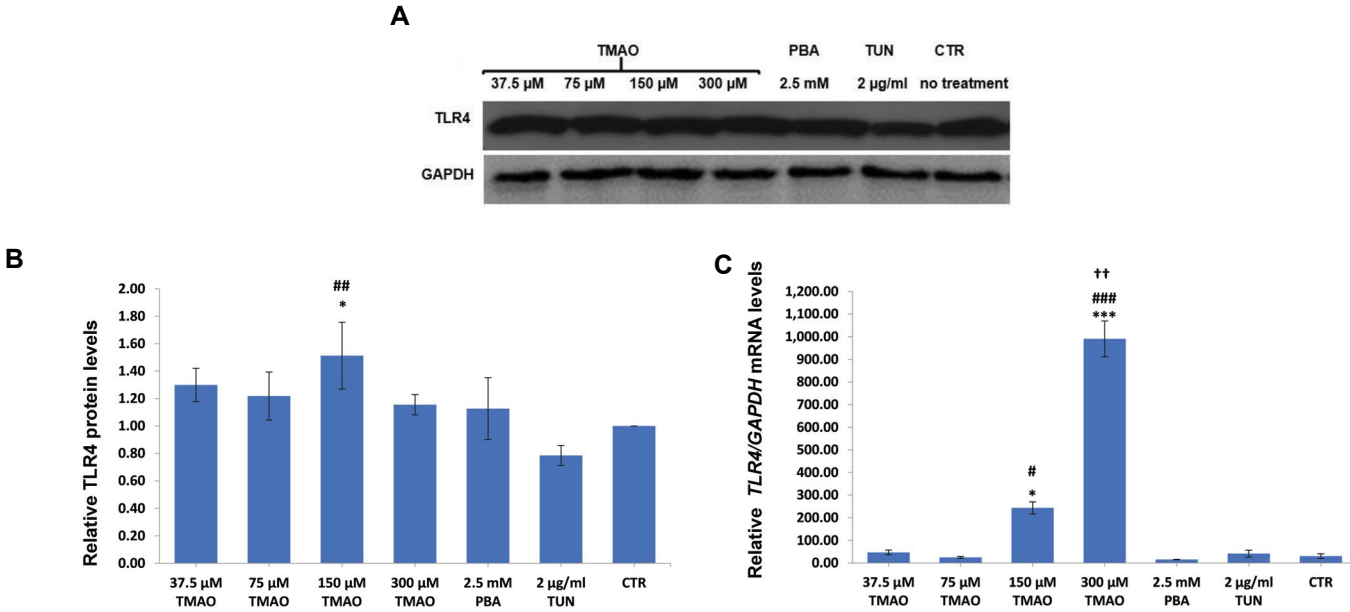

Fig.3: Protein and mRNA levels of TLR4 in macrophages (J774A.1 cell line) treated with TMAO (for 24 hours), PBA (for 8 hours), and TUN (for 18 hours). **A.** Western blotting bands. **B.** Relative TLR4 protein levels. **C.** Relative *TLR4* mRNA levels. Only 150 and 300 µM of TMAO significantly increased protein or mRNA levels of TLR4. Values are mean ± standard error of three or four separate measurements. P<0.05 were considered significant. *; P<0.05, ***; P<0.001 in comparison with the control, ##, ###; P<0.05, P<0.01, and P<0.001 respectively in comparison with the TUN group, ††; P<0.01 in comparison with the PBA group, TMAO; Trimethylamine-N-Oxide, PBA; 4-Phenylbutyric acid, TUN; Tunicamycin, and CTR; Control.

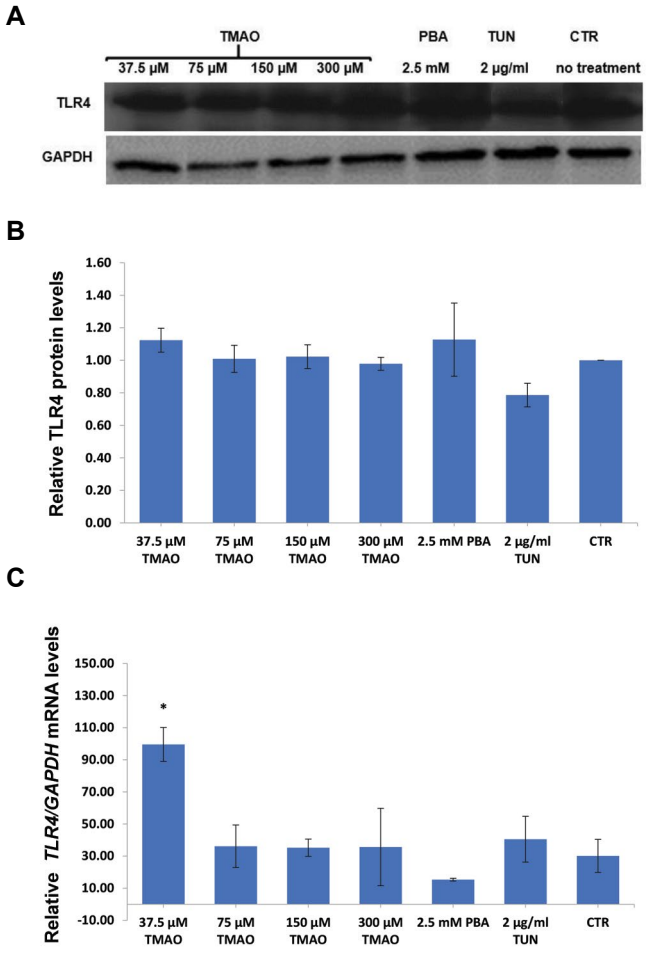

Fig.4: Protein and mRNA levels of TLR4 in macrophages (J774A.1 cell line) treated with TMAO (for 48 hours), PBA (for 8 hours), and TUN (for 18 hours). **A.** Western blotting bands. **B.** Relative TLR4 protein levels. **C.** Relative *TLR4* mRNA levels. Only 37.5 µM of TMAO significantly increased the mRNA levels of *TLR4*. Values are mean ± standard error of three or four separate measurements. P<0.05 were considered significant. *; P<0.05 in comparison with control, TMAO; Trimethylamine-N-Oxide, PBA; 4-Phenylbutyric acid, TUN; Tunicamycin, and CTR; Control.

Discussion

Macrophages play a major role in inflammation under stress conditions similar to that in atherosclerosis. In the present study, we induced ER stress in the murine macrophages (J774A.1 cell line) using TMAO as has been described previously (14). Our results showed that TMAO can induce the expression of TLR4 in macrophages, at both protein and mRNA levels, in a concentration and time-dependent manner.

The trend of *TLR4* changes in response to treatment time and concentration of TMAO was statistically significant, although it did not have a particular upward or downward direction. Cellular responses to ER stress are physiologically short term, adaptable and strongly dependent on the concentration and duration of treatment. The pattern of GRP78 changes in our previous studies also confirms this finding. GRP78 is known as the main marker of ER induction (14). The specific concentration and time for tunicamycin (2 µg/ml for 18 hours, as positive control) and 4-PBA (2.5 mM for 8 hours, as negative control) treatments used in this study, were based on our prior findings (23-26).

In general, 24-hour treatments of TMAO led to significant elevations in expression of both TLR4 gene and protein. Where higher concentrations showed greater effects with shorter incubation times. Conversely, lower concentrations of TMAO had a greater effect when the treatment time was longer. Concentrations of 37.5, 75, and 150 µM caused a further increase in the 18- and 24-hour treatments compared to control.

As expected, the *TLR4* mRNA pattern of changes is not fully consistent with its protein level. The stability and half-life of mRNA is shorter and more variable than protein. Therefore, for a treatment to produce a significant effect on the protein level, the mRNA level must be changed to a greater extent. However, sometimes a single mRNA molecule is used several times for translation without the need for multiple productions of mRNA transcripts. Moreover, similar to cations TMAO has a potential to form an electrostatic bond with mRNA and stabilizes its tertiary structure *in vitro*. This effect may only occurs at certain concentrations of TMAO (27).

Our work is the first experimental (*in vitro*) study that directly measured the effect of TMAO on the expression of *TLR4* in macrophages. In this study we showed that TMAO directly induced the expression of *TLR4*. The enhancing effect of TMAO on the expression of *TLR4* has been demonstrated in cultured endothelial cells (28), cardiac fibroblast as well as in animal models (29).

TMAO is known to correlate with the pathogenesis of different inflammatory diseases. where it plays a major role in the initiation or promotion of inflammation (3, 4, 6, 7, 8, 15-17, 30-32) . TMAO stimulates the mitogen-activated protein kinase as well as nuclear factor-κB cascade to induce the inflammatory markers (15). Furthermore, our previous work has also revealed the promoting effect of TMAO on the expression of proinflammatory cytokines in human macrophages (33).

There are several mechanisms to elucidate the role of TMAO in the development of TLR4-mediated inflammation. TLRs are the major sensors that activate cellular inflammation (34). They recognize different endogenous and exogenous ligands to stimulate the production of proinflammatory cytokine (35). TMAO is an endogenous ligand that directly interacts with TLR4 to activate the inflammation, like what happens to oxidized-low density lipoprotein (ox-LDL) (36).

TMAO is also supposed to be correlated with inflammation of macrophages through an indirect activation of TLR4 mediated by HSPs. Our previous studies have shown that TMAO induces the expression of HSPs in murine macrophages (14, 21). Extracellular form of HSPs binds to TLR4 (13). This interaction in turn stimulates the production of reactive oxygen species (ROS) and cytokines (18, 37).

TMAO-dependent production of ROS during inflammation of vascular cells was also showed by Chen et al. (38). Cluster of differentiation 36 (CD36) is another cell surface receptor of macrophages that identifies the endogenous ligands produced during atherosclerosis. It may facilitates the TLR4 signaling pathway when interacts with endogenous ligands such as TMAO (39). Wang and his colleagues showed that TMAO increases the expression of CD36 in murine macrophages (2). The ability of TMAO to alter the expression of ATP-Binding Cassette Transporter A1 (ABCA1) as well as macrophage Scavenger Receptor A1 (SRA-1) cannot be ignored for the TMAO-dependent mechanism of inflammation (40).

Conclusion

In macrophages TMAO treatment can induce changes in TLR4 protein and mRNA levels in a concentration and time-dependent pattern. The present study along with previous studies may in part elucidate the mechanism by which TMAO induces the macrophage inflammatory reactions in response to induction of ER stress such as what happens during atherosclerosis. From this perspective, our findings provide a documentation to support a direct contribution of TLR4 to pathogenesis of TMAO-induced macrophage inflammation. To confirm this conclusion, more detailed studies are needed to investigate the direct interaction of TMAO with *TLR4* of macrophages. Bioinformatics studies such as investigation of docking and molecular dynamics for binding TMAO to TLR4, or using specific labeled isotopes and functional assays may be useful for this purpose.

Acknowledgments

This study was funded by the research vice-chancellor of the Kurdistan University of Medical Sciences. We also thank the head of Cellular and Molecular Research Centre of Kurdistan University of Medical Sciences for their valuable assistance. The authors have no conflicts of interest.

Authors' Contributions

Z.V.; Supervised and designed the study and performed data collection, evaluation, statistical analysis, and drafting. M.A., M.S.H.; Contributed to the molecular experiments and RT-qPCR analysis. A.A.; Helped to perform the laboratory works of the blotting stages in the western blotting experiments. P.A.; Contributed to interpretation of the data and the conclusion. All authors performed editing and approving the final version of this manuscript for submission, also approved the final draft.

References

1. Yancey PH, Clark ME, Hand SC, Bowlus RD, Somero GN. Living with water stress: evolution of osmolyte systems. Science. 1982; 217(4566): 1214-1222.
2. Wang Z, Klipfell E, Bennett BJ, Koeth R, Levison BS, Dugar B, et al. Gut flora metabolism of phosphatidylcholine promotes cardiovascular disease. Nature. 2011; 472(7341): 57-63.
3. Chen YM, Liu Y, Zhou RF, Chen XL, Wang C, Tan XY, et al. Associations of gut-flora-dependent metabolite trimethylamine-N-oxide, betaine and choline with non-alcoholic fatty liver disease in adults. Sci Rep. 2016; 6: 19076.
4. Xu R,Wang Q. Towards understanding brain-gut-microbiome connections in Alzheimer's disease. BMC Syst Biol. 2016; 10 Suppl 3: 63.
5. Croyal M, Saulnier PJ, Aguesse A, Gand E, Ragot S, Roussel R, et al. Plasma trimethylamine N-oxide and risk of cardiovascular events in patients with type 2 diabetes. J Clin Endocrinol Metab. 2020; 105(7): 2371-2380.
6. Missailidis C, Hallqvist J, Qureshi AR, Barany P, Heimburger O, Lindholm B, et al. Serum trimethylamine-N-oxide is strongly related to renal function and predicts outcome in chronic kidney disease. PLoS One. 2016; 11(1): e0141738.
7. Delzenne NM, Cani PD. Gut microbiota and the pathogenesis of insulin resistance. Curr Diab Rep. 2011; 11(3): 154-159.
8. Oellgaard J, Winther SA, Hansen TS, Rossing P, von Scholten BJ. Trimethylamine N-oxide (TMAO) as a New potential therapeutic target for insulin resistance and cancer. Curr Pharm Des. 2017; 23(25): 3699-3712.
9. Liu Y, Dai M. Trimethylamine N-oxide generated by the gut microbiota is associated with vascular inflammation: new insights into atherosclerosis. Mediators Inflamm. 2020; 2020: 4634172.
10. Weber C, Noels H. Atherosclerosis: current pathogenesis and therapeutic options. Nat Med. 2011; 17(11): 1410-1422.
11. Malhotra JD, Kaufman RJ. The endoplasmic reticulum and the unfolded protein response. Semin Cell Dev Biol. 2007; 18(6): 716-731.
12. Zhou AX, Tabas I. The UPR in atherosclerosis. Semin Immunopathol. 2013; 35(3): 321-332.
13. Shomali N, Hatamnezhad L S, Tarzi S, Tamjidifar R, Xu H, Shotorbani SS. Heat shock proteins regulating Toll-like receptors and the immune system could be a novel therapeutic target for melanoma. Curr Mol Med. 2021; 21(1): 15-24.
14. Mohammadi A, Gholamhoseyniannajar A, Yaghoobi MM, Jahani Y, Vahabzadeh Z. Expression levels of heat shock protein 60 and glucose-regulated protein 78 in response to trimethylamine-N-oxide treatment in murine macrophage J774A.1 cell line. Cell Mol Biol (Noisy-le-grand). 2015; 61(4): 94-100.
15. Seldin MM, Meng Y, Qi H, Zhu W, Wang Z, Hazen SL, et al. Trimethylamine N-oxide promotes vascular inflammation through signaling of mitogen-activated protein kinase and nuclear factor-κB. J Am Heart Assoc. 2016; 5(2): e002767.
16. Chistiakov DA, Bobryshev YV, Kozarov E, Sobenin IA, Orekhov AN. Role of gut microbiota in the modulation of atherosclerosis-associated immune response. Front Microbiol. 2015; 6: 671.
17. Warrier M, Shih DM, Burrows AC, Ferguson D, Gromovsky AD, Brown AL, et al. The TMAO-Generating enzyme flavin monooxygenase 3 is a central regulator of cholesterol balance. Cell Rep. 2015; 10(3): 326-338.
18. Falck-Hansen M, Kassiteridi C, Monaco C. Toll-like receptors in atherosclerosis. Int J Mol Sci. 2013; 14(7): 14008-14023.
19. Seneviratne AN, Sivagurunathan B, Monaco C. Toll-like receptors and macrophage activation in atherosclerosis. Clin Chim Acta. 2012; 413(1-2): 3-14.
20. Zhou Y, Little PJ, Downey L, Afroz R, Wu Y, Ta HT, et al. The role of toll-like receptors in atherothrombotic cardiovascular disease. ACS Pharmacol Transl Sci. 2020; 3(3): 457-471.
21. Mohammadi A, Vahabzadeh Z, Jamalzadeh S, Khalili T. Trimethylamine-N-oxide, as a risk factor for atherosclerosis, induces stress in J774A.1 murine macrophages. Adv Med Sci. 2017; 63(1): 57-63.
22. Ruijter JM, Ramakers C, Hoogaars WMH, Karlen Y, Bakker O, van den Hoff MJB, et al. Amplification efficiency: linking baseline and bias in the analysis of quantitative PCR data. Nucleic Acids Res. 2009; 37(6): e45.
23. Cawley K, Deegan S, Samali A, Gupta S. Assays for detecting the unfolded protein response. Methods Enzymol. 2011; 490: 31-51.
24. Kennedy D, Samali A, Jager R. Methods for studying ER stress and UPR markers in human cells. Methods Mol Biol. 2015; 1292: 3-18.
25. Samali A, Fitzgerald U, Deegan S, Gupta S. Methods for monitoring endoplasmic reticulum stress and the unfolded protein response. Int J Cell Biol. 2010; 2010: 830307.
26. Wiley JC, Meabon JS, Frankowski H, Smith EA, Schecterson LC, Bothwell M, et al. Phenylbutyric acid rescues endoplasmic reticulum stress-induced suppression of APP proteolysis and prevents apoptosis in neuronal cells. PLoS One. 2010; 5(2): e9135.

27. Denning EJ, Thirumalai D, MacKerell AD, Jr. Protonation of trimethylamine N-oxide (TMAO) is required for stabilization of RNA tertiary structure. Biophys Chem. 2013; 184: 8-16.
28. Singh GB, Zhang Y, Boini KM, Koka S. High mobility group Box 1 mediates TMAO-induced endothelial dysfunction. Int J Mol Sci. 2019; 20(14): 3570.
29. Li X, Geng J, Zhao J, Ni Q, Zhao C, Zheng Y, et al. Trimethylamine N-oxide exacerbates cardiac fibrosis via activating the NLRP3 inflammasome. Front Physiol. 2019; 10: 866.
30. Al-Obaide MAI, Singh R, Datta P, Rewers-Felkins KA, Salguero MV, Al-Obaidi I, et al. Gut microbiota-dependent trimethylamine-n-oxide and serum biomarkers in patients with T2DM and advanced CKD. J Clin Med. 2017; 6(9): 86.
31. Gao X, Liu X, Xu J, Xue C, Xue Y, Wang Y. Dietary trimethylamine N-oxide exacerbates impaired glucose tolerance in mice fed a high fat diet. J Biosci Bioeng. 2014; 118(4): 476-481.
32. Liu X, Liu H, Yuan C, Zhang Y, Wang W, Hu S, et al. Preoperative serum TMAO level is a new prognostic marker for colorectal cancer. Biomark Med. 2017; 11(5): 443-447.
33. Abdi M, Vahabzadeh Z, Ghanivash A, Farhadi L, Hakhamaneshi MS, Andalibi P. Investigation of the effect of trimethylamine-N-oxide on the proinflammatory cytokine genes expression in U937-derived macrophages. Scientific Journal of Kurdistan University of Medical Sciences. 2018; 23(3): 1-9.
34. Curtiss LK,Tobias PS. Emerging role of Toll-like receptors in atherosclerosis. J Lipid Res. 2009; 50 Suppl(Suppl): S340-S345.
35. Cole JE, Georgiou E, Monaco C. The expression and functions of toll-like receptors in atherosclerosis. Mediators Inflamm. 2010; 2010: 393946.
36. Beutler B. Inferences, questions and possibilities in Toll-like receptor signalling. Nature. 2004; 430(6996): 257-263.
37. Xu Q. Role of heat shock proteins in atherosclerosis. Arterioscler Thromb Vasc Biol. 2002; 22(10): 1547-1559.
38. Chen ML, Zhu XH, Ran L, Lang HD, Yi L, Mi MT. Trimethylamine-N-oxide induces vascular inflammation by activating the NLRP3 inflammasome through the SIRT3-SOD2-mtROS signaling pathway. J Am Heart Assoc. 2017; 6(9): e006347.
39. Curtiss LK,Tobias PS. The toll of toll-like receptors, especially toll-like receptor 2, on murine atherosclerosis. Curr Drug Targets. 2007; 8(12): 1230-1238.
40. Mohammadi A, Gholamhoseynian Najar A, Yaghoobi MM, Jahani Y, Vahabzadeh Z. Trimethylamine-N-oxide treatment induces changes in the ATP-binding cassette transporter A1 and scavenger receptor A1 in murine macrophage J774A.1 cells. Inflammation. 2016; 39(1): 393-404.

Original Article

Global Scientific Research on SARS-CoV-2 Vaccines: A Bibliometric Analysis

Fakher Rahim, Ph.D.[1], Aida Khakimova, Ph.D.[2]*, Ammar Ebrahimi, Ph.D.[3], Oleg Zolotarev, Ph.D.[4], Fatemeh Rafiei Nasab, M.Sc.[5]

1. Thalassemia and Hemoglobinopathy Research Centre, Ahvaz Jundishapur University of Medical Sciences, Ahvaz, Iran
2. Department of Development of Scientific and Innovation Activities, Russian New University, Moscow, Russia
3. Department of Medical Biotechnology, School of Paramedicine, Guilan University of Medical Sciences, Rasht, Iran
4. Department of Information Systems in Economics and Management, Russian New University, Moscow, Russia
5. Department of Scientometrics, Deputy of Research and Technology Affairs, Ahvaz Jundishapur University of Medical Sciences, Ahvaz, Iran

Corresponding Address: Department of Development of Scientific and Innovation Activities, Russian New University, Moscow, Russia
Email: aida_khatif@mail.ru

Received: 30/September/2020, Accepted: 08/June/2021

Abstract

Objective: We performed this bibliometric analysis to identify global scientific research on the SARS-CoV-2 vaccines.

Materials and Methods: This bibliometric analysis study inclusive search of English-language publications related to the SARS-CoV-2 vaccines was conducted in the Scopus, PubMed, and Dimensions databases without year limitations. The results of bibliometric analysis comprised a time-dependent citation density trend, the name of the journal, journal impact factor (IF), year of publication, type of article, category, subscription or affiliation, co-authorship, and co-occurrence network.

Results: A study of the scientific literature from three databases (Scopus, PubMed, Dimensions) shows that investigators have focused more on studying the structure of the coronavirus at different levels (organismic, cellular, and molecular). In addition, the method of virus penetration into the cell and features of the influence of coronavirus on animals are well-studied. Various methods and strategies are being used to develop the vaccines, including both animal-tested methods and computer models. The Dimensions database is the most representative in terms of coverage of research on development of the SARS-CoV-2 vaccines.

Conclusion: This research is a scientific investigation based on bibliometric analysis of papers related to the SARS-CoV-2 vaccines. The Dimensions database provides the most representative research coverage on the creation of a vaccine against coronavirus. It is characterized by a large number of formed verbose terms (length of more than four words) related to coronavirus, which makes it possible to track trends in the development of methods for creating a vaccine.

Keywords: Bibliometric Analysis, COVID-19/SARS-CoV-2, Vaccine

Cell Journal(Yakhteh), Vol 23, No 5, October 2021, Pages: 523-531

Citation: **Rahim F, Khakimova A, Ebrahimi A, Zolotarev O, Rafiei Nasab F. Global scientific research on SARS-CoV-2 vaccines: a bibliometric analysis. Cell J. 2021; 23(5): 523-531. doi: 10.22074/cellj.2021.7794.**

Introduction

The COVID-19 outbreak has caused many economic and psychological effects, and many casualties (1). This virus has spread worldwide with indescribable speed over a short period of time. According to experts, the COVID-19 pandemic could last for years; hence, numerous scientists worldwide are working to eradicate this virus as soon as possible (2). After the increase in cases and global spread, the World Health Organization (WHO) announced that the new coronavirus is the sixth public health emergency worldwide (3).

Diagnosis of a COVID-19 infection is generally based on laboratory and radiological assessments, and radiological examinations are extremely important in early diagnosis and treatment of this disease (4). Severe lung damage due to COVID-19 infection has resulted in high mortality rates in patients who are infected and requirements for mechanical ventilation are also high (5). There is no specific antiviral treatment for the COVID-19 infection, and the mainstay is supportive care that includes sustaining vital signs, oxygen therapy, and the reduction of complications such as multiple organ dysfunction and failure (6). Due to the lack of standard treatment and effective vaccines for this infection, prevention of infection is the best recommendation.

A vaccine is a biological preparation that protects the body against certain infectious diseases. Vaccines usually contain a pathogen, which is similar to the microorganism that causes the disease and is often obtained from a sample of weak or dead microbes, toxins, or one of its surface proteins. Vaccines are either for prevention (to prevent or help cure an infection by a natural or artificial pathogen) or for treatment (such as a cancer vaccine that has not yet been discovered). SARS-CoV-2 vaccines fall into two groups of genetic vaccines that use one or more of

the genes of the coronavirus to stimulate an immune response or a vaccine that carries the virus where the virus is used to deliver the corona virus gene to cells and stimulate an immune response (7). Studies for SARS-CoV-2 vaccines development are ongoing; despite significant progress in vaccine development, challenges still exist (8). The development of a safe, effective vaccine is a long and complicated process that typically takes 10 to 15 years (9). Currently more than 100 candidates for the SARS-CoV-2 vaccines are in various stages of development and a small number are in the early phases of human clinical trials (10). SARS-CoV-2 vaccines approved by the WHO are in clinical trials (11) and a close competition exists between them to achieve a positive result.

In October, 2020, the US Food and Drug Administration (FDA) approved an antiviral drug, Remdesivir (GS-5734), for the treatment of patients hospitalised with COVID-19. This is the first and only approved drug for treatment of COVID-19 in the United States. Remdesivir, an intravenous (IV) injectable drug, inhibits the substances that increase viral replication. Experts warn against the simultaneous use of this drug with hydroxychloroquine because hydroxychloroquine inhibits the therapeutic effects of Remdesivir (12). Remdesivir was originally developed to treat Ebola, but it was not effective and eventually discarded. This appears to be happening again in patients with COVID-19 infection.

The results of recent studies where Remdesivir was used to reduce the complications of COVID-19 infection showed that this drug had little effect on patient recovery (13).

Bibliometric analysis is a tool to determine the status of research conducted in a particular field (14). Trends and possible gaps in knowledge play an important role in management and decision making in science and technology (15). Bibliometric analysis mainly allows the development of analytical methods and bibliometric indicators from statistical criteria, and it is a tool that manages information records related to publications, citations, patents, reports, etc. (16). This analysis also provides additional information about data such as author(s), affiliation(s), and keywords, in addition to integrating information to develop research areas on a specific topic or disciplines.

Despite rapid response from scientists during COVID-19 pandemic, vaccines and antibody protection are still out of reach; however, in acute cases, the US FDA may allow emergency use of promising vaccines that have not yet fully passed safety tests (17). However, for at least six months, researchers will not know the benefits of a vaccine. People exposed to the virus should hope to strengthen their immune system and receive supportive care from doctors and nurses to fight this disease.

The necessity and importance of the present research is that the findings, which include articles from a time period on SARS-CoV-2 vaccines, can show the status of research in this field, reference resources, and reveal the strengths and weaknesses of these researches. Future researchers can fill the information gap in this field by conducting research. In this study, we intend to identify global scientific research on SARS-CoV-2 vaccines by using bibliometric analysis.

Materials and Methods

Search method and strategy

We performed a search in the Scopus database by October 2020 based on a protocol published by Mecenas et al. (18) in 2020. We searched the Scopus database for titles, abstracts, and keywords. A total of 1659 publications were found for 2019-2020 (1657 publications for 2020, 1 publication for 2019). We also performed a search in the PubMed database on 22/07/2020 and located 6727 articles, of which 6225 were published from 01/01/2019-31/07/2020. We searched the Dimensions database for "Vaccine coronavirus" in titles and abstracts and found 2326 publications for 2019-2020 (2169 publications for 2020, 157 publications for 2019). Of these, publications from PubMed - 1289. Table S1 (See Supplementary Online Information at www.celljournal.org) provides the detailed search strategies for each selected database.

Data extraction

Data collection in this study was conducted with a number of articles and by using a researcher-made form appropriate to the objectives of the research. The studied variables included: number of universities, number of journals in each university, number of articles published, number of citations, countries, publication types, first author and contact author, and the number of articles published in each of the fields of SARS-CoV-2 vaccines. We used the VOSviewer toolkit to conduct a co-occurrence analysis for the Scopus, PubMed, and Dimensions databases. An assessment was made of the intensity of the use of one term with another. The minimum threshold for cluster formation was set in a different number of terms for different databases.

Statistical analysis

For data processing, Excel software and descriptive statistics indicators such as mean value were used. (version 1.6.15, Leiden, The Netherlands) was used for visualization. A $P<0.05$ was considered as significant.

Results

Citation analysis

Table 1 lists the ten top-cited results. There were 1897 citations and three papers had at least 200 citations. The first paper had 514 citations and was published by Wrapp et al. (19) in the Proceedings of Department of Molecular Biosciences, University of Texas at Austin (Austin, TX, USA).

Table 1: The top-cited studies on SARS-CoV-2 vaccines

	Title	Citation type	PMID	DOI	IF
1	Cryo-EM Structure of the 2019-nCoV Spike in the Perfusion Conformation	514 Original	32075877	10.1126/science.abb2507	41.845
2	Structure, Function, and Antigenicity of the SARS-CoV-2 Spike Glycoprotein	390 Original	32155444	10.1016/j.cell.2020.02.058	38.637
3	Angiotensin-converting Enzyme 2 (ACE2) as a SARS-CoV-2 Receptor: Molecular Mechanisms and Potential Therapeutic Target Open Access	232 Review	32125455	10.1007/s00134-020-05985-9	17.679
4	Drug Treatment Options for the 2019-New Coronavirus (2019-nCoV) Open Access	178 Communication	31996494	10.5582/bst.2020.01020	1.690
5	Characterization of Spike Glycoprotein of SARS-CoV-2 on Virus Entry and Its Immune Cross-reactivity with SARS-CoV	138 Original	32221306	10.1038/s41467-020-15562-9	12.121
6	Preliminary Identification of Potential Vaccine Targets for the COVID-19 Coronavirus (SARS-CoV-2) based on SARS-CoV Immunological Studies Open Access	114 Original	32106567	10.3390/v12030254	3.816
7	Structure of Mpro from SARS-CoV-2 and Discovery of Its Inhibitors Open Access	96 Original	32272481	10.1038/s41586-020-2223-y	42.778
8	Characterization of the Receptor-binding Domain (RBD) of 2019 Novel Coronavirus: Implication for Development of RBD Protein as a Viral Attachment Inhibitor and Vaccine	80 Original	32203189	10.1038/s41423-020-0400-4	8.484
9	A SARS-CoV-2 Protein Interaction Map Reveals Targets for Drug Repurposing Open Access	78 Original	32353859	10.1038/s41586-020-2286-9	42.778
10	Emergence of Genomic Diversity and Recurrent Mutations in SARS-CoV-2	77 Review	32387564	10.1016/j.meegid.2020.104351	2.611

PMID; PubMed ID, DOI; Digital object identifier, and IF; Impact factor 2019.

Journals

The "Journal of Bimolecular Structure and Dynamics"has an extremely large number of contributions to COVID-19 research with 33 publications followed by "Nature" with 15 papers and "Medical Hypotheses" with 14 papers. Altogether, the ten highest-ranking journals issued 129 articles, which accounted for 17.25% of all publications in this area from a total of 748 (100%) publications. Table 2 lists the top ten funding agencies and highest-ranking journals.

A total of 30 (4.02%) publications were supported by the National Natural Science Foundation of China and 29 were funded by the National Institutes of Health (03.88%) (Table 2).

Journal impact factor

Impact factors (IFs) for the journals with the top-cited articles ranged from 1.322 to 42.778 (median: 3.324). Overall, 52 of the top-cited studies were published in journals that had IFs above 15 (Table 2). Finally, the correlations between the number of top-cited papers and journal IFs did not show any statistical significance (P>0.05).

Publication type

Overall, 1868 articles were cited 12 675 times and 1089 review papers were cited 9710 times. The articles were had a higher average citation per study (429 times) compared to the review papers, which were cited 378 times. Medicine was the most popular research category, followed by biochemistry, genetics, immunology, and microbiology. In terms of research category, there were 60 published studies that pertained to clinical research, of which 11 papers were about therapeutic vaccines (eight full papers and three protocols, including nine that pertained to phase I/II research studies and two phase III studies) (20-30). Table S2 (See Supplementary Online Information at www.celljournal.org) provides detailed information about these clinical trials.

Language and year

All of these papers were published in English from 2019 to 2020.

Table 2: Top funding sources and journals for studies about SARS-CoV-2 vaccines

No.	Field	IF (2019)	N	%
		Journal		
1	Journal of Biomolecular Structure and Dynamics	3.22	33	4.41
2	Nature	42.778	15	2.01
3	Medical Hypotheses	1.322	14	1.87
4	Frontiers in Immunology	6.429	11	1.47
5	Journal of Medical Virology	2.049	11	1.47
6	Cell	38.637	10	1.34
7	Chaos Solitons and Fractals	3.380	10	1.34
8	Vaccine	3.269	9	1.2
9	Cell Host and Microbe	15.923	8	1.07
10	Diabetes and Metabolic Syndrome Clinical Research and Reviews	1.940	8	1.07
		Funding sponsors		
1	National Natural Science Foundation of China	-	30	4.02
2	National Institutes of Health	-	29	3.88
3	National Institute of Allergy and Infectious Diseases	-	16	2.14
4	Bill and Melinda Gates Foundation	-	10	1.34
5	National Basic Research Program of China (973 (Program	-	8	1.07
6	National Science Foundation	-	7	0.94
7	Chinese Academy of Sciences	-	6	0.8
8	National Research Foundation of Korea	-	6	0.8
9	Science and Engineering Research Board	-	6	0.8
10	Welcome Trust	-	6	0.8

N; Number, %; Percentage, and IF; Impact factor.

Country

The United States produced the most publications with 190 papers (25.40%), followed by India (126 publications, 16.84%) and China (88 papers, 11.76%). The United States ranked first in terms of gross domestic product (GDP) and articles per million population, with 0.009 articles per billion GDP (Table 3).

Co-authorship network by authors

In the Scopus database, we found 1659 articles of which there were 6545 authors. From the 6545 authors, 59 authors had at least five published papers.

The co-authorship Scopus network included 59 authors in nine clusters. However, clusters 8 and 9 included only one author (Fig.S1A, See Supplementary Online Information at www.celljournal.org). Table S3 (See Supplementary Online Information at www.celljournal.org) lists clusters 1-7. We located 6225 articles in PubMed and 26 509 authors in the corpus. For comparison with the co-authorship network obtained for the corpus from Scopus, we selected 59 authors who had at least six publications. The co-authorship PubMed network included 59 authors in 19 clusters (Fig.S1B, See Supplementary Online Information at www.celljournal.org). There were 2326 articles from the Dimensions database with 10 356 authors in the corpus. We selected 59 of the most cited authors who had at least five publications to compare the co-authorship network obtained for the corpora from Scopus and PubMed. All authors of the articles were selected for consideration. The co-authorship Dimensions-network included 59 authors in ten clusters (Fig.S1C, See Supplementary Online Information at www.celljournal.org).

Only nine authors were present in the three text corpora (Bonilla-Aldana D.K., Rodriguez-Morales A.J., Sah R., Bottazzi M.E., Du L., Hotez P.J., Jiang S., Kumar S., and Zhang Y.) (Fig.1).

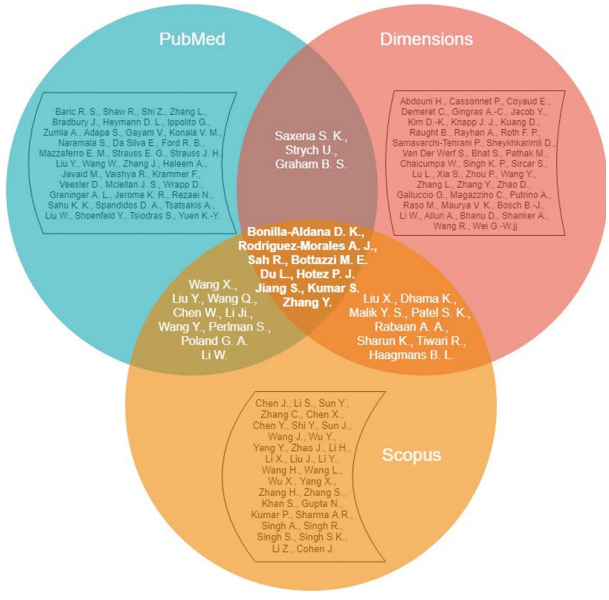

Fig.1: Comparison of the most cited authors of articles in three databases (Scopus, PubMed, Dimensions) that pertain to the vaccine against SARS-CoV-2.

Table 3: Adjusted gross domestic product (GDP) and articles that pertained to studies on the SARS-CoV-2 vaccines per million population

No.	Country/territory	Number	(%)	N per million population	N per billion GDP
1	United States	190	25.4	5.8	0.009
2	India	126	16.84	9.31	0.04
3	China	88	11.76	6.31	0.006
4	United Kingdom	59	7.89	8.87	0.02
5	Italy	53	7.09	8.77	0.02
6	Australia	27	3.61	1.08	0.01
7	Germany	26	3.48	3.15	0.006
8	Pakistan	26	3.48	1.22	0.08
9	Canada	25	3.34	6.74	0.01
10	France	23	3.07	3.73	0.009

Co-authorship network by organizations

Out of 5185 organizations of the corpus in the Scopus database, five had connections and published at least five scientific papers. There were 34 organizations that had at least three publications. We identified 34 organizations that formed 22 clusters in the co-authorship network (Fig. S2A, See Supplementary Online Information at www.celljournal.org).

Out of 15 718 organizations of the corpus from PubMed, 82 had at least three publications. We selected 34 organizations to compare with the co-authorship network obtained for the corpus from Scopus. The co-authorship PubMed network included 34 organizations in 14 clusters (Fig.S2B, See Supplementary Online Information at www.celljournal.org). Of the 1684 organizations of the corpus from the Dimensions database, 34 organizations had at least 12 publications. The 34 organizations formed a co-authorship network of six clusters (Fig.S2C, See Supplementary Online Information at www.celljournal.org). Table S4 (See Supplementary Online Information at www.celljournal.org) shows the first six clusters. We compared the composition of clusters of co-authorship networks by organizations obtained by the corpora from the Scopus, PubMed and Dimensions databases in Table S4 (See Supplementary Online Information at www.celljournal.org).

Co-occurrence network map of keywords

A co-occurrence analysis of keywords was performed that displayed the existing links between keywords used in the publications. In the central part of the map, the terms most frequently encountered in publications are displayed. The keywords/terms were extracted from the title field. A term is presented as a chain of elements (nouns with definitions) with a noun at the end of the phrase [van Eck and Waltman, (31)] (Fig. S3, See Supplementary Online Information at www.celljournal.org).

In our analysis of the corpus from Scopus, we set the threshold of the minimum number of keyword occurrences at ten. This analysis resulted in 39 keywords out of a total of 3625 (Table S5, See Supplementary Online Information at www.celljournal.org). For correct comparison, we choose the same number of terms in the corpus of the Dimensions database. A threshold for the minimum number of keyword occurrences was set at 15. The analysis resulted in 71 keywords out of a total of 4865. We used VOSviewer, which automatically extracted 40% of the least relevant terms; therefore, we chose 43 terms. The common terms “use”, “India”, “time”, and “knowledge” were excluded from the general list (Table S6, See Supplementary Online Information at www.celljournal.org). For correct comparison, we chose the same number of terms in the corpus of the PubMed database. We set the threshold of a minimum number of keyword occurrences at 90. The analysis resulted in 88 keywords out of a total of 26 884. VOSviewer filtered out about 40% of the terms; hence, 53 terms were chosen. We excluded 14 common terms such as “Saudi Arabia”, “vitro”, “South Korea”, and “lesson” from the general list (Table S7, See Supplementary Online Information at www.celljournal.org). Only five terms were present in the three text corpora (COVID -19), China, novel coronavirus, prevention, nCoV) (Fig.2).

The previous experiment was limited in the number of terms. In addition, manual filtering of terms might have affected the result. So, we repeated the experiment with more terms. We choose the conditions of mapping (minimal number of occurrences, minimal cluster size) such that the number of terms approximated 450 and the number of clusters was four (Fig.S4, See Supplementary Online Information at www.celljournal.org).

For correct comparison, we choose the same number of terms in the corpora of the PubMed and Dimensions databases. A threshold of a minimum number of keyword occurrences equal to four for PubMed and three for Dimensions was set. The analysis resulted in 783 keywords out of a total of 10 784 for PubMed and 577 out of 4865 for Dimensions, except for the 40% that were deleted by VOSviewer. Finally, we chose 462 terms for PubMed and 459 terms for the Dimensions database. We

did not exclude any terms from the final list. In order to have four clusters, we set limits of at least 60 words in a cluster for PubMed and 80 for the Dimensions database.

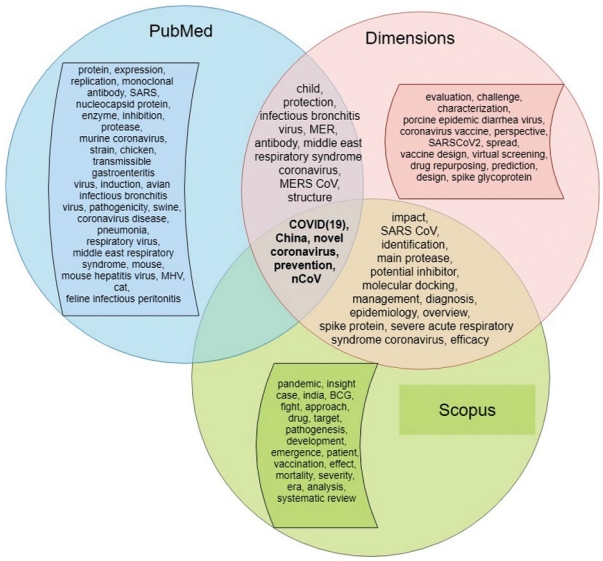

Fig.2: A comparison of the key terms from different corpora (Scopus, PubMed, Dimensions).

The main keywords for each of the four clusters (Top-20) from term co-occurrence maps (rank based on total link strength) are presented in Table S8 (See Supplementary Online Information at www.celljournal.org) for the Scopus database, Table S9 (See Supplementary Online Information at www.celljournal.org) for the PubMed database, and Table S10 (See Supplementary Online Information at www.celljournal.org) for the Dimensions database.

Table S10 (See Supplementary Online Information at www.celljournal.org) presents a comparison of the received terms (450 units) from different corpora. The common vocabulary, general scientific vocabulary, and general medical vocabulary were excluded (Fig.3).

We compared the names of coronavirus diseases used in the resultant text corpora (Table S11, See Supplementary Online Information at www.celljournal.org) and analysed the vocabulary of the terms. We divided the terms into the following groups: i. Common vocabulary, ii. General scientific vocabulary, iii. General medical vocabulary, and iv. Thematic vocabulary. The first group included the following terms: Germany, entry, 21st century, general population, Hubei Province, policy, adult, age, era, future perspective, human, nature, social media, Africa, alternative, communication, community, decision, delay, February, belief, adolescent, adoption, climate change, difference, human right, seasonality, Seattle, disruption, billion compound, chapter, characteristics, characterization, female, goal, Google Scholar, government, guidance, mankind, market, performance, period, week, whole world, Wuhan city, emergence, environment, worldwide, and Wuhan.

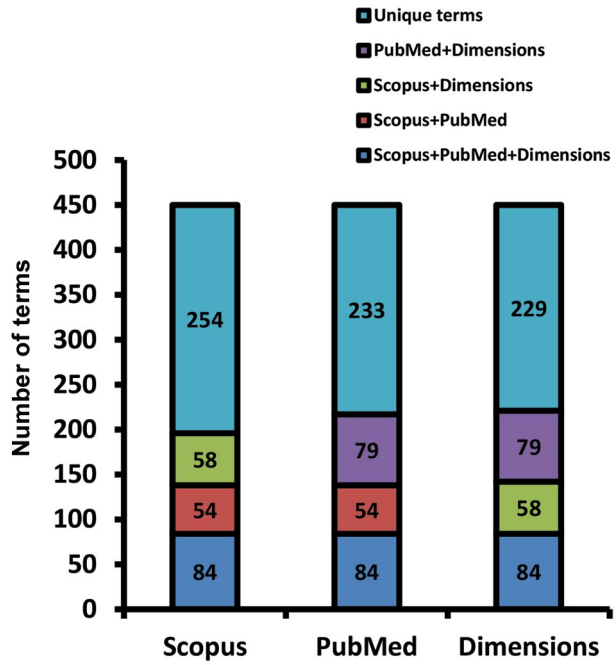

Fig.3: The ratio of repetitive and unique terms in different corpora. There were a total of 450 units for all corpora.

The second group included the following terms: discovery, comparison, assessment, bibliometric analysis, biomedical research, correlation, systematic review, cross-sectional study, meta-analysis, current knowledge, validation, current review, observational study, current study, database, further investigation, mathematical model, publication, PubMed, comparative analysis, mathematical assessment, mathematical prediction, computational, deep learning, computational approach, science, scientist, computational investigation, and computational method.

The third group included the following terms: diagnostic, clinical manifestation, cancer patient, case report, silico approach, human health, clinical consideration, clinical course, clinical features, clinical implication, clinical management, hospitalisation, hospitalised child, prophylactic, hospitalised patient, blood, patients, breath, morbidity, mortality, therapeutic approach, therapeutic strategy, cancer, clinical experience, clinical sample, cardiovascular disease, clinical data, clinical evidence, clinical presentation, clinical study, healthcare, healthcare system, healthcare worker, supportive care, clinical symptom, clinical treatment, clinical use, and clinician. Terms from the fourth group are presented in Table S12 (See Supplementary Online Information at www.celljournal.org).

Figure S5 (See Supplementary Online Information at www.celljournal.org) shows the relationship of the

terms of each group between corpora from the different databases. The most common terms in publications related to research in the field of vaccine and coronavirus was "sars cov" in the PubMed database, which was organized based on the time of appearance (Fig.S6, See Supplementary Online Information at www.celljournal.org).

Discussion

This is the first bibliometric research that summarizes numerous characteristics of the investigations of the SARS-CoV-2 vaccines. An understanding of the features of global researches on SARS-CoV-2 vaccines may be beneficial. In this bibliometric study, we reviewed the literature from three databases - Scopus, Dimensions, and PubMed. We identified 1659 articles from Scopus and 6545 authors in the corpus, of which 59 authors had at least five publications. The co-authorship network includes these authors in nine clusters.

For 6225 articles from PubMed, 26 509 authors were listed in the corpus with the co-authorship network that includes 59 authors in 19 clusters. Moreover, for 2326 articles from the Dimensions database, 10 356 authors were in the corpus, of which 59 authors who had at least five publications with the co-authorship network of ten clusters were included. As can be deduced from the results, although there have been many studies on the SARS-CoV-2 vaccine, as well as number of vaccine showed acceptable efficacy against SARS-CoV-2; therefore, we cannot with certainty expect a fully safe and effective vaccine against this disease, especially for various age groups and various viral strains (32).

To our surprise, we found that that at most, there were 9 authors duplicated in all three corpora of the publications. Scopus and PubMed had nine, whereas Scopus and Dimensions had eight, and PubMed and Dimensions had three mutual authors. There were 33 (55.9%) non-recurring authors in the Scopus-network, 37 (62.7%) in the PubMed network, and 39 (66.1%) in the Dimensions network. It should be noted that Chinese and Indian authors prevailed among Scopus authors. There is a prevalence of European authors in PubMed and the Dimensions database is comprised of European, Chinese, and Indian authors.

To date, there are more than 300 approved candidates for the SARS-CoV-2 vaccines, and 32 have already undergone clinical trials. In addition, the paradox of vaccine production has been raised in some countries (33). Vaccines can help prevent the spread of disease by stimulating the immune system. Our knowledge of COVID-19 is far less than our ignorance, and the complexity of this disease makes us think more deeply about a vaccine. In the first stage, the vaccine is tested on a small number of subjects in order to prove that it is safe. In the second phase, the vaccine will be tested on a larger number of patients to evaluate its effectiveness. Both safety and efficacy of a vaccine are very important and vital (34).

The organizations that were identified in the mapping of co-authorship also differed for the three corpora. Organizations that met twice were: University College London, Fudan University, University of Washington, Tehran University of Medical Sciences (Tehran, Iran), Ohio State University, and Yale University. No organization met three times. In a preliminary experiment, our comparison showed considerable variation in terminology. Common words comprised disease names (COVID19, novel coronavirus, nCoV), disease prevention, and country of origin (China). Although unlikely, the COVID-19 outbreak could abruptly end before a safe and effective vaccine is available; therefore, we must continue our efforts to find such vaccines in order to be prepared to fight this disease if an outbreak recurs (35). Given that all scientists and research and development centres are in a race and competition to develop the SARS-CoV-2 vaccines, it is necessary to accelerate and streamline that process because a vaccine may be the only approach that enables the development of immunity to SARS-CoV-2 across a population (36).

As a result, scientific biomedical information databases are often used by physicians and researchers. In this article, we compared different aspects of basic biomedical scientific information databases. PubMed is a very significant resource for physicians and researchers, whereas Scopus covers a wider range of journals and citation analysis capabilities compared to the other databases (37). At the same time, both the PubMed and Dimensions corpora overlapped in eight terms. The Scopus and Dimensions corpora overlapped in 13 terms. Both the Scopus and PubMed corpora did not overlap in any of the terms. In order to clarify terminological mapping, we conducted research on a large number of terms. The results of the previous study could have been influenced by human factor because we excluded a number of uninformative terms at the last stage. In the current study, we considered all terms without exception. The main term common to the Scopus and PubMed databases was 2019-COV. The PubMed and Dimensions databases had eight terms in common (new coronavirus, novel coronavirus covid, novel coronavirus SARS-CoV, porcine deltacoronavirus, porcine epidemic diarrhoea virus, SARS CoV2, SARSCoV2 infection, and severe acute respiratory syndrome). Therefore, PubMed had more research with animal models on COVID-19 diseases compared to the other databases (38). In addition, more accurate names of this disease were used in this corpus, which was not surprising given the medical nature of this database.

We analysed the lexical groups of the terms, of which the thematic vocabulary group is of interest as it contains terms related to the field of vaccine development (39). Surprisingly, the Dimensions database had the most topic-specific words (249 words), followed by Scopus (221 words) and PubMed (193 words). However, there were

words that were repeated in the three corpora. Among the general terms, there were terms that provided an idea that to design a vaccine toolkit, animal models are essential, using approaches such as immune-informatics, virtual screening, molecular dynamics simulation, which are popular methods for vaccine development so far (40).

The structure of the coronavirus is being studied. Animal models are mentioned in the PubMed and Dimensions corpora. Hence, in term of Scopus terms, penetration of the virus into the cell and the body's response to the virus were frequent terms. PubMed has frequent immunological terms, but the largest number of specific terms were identified in the Dimensions database. Thus, the corpus from the Dimensions database provided a more complete picture of the research topics for SARS-CoV-2 vaccine development. This could help health policy makers make decisions about incorporating new researches into vaccine development (41).

We attempted to analyse temporal dynamics using the PubMed corpus as an example by taking into account the medical specifics of this database because these collections were less represented in the Dimensions and Scopus databases. The time slot is wider in the PubMed database. Unlike other databases, PubMed contains many articles about previous strains of coronaviruses. Nevertheless, the interval of publication activity was small. Hence, we decided to consider temporal dynamics in future studies.

There were 10874 terms in the PubMed collection. We chose 147 terms because they were the most relevant and popular. The clustering of these terms resulted in ten clusters. There were eight clusters with the minimum cluster size that equalled one.

Conclusion

This study is a scientific bibliometric analysis of studies on SARS-CoV-2 vaccines. A comparative analysis of scientific literature was carried out for three bases: Scopus, PubMed, and Dimensions. As a result, we determined that tremendous attention is paid to the study of the coronavirus structure at the organismic, cellular and molecular levels. Penetration of the virus into the cells is well-studied. A variety of methods and strategies are being used to develop a vaccine. The features of the influence and development of coronavirus on animals are well understood. Both animal and computer models are being used to create a vaccine for humans. The most representative from the point of view of the coverage of research on the creation of a vaccine against coronavirus is in the Dimensions database. It is characterized by a large number of formed verbose terms (more than four words) related to coronavirus, which makes it possible to track trends in the development of methods for creating a vaccine.

Acknowledgements

The reported study was funded by Russian Fund of Basic Research (RFBR) and National Natural Science Foundation of China (NSFC), project numbers 21-51-53001 and 20-24-70001. There is no conflict of interest in this study.

Authors' Contributions

F.R., A.Kh., A.E., O.Z., F.R.N.; Were involved in the study design, and drafting and editing the manuscript. F.R., A.Kh.; Were involved in the experimental studies. F.R., O.Z., F.R.N.; Were involved in primer design, search, and data analysis. F.R., A.Kh.; Were involved in the revising the manuscript. All authors have read and approved the final manuscript.

References

1. Ahmad T, Haroon, Baig M, Hui J. Coronavirus disease 2019 (COVID-19) pandemic and economic impact. Pak J Med Sci. 2020; 36(Covid19-s4): S73-S78.
2. Scudellari M. How the pandemic might play out in 2021 and beyond. Nature. Available from: https://www.nature.com/articles/d41586-020-02278-5. 2020 (05 Aug 2020).
3. Eurosurveillance Editorial Team. Note from the editors: World Health Organization declares novel coronavirus (2019-nCoV) sixth public health emergency of international concern. Euro Surveill. 2020; 25(5): 200131e.
4. Zhai P, Ding Y, Wu X, Long J, Zhong Y, Li Y. The epidemiology, diagnosis and treatment of COVID-19. Int J Antimicrob Agents. 2020; 55(5): 105955.
5. Khafaie MA, Rahim F. Cross-country comparison of case fatality rates of COVID-19/SARS-COV-2. Osong Public Health Res Perspect. 2020; 11(2): 74-80.
6. Shih HI, Wu CJ, Tu YF, Chi CY. Fighting COVID-19: a quick review of diagnoses, therapies, and vaccines. Biomed J. 2020; 43(4): 341-354.
7. Izda V, Jeffries MA, Sawalha AH. COVID-19: a review of therapeutic strategies and vaccine candidates. Clin Immunol. 2021; 222: 108634.
8. Zhu FC, Guan XH, Li YH, Huang JY, Jiang T, Hou LH, et al. Immunogenicity and safety of a recombinant adenovirus type-5-vectored COVID-19 vaccine in healthy adults aged 18 years or older: a randomised, double-blind, placebo-controlled, phase 2 trial. Lancet. 2020; 396(10249): 479-88.
9. Bregu M, Draper SJ, Hill AVS, Greenwood BM. Accelerating vaccine development and deployment: report of a Royal Society satellite meeting. Philos Trans R Soc Lond B Biol Sci. 2011; 366(1579): 2841-2849.
10. Thanh Le T, Andreadakis Z, Kumar A, Gómez Román R, Tollefsen S, Saville M, et al. The COVID-19 vaccine development landscape. Nat Rev Drug Discov. 2020; 19(5): 305-306.
11. Funk CD, Laferrière C, Ardakani A. A snapshot of the global race for vaccines targeting SARS-CoV-2 and the COVID-19 pandemic. Front Pharmacol. 2020; 11: 937.
12. Santoro MG, Carafoli E. Remdesivir: from Ebola to COVID-19. Biochem Biophys Res Commun. 2021; 538: 145-150.
13. Doggrell SA. Remdesivir, a remedy or a ripple in severe COVID-19? Expert Opin Investig Drugs. 2020; 29(11): 1195-1198.
14. Jing R, Vunnam RR, Yang Y, Karevoll A, Vunnam SR. Current status of treatment options, clinical trials, and vaccine development for SARS-CoV-2 infection. J Pure Appl Microbiol. 2020; 14(1): 733-740.
15. Khakimova A, Yang X, Zolotarev O, Berberova M, Charnine M. Tracking knowledge evolution based on the terminology dynamics in 4p-medicine. Int J Environ Res Public Health. 2020; 17(20): 7444.
16. Wallin JA. Bibliometric methods: pitfalls and possibilities. Basic Clin Pharmacol Toxicol. 2005; 97(5): 261-275.
17. Tu YF, Chien CS, Yarmishyn AA, Lin YY, Luo YH, Lin YT, et al. A review of SARS-CoV-2 and the Ongoing clinical trials. Int J Mol Sci. 2020; 21(7): 2657.
18. Mecenas P, Bastos RTRM, Vallinoto ACR, Normando D. Effects of temperature and humidity on the spread of COVID-19: a systematic review. PLoS One. 2020; 15(9): e0238339.
19. Wrapp D, Wang N, Corbett KS, Goldsmith JA, Hsieh CL, Abiona O,

et al. Cryo-EM structure of the 2019-nCoV spike in the prefusion conformation. Science. 2020; 367(6483): 1260-1263.
20. Junqueira-Kipnis AP, Dos Anjos LRB, Barbosa LCS, da Costa AC, Borges KCM, Cardoso A, et al. BCG revaccination of health workers in Brazil to improve innate immune responses against COVID-19: A structured summary of a study protocol for a randomised controlled trial. Trials. 2020; 21(1): 881.
21. Palacios R, Patiño EG, de Oliveira Piorelli R, Conde MTRP, Batista AP, Zeng G, et al. Double-blind, randomized, placebo-controlled phase III Clinical trial to evaluate the efficacy and safety of treating healthcare professionals with the adsorbed COVID-19 (inactivated) vaccine manufactured by sinovac - PROFISCOV: a structured summary of a study protocol for a randomised controlled trial. Trials. 2020; 21(1): 853.
22. Sahin U, Muik A, Derhovanessian E, Vogler I, Kranz LM, Vormehr M, et al. COVID-19 vaccine BNT162b1 elicits human antibody and T(H)1 T cell responses. Nature. 2020; 586(7830): 594-599.
23. Giamarellos-Bourboulis EJ, Tsilika M, Moorlag S, Antonakos N, Kotsaki A, Domínguez-Andrés J, et al. Activate: randomized clinical trial of BCG vaccination against infection in the elderly. Cell. 2020; 183(2): 315-323. e9.
24. Logunov DY, Dolzhikova IV, Zubkova OV, Tukhvatullin AI, Shcheblyakov DV, Dzharullaeva AS, et al. Safety and immunogenicity of an rAd26 and rAd5 vector-based heterologous prime-boost COVID-19 vaccine in two formulations: two open, non-randomised phase 1/2 studies from Russia. Lancet. 2020; 396(10255): 887-897.
25. Xia S, Duan K, Zhang Y, Zhao D, Zhang H, Xie Z, et al. Effect of an Inactivated vaccine against SARS-CoV-2 on safety and immunogenicity outcomes: interim analysis of 2 randomized clinical trials. JAMA. 2020; 324(10): 951-960.
26. Mulligan MJ, Lyke KE, Kitchin N, Absalon J, Gurtman A, Lockhart S, et al. Phase I/II study of COVID-19 RNA vaccine BNT162b1 in adults. Nature. 2020; 586(7830): 589-593.
27. Jackson LA, Anderson EJ, Rouphael NG, Roberts PC, Makhene M, Coler RN, et al. An mRNA vaccine against SARS-CoV-2 - preliminary report. N Engl J Med. 2020; 383(20): 1920-1931.
28. Folegatti PM, Ewer KJ, Aley PK, Angus B, Becker S, Belij-Rammerstorfer S, et al. Safety and immunogenicity of the ChAdOx1 nCoV-19 vaccine against SARS-CoV-2: a preliminary report of a phase 1/2, single-blind, randomised controlled trial. Lancet. 2020; 396(10249): 467-478.
29. Zhu FC, Guan XH, Li YH, Huang JY, Jiang T, Hou LH, et al. Immunogenicity and safety of a recombinant adenovirus type-5-vectored COVID-19 vaccine in healthy adults aged 18 years or older: a randomised, double-blind, placebo-controlled, phase 2 trial. Lancet. 2020; 396(10249): 479-488.
30. Zhu FC, Li YH, Guan XH, Hou LH, Wang WJ, Li JX, et al. Safety, tolerability, and immunogenicity of a recombinant adenovirus type-5 vectored COVID-19 vaccine: a dose-escalation, open-label, non-randomised, first-in-human trial. Lancet. 2020; 395(10240): 1845-1854.
31. van Eck NJ, Waltman L. Citation-based clustering of publications using CitNetExplorer and VOSviewer. Scientometrics. 2017; 111(2): 1053-1070.
32. The Lancet Infectious Diseases. COVID-19: endgames. Lancet Infect Dis. 2020; 20(5): 511.
33. Graham F, Castelvecchi D, Phillips N. Daily briefing: This is the state of COVID-19 vaccine development now. Nature. 2020. Available from: https://www.nature.com/articles/d41586-020-01083-4 (30 Sep 2020).
34. Al-Kassmy J, Pedersen J, Kobinger G. Vaccine candidates against coronavirus infections. where does COVID-19 stand? Viruses. 2020; 12(8): 861.
35. Lurie N, Saville M, Hatchett R, Halton J. Developing Covid-19 vaccines at pandemic speed. N Engl J Med. 2020; 382(21): 1969-1973.
36. Callaway E. Scores of coronavirus vaccines are in competition — how will scientists choose the best? Nature. 2020. Available from: https://www.nature.com/articles/d41586-020-01247-2 (30 Sep 2020).
37. Falagas ME, Pitsouni EI, Malietzis GA, Pappas G. Comparison of PubMed, Scopus, Web of Science, and Google Scholar: strengths and weaknesses. FASEB J. 2008; 22(2): 338-342.
38. Leenaars M, Hooijmans CR, van Veggel N, ter Riet G, Leeflang M, Hooft L, et al. A step-by-step guide to systematically identify all relevant animal studies. Lab Anim. 2012; 46(1): 24-31.
39. Report of CIOMS/WHO Working Group on Vaccine Pharmacovigilance. Definition and application of terms for vaccine pharmacovigilance. Geneva: WHO Press; 2012. Available from: https://www.who.int/vaccine_safety/initiative/tools/CIOMS_report_WG_vaccine.pdf (21 Jan 2020).
40. Parvizpour S, Pourseif MM, Razmara J, Rafi MA, Omidi Y. Epitope-based vaccine design: a comprehensive overview of bioinformatics approaches. Drug Discov Today. 2020; 25(6): 1034-1042.
41. González-Lorenzo M, Piatti A, Coppola L, Gramegna M, Demicheli V, Melegaro A, et al. Conceptual frameworks and key dimensions to support coverage decisions for vaccines. Vaccine. 2015; 33(9): 1206-1217.

Original Article

miR-155, miR-21, and let-7a Expressions in MCF-10A and MCF-7 Cell Lines after Low to High Dose Irradiation

Afsaneh Zare, M.Sc.[1], Reza Fardid, Ph.D.[1, 2*], Gholam Hossein Tamadon, Ph.D.[3, 4], Mohammad Amin Mosleh-Shirazi, Ph.D.[2, 5]

1. Department of Radiology, School of Paramedical Sciences, Shiraz University of Medical Sciences, Shiraz, Iran
2. Ionizing and Non-Ionizing Radiation Protection Research Centre, School of Paramedical Sciences, Shiraz University of Medical Sciences, Shiraz, Iran
3. Department of Laboratory Sciences, School of Paramedical Sciences, Shiraz University of Medical Sciences, Shiraz, Iran
4. Diagnostic Laboratory Sciences and Technology Research Centre, School of Paramedical Sciences, Shiraz University of Medical Sciences, Shiraz, Iran
5. Physics Unit, Department of Radio-Oncology, School of Medicine, Shiraz University of Medical Sciences, Shiraz, Iran

**Corresponding Address: P.O.Box: 71348-14336, Department of Radiology, School of Paramedical Sciences, Shiraz University of Medical Sciences, Shiraz, Iran*
Email: rfardid@gmail.com

Received: 13/January/2020, Accepted: 04/April/2020

Abstract

Objective: Ionizing radiation is a tremendous risk factor for cancer development. MicroRNAs (miRNAs) are regulators that utilize cell pathways, which are implicated in human cancer prognosis. In addition, miRNAs respond to anti-cancer therapy and proliferation after irradiation. However, the changes in miRNA expression profiles in response to irradiation have not been comprehensively analysed. The present study was designed to assess potential changes that occur in miRNA expression following irradiation.

Materials and Methods: In this experimental study, we used quantitative real-time polymerase chain reaction (qRT-PCR) to measure the expressions of miR-155, miR-21, and let-7a in MCF-10A (normal breast cells) and MCF-7 (breast cancer cells) six hours after the cells were exposed to five different irradiation doses (50, 100, 400, 2000, and 4000 mGY).

Results: After irradiation from the low to high doses, we observed an upsurge in miR-155 (more than 100%) expression and reduction in let-7a (more than 87%) expression. However, there was an increase and a reduction in miR-21 expression (more than 100%).

Conclusion: Irradiation can play an important role in cancer development in normal breast cells (MCF-10A) at low dose irradiation. However, the results showed little difference at high doses of radiation.

Keywords: Breast Cancer, Ionizing Radiation, Let-7a, MiR-155, MiR-21

Cell Journal(Yakhteh), Vol 23, No 5, October 2021, Pages: 532-537

Citation: **Zare A, Fardid R, Tamadon GhH, Mosleh-Shirazi MA. miR-155, miR-21, and let-7a expressions in MCF-10A and MCF-7 cell lines after low to high dose irradiation. Cell J. 2021; 23(5): 532-537. doi: 10.22074/cellj.2021.7411.**

Introduction

Breast cancer is a complicated disease with genetic diversity that encompasses a wide range of changes in structure and gene expression. Since breast cancer is very prevalent and is the second cause of mortality amongst women, further research is vital in this field (1).

MicroRNAs (miRNAs) play important role in the diagnosis and treatment of cancers (2). MiRNAs comprise 19-25 nucleotides and they play a role in the arrangement of gene expressions. There are a few studies on radiation and miRNAs (3). In addition, miRNAs play a major role in several processes, such as apoptosis, differentiation, cell migration, and proliferation (4). Recently, the number of identified miRNAs in the process of gene arrangement has significantly increased (3). In order to achieve their intended target, miRNAs can play the role of tumour suppressor or oncogene (5).

MiRNAs can be potential candidates for breast cancer biomarker and used for early prognosis and diagnosis (6). MiR-155 increases in several cancers, including breast cancer (7). Recently, the influence of evidence-based miR-155 on suppressor of cytokine signalling 1 (SOCS1) was found to play a role in tumour suppression. An increase in miR-155 results in a decrease in SOCS1 levels (8). In addition, in another study the impact of miR-155 on caspase3 was observed as a suppressor with a major role in apoptosis (9).

In a study of rat breast cancer epithelial cells, miR-155, an inter-mediator in the TGFB pathway, was found to have a central role in cell formation epithelial-mesenchymal transition (EMT) and increased considerably (10). In general, although miR-155 increases in breast cancer, in

some research, a decrease in miR-155 in some hormonal receptors has been seen (11). Increases in miR-21 have been reported in some cancers, including breast cancer (12, 13). The increase in miR-21 in cancer cells was shown to be specific when compared to normal breast cells (13). An investigation of 199 breast cancer patient and 21 healthy control by real-time polymerase chain reaction (qRT-PCR) showed a significant level of miR-21 (14). The amount of miR-21 expression in grades 2 and 3 cancer cells is higher than grade 1. MiR-21 is one of the major regulators of miRNAs in different cell pathways; this miRNA regulates metastasis and can control cell viability. Tropomyosin-1 is an important growth-inhibiting protein that is negatively regulated by miR-21 (15-17).

Let-7a is part of the first known miRNAs, with a 12 member's family (18). Let-7a regulates many targets in cell pathways and the levels of these targets increase in breast cancer. There is a negative feedback between let-7a and lin-28 (19). Gene producer let-7a is on chromosome 13, a fragile part of the gene that is constantly being deleted. Studies have shown that in undifferentiated cells, let-7a is also absent and the chance of cancer is also increased (20). The results of one study showed a decrease in let-7a in breast cancer cells (BT-IC) and an increase in let-7a in differentiated cells (21). Dingo and colleagues reported a role for let-7a in breast cancer metastasis by RKIP regulation. RKIP is a gene suppressor in breast cancer cells (22). The changes in miRNA expression profiles in response to irradiation have not been comprehensively analyzed. The present study was designed to assess potential changes that occur in miRNA expression following irradiation.

Materials and Methods

This experimental research was designed to examine the effect of ionizing radiation on expression changes in three miRNAs - miR-155, miR-21, and let-7a. This study was conducted at Shiraz University of Medical Sciences with the support of the Vice Chancellor for Research and was registered by the Ethics Committee (IR.SUMS.REC.1397.538).

Cell culture

We obtained both human breast cancer cell lines (MCF-7) and human normal breast cell line (MCF-10A) from Pasteur institute of Iran (Tehran, Iran). The cells were supplemented with 10% foetal bovine serum (FBS, Merck, Germany) and 1% penicillin-streptomycin (Merck, Germany), and cultivated in 20 flasks in medium at 37˚C and 5% CO_2 under carefully controlled conditions. Each group was cultured in three flasks and twice testing was performed for each flask.

Ionizing radiation treatment

The cultured cells were irradiated with different doses of ionizing radiation. The cells received 50, 100, 400, 2000, and 4000 mGY administered by a linak accelerator (Elekta Company, Sweden) at 6 mv and source-skin distance (SSD) of 100 cm and a dose rate of 200 mu/minutes. The experiments were conducted at Namazi Hospital, Shiraz, Iran. The irradiated cells were maintained at 37˚C and 5% CO_2 for six hours prior to total RNA extraction conducted in accordance with the manufacturer's instructions.

RNA extraction

Total RNA was extracted from the cultivated MCF-7 and MCF-10A cell lines using TRIzol reagent (Invitrogen, Carlsbad, CA, USA) in accordance with the manufacturer's instructions. Both the RNA concentration and integrity were quantified in each sample by a NanoDrop (Bioner, South Korea) instrument before the samples were stored at -70˚C.

cDNA synthesis and real-time polymerase chain reaction

cDNA synthesis was conducted with a KIT protocol (Exiqon, Denmark) according to the manufacturer's instructions. An average of 2 µl of the total miRNAs was used for cDNA synthesis based on the evaluation of the NanoDrop instrument. For recognizing miRNAs expression and RT-PCR, we used 10 ml of ROX and SYBR-green (Exiqon, Denmark), 1 µl cDNA, 1 µl primer, and 8 µl DEPC Water (DW) according to the manufacturer's instructions. In order to specify the amount of miRNA expression and for RT-PCR analysis, we used Oligo-dT primer to design specific primers for miR-155, MiR-21, and let-7a. MiR-5s was purchased from mentioned company (Exiqon, Denmark), for internal control. The expression levels of these three miRNAs were evaluated by an ABI Step One QPCR according to the manufacturer's instructions. Briefly, all samples were incubated for 60 minutes at 42˚C, followed by heat inactivation of the reverse transcriptase (RT-enzyme) at 95˚C for 5 minutes. Additionally, 5S rRNA gene was used as an internal control. The RT-PCR reactions were performed at 95˚C for 10 minutes, followed by 40 cycles at 95˚C for 10 seconds, and 60˚C for one minute with an ABI 7500 qRT-PCR system (Applied Biosystems, Foster City, CA, USA).

Bioinformatics analysis

Identification of putative and validated target genes among the differentially expressed genes for all the studied seven miRNAs was performed by using Web-based software analysis. The corresponding gene, miRBase ID, and sequence of each miRNA in this study were assigned before analysis. The Web-based software used to investigate the miRNA targets were: miRTarBase (http://miRtarbase.mbc.nctu.edu.tw), miRecords (http://miRecords.biolead.org/), TargetScan (http://www.targetscan.org/), miRanda (http://www.microrna.org), DIANA microT (http://diana.imis.athena-innovation.gr/DianaTools), and miRwalk (http://zmf.umm.uni-heidelberg.de/apps/zmf/miRwalk2/).

Statistical analysis

All experiments were performed in duplicate. Data

were analysed by software used in an ABI instrument by taking into consideration the obtained cycle threshold (CT) numbers and the estimated melting curve using device for any miRNA in each irradiation. We had a CT number which was normalized to internal control (miR-5s) by Graph Pad Prism 5.0 (Graph Pad Software, Inc., La Jolla, CA, USA), finally use $2^{(-\Delta\Delta ct)}$ were expressed as log2 values.

Results

The MCF-7 and MCF-10A cell lines were cultivated under appropriate conditions and subsequently irradiated with varying doses (50, 100, 400, 2000, or 4000 mGY). After six hours, we evaluated miRNA expression levels by qRT-PCR. Irradiation from low to high doses showed an increase in miR-155 expression in the cancer cell line in comparison with normal cells, and this represented the probability of breast cancer at the various doses. Down-regulation occurred between the 100 to 400 mGY doses, which could be considered a reduction related to the chance of breast cancer at the 400 mGY dose compared to the lower doses. We observed up-regulation in the doses after 400 mGY (Fig.1).

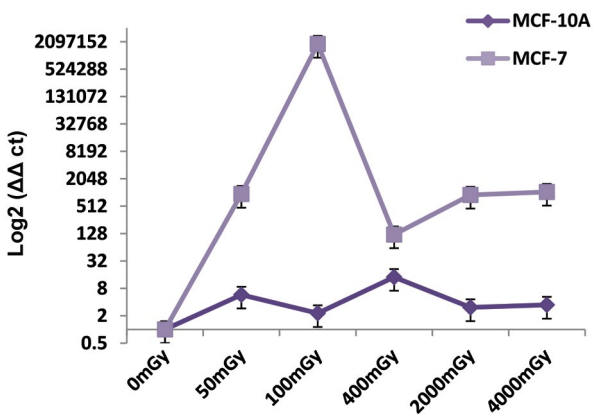

Fig.1: The relative expression of miR-155 in the MCF-10A and MCF-7 cell lines after irradiation at 50, 100, 400, 2000, and 4000 mGY. MicroRNA (miRNA) expressions were assessed after six hours. There is a chance for breast cancer in the low to high doses.

MiR-21 expression was up-regulated and down-regulated in the cancer cells in comparison with the normal cells. There was up-regulation in 50 and 100 mGY doses; hence, it could be said that the probability of breast cancer increased in this dose due to the increase in miR-21 expression in breast cancer. However, we had a decrease in the expression of miR-21 in the cancer cells compared to normal cells at the 200 mGY dose, followed by an overlap to 4000 mGY. The minimum possibility to develop cancer in miR-21 after irradiation was 400 mGY where we had a significant difference between normal cells and cancer cells (Fig.2).

The reduction in let-7a in cancer cells compared to normal cells is a fact. Overally, we observed a decrease in let-7a expression in cancer cells compared with normal ones, which could be considered as an increased chance for breast cancer in the low to high doses. There was no significant increase or decrease in let-7a expression in the low to high doses; however, the most significant amount change to level of let-7a expression between normal and cancer cells was observed at the 400 mGY dose (Fig.3).

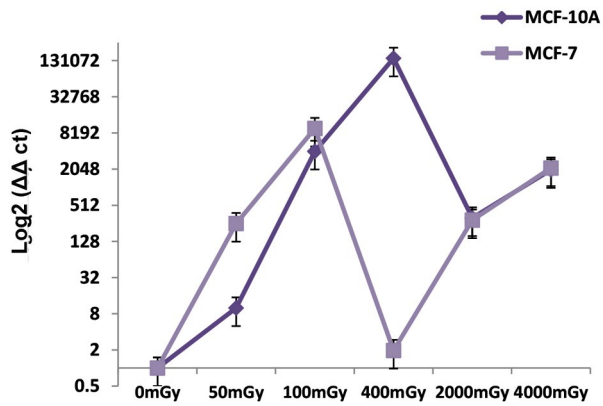

Fig.2: Relative expression of miR-21 in the MCF-10A and MCF-7 cell lines after irradiation at 50, 100, 400, 2000, and 4000 mGY. MicroRNA (miRNA) expressions were assessed after six hours. Up-regulation and down-regulation were observed at different doses.

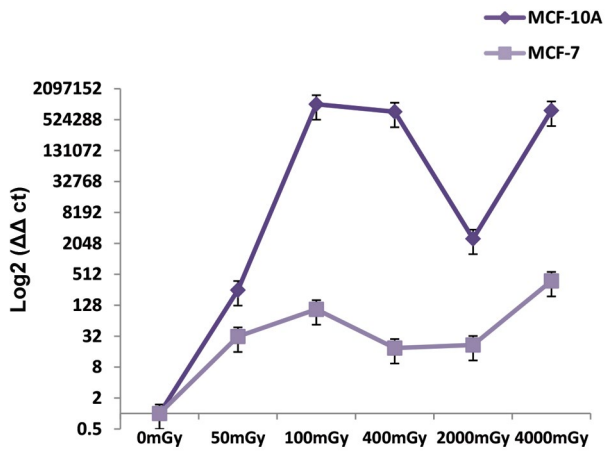

Fig.3: Relative expression of let-7a in the MCF-10A and MCF-7 cell lines after irradiation at 50, 100, 400, 2000, and 4000 mGY. MicroRNA (miRNA) expression was assessed after six hours. There is a chance of breast cancer in the low dose to high doses.

The MCF-7 cancer cell line was affected by let-7a down-regulation and miR-155 and miR-21 up-regulation. In terms of the irradiation effect, we observed a similarity in expressions of miR-155 and miR-21 in the cancer cells after irradiation. The higher probability of breast cancer was observed at the 100 mGY dose and the minimum probability was at the 400 mGY dose. For let-7a, the most significant effect was observed with the least possible expression, which occurred with the 400 mGY dose and the least irradiation effect was at 4000 mGY, which had the most expression (Fig.4).

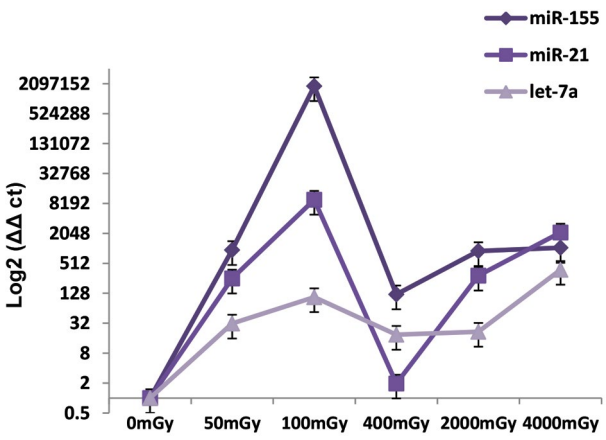

Fig.4: Relative expressions of miR-155, miR-21, and let-7a in the MCF-7 cell line after irradiation at 50, 100, 400, 2000 and 4000 x-rays. MicroRNA (miRNA) expression was assessed after six hours.

The changes in expressions of miR-155, miR-21 and let-7a in the MCF-10A cell line (normal cells) are seen in the form of increase and decrease on different doses. In the case of let-7a, probability of breast cancer increased at the 2000 mGY dose compared to the 4000 mGY dose, due to a reduction in expression level. MiR-21 expression in normal cells at different doses showed that the probability of breast cancer has increased followed by a decrease at 2000 mGY compared to 400 mGY. MiR-155 expression in normal cells had no significant decrease or increase; however, it can be said that probability of breast cancer after irradiation was high at the 400 mGY dose compared to the other doses because we observed the highest expression (Fig.5).

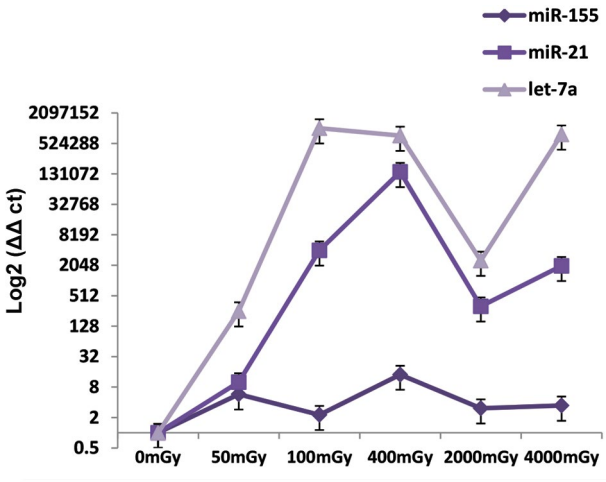

Fig.5: Relative expressions of miR-155, miR-21, and let-7a in the MCF-10A cell line after irradiation at 50, 100, 400, 2000, and 4000 mGY. MicroRNA (miRNA) expression was assessed after six hours.

Discussion

There are recent significant developments in the field of molecular analysis and problem-solving aetiology. MiRNAs are a new category of endogenous RNA molecules that have aroused great interest in the scientific community. MiRNAs are often expressed in cancer. A new source of upstream molecular factors of gene expression has been discovered, which warrants extensive research to clarify their roles in cancer.

We studied the association between miRNAs and breast cancer. The role of miRNAs as an effective diagnostic factor for breast cancer was the focus of our research. MiRNAs have important roles in cancer diagnosis that are very important like germ cell tumours (23). Although one of the most important factors that influences the process of cancer is radiation, there are few studies of irradiation on miRNAs and breast cancer. A recent study showed the effect of different radiation doses on two types of cancer cell lines through the miRNA pathway (24). miRNAs are also used to treat breast cancer (25).

A double strand break (DSB) is a fatal damage caused by ionizing radiation that should be restored; one of the major components in this restoration is RAD51.

Gasparini et al. (26) reported that the increase in miR-155 in breast cancer cells would lead to a reduction in RAD51 levels and would affect the cell response to radiation. Consequently, along with radiation and an increase in miR-155 and consequent decrease in RAD51, cell sensitivity to radiation will increase. The results of the present study indicated increased miR-155 expression in the normal cell line compared to the cancer cell line, which could increase radio-sensitivity and the chance of breast cancer. Although in different doses we observed an increase and decrease. An important finding of miR-155 is the relationship with BRCA1. Chang et al. (27) showed that BRCA1 play an important role in damage to DNA repair and cell cycle. The function of BRCA1 will decrease with cell mutations and increases in miR-155. Based on the results of our research, an increase in miR-155 expression and a decrease in the performance of BRCA1 can lead to an increased chance for breast cancer.

One direct target of miR-21 is CDC25a, which has a tremendous effect on cell repair and increase of checkpoint arrest (28, 29). Also, miR-21 can be use as a radio-resistance, since, with increasing radiation dose and the need for DNA repair, an increase in miR-21 and CDC25a has been observed and this result can be seen in the 100 mGY dose. Although miR-21 is observed in breast cancer, there is no clear pattern of gene target of this miRNA, like PTEN; therefore, additional investigation is necessary (15) .

Let-7a has a key role in proliferation, differentiation and tumour suppression (30). There are contradictory results regarding increases or decreases in let-7a after radiation. The results of a study on lung cancer indicated down-regulation of let-7a. There was up-regulation in the entire let-7a family in a glioma cell line (31). In addition, the p53 path in determining the amount of let-7a expression is interesting after

radiation. In a study after ionizing radiation (IR), we observed down-regulation of let-7a in cells sensitive to radiation, such as the lungs and bone marrow, while there was up-regulation in let-7a in cells resistant to radiation, like the brain and muscles (32). This change could come from several factors, including the type and amount of radiation and paths involved in let-7a regulations (e.g., line 28 and RAS) (33). We observed a significant decrease in let-7a in the cancer cells compared to the normal cells; hence, it can be inferred that there was a chance of breast cancer from the low dose to the high dose of irradiation.

Conclusion

According to the results from various studied that investigated the relationship between miRNAs and radiation, we concluded that irradiation affects breast and other cancers. Our findings showed up-regulation of miR-155 and let-7a with an increase in irradiation dose. It could be said that the probability of breast cancer increases following irradiation in normal and cancer cells. However, we did not see miR-21 up-regulation with increased irradiation. We observed up-regulation and down-regulation at different doses. We could not say that the probability of breast cancer increased after irradiation in miR-21. The current and previous research studies could be a promising approach for the effect of radiation on miRNA expression. The role of miRNAs in breast cancer is suggested in diagnostic radiology and radiotherapy and in radiation accidents.

Acknowledgements

This article is part of a thesis written by Afsaneh Zareh, M.Sc. of radiobiology and radiation protection, and is financially supported by the Research Council of Shiraz University of Medical Sciences (97-01-10-17034). There is no conflict of interest in this study.

Authors' Contributions

A.Z., R.F., G.H.T..; Participated in study design, data collection and evaluation, drafting and statistical analysis. A.Z., R.F., M.A.M.-S.; Contributed extensively in interpretation of the data and the conclusion. A.Z., R.F.; Conducted molecular experiments and RT-qPCR analysis. All authors performed editing and approving the final version of this manuscript for submission, also approved the final draft.

References

1. Bartel DP. MicroRNAs: target recognition and regulatory functions. Cell. 2009; 136(2): 215-233.
2. Yanaihara N, Harris CC. MicroRNA involvement in human cancers. Clin Chem. 2013; 59(12): 1811-1812.
3. Luo H, Yount C, Lang H, Yang A, Riemer EC, Lyons K, et al. Activation of p53 with Nutlin-3a radiosensitizes lung cancer cells via enhancing radiation-induced premature senescence. Lung Cancer. 2013; 81(2): 167-173.
4. Bachour T, Bennett K. The role of microRNAs in breast cancer. J Assoc Genet Technol. 2011; 37(1): 21-28.
5. Masood N, Basharat Z, Khan T, Yasmin A. Entangling relation of micro RNA-let7, miRNA-200 and miRNA-125 with various cancers. Pathol Oncol Res. 2017; 23(4): 707-715.
6. Adhami M, Haghdoost AA, Sadeghi B, Malekpour Afshar R. Candidate miRNAs in human breast cancer biomarkers: a systematic review. Breast Cancer. 2018; 25(2): 198-205.
7. Drusco A, Croce CM. MicroRNAs and cancer: a long story for short RNAs. Adv cancer Res. 2017; 135: 1-24.
8. Jiang S, Zhang HW, Lu MH, He XH, Li Y, Gu H, et al. MicroRNA-155 functions as an OncomiR in breast cancer by targeting the suppressor of cytokine. Cancer Res. 2010; 70(8): 3119-3127.
9. Mattiske S, Suetani RJ, Neilsen PM, Callen DF. The oncogenic role of miR-155 in breast cancer. Cancer Epidemiol Biomarkers Prev. 2012; 21(8): 1236-1243.
10. Kong W, He L, Coppola M, Guo J, Esposito NN, Coppola D, et al. MicroRNA-155 regulates cell survival, growth, and chemosensitivity by targeting FOXO3a in breast cancer. J Biol Chem. 2010; 285(23): 17869-17879.
11. Chen J, Wang BC, Tang JH. Clinical significance of MicoRNA-155 expression in human breast cancer. J Surg Oncol. 2012; 106(3): 260-266.
12. Hwang JH, Voortman J, Giovannetti E, Steinberg SM, Leon LG, Kim YT, et al. Identification of microRNA-21 as a biomarker for chemoresistance and clinical outcome following adjuvant therapy in resectable pancreatic cancer. PLoS One. 2010; 5(5): e10630.
13. Yan LX, Huang XF, Shao Q, Huang MY, Deng L, Wu QL, et al. MicroRNA miR-21 overexpression in human breast cancer is associated with advanced clinical stage, lymph node metastasis and patient poor prognosis. RNA. 2008; 14(11): 2348-2360.
14. Han JG, Jiang YD, Zhang CH, Yang YM, Pang D, Song YN, et al. A novel panel of serum miR-21/miR-155/miR-365 as a potential diagnostic biomarker for breast cancer. Ann Surg Treat Res. 2017; 92(2): 55-66.
15. Qi LQ, Bart J, Tan LP, Platteel I. Expression of miR-21 and its targets (PTEN, PDCD4, TM1) in flat epithelial atypia of the breast in relation to ductal carcinoma in situ and invasive carcinoma. BMC Cancer. 2009; 9(1): 163.
16. Negrini M, Nicoloso MS, Calin GA. MicroRNAs and cancer-new paradigm in molecular oncology. Curr Opin Cell Biol. 2009; 21(3): 470-479.
17. Nicloso MS, Spizzo R, Shimizu M, Rossi S, Calin GA. MicroRNA-the micro steering wheel ot tumor metastase. Nat Rev Cancer. 2009; 9(4): 293-302.
18. Le Quesne JL, Caldas C. MicroRNA and breast cancer. Mol Oncol. 2010; 4(3): 230-241.
19. Heo I, Joo C, Cho J, Ha M, Han J, Kim VN. Lin28 mediates the terminal uridylation of let-7 precursor MicroRNA. Mol Cell. 2008; 32(2): 276-284.
20. Shell S, Park SM, Radjabi AR, Schickel R, Kistner EO, Jewell DA, et al. Let-7 expression defines two differentiation stages of cancer. Proc Natl Acad Sci USA. 2007; 104(27): 11400-11405.
21. Yu F, Yao H, Zhu P, Zhang X, Pan Q, Gong C, et al. let-7 regulates self renewal and tumorigenicity of breast cancer cells. Cell. 2007; 131(6): 1109-11023.
22. Hagan S, Al-Mulla F, Mallon E, Oien K, Ferrier R, Gusterson B, et al. Reduction of Raf-1 kinase inhibitor protein expression correlates with breast cancer metastasis. Clin Cancer Res. 2005; 11(20): 7392-7397.
23. Dieckmann KP, Radtke A, Geczi L, Matthies C, Anheuser P, Eckardt U, et al. Serum levels of MicroRNA-371a-3p (M371 Test) as a new biomarker of testicular germ cell tumors: results of a prospective multicentric study. J Clin Oncol. 2019; 37(16): 1412-1423.
24. Dehghan Kouhestani S, Forouzandeh M, Aghili M. Analysis of microRNAs expression changes in human breast cancer cell lines following exposure to ionizing radiation. Int J Radiat Res. 2018; 16(3): 383-388.
25. Mehrgou A, Akouchekian M. Therapeutic impacts of microRNAs in breast cancer by their roles in regulating processes involved in this disease. J Res Med Sci. 2017; 22: 130.
26. Gasparini P, Lovat F, Fassan M, Casadei L, Cascione L, Jacob NK, et al. Protective role of miR-155 in breast cancer through RAD51 targeting impairs homologous recombination after irradiation. Proc Natl Acad Sci USA. 2014; 111(12): 4536-4541.
27. Chang S, Wang RH, Akagi K, Kim KA, Martin BK, Cavallone L, et al. Tumor suppressor BRCA1 epigenetically controls oncogenic

microRNA-155. Nat Med. 2011; 17(10): 1275-1282.
28. Wang P, Zou F, Zhang X, Li H, Dulak A, Tomko RJ, et al. microRNA-21 negatively regulates Cdc25A and cell cycle progression in colon cancer cells. Cancer Res. 2009; 69(20): 8157-8165.
29. Medema RH, Macůrek L. Checkpoint control and cancer. Oncogene. 2012; 31(21): 2601-2113.
30. Viswanathan SR, Daley GQ. Lin28: A microRNA regulator with a macro role. Cell. 2010; 140(4): 445-449.
31. Chaudhry MA, Sachdeva H, Omaruddin RA. Radiation-induced micro-RNA modulation in glioblastoma cells differing in DNA-repair pathways. DNA Cell Biol. 2010; 29(9): 553-561.
32. Saleh AD, Savage JE, Cao L, Soule BP, Ly D, DeGraff W, et al. Cellular stress induced alterations in microRNA let-7a and let-7b expression are dependent on p53. PLoS One. 2011; 6(10): e24429.
33. Piskounova E, Polytarchou C, Thornton JE, LaPierre RJ, Pothoulakis C, Hagan JP, et al. Lin28A and lin28B inhibit let-7 microRNA biogenesis by distinct mechanisms. Cell. 2011; 147(5): 1066-1079.

Original Article

Coenzyme Q10 Modulates Apoptotic Effects of Chronic Administration of Methadone on NMRI Mouse Hippocampus

Maryam Vaselbehagh, M.Sc.[1], Mehdi Sadegh, Ph.D.[2], Hadi Karami, Ph.D.[3], Saied Babaie, Ph.D.[1], Mohammad Hassan Sakhaie, Ph.D.[1*]

1.Department of Anatomy, Faculty of Medicine, Arak University of Medical Sciences, Arak, Iran
2. Department of Physiology, Faculty of Medicine, Arak University of Medical Sciences, Arak, Iran
3. Department of Molecular Medicine and Biotechnology, Faculty of Medicine, Arak University of Medical Sciences, Arak, Iran

Corresponding Address: P.O.Box: 3848176941, Department of Anatomy, Faculty of Medicine, Arak University of Medical Sciences, Arak, Iran
Email: mh.sakhaie@arakmu.ac.ir

Received: 04/January/2020, Accepted: 11/April/2020

Abstract

Objective: Methadone is one of the widely used drug substances prescribed in treatment of opioid dependence and pain management; however, several studies have shown its neurotoxic effects on individuals and animal models. The purpose of this study was to assess neuroprotective effects of Coenzyme Q10 (CoQ10) on neurotoxicity induced by methadone in hippocampus of adult NMRI male mice.

Materials and Methods: In this experimental study, 48 adult NMRI male mice were randomly divided into 4 groups (n=12 in each) including Methadone, Methadone with sesame oil, Methadone with CoQ10 and saline. The injections of methadone, saline and sesame oil were performed intraperitoneally for 20 days. 24 hours after last injection, half of the animals in each group (n=6) were randomly assessed for evaluating of spatial memory by radial maze. Following behavioral study, animals were sacrificed, and their brains were removed to evaluate pyknotic cells through histological assessment. The remaining were used to study the expression of *Arc, Bax, Bcl-2* and *Bdnf* genes.

Results: Results of the present study showed that daily administration of methadone increased the number of pyknotic neurons in the CA1 hippocampus and altered the expression of *Bax, Bdnf, Arc* and *Bcl-2*. However, it did not alter spatial memory comparing to saline group. CoQ10 treatment significantly reduced the number of pyknotic cells and expression of *Bax, Bdnf, Arc* when compared to the vehicle group treated by sesame oil. However, the expression of Bcl-2 significantly increased as a result of CoQ10 treatment.

Conclusion: CoQ10 reduced the neuronal damage caused by methadone in the hippocampus CA1.

Keywords: Apoptosis, *Bdnf*, CoQ10, Hippocampus, Methadone

Cell Journal(Yakhteh), Vol 23, No 5, October 2021, Pages: 538-543

Citation: **Vaselbehagh M, Sadegh M, Karami H, Babaie S, Sakhaie MH. Coenzyme Q10 modulates apoptotic effects of chronic administration of methadone on NMRI mouse hippocampus. Cell J. 2021; 23(5): 538-543. doi: 10.22074/cellj.2021.7384.**

Introduction

Methadone is a synthetic opioid derivative prescribed for treatment of pain syndrome and opioid-related dependencies to avoid withdrawal symptoms (1). Despite the extensive therapeutic use of methadone, some studies have shown it has destructive and harmful effects on perception and cognition in individuals (2).

It's been shown that, the expression of some genes is changed within the body as a result of drug abuse (3). *Bdnf* is a member of the neurotrophic factor family, which plays a role in regulating survival and differentiation of neurons in the central and peripheral nervous system (4). *Arc*, a member of the immediate-early gene (IEG) family, is another neuroplastic protein that plays a vital role in learning and memory-related process (5). *Arc* causes a series of changes in the pattern of neuronal activity relative to synaptic plasticity and thus, optimizes the storage of information in the nervous system (6). Long-term consumption of methadone increases the expression of pro-apoptotic proteins in the cerebral cortex and hippocampus (7, 8), leading to cell death activation through mitochondrial-mediated pathway, and ultimately dendritic atrophy, abnormal neurogenesis, and neurodegeneration (9). Members of *Bcl-2* family proteins have a crucial role in survival and cell death regulation, from which *Bax* is an important proapoptotic player that induces mitochondrial-mediated pathway of apoptosis via oligomerization and induction of mitochondrial membrane disruption (10).

In neurodegenerative disease oxidative stress disrupts glutathione homeostasis and produces reactive oxygen species (ROS) (11). An excessive increase in ROS generation and a reduction in defensive antioxidants lead to oxidative damage to DNA, lipids and proteins and therefore leading to cell damage (12). Neuronal cells in CNS have a lower antioxidant capacity than glia,

that makes them more susceptible to such injuries (13, 14) and hence increasing the antioxidant defense could provide neuroprotective effects. CoQ10 is a natural fat-soluble antioxidant that found in cellular organelles such as peroxisome, lysosomes, Golgi vesicles, and inner mitochondrial membrane (15, 16). It has been considered as a neuroprotective agent for treatment of neurodegenerative diseases. Q10 reduces the damage to hippocampal neurons (17), prevents nerve damage, and inhibits lipid peroxidation by reducing radical species production (18).

Because of the extensive use of methadone in the treatment of addiction and its negative effects on learning disruption and neuronal damage in the brain, the aim of this study was to evaluate the neuroprotective potential of Q10 as a complementary therapy in reducing methadone-induced neuronal damage.

Materials and Methods

Animals and treatment groups

All experimental procedures were approved by the Review Board and Ethics Committee of Arak University of Medical Sciences (IR.ARAKMU.REC.1395.318). Forty eight adult NMRI male mice (30-35 g) were obtained from Razi Institute (Karaj, Iran). Animals were housed in 12-hour light/dark cycles and water and food were freely available. Mice were assigned into 4 following groups (n=12 in each) and treatments were administrated for 20 consecutive days: i. Saline group, ii. Methadone group: received methadone 10 mg/kg (i.p) daily, iii. Methadone+sesame oil group; received methadone 10 mg/kg (i.p) following the injection of sesame oil 0.2 ml/day (i.p), and iv. Methadone+Q10 group: received methadone 10 mg/kg (i.p) following the injection of Q10 dissolved in sesame oil 10 mg/kg daily for 20 consecutive days.

Twenty four hours after the last injection, mice from each group were randomly divided into 2 subgroups: half of them were assigned for behavioral study, then they were sacrificed and their brains were processed for morphological studies of pyknotic cells. Other half were used for gene expression analyses of *Arc, Bax, Bcl-2* and *Bdnf*.

Histological study

The animals were killed by cervical dislocation, the brains were removed and fixed overnight in formalin10%. After paraffin embedding, coronal sections with 5µm thickness were prepared from -1.5 to -2.5 mm post bregma (in accordance with the mouse brain atlas, 2004). Sections were then dehydrated in the ascending alcohols series, stained with cresyl violet and mounted on glass slides. The slides were examined under a light microscope using an x40 objective lens (BX51, Japan) and images were captured by a digital camera (Olympus, DP 11, Japan). The number of pyknotic cells in each CA1 hippocampus were counted in three random areas of each section and five sections were analyzed for each sample. Pyknotic cells were characterized by their darkly stained condensed chromatin, a smaller volume and light or absent cytoplasm.

Spatial learning test with radial arm maze

For assessment of memory and learning task, a radiating eight black Plexiglas arms maze with a central round platform was used as previously described with few modifications (19). Briefly the diameter of arms was 50×15×15 cm and each of arms numbered from 1 to 8. There was a removable door in the entrance of every arm of maze and at the end of it a well for hiding of food bite. Various intra and extra maze visual cues were sited through the testing room to help the animal for spatial memory task. Trials were performed daily 9:00 to 12:00 am. Habituation phase was done one day before the training session in which each mouse was placed in the RAM for adjustment of apparatus environment.

During the training phase, the animal was placed to the central platform and allowed for 30 seconds to become familiar with the place. After that the entry of all doors were opened and animal was allowed to freely explore the maze for 5 minutes. Four fixed arms were baited, and the others arranged in the same configuration throughout the entire experiment. The final time of spatial memory experiment were calculated when the mouse visited all four baited arms once or after 5 minutes, since the start of the trial.

Training session was done daily, for 5 continuous days. Access to food was restricted two hours before each trial. Following each trial, the apparatus was cleaned with 40% ethanol to avoid of olfactory cues.

To evaluate spatial learning and memory, two types of errors were calculated: i. Working memory errors (WME): the number of entries into a baited arm during each trial session. ii. Reference memory errors (RME): the number of entries into a non- baited arm during each trial.

Gene expression study

After decapitation, the hippocampus was dissected and stored at nitrogen -80˚C until use. Total RNA was extracted using RNA plus extraction kit (Sinaclon, Iran). Three microgram RNA was reverse transcribed using oligo-dT primer (Yekta Tajhiz Azma, Iran) and reverse transcriptase (Yekta Tajhiz Azma, Iran) based on manufacturer's protocol. The reaction mixtures were incubated at 42˚C for 60 minutes and then inactivated at 70˚C for 10 minutes. Resulting cDNA was subjected to quantitative real-time polymerase chain reaction (q-PCR) by using SYBR1 Green Mix (Yekta Tajhiz Azma, Iran) on a Light Cycler 96 System (Roche Diagnostics GmbH, Germany). The following conditions were used for q-PCR: initial heating for 10 minutes at 95˚C, 45 cycles of amplification, each

composed of 15 seconds at 95˚C, 60 seconds at the annealing temperature, and 60 seconds at 72˚C. The annealing temperatures were 55˚C, 53˚C, 53˚C, 53˚C and 54˚C for *β-actin*, *Arc, Bdnf, Bcl-2* and *Bax,* respectively. Reactions were performed in triplicates. *β-actin* was used as an endogenous control to minimize the effect of sample variations. The fold changes in gene expression were calculated using ΔΔCt method. Primer were designed using Allele ID 7 software (Table 1).

Table 1: Designed primers for the gene expression study

Gene name	Primer sequence (5´-3´)	Amplicon size
Arc	F: ACGACACCAGGTCTCAAG	159
	R: GCACCTCCTCTTTGTAATCC	
Bax	F: CTGAGCTGACCTTGGAGC	413
	R: GACTCCAGCCACAAAGATG	
Bcl-2	F: CACCCCTGGCATCTTCTCCT	349
	R: GACTCCAGCCACAAAGATG	
Bdnf	F: CACCCCTGGCATCTTCTCCT	118
	R: GTTGACGCTCCCCACACACA	
β-actin	F: GCGCCCATGAAAGAAGTAAA	536
	R: GGGCCGCTCTAGGCACCAA	

Statistical analysis

Data are presented as mean ± SEM. Statistical analyses were performed using GraphPad Prism V8.4.0 (GraphPad Software, San Diego, CA, USA). One-way analysis of variance (ANOVA) was used for histological, WME, RME and gene expression data, followed by Bonferroni post-hoc test for further pair-wise comparisons. Latency of spatial learning was analyzed by repeated measures ANOVA followed by Bonferroni post-hoc test. P<0.05 was regarded as statistically significant.

CoQ10 reduced the number of Methadone-induced pyknotic cells in CA1

As demonstrated in Figure 1, the numbers of pyknotic cells in CA1 significantly increased in the methadone group when compared to the control group (treated with saline) (P<0.001). Daily administration of CoQ10 to the mice treated with Methadone, significantly reduced the effect of methadone on pyknotic cells number (P<0.05). In addition, injection of Sesame oil without CoQ10 to the mice treated with Methadone showed no significant effects.

CoQ10 did not alter the effects of methadone on spatial memory

RMA analyses demonstrated there were no significant differences in mean values of latency to finish the four baited arms ($F_{12, 60}$=1.4, Fig.2A) among experimental groups. Similarly, the mean number of entries into the baited arm during the trials (working memory errors, Fig.2B) and mean number of entries into a non -baited arm (reference memory errors, Fig.2C) remained unchanged.

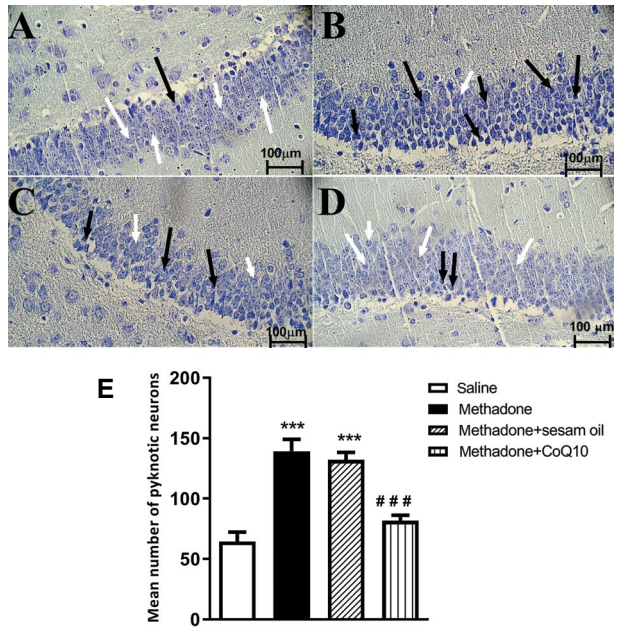

Fig.1: Nissl staining showed CoQ10 reduced the number of pyknotic cells in CA1 area. Statistical analysis demonstrated a significant increase of the pyknotic cells in methadone and methadone+sesame oil groups. CoQ10 significantly decreased pyknotic cells. Black arrows show pyknotic cells and white arrows show normal neurons. **A.** Saline, **B.** Methadone, **C.** Methadone+sesame oil, **D.** Methadone+CoQ10 group (scale bar: 100 µm). **E.** Mean values of the experimental groups. ***; P<0.001 compared with saline, ###; P<0.05 compared with methadone. All data are expressed as mean ± SEM.

CoQ10 modified the effects of methadone on hippocampal gene expression

The results of quantitative PCR showed a significant enhancement in relative expression of *Bdnf* and *Arc* in all groups received methadone compared to the saline group (P<0.05). However, CoQ10 treatment significantly inhibited upregulation of both genes (P<0.05) in comparison with methadone group and methadone+ sesame oil group (Fig.3A, B).

The relative expression of *Bcl-2* was significantly reduced in methadone group compared to the saline group (P<0.05), however; the relative expression of *Bax* was significantly increased (P<0.05). Treated animals with CoQ10 showed significant increase in *Bcl-2* expression compared to methadone group and methadone+sesame

oil (P<0.05, Fig.3C). In addition, relative expression of *Bax* was significantly reduced in methadone+CoQ10 group in comparison with methadone group and methadone+sesame oil group (P<0.05, Fig.3D). Also, *Bax/Bcl-2* ratio demonstrate a significant increase in the methadone group and methadone+sesame oil group compared to Saline group while CoQ10 administration with methadone significantly reduced this effect (P<0.01, Fig.3E).

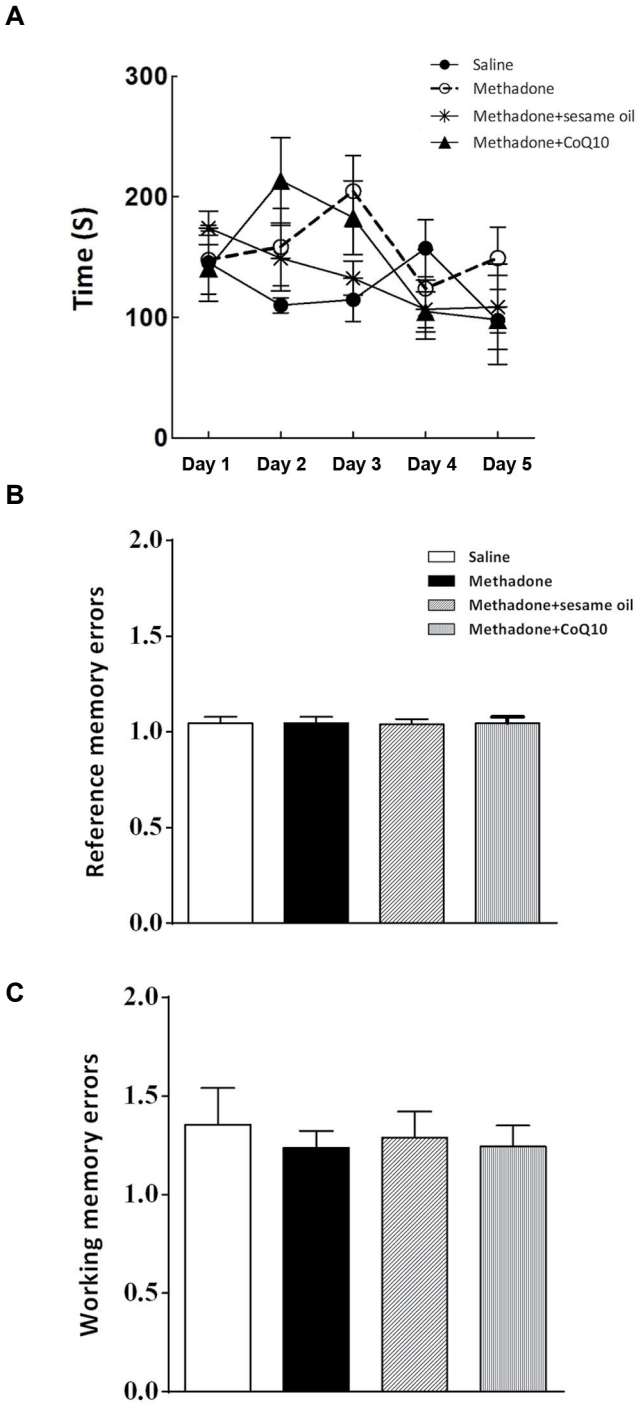

Fig.2: CoQ10 did not change the effects of methadone on spatial memory. **A.** Repeated measured ANOVA analysis showed no significant differences among experimental groups in latency. One-way ANOVA showed no significant differences among experimental groups in **B.** Working memory and **C.** Reference memory errors. The data are presented as mean ± SEM.

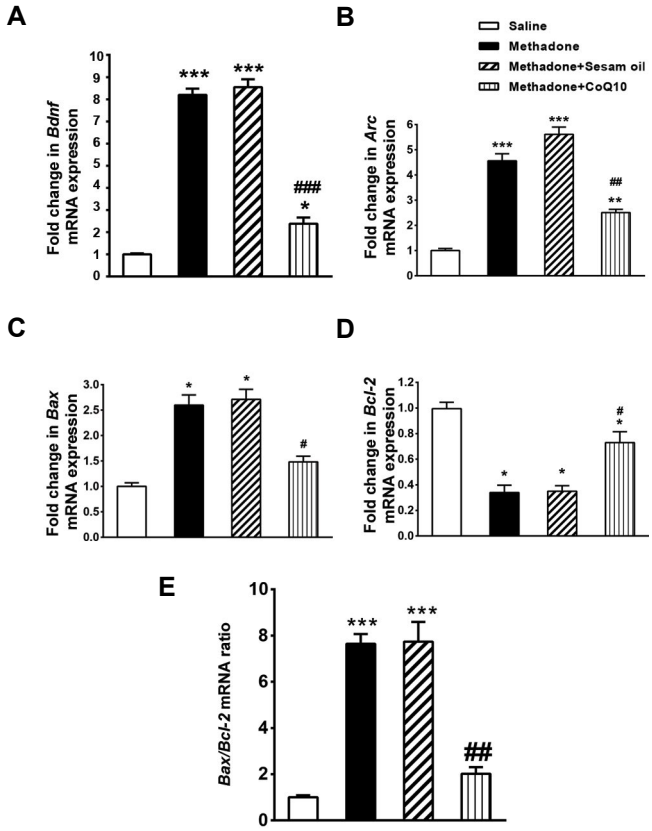

Fig.3: CoQ10 modified the effects of methadone on hippocampal gene expression. **A-C.** The relative expression of *Bdnf*, *Arc* and *Bax* in methadone group showed a significant increase compared to the saline group (P<0.001). **D.** However, relative expression of *Bcl-2* in methadone group showed a significant decrease compared to the saline group (P<0.01). **E.** In addition, *Bax/Bcl2* mRNA ratio significantly increased by methadone. Administration of CoQ10 following methadone significantly attenuated these effects. All data are expressed as mean ± SEM. *; P<0.05: relative to the saline group, **; P<0.01: relative to the saline group, ***; P<0.001: relative to the saline group, #; P<0.05: relative to methadone group, ##; P<0.01: relative to methadone group, and ###; P<0.001: relative to methadone group.

Discussion

Results of the present study suggested that chronic administration of methadone led to an increase in number of pyknotic cells in CA1 area of hippocampus, while did not affect spatial memory assessed by radial maze analysis. In addition, the rate of mRNA expression of *Bax* gene increased, while the expression of anti-apoptotic gene *Bcl-2* declined. Methadone administration also increased the expression of the *Bdnf* and *Arc* genes. CoQ10 significantly reduced pyknotic cells and *Bax* gene expression, butincreased gene expression of *Bcl-2, Bdnf* and *Arc*.

Perez-Alvarez et al. (20) examined the effects of methadone on mitochondria in the SH-SY5Y cells and showed that high accumulation of methadone resulted in cell death.Therefore, the use of opiates may also lead to irreversible neuronal damage and death of neurons. In agreement with this result our histological finding indicated increased pyknotic cells in the CA1 hippocampus after methadone administration.

Friesen et al. (21) showed that methadone inhibited

proliferation of myeloid leukemia cell line (HL-60) and induced cell death through caspase 3, 9 activation and diminishing of anti-apoptotic genes expression. Changes in calcium homeostasis in the presence of methadone can induce ROS production and finally cell death (20). Therefore, we aimed to evaluate the protective effects of coenzyme Q10 (CoQ10) against the adverse effects of methadone.

In the spatial memory test, our results showed no significant difference in the learning capacity of mice chronically treated with methadone when compared to the control group. This finding was consistent with the results of a study conducted by Cummins et al. (22) in which, chronic use of methadone showed no statistically significant difference in memory tests.

In agreement with our findings Sadegh et al. (23) evaluated the effects of repeated injections of morphine on spatial memory and found no significant differences among experimental groups. However, they had shown hippocampus CA1 synaptic plasticity changed in morphine dependent rats due to chronic morphine consumption (24). Hence, it's possible that methadone, similar to morphine, also affect the hippocampal neurons with no sign of behavioral learning.

Our histological findings showed increased number of pyknotic cells in the hippocampus CA1 of methadone administrated animals suggesting cell death induction. Previous molecular studies have shown chronic administration of morphine and other opiates deceased the number of hippocampal progenitor cells and newly BrdU positive cells in dentate gyrus (25, 26). Opiates might directly act on the progenitor cell population. In another study, TUNEL assay analysis indicated that chronic treatment of high dose morphine and it's withdrawal, induced apoptotic cell death in the brain tissue (27).

Interestingly, the results of our study indicated that CoQ10 treatment can reduce the number of pyknotic cells in hippocampal CA1 following hippocampal methadone injury. Natural antioxidants, such as CoQ10, are effective in improving mitochondrial complexes dysfunction and inhibition of oxidative stress damages. Hwang et al. (28) demonstrated that pretreatment of CoQ10 significantly prevented motor deterioration in a rat model of spinal cord ischemia-reperfusion damage, as a result of reduction in oxidative stress and neuronal apoptosis. Similarly, CoQ10 pretreatment could alleviate hippocampal neuronal loss and aberrant mossy fiber induced by kainic acid as a model of temporal lobe epilepsy referred to its potential to modulate the production of oxidative stress (29). Neuroprotective function of CoQ10 is associated with its scavenging capacity on free radicals (30). In our study methadone increased *Bdnf* gene expression in hippocampal tissue of methadone group compared to the saline group. In line with these results, Baydyuk proposed that *Bdnf* plays a vital role in maintenance and proper function of neuronal population. It also improves the survival of the immature striatal neurons and facilitates establishment of striatal connections during brain development. Furthermore it plays a crucial role in opioid-induced plasticity (31, 32).

Analysis of a human study indicated that the serum levels of *Bdnf* increased in the methadone maintenance treatment patients compared to healthy controls (33). In alignment with our study Rouhani et al. showed morphine administration increased the expression of *Bdnf* gene in hippocampus of rats with a dose dependent manner (3).

The mechanism of the action of multiple protective effects of *Bdnf* against brain injury are related to its antiapoptosis, antiinflammation and antineurotoxicity effects (34). Therefore, the increased level of hippocampal *Bdnf* in our study could be a protective response triggering as a result of neuronal cell damages. Treatment with CoQ10 could reduce the level of *Bdnf* gene expression to almost the baseline.

The results of this study showed that methadone increased the expression of *Bax* and reduced the expression of *Bcl-2* when compared to the saline group. In consistent with our results, Tramullas et al. demonstrated that the chronic consumption of methadone and heroin in animals increased pro-apoptotic proteins and their activity in the cortex and hippocampus (7, 35). But after treatment with CoQ10, the expression of *Bax* decreased and the expression of *Bcl-2* increased. Similar to our study, Gholipour et al. (17) showed that CoQ10 could reduce apoptosis induced by methamphetamine through reducing apoptotic factors and increasing the anti-apoptotic pathways in the rat brain. Lee et al. (36) provided evidence that CoQ10 promotes survival in ischemic mouse retinal cells by inhibiting oxidative stress and blocking the *Bax/Bad* mediated mitochondrial apoptotic pathway. CoQ10 is also able to activate the phosphatidylinositol-3-kinases (PI3K) pathway in neurons and significantly reduces the amount of ROS production (37). As a limitation of this study we did not asses the ROS alterations in our experimental groups and it should be considered for the future studies.

In summary, for the first time our results showed methadone increased hippocampal gene expression of *Arc* and CoQ10 when administrated with methadone was able to prevent this effect. As an immediate early gene, *Arc* contributes to the synaptic plasticity and memory formation. Previous studies have shown that chronic morphine administration increased mRNA expression of immediate early genes such as *Arc* in the hippocampus (3, 38). Also, it has been shown that *Arc* is able to block cellular pathways associated with apoptosis (13). Therefore, it is possible that increased expression of *Arc* occurring following chronic methadone administration works as a protective feedback mechanism against the apoptotic effects of methadone. In addition, CoQ10 might preventthe expression of *Arc* gene by blocking the apoptotic effects of methadone.

Conclusion

Finding of our study showed that CoQ10 reduced the neuronal damage and complications of methadone on hippocampus CA1, probably by modifying the expression of pro-apoptotic and anti-apoptotic genes. CoQ10 might be considered as complementary therapy to prevent

adverse effects of methadone on hippocampus.

Acknowledgments

This study was financially supported by Arak University of Medical Sciences. There is no conflict of interest in this study.

Authors' Contributions

M.V., M.H.S., M.S., H.K.; Participated in study design, data collection and evaluation, drafting and statistical analysis. M.V., S.B., M.S.; Performed behavioral study and prepared histological study to this component of the study. M.H.S., M.S., H.K.; Contributed extensively to interpretation of the data and the conclusion. M.V., H.K.; Conducted molecular experiments and RT-qPCR analysis. All authors performed editing and approving the final version of this manuscript for submission, also approved the final draft.

References

1. Sankararaman A, Masiulis I, Richardson DR, Andersen JM, Mørland J,Eisch AJ. Methadone does not alter key parameters of adult hippocampal neurogenesis in the heroin-naïve rat. Neurosci Lett. 2012; 516(1): 99-104.
2. Ahmad-Molaei L, Hassnian-Moghaddam H, Farnaghi F, Tomaz C, Haghparast A. Delay-dependent impairments in memory and motor functions after acute methadone overdose in rats. Front Pharmacol. 2018; 9: 1023.
3. Rouhani F, Khodarahmi P, Naseh V. NGF, BDNF and Arc mRNA expression in the hippocampus of rats after administration of morphine. Neurochem Res. 2019; 44(9): 2139-2146.
4. Kowiański P, Lietzau G, Czuba E, Waśkow M, Steliga A, Moryś J. BDNF: a key factor with multipotent impact on brain signaling and synaptic plasticity. Cell Mol Neurobiol. 2018; 38(3): 579-593.
5. Gallo FT, Katche C, Morici JF, Medina JH, Weisstaub NV. Immediate early genes, memory and psychiatric disorders: focus on c-Fos, Egr1 and Arc. Front Behav Neurosci. 2018; 12: 79.
6. Bramham CR, Alme MN, Bittins M, Kuipers SD, Nair RR, Pai B, et al. The Arc of synaptic memory. Exp Brain Res. 2010; 200(2): 125-140.
7. Tramullas M, Martínez-Cué C, Hurlé MA. Chronic methadone treatment and repeated withdrawal impair cognition and increase the expression of apoptosis-related proteins in mouse brain. Psychopharmacology. 2007; 193(1): 107-120.
8. Nouri F, Afarinesh MR, Sheibani V, Foroumadi A, Esmaeili Mahani S, Mahmoudi M, et al. Concomitant abuse of methadone and methamphetamine could impair spatial learning and memory in male rats. Learn Motiv. 2019; 65: 43-51.
9. Wang Y, Li W, Li Q, Yang W, Zhu J, Wang W. White matter impairment in heroin addicts undergoing methadone maintenance treatment and prolonged abstinence: a preliminary DTI study. Neurosci Lett. 2011; 494(1): 49-53.
10. Renault Thibaud T, Floros Konstantinos V, Elkholi R, Corrigan KA, Kushnareva Y, Wieder Shira Y, et al. Mitochondrial shape governs bax-induced membrane permeabilization and apoptosis. Mol Cell. 2015; 57(1): 69-82.
11. Johnson WM, Wilson-Delfosse AL, Mieyal J. Dysregulation of glutathione homeostasis in neurodegenerative diseases. Nutrients. 2012; 4(10): 1399-1440.
12. Salim S. Oxidative stress and the central nervous system. J Pharmacol Exp Ther. 2017; 360(1): 201-205.
13. Bell KFS, Al-Mubarak B, Martel MA, McKay S, Wheelan N, Hasel P, et al. Neuronal development is promoted by weakened intrinsic antioxidant defences due to epigenetic repression of Nrf2. Nat Commun. 2015; 6: 7066.
14. Fernandez-Fernandez S, Almeida A, Bolanos JP. Antioxidant and bioenergetic coupling between neurons and astrocytes. Biochem J. 2012; 443(1): 3-11.
15. Sikorska M, Lanthier P, Miller H, Beyers M, Sodja C, Zurakowski B, et al. Nanomicellar formulation of coenzyme Q10 (Ubisol-Q10) effectively blocks ongoing neurodegeneration in the mouse 1-methyl-4-phenyl-1, 2, 3, 6-tetrahydropyridine model: potential use as an adjuvant treatment in Parkinson's disease. Neurobiol Aging. 2014; 35(10): 2329-2346.
16. Balakrishnan P, Lee BJ, Oh DH, Kim JO, Lee YI, Kim DD, et al. Enhanced oral bioavailability of Coenzyme Q10 by self-emulsifying drug delivery systems. Int J Pharm. 2009; 374(1-2): 66-72.
17. Gholipour F, Shams J, Zahiroddin A. Protective effect of coenzyme q10 on methamphetamine-induced apoptosis in adult male rats. Novel Biomed. 2017; 5(3): 127-132.
18. Sakhaie MH, Soleimani M, Pirhajati V, Soleimani Asl S, Madjd Z, Mehdizadeh M. Coenzyme Q10 ameliorates trimethyltin chloride neurotoxicity in experimental model of injury in dentate gyrus of hippocampus: a histopathological and behavioral study. Iran Red Crescent Med J. 2016; 18(8).
19. Schrott LM, Franklin LTM,Serrano PA. Prenatal opiate exposure impairs radial arm maze performance and reduces levels of BDNF precursor following training. Brain Res. 2008; 1198: 132-140.
20. Perez-Alvarez S, Cuenca-Lopez MD, de Mera RMMF, Puerta E, Karachitos A, Bednarczyk P, et al. Methadone induces necrotic-like cell death in SH-SY5Y cells by an impairment of mitochondrial ATP synthesis. Biochim Biophys Acta. 2010; 1802(11): 1036-1047.
21. Friesen C, Roscher M, Alt A, Miltner E. Methadone, commonly used as maintenance medication for outpatient treatment of opioid dependence, kills leukemia cells and overcomes chemoresistance. Cancer Res. 2008; 68(15): 6059-6064.
22. Cummins E, Allen CP, Ricchetti A, Boughner E, Christenson K, Haines M, et al. The effects of acute and chronic steady state methadone on memory retrieval in rats. Psychopharmacology (Berl). 2012; 222(2): 225-235.
23. Sadegh M, Fathollahi Y, Naghdi N, Semnanian S. Morphine deteriorates spatial memory in sodium salicylate treated rats. Eur J Pharmacol. 2013; 704(1-3): 1-6.
24. Sadegh M, Fathollahi Y, Semnanian S. The chronic treatment in vivo of salicylate or morphine alters excitatory effects of subsequent salicylate or morphine tests in vitro in hippocampus area CA1. Eur J Pharmacol. 2013 ; 721(1-3): 103-108
25. Zhang Y, Xu C, Zheng H, Loh HH, Law PY. Morphine modulates adult neurogenesis and contextual memory by impeding the maturation of neural progenitors. PLoS One. 2016; 11(4): e0153628.
26. Zhang Y, Loh HH, Law PY. Effect of opioid on adult hippocampal neurogenesis. Sci World J. 2016; 2016.
27. Emeterio EPS, Tramullas M, Hurlé MA. Modulation of apoptosis in the mouse brain after morphine treatments and morphine withdrawal. J Neurosci Res. 2006; 83(7): 1352-1361.
28. Hwang JY, Min SW, Jeon YT, Hwang JW, Park SH, Kim JH, et al. Effect of coenzyme Q10 on spinal cord ischemia-reperfusion injury. J Neurosurg Spine. 2015; 22(4): 432-438.
29. Baluchnejadmojarad T, Roghani M. Coenzyme q10 ameliorates neurodegeneration, mossy fiber sprouting, and oxidative stress in intrahippocampal kainate model of temporal lobe epilepsy in rat. J Mol Neurosci. 2013; 49(1): 194-201.
30. Hargreaves IP. Coenzyme Q10 as a therapy for mitochondrial disease. Int J Biochem Cell Biol. 2014; 49: 105-111.
31. Baydyuk M, Xu B. BDNF signaling and survival of striatal neurons. Front Cell Neurosci. 2014; 8254.
32. Cowansage KK, LeDoux JE, Monfils MH. Brain-derived neurotrophic factor: a dynamic gatekeeper of neural plasticity. Curr Mol Pharmacol. 2010; 3(1): 12-29.
33. Tsai MC, Huang TL. Brain-derived neurotrophic factor (BDNF) and oxidative stress in heroin-dependent male patients undergoing methadone maintenance treatment. Psychiatry Res. 2017; 249: 46-50.
34. Chen A, Xiong LJ, Tong Y, Mao M. The neuroprotective roles of BDNF in hypoxic ischemic brain injury. Biomed Rep. 2013; 1(2): 167-176.
35. Tramullas M, Martíne z-Cué C, Hurlé MA. Chronic administration of heroin to mice produces up-regulation of brain apoptosis-related proteins and impairs spatial learning and memory. Neuropharmacology. 2008; 54(4): 640-652.
36. Lee D, Kim KY, Shim MS, Kim S, Ellisman MH, Weinreb RN, et al. Coenzyme Q10 ameliorates oxidative stress and prevents mitochondrial alteration in ischemic retinal injury. Apoptosis. 2014; 19(4): 603-614.
37. Choi H, Park HH, Koh SH, Choi NY, Yu HJ, Park J, et al. Coenzyme Q10 protects against amyloid beta-induced neuronal cell death by inhibiting oxidative stress and activating the P13K pathway. Neurotoxicology. 2012; 33(1): 85-90.
38. Yip KW, Reed JC. Bcl-2 family proteins and cancer. Oncogene. 2008; 27(50): 6398-6406.

Original Article

The Role of MicroRNA 143 and MicroRNA 206 in The Regulation of Apoptosis in Mouse Lukemia Cancer Cells and Spermatogonial Cells

Azar Shams, Ph.D.[1, 2], Ronak Shabani, Ph.D.[1, 2], Mohammad Najafi, Ph.D.[3], Mahdi Karimi, Ph.D.[4], Vahid Pirhajati, Ph.D.[5], Mohammad Asghari Jafarabadi, Ph.D.[6, 7], Hamid Reza Asgari, Ph.D.[2], Chad B. Maki, D.V.M.[8], Seyed Mohsen Razavi, M.D.[9], Morteza Koruji, Ph.D.[1, 2*]

1. Stem Cell and Regenerative Medicine Research Center, Iran University of Medical Sciences, Tehran, Iran
2. Department of Anatomical Sciences, School of Medicine, Iran University of Medical Sciences, Tehran, Iran
3. Department of Biochemistry, School of Medicine, Iran University of Medical Sciences, Tehran, Iran
4. Department of Nanotechnology, School of Medicine, Iran University of Medical Sciences, Tehran, Iran
5. Neuroscience Research Center, Iran University of Medical Sciences, Tehran, Iran
6. Department of Statistics and Epidemiology, School of Medicine, Zanjan University of Medical Sciences, Zanjan, Iran
7. Center for The Development of Interdisciplinary Research in Islamic Sciences and Health Sciences, Tabriz University of Medical Sciences, Tabriz, Iran
8. VetCell Therapeutics USA, 2917 Daimler Street, Santa Ana CA 92705, USA
9. Oncopathology Research Center, Faculty of Medicine, Iran University of Medical Sciences, Tehran, Iran

**Corresponding Address: P.O.Box: 14665354, Stem Cell and Regenerative Medicine Research Center, Iran University of Medical Sciences, Tehran, Iran*
Email: koruji.m@iums.ac.ir

Received: 11/May/2020, Accepted: 21/July/2020

Abstract

Objective: In cancer treatments, smart gene delivery via nanoparticles (NPs) can be targeted for cancer cells, while concurrently minimizing damage to healthy cells. This study assessed the efficiency of poly lactic-co-glycolic acid (PLGA)-miR 143/206 transfection on apoptosis in mouse leukemia cancer cells (El4) and spermatogonial stem cells (SSCs).

Materials and Methods: In this experimental study, neonatal mouse spermatogonia cells and EL4 cancer cell lines were used. MicroRNA-PLGA NPs were prepared, characterized, and targeted with folate. Several doses were evaluated to obtain a suitable miR dose that can induce appropriate apoptosis in EL4 cells, while not harming SSCs. Cells were treated separately at 3 doses of each miR (for miR 143, doses of 25, 50 and 75 nmol and for miR 206, doses of 50, 100 and 150 nmol). The experiments were performed at 24, 48 and 72 hours. Viability and apoptosis were investigated by MTT and Annexin Kits.

Results: Based on MTT assay results, the optimal dose of miR 143 was 75 nmol (59.87 ± 2.85 % SSC and 35.3 ± 0.78 % EL4) (P≤0.05), and for miR 206, the optimal dose was 150 nmol (54.82 ± 6.7 % SSC and 33.92 ± 3.01% EL4) (P≤0.05). The optimal time was 48 hours. At these doses, the survival rate of the EL4 cells was below the half maximal inhibitory concentration (IC_{50}) and SSC survival was above 50%. Annexin V staining also confirmed the selected doses (for miR 143 total apoptosis was 6.62% ± 1.8 SSC and 37.4% ± 4.2 EL4 (P≤0.05), and miR 206 was (10.98% ± 1.5 SSC and 36.4% ± 3.7 EL4, P≤0.05).

Conclusion: Using intelligent transfection by NPs, we were able to induce apoptosis on EL4 cells and maintain acceptable SSC survival rates.

Keywords: Apoptosis, Cancer, MicroRNA, Poly Lactic-Co-Glycolic Acid, Smart Gene Delivery

Cell Journal(Yakhteh), Vol 23, No 5, October 2021, Pages: 544-551

Citation: Shams A, Shabani R, Najafi M, Karimi M, Pirhajati V, Asghari Jafarabadi M, Asgari HR, Maki CB, Razavi SM, Koruji M. The role of MicroRNA 143 and MicroRNA 206 in the regulation of apoptosis in mouse lukemia cancer cells and spermatogonial cells. Cell J. 2021; 23(5): 544-551. doi: 10.22074/cellj.2021.7606.

Introduction

Chemotherapy and radiotherapy cause serious damage to spermatogonial stem cells (SSCs), resulting in early loss of SSCs and temporary infertility. The proportion of azoospermic as late effect of cancer was reported 18%, specifically for leukaemias (1).

Today, there are promising ways to manage the consequences of infertility in adulthood such as transplantation of SSCs (2) or testicular tissue transplantation (3). Adult males will have a chance to maintain fertility through ejaculation and cryogenic preservation before starting treatment, but this is not an option in pre-puberty. A promising method to preserve fertility in children with cancer is via testicular biopsy before the onset of cancer treatment, followed by isolation, proliferation, maintenance and transplantation (4, 5). But, a major concern with this method is the possibility of tissue contamination with cancer cells which introduces the risk of recurrence of the cancer (6, 7). At this time, magnetic-activated cell sorting (MACS) and fluorescence-

activated cell sorting (FACS) are the most utilized techniques to eliminate cancerous cells, but they are not sensitive enough to completely eliminate tumor cells (8). Because of different spermatogonial cell markers as well as the variability of cell size, the efficiency of MACS has lessened and the survivability of cells with this method is questionable (9). Therefore, rather than focusing on positive SSC selection, the development of new methods for eliminating cancer cells can provide a more effective solution.

Nanoparticles (NPs), which have the ability to deliver targeted therapies to specific cell types through their structural changes and physical reformation, (change in their shape, size, and physical and chemical properties), have increased the success rate of a new therapeutic strategy (10). Many microRNAs (MiRs) are used to induce apoptosis in cancer cells. MiRs are subgroups of non-coding RNAs that are about 20-25 nucleotides long and affect the expression of genes after transcription, among these MiR 143 and MiR 206 play a more prominent role. Many studies have shown the effects of these MiRs on induction of apoptosis in cervical cancer cells (11), oral squamous cells (12) and human epithelial cells (13). Transfection of MiRs via NPs in order to induce apoptosis has been very promising. Among the NPs, poly lactic-co-glycolic acid (PLGA), due to its high biocompatibility and bioavailability, non-toxicity, non-immunogenicity and food and drug administration (FDA) approval, is used extensively (14). In addition, targeting drug carriers to cancer cells can increase treatment efficacy. Conjugated NPs with folic acid can facilitate the entry of NPs into cells (15). Cancer cells have large amounts of folic acid receptors on the surface of their cell membranes, which makes it easier to target NPs to this type of cell as compared with normal or non-cancerous cells (16).

In human testicular biopsy samples, there is no threshold for the risk of recurrence in the form of a transplant, and this ambiguity requires more sensitivity to clean up and purify the SSCs. So far, no studies have measured the effects of these apoptotic inducers on cancer and spermatogonia cells from a fertility perspective. Therefore, we assessed the efficiency of PLGA- MiR transfection on apoptosis in mouse leukemia cancer cells (El4 cells) and SSCs to determine the optimal effective dose to eliminate EL4 cells, while maintaining adequate SSC viability.

Materials and Methods

In this experimental study, MiR 143 and MiR 206, including primer and fluorescent marker (FAM), were purchased from pishgam co. Sequence data for these have been submitted to the GenBank databases under accession numbers (Mir 206: MI0000490 , Mir 143: NR_029684). PLGA (Resomer RG502H), with a 50:50 mole ratio of glycolic acid to lactic acid and a molecular weight of 12,000 g/mol and polyvinyl alcohol (89 mol% hydrolyzed) (Sigma, St Louis, MO, USA) same as previous study (17).

Fifty neonatal NMRI mice 3-6 days were used to extract spermatogonia cells. The research was approved by the Research Ethics Committee of Iran University of Medical Sciences (IR.IUMS.FMD.REC.1396.9321113001).

Cancerous cell line (EL4 cells)

EL4 cancer cell line was purchased from the Pasteur Institute (Tehran, Iran). To confirm cell line characteristics, flow cytometry with a H-2kb specific marker was used (Abcam, UK). Based on our perivous studies (17, 18), EL4 cells were cultured at 37˚C in a 5% CO_2, in DMEM/F12 (Gibco, USA) with 2% FBS, penicillin (100 U/mL) and streptomycin (100 µg/mL). To evaluate the functionalities of EL4 cells and their tumorigenicity, 5×10^5 cells in a volume of 10 µl was injected with a suitable diameter needle (70 µm) and under a stereomicroscope (Olympus, SZ1145, Japan) through the efferent ductile, rete testis and ultimately into the seminiferous tubules in mouse reciepent.

Spermatogonial stem cell culture

A total of 50 NMRI neonate mice were used for SSC extraction. Testicles were kept on ice after separation from the animal until they were transferred to the culture medium. After washing in PBS and DMEM/F12, the testes capsules were isolated. After two phases of enzymatic digestion with the enzymes hyaluronidase (1 mg/ml), collagenase IV (4 mg/ml) and trypsin (0.25%), SSCs were extracted and cultured for 2 weeks.

To confirm SSC phenotype, flow cytometry analysis with Plzf marker with Alexa flour anti-mouse Plzf antibody was used (biosciences). Additionally, polymerase chain reaction (PCR) was used to examine specific genes associated with SSCs (*Plzf, Gfrα1, Oct4* and *Gapdh* as a housekeeping gene).

Oct4-
F: 5′GAACTAGCATTGAGAACCGT3′
R: 5′CATACTCGAACCACATCCTTC3′

Plzf-
F: 5′CCCGTTGGGGGTCAGCTAGAA3′
R: 5′CTGCAAGGTGGGGCGGTGTAG3′

Gfrα1-
F: 5′AATTGTCTGCGTATCTACTGG3′
R: 5′ACATCTGATATGAACGGGAC3′

Gapdh-
F: 5′CTGCTGGACAAGTGAGTCCC3′
R: 5′CCAAGTACCCTGGCCTCATC3′

Total RNA were extracted using RNA extraction kit (Qiagen, Germany) besed on the manufacturer's instructions. RNA was checked by a 260/280 nm ratio measurement, Reverse-transcription PCR (RT-PCR) was done by using complementary deoxyribonucleic acid (cDNA), primers and with PCR Master Mix 2X kit (Fermentas, St. Leon-Rot, Germany). To calculate gene expression Gene Runner software (version 3.02; Hastings Software Inc, New York, NY, USA) was used. The following conditions were used: Incubation at 95˚C for 3

minutes, denaturation for 30 seconds at 95˚C, Annealing for 30 seconds at the specific temperature associated with each primer and extension for 1 minute at 72˚C. After completion of the reaction, 5-10 µl of PCR solution on 1.2% agarose gel was analysed.

Preparing MiR-PLGA

In order to encapsulate MiR in the PLGA polymer structure, emulsion-solvent penetration was used. Tween 80 and span 80 surfactants were used as emulsifying agents. Polyvinyl alcohol was used as a stabilizer. Briefly, it should be noted that all appliances were deprotected with DEPC-treated water and glass containers were baked for 4 hours at 240˚C in order to remove any RNase enzymes. In order to obtain the desired Nano capsule, the internal water phase was initiated by the formation of polyethyleneimine (PEI) 25KDa and MiR with a mass ratio of 3 to 1. In practice, however, different ratios of PEI were used at this stage and eventually a synthesis was selected that had the appropriate zeta potential and was capable of loading the minimal genetic material required by agarose gel retention test. At first, a 0.1% solution of PEI was prepared in DEPC water. The MiR solution was also prepared using DEPC water at a concentration of 100 picomoles per microliter. Then, 80 µl of PEI containing 90 µg of PEI and 40 µl of MiR containing 30 µg of MiR were combined and the volume was adjusted to 500 µl PBS and maintained for 30 minutes in a thermal shaker at 37˚C. Because MiR was labeled, the entire process was performed in the dark.

To prepare the organic phase in solvent evaporation, 10 mg of PLGA was dissolved in 2 ml of organic solvent of ethyl acetate. To form the initial emulsion, 500 µl of internal aqueous phase with 0.5 ml of span 80 solutions at a concentration of 5 mg/ml was added to the organic phase and, using a vortex and ultrasonic bath, an initial water emulsion in oil was created. In the final step, 4 ml of PVA 0.5% was added and was agitated with a magnetic stirrer for 4 hours. In order to separate and purify, centrifugation at 12,000 rpm for 30 minutes and washing steps were performed two times and were finally resuspended in distilled water. This was performed so that the polyplexes were not loaded and the extra surfactants in the aqueous phase were removed from the surface of the NPs.

Surface modification of MiR-PLGA with folate

One mmol of folic acid in 20 ml DMSO with 1 mmol of ethyl dimethylaminopropyl carbodiimide (EDC) and 2 mmol of N-Hydroxysuccinimide (NHS) was dissolved in with a magnetic stirrer for 12 hours at room temperature. Then, to remove excess material, the solution was filtered and added to the ethylenediamine (EDA) as a linker, and pyridine (0.2/ml) and acetonitrile added to precipitate the folate. The precipitate was washed 3 times with diethyl ether and then dried to give a yellow deposit. 10 mg of MiR-PLGA was dissolved in 5 ml phosphate-buffered saline (PBS, Abcam, UK) at pH=7.4 and sonicated for 1 minute. 1 mg/ml EDC and 1 mg/ml of NHS were dissolved in DW and each of them washed, and about 500 µl was added to the above solution and agitated with a magenetic stirrer at room temperature for 2 hours and then centrifuged for 20 minutes to remove EDC and NHS. Following, folic acid was added to the product with the ratio of 1 mg/ml in PBS, incubated overnight at room temperature, agitated with the magenetic stirrer and then centrifuged. Using the same procedure as a previous study (17) the obtained solution was mixeded at room temperature once more and then the extra non-conjugated material was picked up by ultracentrifugation. Finally, the residual solution was lyophilized and stored. Conjugation of folate on the PLGA surface was confirmed by fourier transform infrared spectroscopy (FTIR) analysis.

The dynamic light scattering

A portion of dried powder of MiR-PLGA was dissolved in 1 ml of PBS with pH=7.4, using ultrasonic bath. Zeta potential was measured using a zeta meter device.

Transmission electron microscopy

The shape of NPs were evaluated by transmission electron microscopy (TEM, LEO 906; Carl Zeiss). The solution was sonicated for 5 minutes, then one drop of NP suspension (1 mg/mL) was put on a carbon-coated copper TEM grid and dried in the air. Finally,the sample was imaged by a KV 100.

Fourier transform infrared spectroscopy analysis

Using FTIR, the chemical structure of the NPs was studied. The test was carried out on 3 samples including polymer, folic acid and loaded NPs with a surface texture with folic acid. Approximately 2-3 milligrams of sample with potassium bromide powder was converted to a tablet using a 12-ppm hydraulic press and then FTIR spectra were collected.

Evaluation of miR-PLGA-folic acid uptake

Uptake was measured by fluorescence of MiR-PLGA incubated with EL4 cells in the culture medium.

Dosimetry

Due to the fact that treatment with MiR -PLGA-Folic acid was performed on SSCs as healthy cells, it was necessary to obtain a optimal MiR dose that can induce appropriate apoptosis in EL4 cells, but remain non-harmful to SSCs. So several doses were evaluated in the dosimetry stage (based on several previous studies (19, 20). Cells (EL4s and SSCs) were treated separately at 3 doses (for MiR 143, 25, 50 and 75 nmol and for MiR 206, 50, 100 and 150 nmol). The experiments were performed at 24, 48 and 72 hrs to investigate the most optimal time for transfection. Each experiment was repeated 3 times.

Cytotoxicity assay

MTT was used to assay the toxicity MiR-PLGA-

Folic Acid and the survival rate of EL4 cells and SSCs. 2×10^4 cells per well were seeded in two 96-well plates for each cell type. After treating with various doses (for MiR 143 : 25, 50, 75 nmol and for MiR 206: 50, 100, 150 nmol) the culture medium was extracted from the well and 10 µl/well MTT solution (5 mg/ml) was added, incubated at incubator for 3 hours, and then the medium was washed with 100 µl of DMSO. The absorbance was evaluated at 570 nm using a MiR plate reader. The experiments were repeated 3 times.

Apoptosis evaluation by using Annexin V-FITC apoptosis detection kit in dosimetry stage

Initially, 2×10^4 SSCs and EL4 cellss were removed after treatment. Then, 500 µl of the binding buffer was added to the cell plate. In the next step, 5 µl of Annexin V-FITC and 5 µl of propidium iodide (PI) (21, 22) were added. At room temperature, it was incubated in foil for 10 minutes, then flow cytometry was performed and the percentage of apoptosis in both healthy and cancerous groups was evaluated.

Evaluation of apoptotic gene expression

To determine the optimal dose of microRNA, after treatment of cancer cells, expression levels of apoptotic genes including *Bax*, *Bcl2* and *Caspase* 3 were evaluated by Q-PCR.

Bax-
F: 5′TGGGATGAATGGGGGAAGGGGAAA3′
R: 5′AAGGGGACCTGAGGTTTATTGGCG3′

Bcl2-
F: 5′ATGGCGCAAGCCGGGAGAAC3′
R: 5′CGCGTCCGCATCTCCAGCAT3′

Caspase 3-
F: 5′CTCTGGTACGGATGTGGACG3′
R: 5′CCCCTTCATCACCATGGCTT3′

Statistical analysis

To compare quantitative apoptosis data between different times, one-way analysis of variance (ANOVA) test was performed. To evaluate the effects of different cytotoxic concentrations of MiR at different times (group and time, and their interaction) as well as the effects of different concentrations of MiR at different times on the number of cells, two-way ANOVA was performed. Tukey's multiple comparison was also performed. All data was analyzed by the software version 25. SPSS at level of $P\leq0.05$.

Results

Cell culture and confirmation

SSCs were cultured in DMEM/F12 medium containing 2% fetal bovine serum (FBS, Gibco, USA) with glial cell line-derived neurotrophic factor (GDNF, Sigma, USA) 10 ng/ml for 2 weeks. Colony formation began after 24 hours (Fig.1A). EL4 cells were cultured in suspension (Fig.1B). The cell line was confirmed by flow cytometry analysis at the time of purchase as it was approximately 99% positive for EL4 cell-specific marker H2Kb (data not shown). Transplantation of EL4 cells confirmed their tumorigenicity potential as tissue histological examination revealed that the normal structure of the tubules had disappeared, and the leukemia cells had penetrated the interstitial tissue (Fig.1C, D). SSC was confirmed by expression of *Plzf, Gfrα-1* and *Oct4* by PCR (Fig.1E). Additionally, based on flow cytometry analysis, the percentage of SSCs was 42.8% and 74.6% after one and two weeks of culture respectively (data not shown).

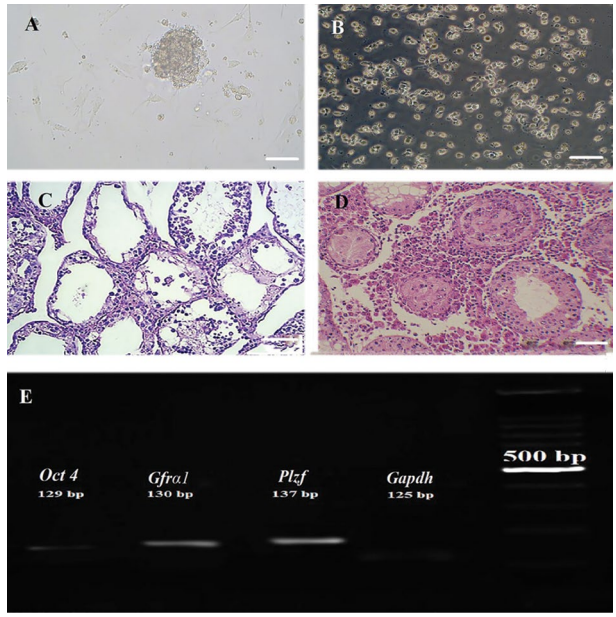

Fig.1: Cell culture and confirmation. **A.** The structure and nature of the cells of spermatogonia and cancer cells in the culture medium. Spermatogonia cells are colonized and sticky. **B.** Cancer cells have a rounded structure and a non-sticky nature. **C.** Tissue cross-sectional image of azoospermia mice, the structure of seminiferous tubules is observed without the presence of spermatogonia. **D.** Cross-section of mice testicular after tumor cell transplantation, the changing of the structure of the seminiferous tubules and infiltration of leukaemic cells are observed due to invasive tumor cells. **E.** Results of driving PCR products related to spermatogonia cells. The expression of (*Gapdh, Plzf, Gfrα-1, Oct4*) was proven by the reverse transcription polymerase chain reaction (RT-PCR) (scale bar: 100 µm).

Determination of particle size and charge with DLS

To assure that the folic acid modification process on the surface of the prepared NPs was complete, the FTIR spectrum of polymer, folic acid, and polymer with folic acid are shown in Figure 2A. The specimens were measured in terms of particle size by using DLS. The surface load obtained in the Zeta bar in the sample of the loaded NP was -18 mv. The average particle size obtained with DLS was 69.8 nm (Fig.2B), and morphology by TEM showed a smooth and spherical surface in all NPs (Fig.2C). In order to meet a suitable mass ratio for 25 kDa polyethylene, we selected a 3:1 ratio (N:P equivalent of 20:1, Fig.2D).

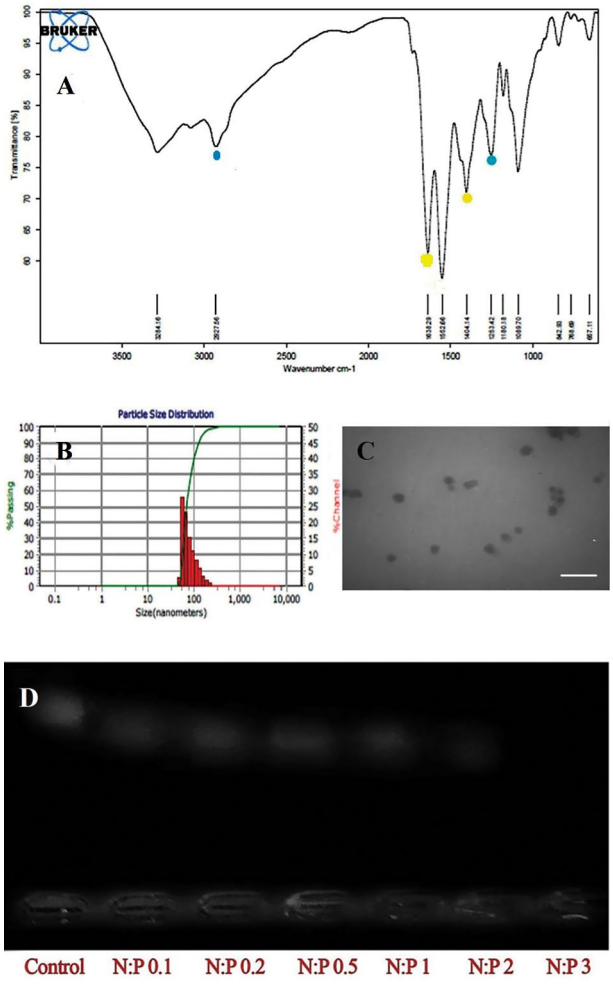

Fig.2: Nanoparticle evaluation tests. **A.** FTIR spectrum of polymer, folic acid and polymer coated with folic acid. The presence of the peaks of 1638 and 1404 (yellow spot) indexes of folic acid, 1263 and 2927 index loaded nanoparticles (blue spot). **B.** The particle size based on the DLS test. **C.** Transmission electron microscope showed a smooth and spherical surface in all nanoparticles. The average particle size was 69 nm (scale bar: 100 nm). **D.** Inhibition test for polyethylene amine electrophoresis gel.

Toxicity of different doses MiR-PLGA-folic acid

SSCs and EL4 cells were incubated by different doses of NPs containing MiR 143 (25, 50 and 75 nmol) and MiR 206 (50, 100 and 150 nmol) at 24, 48 and 72 hours. There was no significant difference between the 24 hrs data and the control group and therefore this time was removed from our study. Additionally, data for 72 hours was less valuable than data for 48 hours due to cell doubling characteristics, so 48 hours was chosen as the optimal time. Each experiment was repeated 3 times.

Based on MTT assay results, by two-way ANOVA, the optimal dose of MiR 143 was 75 nmol (59.87 ± 2.85% SSC and 35.3 ± 0.78 % EL4, P≤0.05) after 48 hours, and for MiR 206 it was 150 nmol (54.82 ± 6.7% SSC and 33.92 ± 3.01% EL4, P≤0.05) after 48 hours. In these doses, the survival rate of the EL4 cells and SSCs was below the half maximal inhibitory concentration (IC_{50}) and above 50% respectively (P≤0.05, Fig.3).

Determination of apoptosis rate at the optimal dose of microRNAs

Evaluation of apoptosis by the annexin kit also confirmed the optimal doses selected by MTT, for MiR 143, total apoptosis was (6.62 ± 1.8% for SSCs and 37.4 ± 1.2% for EL4 cells, P≤0.05), and for MiR 206, total apoptosis was (10.98 ± 1.5% for SSCs and 36.4 ± 3.7% for EL4 cells, P≤0.05) after 48 hours. In fact, using intelligent NPs at the same concentration, we were able to induce apoptosis in EL4 cells without any significant damage to the SSCs (Fig.4). Fluorescence microscopy images depict the extent of microRNA penetration into the cells (Fig.5).

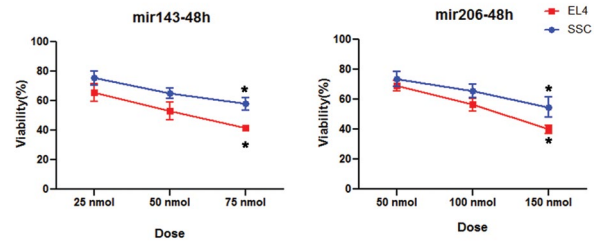

Fig.3: MTT test data. Based on MTT test, 48 hours after treatment with miR-PLGA-Acid folic, the highest rate of toxicity were observed in EL4 compared to SSC. *; Significant difference vs. other groups in the same cell (P≤0.05).

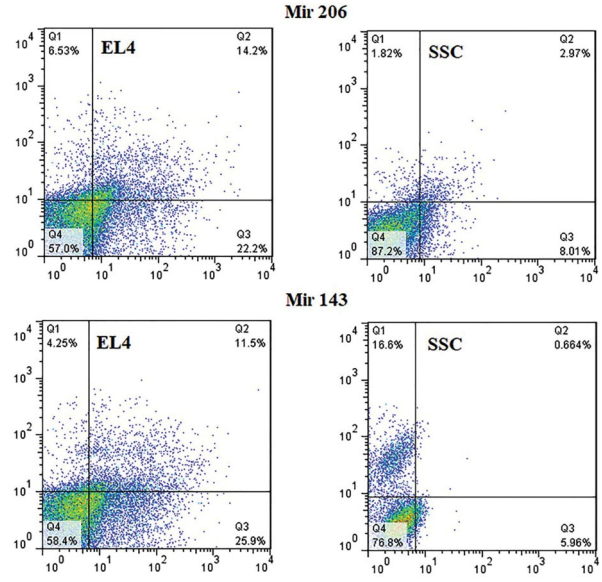

Fig.4: Based on the annexin assay, 48 hours after treatment with miR-PLGA-Acid folic, the highest rate of apoptosis were observed in EL4 compared to spermatogonial stem cell (SSC). The cells and microRNAs are shown separately in the image. Q1; Necrosis, Q2; Early apoptosis, Q3; Late apoptosis, and Q4; Survival rate.

Tukey's multiple comparison test showed that *Bax* gene expression was significantly increased in cancer cells at the optimal dose of both microRNAs as compared to the control group (P≤0.04). *Bcl2* gene expression was decreased in both groups as compared to the control group, although there was no significant difference. There were significant correlations in the Mir 143 group (P≤0.01) and in the Mir 206 group (P≤0.048) as compared to the control group. *Caspase 3* expression was also significantly increased in the experimental groups (P≤0.01), but there was no significant relationship between the two treatment groups (Table 1).

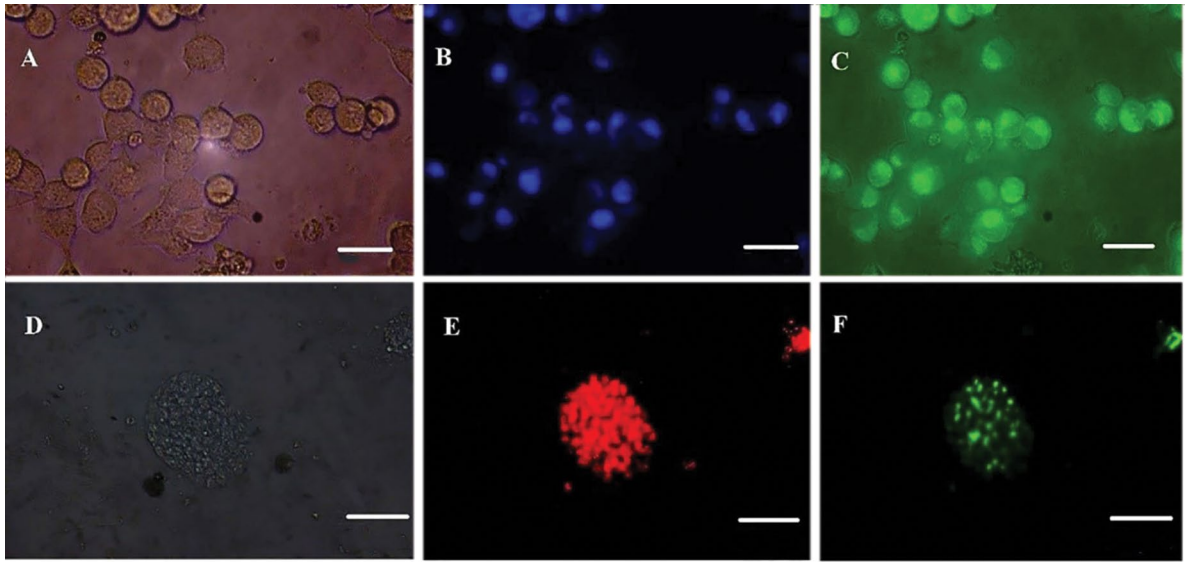

Fig.5: Fluorescent imaging of cells treated with PLGA-micro RNAs. **A.** Light microscope image of EL4 cells, **B.** Hoechst stained EL4 cells in blue, **C.** Fluorescent image of FAM-labeled green dyes inside EL4 cells at 570 nm wavelength, **D.** Spermatogonia colony, **E.** Plzf labeled spermatogonia, and **F.** Fluorescent image of FAM-labeled red dyes inside spermatogonial cells at 570 nm (scale bar: 50 µm).

Table 1: Expression of genes associated with the apoptosis process in EL4

PLGA-MiR treatment groups (48 hours incubation)	*Caspase 3*	*Bcl2*	*Bax*
PLGA-MicroRNA 143 treatment group	1.36 ± 0.2^{a}	$0.23 \pm 0.02^{a, b}$	$2.86 \pm 0.08^{a, b}$
PLGA-MicroRNA 206 treatment group	1.66 ± 0.15^{a}	$0.30 \pm 0.01^{a, b}$	$3.08 \pm 0.03^{a, b}$
Control	0.85 ± 0.04	0.49 ± 0.04	0.03 ± 0.01

Data are presented as mean ± SD. [a]; There was a significant difference between the expression levels of the target gene in the treatment groups compared to control (P≤0.05), and, [b]; There was a significant difference between two treatment groups in terms of gene expression (P≤0.05).

Discussion

The importance of MiRs in cancer is highlighted by the observation that ~50% of MiR genes are located in cancer-associated genomic regions or fragile sites (23). Studies have conclusively demonstrated that miRNAs are involved as tumor suppressors. In this study, we used two effective microRNAs, (143 and 206), to assess their effects on apoptosis in cancer cells. In our study, we showed apoptotic effects of these microRNAs on EL4 cells.

In this study, as in previous studies, we used the standard method of isolating and culturing spermatogonia cells and cancer cells, also, confirming them with appropriate PCR and flow cytometry methods (17, 18, 24).

In gene transfection, the method that should be used is the one that has the lowest toxicity, the highest level of performance and the lowest cost, while also having the ability to make a specific transfer (25). To overcome gene therapy problems and to improve efficiency, we used PLGA as the core and cationic PEI as a biodegradable shell.

We synthesized PLGA below 100 nm, which was a turning point in our study. In general, smaller NPs have a higher surface area to volume ratio than larger NPs, which increases the efficiency and interaction of NPs with the cell (26). In a study by Li et al. (27) with a size of 150 nm reached 70% absorbtion rate at 48 hours, In this study, with a nanoparticle size of approximately ≈ 70 nm based on flow cytometry data, we obtained a 62.54% uptake rate at 48 hours. Mohammadian et al. (28) also achieved the best result with a size of 15-60 nm at the same incubation time. The particles below 100 nm seem to be in best state for transfection (29). In agreement with other studies, the highest efficacy was observed after 48 hours of incubation (30, 31) that may increase at longer incubation times, only by non-selective passive uptake which is not desirable (32).

We also showed that with precise dosimetry, the NPs can prevent significant damage to SSCs. Folic acid, in the presence of a cell surface receptor, simply enters the cell and is absorbed through receptor-dependent endocytosis mechanism into the cell. Therefore, it is one of the most commonly targeted sites. Additionally, it is a preferred target because of many benefits, such as non-immunogenicity, small size, non-toxicity, and ease of handling (33). Due

to the fact that, this receptor is expressed in cancer cells more than in healthy cells, by selecting folic acid as the targeting agent for nanoparticles, we tried to target cancer cells and preserve SSC, NPs moving towards cancer cells in order to preserve SSC, which we largely achieved. But at the same time, the small size of our NPs was like a double-edged sword, which was both more suitable for transfusion and increased peneteration into the cell. At the same time, it played a role in penetration of these NPs into SSC, which ultimately affected these cells. Certainly, further studies could help optimize this method to reduce non-selective influence.

We also benefited from the use of PEI as a water-soluble polymer for effective transfection. Because of high cationic charge at normal pH, this polymer is able to connect through a electrostatic bond to microRNA. Therefore, this is a valuable polymer for gene delivery, as demonstrated by other studies (34, 35).

In our study, various doses of MiR -PLGA 143/206 conjugated with folic acid were tested on tumor cells (EL4 cells) and healthy cells (SSCs). We chose doses based on previous studies, but we found a different effective dose. Our appropriate dose of each MiR was selected, based on the optimal decrease in EL4 cell survival and simultaneous SSC protection (i.e. less toxicity and apoptosis). The efficacy of therapeutic approach used in this study is similar to results reported in our perivous studies (17). In similar studies, the survival rate of cancer cells was reduced by increasing the time from 24 to 48 hours and increasing the dose (17, 28). Also, No studies have shown that treatment with a microRNA alone can completely eliminate cancer cells (36-38). In no similar study were both Mir 143 and 206 compared. In this study, based on MTT findings, we found a small difference in the survival rate of EL4 cells in the Mir 143 group which according to Mir 206 was more successful in inducing cell death, annexin assay did not show a significant difference. Both microRNAs appear to have the same effect in inducing cell death in cancer cells.

In this study, we showed that expression of pre-apoptotic gene *Bax2* and *Caspase 3* in cancer cell treared with PLGA-Mir was increased, and *Bcl2* expression decreased which is probably the mechanism of induction of apoptosis in cancer cells (39). A similar result was obtained in a previous study (17). As mentioned earlier, microRNAs activate apoptosis signaling in cancer cells by regulating apoptotic genes (39).

Due to the multivariate nature of cancer, (i.e. the existence of different microRNAs that play a role in either reducing or increasing cancer regulation), we need a method that can utilize the many potentials of microRNAs to control cancer. In this setting, miRNAs can be used as disruptors of cancer cells and sensitization agents, making the malignant mass more susceptible for the next line of treatment (40).

Conclusion

In our first experience of utilizing MiRs for gene therapy on SSCs, we chose two MiRs because we were not certain about success rate,. MiR 206 has been demonstrated to have a tumor-suppressive role. According to this study and other similar studies, the efficacy of microRNAs in inducing apoptosis seems to be limited, and combinational therapy with medications may need to be considered for further efficacy. Taken together, this study suggests that MiR-therapy may lead to the development of novel therapeutic strategies for cancer, and apoptotic MiRs may be a potential therapeutic agent for human tumors and is worthy of further investigation.

Acknowledgments

This study was funded by a grant from Iran University of Medical Sciences (IUMS, number 96-01-30-29861) for a Ph.D. student thesis. We would like to give great thanks to the Nanotechnology Department of Iran University of Medical Sciences. The authors declare that there is no conflict of interest in this study.

Authors' Contributions

A.Sh.; Performed all *in vitro* and *in vivo* experiments and wrote the manuscript. Mo.K., R.Sh.; Participated in study design and drafting, contributed to concept and design and final approval of the manuscript. M.N., Mo.K., Ma.K., V.P., H.R.A., C.B.M.; Contributed extensively in interpretation of the data and the conclusion. M.A.J.; Statistical analysis and interpretation of the data. S.M.R.; Participated in study design. All authors performed editing and approving the final version of this manuscript for submission, also approved the final draft.

References

1. Romerius P, Ståhl O, Moëll C, Relander T, Cavallin-Ståhl E, Wiebe T, et al. High risk of azoospermia in men treated for childhood cancer. Int J Androl. 2011; 34(1): 69-76.
2. Takashima S, Shinohara T. Culture and transplantation of spermatogonial stem cells. Stem Cell Res. 2018; 29: 46-55.
3. Del Vento F, Vermeulen M, de Michele F, Giudice MG, Poels J, des Rieux A, et al. Tissue engineering to improve immature testicular tissue and cell transplantation outcomes: one step closer to fertility restoration for prepubertal boys exposed to gonadotoxic treatments. Int J Mol Sci. 2018; 19(1): 286.
4. Yue Y, Eun JS, Lee MK, Seo SY. Synthesis and characterization of G5 PAMAM dendrimer containing daunorubicin for targeting cancer cells. Arch Pharm Res. 2012; 35(2): 343-349.
5. Koruji M, Movahedin M, Mowla SJ, Gourabi H, Pour-Beiranvand S, Arfaee AJ. Autologous transplantation of adult mice spermatogonial stem cells into gamma irradiated testes. Cell J. 2012; 14(2): 82-89.
6. Struijk RB, Mulder CL, van der Veen F, van Pelt AMM, Repping S. Restoring fertility in sterile childhood cancer survivors by autotransplanting spermatogonial stem cells: are we there yet? Biomed Res Int. 2013; 2013: 903142.
7. Shabani R, Ashtari K, Behnam B, Izadyar F, Asgari H, Asghari Jafarabadi M, et al. In vitro toxicity assay of cisplatin on mouse acute lymphoblastic leukaemia and spermatogonial stem cells. Andrologia. 2016; 48(5): 584-594.
8. Hermann BP, Sukhwani M, Salati J, Sheng Y, Chu T, Orwig KE. Separating spermatogonia from cancer cells in contaminated prepubertal primate testis cell suspensions. Hum Reprod. 2011; 26(12): 3222-3231.

9. He BR, Lu F, Zhang L, Hao DJ, Yang H. An alternative long-term culture system for highly-pure mouse spermatogonial stem cells. J Cell Physiol. 2015; 230(6): 1365-1375.
10. Aghebati-Maleki A, Dolati S, Ahmadi M, Baghbanzhadeh A, Asadi M, Fotouhi A, et al. Nanoparticles and cancer therapy: Perspectives for application of nanoparticles in the treatment of cancers. J Cell Physiol. 2020; 235(3): 1962-1972.
11. Chen Y, Ma C, Zhang W, Chen Z, Ma L. Down regulation of miR-143 is related with tumor size, lymph node metastasis and HPV16 infection in cervical squamous cancer. Diagn Pathol. 2014; 9: 88.
12. Ni ZY, Lin FO, Liu DF, Xiao J. Decreased microRNA-143 expression and its tumor suppressive function in human oral squamous cell carcinoma. Genet Mol Res. 2015; 14(2): 6943-6952.
13. Zhang J, Sun Q, Zhang Z, Ge S, Han ZG, Chen WT. Loss of microRNA-143/145 disturbs cellular growth and apoptosis of human epithelial cancers by impairing the MDM2-p53 feedback loop. Oncogene. 2013; 32(1): 61-69.
14. Bae KH, Chung HJ, Park TG. Nanomaterials for cancer therapy and imaging. Mol Cells. 2011; 31(4): 295-302.
15. Low PS, Kularatne SA. Folate-targeted therapeutic and imaging agents for cancer. Curr Opin Chem Biol. 2009; 13(3): 256-262.
16. Zwicke GL, Mansoori GA, Jeffery CJ. Utilizing the folate receptor for active targeting of cancer nanotherapeutics. Nano Rev. 2012; 3.
17. Shabani R, Ashjari M, Ashtari K, Izadyar F, Behnam B, Khoei S, et al. Elimination of mouse tumor cells from neonate spermatogonial cells utilizing cisplatin-entrapped folic acid-conjugated poly (lactic-co-glycolic acid) nanoparticles in vitro. Int J Nanomedicine. 2018; 13: 2943-2954.
18. Eslahi N, Shakeri-Zadeh A, Ashtari K, Pirhajati-Mahabadi V, Tohidi Moghadam T, Shabani R, et al. In vitro cytotoxicity of folate-silica-gold nanorods on mouse acute lymphoblastic leukemia and spermatogonial Cells. Cell J. 2019; 21(1): 14-26.
19. Wu XL, Cheng B, Li PY, Huang HJ, Zhao Q, Dan ZL, et al. MicroRNA-143 suppresses gastric cancer cell growth and induces apoptosis by targeting COX-2. World J Gastroenterol. 2013; 19(43): 7758-7765.
20. Sun C, Liu Z, Li S, Yang C, Xue R, Xi Y, et al. Down-regulation of c-Met and Bcl2 by microRNA-206, activates apoptosis, and inhibits tumor cell proliferation, migration and colony formation. Oncotarget. 2015; 6(28): 25533-25574.
21. Lee H, Lytton-Jean AKR, Chen Y, Love KT, Park AI, Karagiannis ED, et al. Molecularly self-assembled nucleic acid nanoparticles for targeted in vivo siRNA delivery. Nat Nanotechnol. 2012; 7(6): 389-393.
22. Li TSC, Yawata T, Honke K. Efficient siRNA delivery and tumor accumulation mediated by ionically cross-linked folic acid–poly (ethylene glycol)–chitosan oligosaccharide lactate nanoparticles: For the potential targeted ovarian cancer gene therapy. Eur J Pharm Sci. 2014; 52: 48-61.
23. Si W, Shen J, Zheng H, Fan W. The role and mechanisms of action of microRNAs in cancer drug resistance. Clin Epigenetics. 2019; 11(1): 25.
24. Bashiri Z, Amiri I, Gholipourmalekabadi M, Falak R, Asgari H, Maki CB, et al. Artificial testis: a testicular tissue extracellular matrix as a potential bio-ink for 3D printing. Biomater Sci. 2021; 9(9): 3465-3484.
25. Alabdullah AA, Al-Abdulaziz B, Alsalem H, Magrashi A, Pulicat SM, Almzroua AA, et al. Estimating transfection efficiency in differentiated and undifferentiated neural cells. BMC Res Notes. 2019; 12(1): 225.
26. Fortuni B, Inose T, Ricci M, Fujita Y, Van Zundert I, Masuhara A, et al. Polymeric engineering of nanoparticles for highly efficient multifunctional drug delivery systems. Sci Rep. 2019; 9(1): 2666.
27. Li F, Wang F, Zhu C, Wei Q, Zhang T, Zhou YL. miR-221 suppression through nanoparticle-based miRNA delivery system for hepatocellular carcinoma therapy and its diagnosis as a potential biomarker. Int J Nanomedicine. 2018; 13: 2295-2307.
28. Mohammadian F, Abhari A, Dariushnejad H, Nikanfar A, Pilehvar-Soltanahmadi Y, Zarghami N. Effects of chrysin-PLGA-PEG nanoparticles on proliferation and gene expression of miRNAs in gastric cancer cell line. Iran J Cancer Prev. 2016; 9(4): e4190.
29. Kim JH, Park JS, Yang HN, Woo DG, Jeon SY, Do HJ, et al. The use of biodegradable PLGA nanoparticles to mediate SOX9 gene delivery in human mesenchymal stem cells (hMSCs) and induce chondrogenesis. Biomaterials. 2011; 32(1): 268-278.
30. Zhou M, Chen X, Wu J, He X, Ren R. MicroRNA-143 regulates cell migration and invasion by targeting GOLM1 in cervical cancer. Oncol Lett. 2018; 16(5): 6393-6400.
31. Liu W, Xu C, Wan H, Liu C, Wen C, Lu H, et al. MicroRNA-206 overexpression promotes apoptosis, induces cell cycle arrest and inhibits the migration of human hepatocellular carcinoma HepG2 cells. Int J Mol Med. 2014; 34(2): 420-842.
32. Malhotra M, Sekar TV, Ananta JS, Devulapally R, Afjei R, Babikir HA, et al. Targeted nanoparticle delivery of therapeutic antisense microRNAs presensitizes glioblastoma cells to lower effective doses of temozolomide in vitro and in a mouse model. Oncotarget. 2018; 9(30): 21478-21494.
33. Li W, Szoka FC. Lipid-based nanoparticles for nucleic acid delivery. Pharm Res. 2007; 24(3): 438-449.
34. Wu L, Xie J, Li T, Mai Z, Wang L, Wang X, et al. Gene delivery ability of polyethylenimine and polyethylene glycol dual-functionalized nanographene oxide in 11 different cell lines. R Soc Open Sci. 2017; 4(10): 170822.
35. Zhang T, Xue X, He D, Hsieh JT. A prostate cancer-targeted polyarginine-disulfide linked PEI nanocarrier for delivery of microRNA. Cancer Lett. 2015; 365(2): 156-165.
36. Lei C, Du F, Sun L, Li T, Li T, Min Y, et al. miR-143 and miR-145 inhibit gastric cancer cell migration and metastasis by suppressing MYO6. Cell Death Dis. 2017; 8(10): e3101.
37. Zhao Y, Liu X, Lu Y. MicroRNA-143 regulates the proliferation and apoptosis of cervical cancer cells by targeting HIF-1α. Eur Rev Med Pharmacol Sci. 2017; 21(24): 5580-5586.
38. Park YR, Seo SY, Kim SL, Zhu SM, Chun S, Oh JM, et al. MiRNA-206 suppresses PGE2-induced colorectal cancer cell proliferation, migration, and invasion by targetting TM4SF1. Biosci Rep. 2018; 38(5): BSR20180664.
39. Pileczki V, Cojocneanu-Petric R, Maralani M, Neagoe IB, Sandulescu R. MicroRNAs as regulators of apoptosis mechanisms in cancer. Clujul Med. 2016; 89(1): 50-55.
40. Gulei D, Berindan-Neagoe I. Combined therapy in cancer: the non-coding approach. Mol Ther Nucleic Acids. 2018; 12: 787-792.

Original Article

Circular RNA *circ_0000517* Facilitates The Growth and Metastasis of Non-Small Cell Lung Cancer by Sponging *miR-326/miR-330-5p*

Qiyan Tan, B.Sc.#, Changyu Liu, B.Sc.#, Ying Shen, B.Sc., Tao Huang, M.Sc.*

Department of Laboratory, Hainan People's Hospital, Haikou, Hainan, China

#These authors contributed equally to this Work.

Corresponding Address: Department of Laboratory, Hainan People's Hospital, Haikou, Hainan, China
Email: scy610463@163.com

Received: 22/December/2020, Accepted: 08/June/2021

Abstract

Objective: There is growing evidence showing that circular RNAs (circRNAs) are crucial regulators in modulating the biological behavior of tumors. This work is aimed to probe the role of *circ_0000517* in non-small cell lung cancer (NSCLC) and to elucidate its mechanism of action.

Materials and Methods: In this experimental study, the differentially expressed circRNAs in NSCLC were screened using the GEO database (GSE158695). *Circ_0000517*, *miR-326, miR-330-5p*, and *MMP2* expression levels were determined by quantitative real-time polymerase chain reaction (qRT-PCR) analysis and Western blot. The proliferation, apoptosis, migration, and invasion of NSCLC cells were detected by CCK-8, flow cytometry, and transwell assays. RNA immunoprecipitation (RIP), RNA pull-down, and dual-luciferase reporter gene assays were performed to clarify the association between the *circ_0000517* and *miR-326/miR-330-5p*.

Results: *Circ_0000517* was shown to be up-regulated in NSCLC tissues and cell lines. The up-regulation of *circ_0000517* is closely associated with advanced clinical stage of cancer, lymph node metastasis, and poor prognosis in NSCLC patients. *Circ_0000517* knockdown impeded the proliferation, migration, and invasion of NSCLC cells and enhanced their apoptosis. Mechanistically, *circ_0000517* was demonstrated to up-regulate MMP2 expression via decoying *miR-326* and *miR-330-5p* to facilitate the malignant biological behaviors of NSCLC cells.

Conclusion: This work reveals that *circ_0000517* is implicated in NSCLC cell growth and metastasis through the modulation of miR-326/miR-330-5p/MMP2, providing novel insights into the role of circRNAs in NSCLC progression.

Keywords: miR-326, miR-330-5p, MMP2, Non-Small Cell Lung Cancer

Cell Journal(Yakhteh), Vol 23, No 5, October 2021, Pages: 552-561

Citation: Tan Q, Liu Ch, Shen Y, Huang T. Circular RNA circ_0000517 facilitates the growth and metastasis of non-small cell lung cancer by sponging miR-326/miR-330-5p. Cell J. 2021; 23(5): 552-561. doi: 10.22074/cellj.2021.7913.

Introduction

Lung cancer (LC) is the most common type of tumor and the chief cause of cancer-related death, worldwide (1). Non-small cell lung cancer (NSCLC) is the major subtype of LC, taking up more than 85% of all cases (2). Despite the progress in NSCLC therapy, the survival and prognosis of NSCLC patients are still unfavorable (3-5). Hence, it is important to investigate the molecular mechanisms of the carcinogenesis and development of NSCLC.

CircRNAs are endogenous non-coding RNAs (ncRNAs) that form closed loops by covalently linking together the 3' and 5' ends of one or more exons (6). CircRNAs were discovered in RNA viruses as early as 1976 (7, 8). At first, they were thought to be the products of splicing errors (7). CircRNAs in mammals are with relative stability and high tissue- and cell-specific expression, exerting an important role in regulating the biological processes and pathogenesis (9, 10). For instance, *circ_001783* is overexpressed in breast cancer (BC) tissues and is remarkably linked to a heavier tumor burden and poorer prognosis in BC patients (11). Reportedly, knocking down circ_0000799 inhibits the proliferation and migration of bladder cancer cells *in vitro* and impedes tumor growth *in vivo* (12). *Circ_0000517* is a newly discovered circRNA that is abnormally overexpressed in hepatocellular carcinoma (HCC), and its expression is linked to adverse clinical outcomes (13). Nonetheless, the expression features of *circ_0000517*, its biological functions and its underlying mechanism in NSCLC are still unclear.

Competitive endogenous RNAs (ceRNAs) are RNA transcripts involved in "target mimetic" processes, also known as miRNA "sponges" or miRNA "decoys"(14). It binds competitively to miRNAs through base complementarity with miRNA response elements, thereby decreasing the number of miRNAs targeting mRNAs (15). CircRNAs can function as effective miRNA sponges that disrupt mRNA translation and play a role in cancer progression (16, 17). For instance, *circ_0008039* enhances the proliferation and cycle progression of BC cells through regulating miR-432-5p/E2F3 axis (18). *Circ_0091570* up-regulates ISM1 expression as a sponge for miR-1307 to modulate HCC growth and metastasis (19). Nonetheless, it remains to be further investigated

whether *circ_0000517* may also participate in the ceRNA network in NSCLC.

In this study, the GSE158695 query from the GEO database is analyzed, and *circ_0000517* is discovered to be abnormally overexpressed in NSCLC. Moreover, the research reveals that knocking down *circ_0000517* impedes the proliferation, migration, and invasion of NSCLC cells and enhances apoptosis. Furthermore, we demonstrate that, *circ_0000517* works as a molecular sponge for *miR-326/miR-330-5p* to accelerate NSCLC progression.

Material and Methods

Tissue specimens

In this experimental study, a total of 37 samples of NSCLC tissues and paired paracancerous non-tumor tissues were available from subjects who underwent surgical resection at Hainan People's Hospital. The ages of the participants were from 36 to 65 years, and consent forms were signed by the patients. Before their surgeries, none of the participants had a history of other tumors or underwent radio/chemotherapy. This work was endorsed by the Ethics Committee of Hainan People's Hospital (2019A-3C011). The tissue specimens were frozen in liquid nitrogen shortly after resection and preserved at -196˚C until being used.

Cell lines

Human normal bronchial epithelial cell line (BEAS-2B) and NSCLC cell lines (H1650, H1299, A549, H1975, and HCC827) were obtained from the Shanghai Cell Bank of Chinese Academy of Sciences (Shanghai, China). BEAS-2B cell line and NSCLC cells were maintained in RPMI1640 (Gibco, Grand Island, NY, USA) supplemented with 10% fetal bovine serum (FBS, Gibco, Grand Island, NY, USA), 100 μg/ml streptomycin, and 100 U/ml penicillin (Invitrogen, Carlsbad, CA, USA) at 37˚C with 5% CO_2.

Bioinformatics analysis

Gene expression data of GSE158695 were obtained from the NCBI GEO database and analyzed using the online software GEO2R to screen for differentially expressed circRNAs. GSE158695 contained 6 human samples, including 3 cases of NSCLC tissues and 3 cases of paracancerous tissues. Sangerbox software (Mugu Biotech Company, Hangzhou, China) was used for cluster analysis. The target miRNAs of circ_0000517 were projected by CircInteractome database and StarBase database.

Cell transfection

The NSCLC cells were plated in a 6-well plate at 3×10^5 cells/well. The cells were transfected with small interfering RNAs (siRNAs) targeting *circ_0000517* (si-circ_0000517#1/2/3) and the negative control siRNA (si-NC), miR-326/miR-330-5p mimic (miR-326/miR-330-5p) and control mimic (miR-NC), miR-326/miR-330-5p inhibitor (miR-326 in /miR-330-5p in) and inhibitor NC (miR-NC in), which were synthesized by GeneCopoeia (Shanghai, China). Cell transfection was executed using Lipofectamine 2000 (Invitrogen, Carlsbad, CA, USA).

Preparation of RNA and quantitative real-time polymerase chain reaction analysis

Total RNA was extracted from cells and tissues using the TRIzol reagent (Invitrogen, Carlsbad, CA, USA). The subcellular fractions of NSCLC cells were separated using the PARIS Kit (Ambion, Austin, TX, USA). RevertAid™ First Strand DNA Synthesis Kit (Thermo Fisher Scientific, Waltham, MA, USA) was used for reverse transcription, and quantitative real-time polymerase chain reaction (qRT-PCR) was executed using an SYBR Green PCR Kit (Toyobo, Osaka, Japan) on the 7500 Fast Dx Real-Time PCR Instrument (Applied Biosystems, Foster City, CA, USA). *β-actin* was considered as a control for normalization. MicroRNA detection was conducted using a miDETECT A Track Kit (RiboBio, Guangzhou, China). The small nuclear RNA *U6* expression was employed as a control for normalization. The primers for this research were designed using Primer Premier 5 software. The sequences are presented in Table S1 (See Supplementary Online Information at www.celljournal.org).

RNase R trypsinization experiment

In this study, 20 μg total RNA was incubated with or without RNase R (20 mg/mL, Epicentre Biotechnologies, Shanghai, China) for 15 minutes at 37˚C. Following that, qRT-PCR was implemented to determine circ_0000517 and linear *RPPH1* mRNA expressions.

Cell proliferation experiment

Cell proliferation was examined using the Cell Counting Kit-8 (CCK-8, Dojindo, Tokyo, Japan) assay. Cells were plated in a 96-well plate (3×10^3 cells/well), and cultured for 1, 2, 3 or 4 days. Next, 10 μL of CCK-8 solution was added to each well. Then the cells remained in culture for 1 hour. Next, the absorbance (OD) at 450 nm was determined using a microplate reader (Model 550, Bio-Rad Laboratories, Inc., Hercules, CA, USA).

Flow cytometry analysis

Briefly, to analyze the cell cycle of the transfected cells, the cells were fixed using 75% ethanol and then dyed using propidium iodide (PI, BD Biosciences, San Diego, CA, USA). Then a flow cytometer (BD Biosciences, Franklin Lake, NJ, USA) was used to detect the cell cycle distribution. To analyze the apoptotic rate of transfected cells, a Annexin V-FITC/PI apoptosis detection kit (BD Biosciences, San Jose, CA, USA) was used. The cells were resuspended in 1× binding buffer, and then dyed with AnnexinV-FITC staining solution and PI staining solution in the dark for 15 minutes. Subsequently, the apoptotic cells were analyzed with the flow cytometer.

Transwell experiment

In the Transwell experiment, approximately 1×10^4 transfected cells were suspended in 200 μL of serum-free medium and positioned in the top compartment of each Transwell (8 μm pore size, Corning, NY, USA). Matrigel (BD Biosciences, San Jose, CA, USA) was used to cover the filter in invasion assay, but it was not used in the migration assay. The lower compartment was filled with the medium-containing 10 % FBS as the chemoattractant. The cells were cultured for 48 hours for the invasion experiment and 24 hours for the migration assay. Following that, the cells in the upper compartment were swabbed with cotton swabs, while those on the lower surface of the filter were fixed with 0.1% crystal violet. In three random areas, the number of cells on the filter was recorded under a light microscope (Olympus Corporation, Tokyo, Japan).

Dual-luciferase reporter gene experiment

By inserting the wild-type or mutant-type sequence of *circ_0000517* or *MMP2* 3′UTR containing miR-326/miR-330-5p complementary sites into the psiCHECK-2 vector (Promega, Madison, WI, USA), respectively, wild-type luciferase reporter plasmids (circ_0000517-WT and MMP2 3′UTR-WT) and their mutants (circ_0000517-MUT and MMP2 3′UTR-MUT) were generated. The luciferase reporter plasmids were co-transfected into 293T cells and plated in a 96-well plate with miR-326/miR-330-5p mimics. The miR-NC was employed as the negative control. After 48 hours, the cells were collected and the Dual-Luciferase Assay System (Promega, Madison, WI, USA) was used to assess the activities of Firefly and Renilla luciferase. The relative luciferase activity was normalized to Renilla luciferase activity.

RNA immunoprecipitation assay

The RNA immunoprecipitation (RIP) experiment was executed with an EZ-Magna RIP Kit (Millipore, Billerica, MA, USA). A549 and H1299 cells were lysed in RIP lysis buffer plus cocktail (Roche Diagnostics, Shanghai, China). Supernatants were then incubated with protein A/G magnetic beads coupled with anti-Ago2 or IgG antibodies (Millipore, Billerica, MA, USA). After the immunoprecipitate was incubated with Proteinase K, qRT-PCR was performed to analyze the enrichment of miR-326 and miR-330-5p.

RNA pull-down experiment

By using Biotin RNA Marking Mix (Roche), RNAs were biotin-labeled. After that, the biotinylated RNAs were incubated with A549 and H1299 cell lysates, followed by the incubation of M-280 streptavidin magnetic beads (Invitrogen, San Diego, CA, USA). After rinsing with RNase-free lysis buffer, the RNAs were extracted according to the manufacturer's instructions, and the enrichment of *circ_0000517* was evaluated by qRT-PCR.

Western blot

Total cellular protein was isolated using RIPA lysis buffer and stored on ice after the cells were washed with cold phosphate buffer saline (PBS, Sigma-Aldrich, Louis, MO, USA). Twenty μg of proteins per group were separated with 10% sodium dodecyl sulfate polyacrylamide gel electrophoresis (SDS-PAGE) and transferred onto a polyvinylidene difluoride (PVDF) membrane (Millipore, Burlington, MA, USA) using semi-dry transfer method (Bio-Rad, Hercules, CA, USA). After the membranes were blocked with 5% defatted milk, the membranes were incubated with primary and secondary antibodies according to standard protocols. After that, the protein bands were visualized using the ECL detection kit (Tanon, Shanghai, China). The protein bands were normalized with β-actin. The primary antibodies used in this study were as follows: anti-matrix metalloproteinase-2 (MMP2) (Abcam, ab92536, 1:1000), and anti-β-actin (Abcam, ab7817, 1:3000).

Statistical analysis

All of tests were executed in triplicate. All data were analyzed using SPSS version 19.0 software (SPSS, Inc, Chicago, IL, USA). Student's t test and one-way ANOVA were used to analyze the difference between two groups and among multiple groups, respectively. Correlations were measured by Pearson's correlation analysis. Chi-square test was perform to analyze the association between clinical characteristics and *circ_0000517* expression levels. Kaplan-Meier survival curve was used to compare the prognosis of the NSCLC patients. $P<0.05$ signified statistical significance.

Results

Circ_0000517 was up-regulated in NSCLC tissues and cell lines

At first, a GEO microarray dataset (GSE158695) was analyzed to find candidate genes in three pairs of human NSCLC tissues and normal lung tissues. The result suggested that the expression levels of 84 circRNAs were up-regulated and the expression levels of 101 circRNA expression were down-regulated in NSCLC tissues ($P<0.05$, $|\text{Log2(Change fold)}|>1$, Fig.1A). The top 20 up- and down-regulated circRNAs were exhibited in the heat map (Fig.1B), where *circ_0000517* was remarkably up-regulated in NSCLC tissues (Log2FC=2.665316, $P<0.001$). Additionally, *circ_0000517* expression in 37 pairs of NSCLC tissues and non-tumor tissues was detected by qRT-PCR analysis. The results showed that *circ_0000517* expression was higher in NSCLC tissues than in paracancerous normal tissues (Fig.1C, $P<0.001$). Moreover, relative to the normal bronchial epithelial cell line (BEAS-2B cells), *circ_0000517* expression in NSCLC cell lines (H1650, H1299, A549, H1975, and HCC827 cells) was markedly up-regulated (Fig.1D, $P<0.001$). Additionally, we showed that *RPPH1* was

significantly degraded after RNase R treatment, but RNase R could not degrade *circ_0000517*, suggesting that *circ_0000517* had a closed-loop structure (Fig.1E). Furthermore, *circ_0000517* was found to be predominantly located in the cytoplasm of NSCLC cells (Fig.1F). Next, the half-life time of *circ_0000517* and *RPPH1* mRNA were measured in NSCLC cells treated with actinomycin D, which was used to restrain the transcription process. Our data showed that *circ_0000517* was more stable than *RPPH1* mRNA (Fig.1G). With the median expression level of *circ_0000517* as the cutoff value, the 37 NSCLC patients were divided into low and high expression groups (Fig.1H). A strong association was observed between *circ_0000517* expression and higher clinical stage, and lymphatic metastasis of the patients (Table 1). On the other hand, lower *circ_0000517* expression level in NSCLC tissues predicted a longer survival time of the patients (Fig.1I).

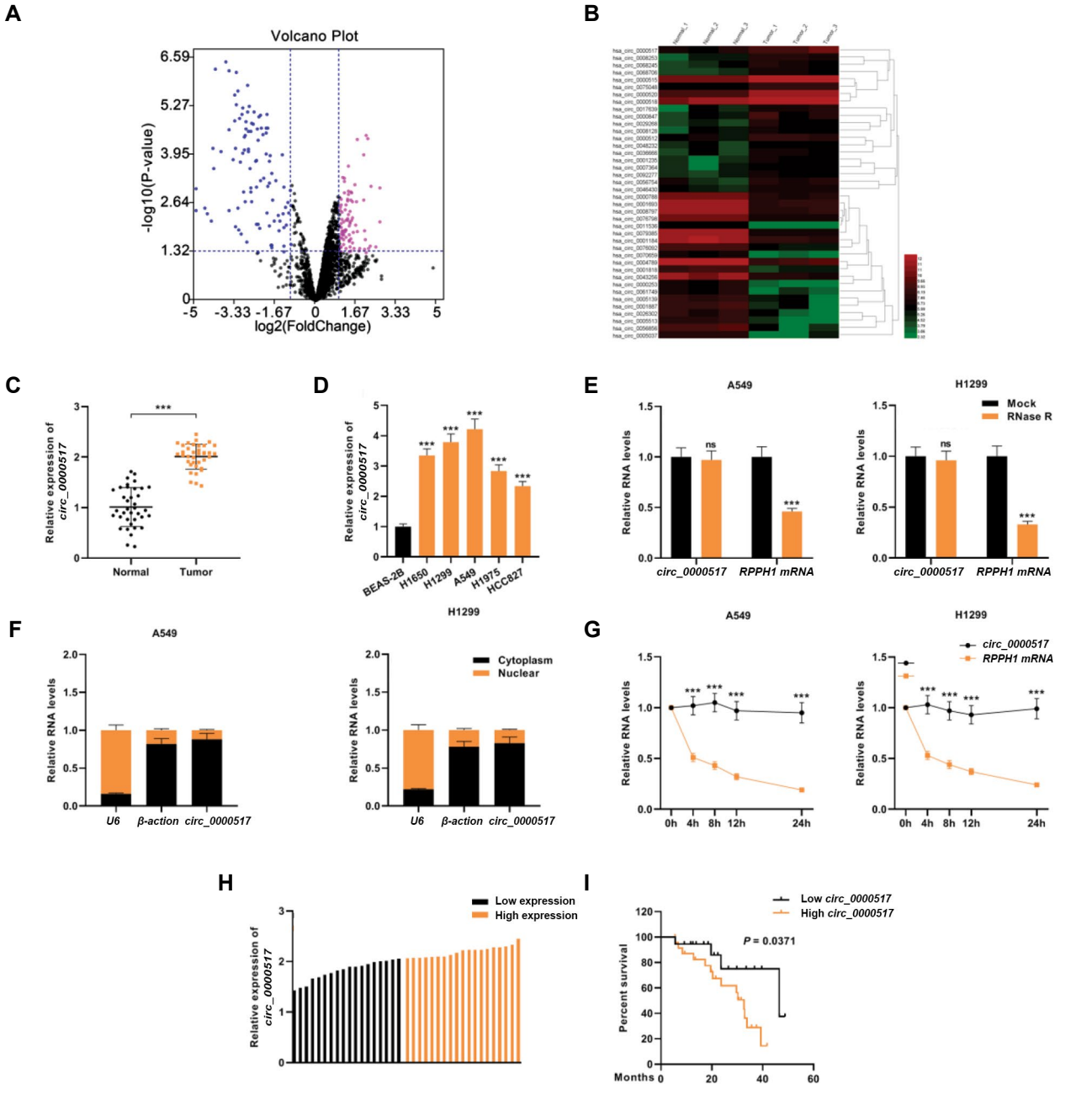

Fig.1: *Circ_0000517* was up-regulated in NSCLC. **A.** Differentially expressed circRNAs in NSCLC tissues (GSE158695) were presented in a volcano plot. The screening condition was | log2FC | >1 and P<0.05. **B.** Cluster heatmap of top 20 up- and down-regulated differentially expressed circRNAs (GSE158695). **C.** *Circ_0000517* expression level in 37 paired NSCLC tissues and matched adjacent normal tissues were examined by qRT-PCR. **D.** *Circ_0000517* expression in diverse human NSCLC cell lines (H1650, H1299, A549, H1975 and HCC827) and the human normal bronchial epithelial cell line (BEAS-2B) was examined by qRT-PCR. **E.** The relative RNA levels were examined by RT-qPCR after treatment with RNase R- or RNase R+ in total RNAs. **F.** *Circ_0000517* expression in the nuclei and cytoplasm of A549 and H1299 cell was examined by qRT-PCR. Our two controls were *β-actin*, which was mostly localized in the cytoplasm, and U6, which was mainly localized in the nuclei. **G.** qRT-PCR was executed to detect the relative levels of *circ_0000517* and *RPPH1* mRNAs at each time point after actinomycin D treatment. **H.** The 37 NSCLC patients were divided into low (n=18) and high expression groups (n=19) according to the median level of *circ_0000517* as the cut-off value. **I.** Kaplan-Meier survival curve was used to analyze the overall survival time of NSCLC patients (in TCGA database) with high or low *circ_0000517* expression levels. ***; P<0.001, NSCLC; Non-small cell lung cancer, and qRT-PCR; Quantitative real-time polymerase chain reaction.

Table 1: The relationship between *circ_0000517* and clinical characteristics in 37 NSCLC patients

Pathological indicators	Number of patients	Relative expression of *circ_0000517*		P value
		High expression	Low expression	
Gender				0.072
Female	17	6	11	
Male	20	13	7	
Age (Y)				0.254
<47	17	7	10	
≥47	20	12	8	
Histology				0.585
Squamous cell carcinoma	32	17	15	
Adenocarcinoma	5	2	3	
Clinical stage				0.013*
I~II	19	6	13	
II~III	18	13	5	
Tumor size (cm)				0.138
<5	14	5	9	
≥5	23	14	9	
Lymphatic metastasis				0.033*
Yes	21	14	7	
No	16	5	11	
Differentiation				0.124
Well+moderate	22	9	13	
Poor	15	10	5	

NSCLC; Non-small cell lung cancer and *; P<0.05.

Knockdown of *circ_0000517* impeded NSCLC cell growth, migration, invasion, but enhanced apoptosis

As shown in Figure 1, *circ_0000517* expression was relatively high in A549 and H1299 cells among all tested NSCLC cell lines, and therefore these two cell lines were selected for the following functional assays. The *circ_0000517* knockdown cell models were generated by transfecting three siRNAs (si-circ 0000517#1/2/3) into A549 and H1299 cells (Fig.2A). Because the knockdown efficiency of si-circ_0000517#2 is the most significant, si-circ_0000517#2 was selected. CCK-8 experiment confirmed that *circ_0000517* knockdown significantly inhibited NSCLC cell proliferation compared with the control group (Fig.2B). Flow cytometry analysis revealed that knocking down *circ_0000517* increased the proportion of A549 and H1299 cells arrested in G0/G1 phase (Fig.2C). Additionally, knocking down *circ_0000517* remarkably increased the apoptotic rate of both cells relative to the control groups (Fig.2D). Moreover, the data of the Transwell experiments showed that knocking down circ_0000517 markedly reduced cell migration and invasion relative to the control (Fig.2E). Our findings indicated that knocking down *circ_0000517* impeded the proliferation, migration, and invasion of NSCLC cells, while enhancing apoptosis.

Circ_0000517 sponged *miR-326/miR-330-5p* in NSCLC cells

The online prediction tools CircInteractome and StarBase were utilized to search for the downstream miRNAs that could bind to *circ_0000517*, and as a result, *miR-326* and *miR-330-5p* were predicted (Fig.3A). To prove the targeting relationship between *circ_0000517* and *miR-326/miR-330-5p*, wild-type circ_0000517 (circ_0000517-WT) and mutant circ_0000517 (circ_0000517-MUT) luciferase reporter vectors containing miR-326/miR-330-5p binding sites were constructed. (Fig.3B). MiR-326/miR-330-5p mimics substantially weakened the luciferase activity of circ_0000517-WT reporter, but had no effect on the luciferase activity of circ_0000517-MUT reporter (Fig.3C). RIP experiment suggested that *circ_0000517* and *miR-326/miR-330-5p* were enriched in micro-ribonucleoprotein complexes containing Ago2 in A549 and H1299 cells (Fig.3D). Moreover, in both A549 and H1299 cells, *circ_0000517* could be pulled down by Bio-miR-326/miR-330-5p-WT, but not Bio-miR-326/miR-330-5p-MUT or Bio-NC (Fig.3E). In A549 and H1299 cells, knocking down *circ_0000517* markedly augmented *miR-326/miR-330-5p* expression (Fig.3F). Furthermore, *miR-326/miR-330-5p* was found to be substantially under-expressed in NSCLC tissues (Fig.3G); and was negatively correlated by *circ_0000517* expression (Fig.3H). Hence, we concluded that *circ_0000517* could probably be a sponge for *miR-326/miR-330-5p* in NSCLC cells.

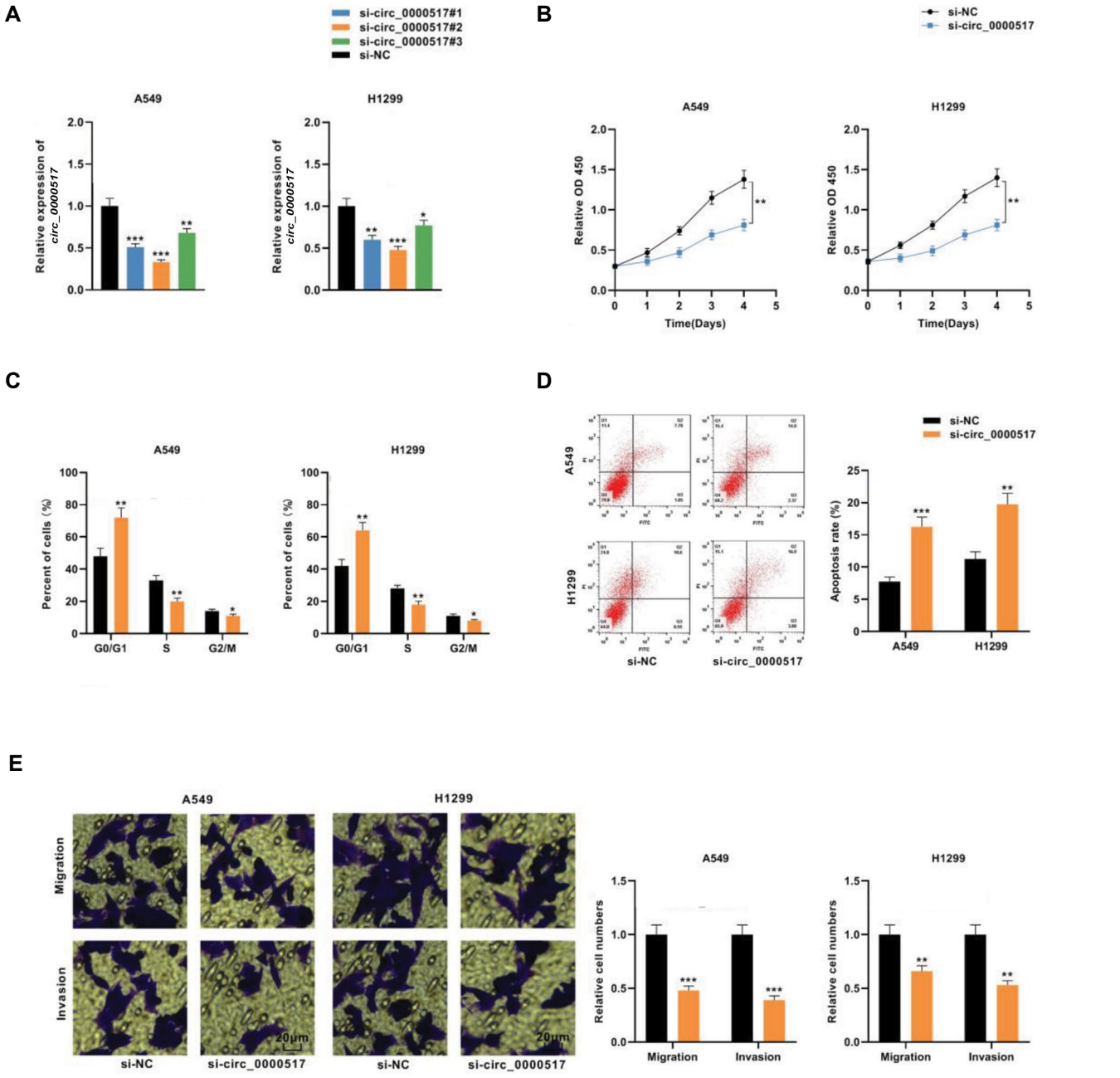

Fig.2: Knockdown of *circ_0000517* impeded the proliferation, migration, and invasion of NSCLC cells. **A.** Three siRNAs against circ_0000517 (si-circ_0000517#1, si-circ_0000517#2, and si-circ_0000517#3) were transfected into A549 and H1299 cells, and *circ_0000517* expression was detected by qRT-PCR. **B.** CCK-8 assay was employed to detect the proliferation of A549 and H1299 cells transfected with si-circ_0000517. **C.** Flow cytometry was used to detect the cell cycle distribution of A549 and H1299 cells transfected with si-circ_0000517. **D.** Flow cytometry was performed to detect the apoptosis rate of A549 and H1299 cells transfected with si-circ_0000517. **E.** Transwell experiment was done to detect the migration and invasion of A549 and H1299 cells transfected with si-circ_0000517 (scale bar: 20 μm). *; P<0.05, **; P<0.01, ***; P<0.001, NSCLC; Non-small cell lung cancer, and qRT-PCR; Quantitative real-time polymerase chain reaction.

miR-326/miR-330-5p targeted MMP2 in NSCLC cells

Using StarBase online database, *MMP2* was predicted to be a common downstream target of *miR-326* and *miR-330-5p* (Tables S2, S3, See Supplementary Online Information at www.celljournal.org). The TCGA database showed that the overall survival of NSCLC patients with high *MMP2* expression was relatively shorter (Fig. S1, See Supplementary Online Information at www.celljournal.org). Additionally, wild-type MMP2 3′UTR (MMP2-WT) and mutant MMP2 3′UTR (MMP2-MUT) luciferase reporter vectors containing the *miR-326/miR-330-5p* binding site were constructed (Fig.4A). The data of the luciferase reporter gene assay showed that miR-326/miR-330-5p mimics remarkably weakened the luciferase activity of MMP2-WT reporter, but exerted no remarkable influence on the luciferase activity of MMP2-MUT reporter (Fig.4B). The data of qRT-PCR revealed that *MMP2* mRNA was overexpressed in NSCLC tissues (Fig.4C). Furthermore, *MMP2* expression in NSCLC tissues was negatively correlated with *miR-326/miR-330-5p* expression and positively correlated with *circ_0000517* expression (Fig.4D, E). Therefore, it was hypothesized that *circ_0000517* positively regulated MMP2 expression by down-regulating *miR-326/miR-330-5p* in NSCLC cells.

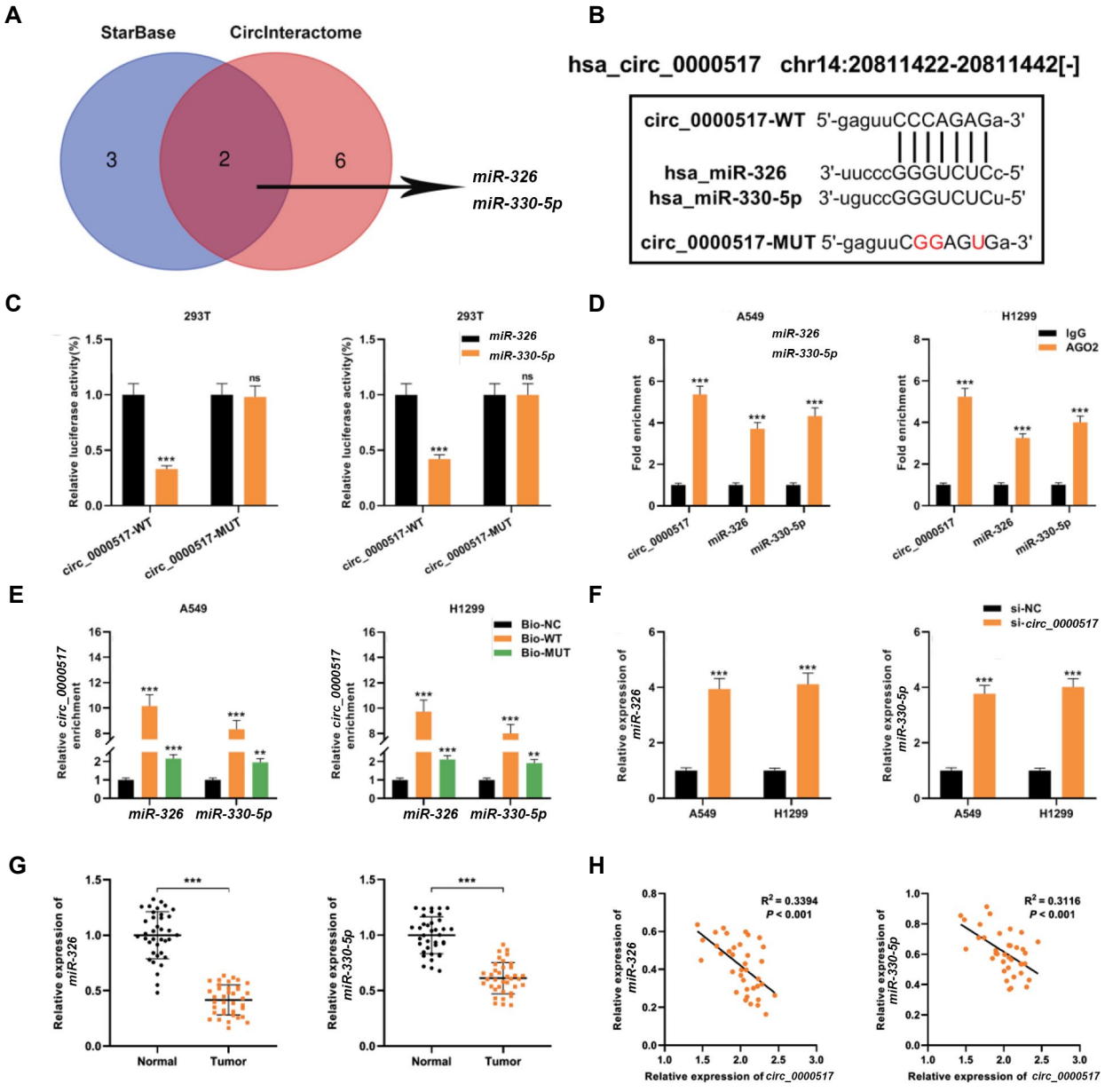

Fig.3: *miR-326* and *miR-330-5p* were downstream targets of *circ_0000517*. **A.** Bioinformatics analysis predicted that the sequence of *miR-326* and *miR-330-5p* matched the sequence of *circ_0000517*. **B.** The schematic diagram shows the putative *miR-326* and *miR-330-5p* binding sites with the circ_0000517, and the circ_0000517-WT and circ_0000517-MUT luciferase reporters that were constructed. **C.** Dual-luciferase reporter assays indicated that *miR-326* and *miR-330-5p* were the direct targets of *circ_0000517*. **D.** The complex containing *circ_0000517* and *miR-326/miR-330-5p* in A549 and H1299 cells were immunoprecipitated by anti-Ago2 antibody in RIP assay. **E.** RNA pull-down experiment was carried out to verify the interactions between *circ_0000517* and *miR-326/miR-330-5p*. **F.** *miR-326* and *miR-330-5p* expression levels in A549 and H1299 cells transfected with si-circ_0000517 were detected by qRT-PCR. **G.** qRT-PCR was employed to examine *miR-326* and *miR-330-5p* expression levels in 37 paired NSCLC tissues and matched adjacent normal tissues. **H.** Pearson's correlation analysis was utilized to evaluate the correlations between *circ_0000517* expression and *miR-326/miR-330-5p* expression in NSCLC tissues. **; P<0.01, ***; P<0.001, ns; Not significant, NSCLC; Non-small cell lung cancer, and qRT-PCR; Quantitative real-time polymerase chain reaction.

Circ_0000517 facilitates NSCLC cell growth and metastasis via the miR-326/miR-330-5p-MMP2 axis

To elaborate on whether *circ_0000517* affected NSCLC progression through the circ_0000517-miR-326/miR-330-5p-MMP2 axis, miR-326/miR-330-5p inhibitors (or control) were transfected into A549 and H1299 cells along with *circ_0000517* knockdown (Fig.5A). Western blot results suggested that knocking down *circ_0000517* impeded MMP2 expression, whereas down-regulating *miR-326/miR-330-5p* reversed this effect (Fig.5B). Besides, functional compensation experiments were executed in A549 cells. CCK-8 experiments showed that the inhibition of *miR-326/miR-330-5p* diminished the suppressive effect of down-regulation of *circ_0000517* on A549 cell proliferation (Fig.5C). Flow cytometry analysis revealed that co-transfection with miR-326/miR-330-5p inhibitors reversed the effects of *circ_0000517* knockdown on cell cycle progression and apoptosis (Fig.5D, E). Furthermore, Transwell experiments revealed that co-transfection of miR-326/miR-330-5p inhibitors counteracted the effects of *circ_0000517* knockdown on migration and invasion of A549 cells (Fig.5F). In summary, *circ_0000517* exerted oncogenic effects in NSCLC by regulating miR-326/miR-330-5p-MMP2 axis.

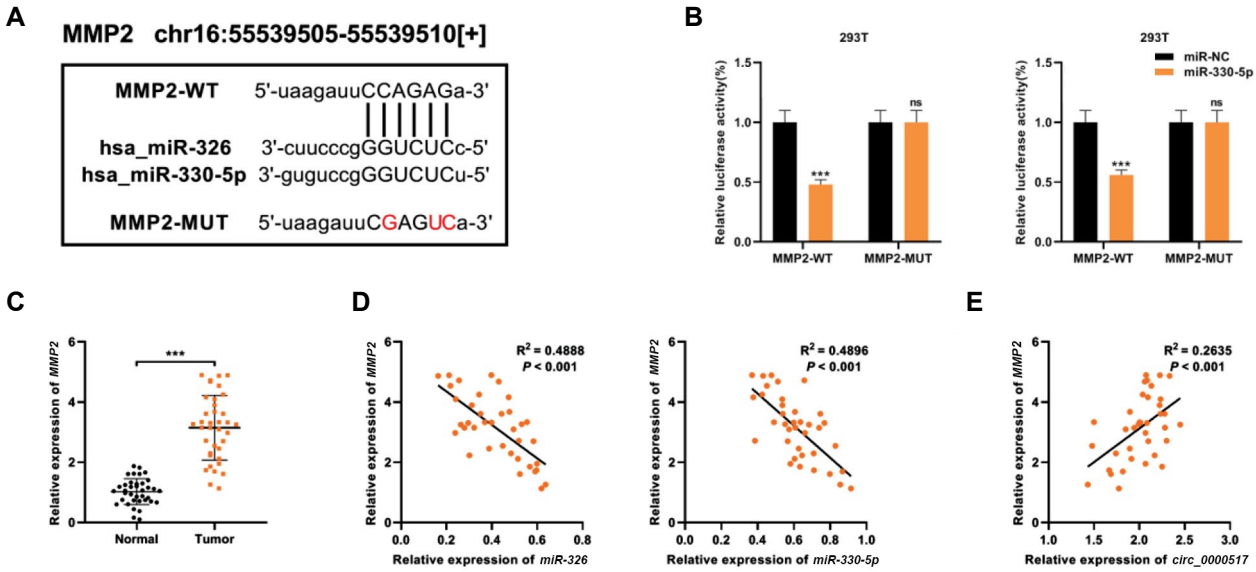

Fig.4: *MMP2* was a common target of *miR-326* and *miR-330-5p*. **A.** Bioinformatics analysis predicted that the sequence of *MMP2* 3′UTR matched the sequences of *miR-326/miR-330-5p*. MMP2-WT and MMP2-MUT luciferase reporter vectors were constructed. **B.** Dual-luciferase reporter assays demonstrated that *MMP2* was the direct target of *miR-326/miR-330-5p*. **C.** qRT-PCR was performed to examine *MMP2* expression in 37 paired NSCLC tissues and matched adjacent normal tissues. **D.** Pearson's correlation analysis was utilized to evaluate the correlations between *MMP2* and *miR-326/miR-330-5p* expression levels in NSCLC tissues. **E.** Pearson's correlation analysis was utilized to evaluate the correlation between *circ_0000517* expression and *MMP2* expression in NSCLC tissues. ***; P<0.001, ns; Not significant, NSCLC; Non-small cell lung cancer, and qRT-PCR; Quantitative real-time polymerase chain reaction.

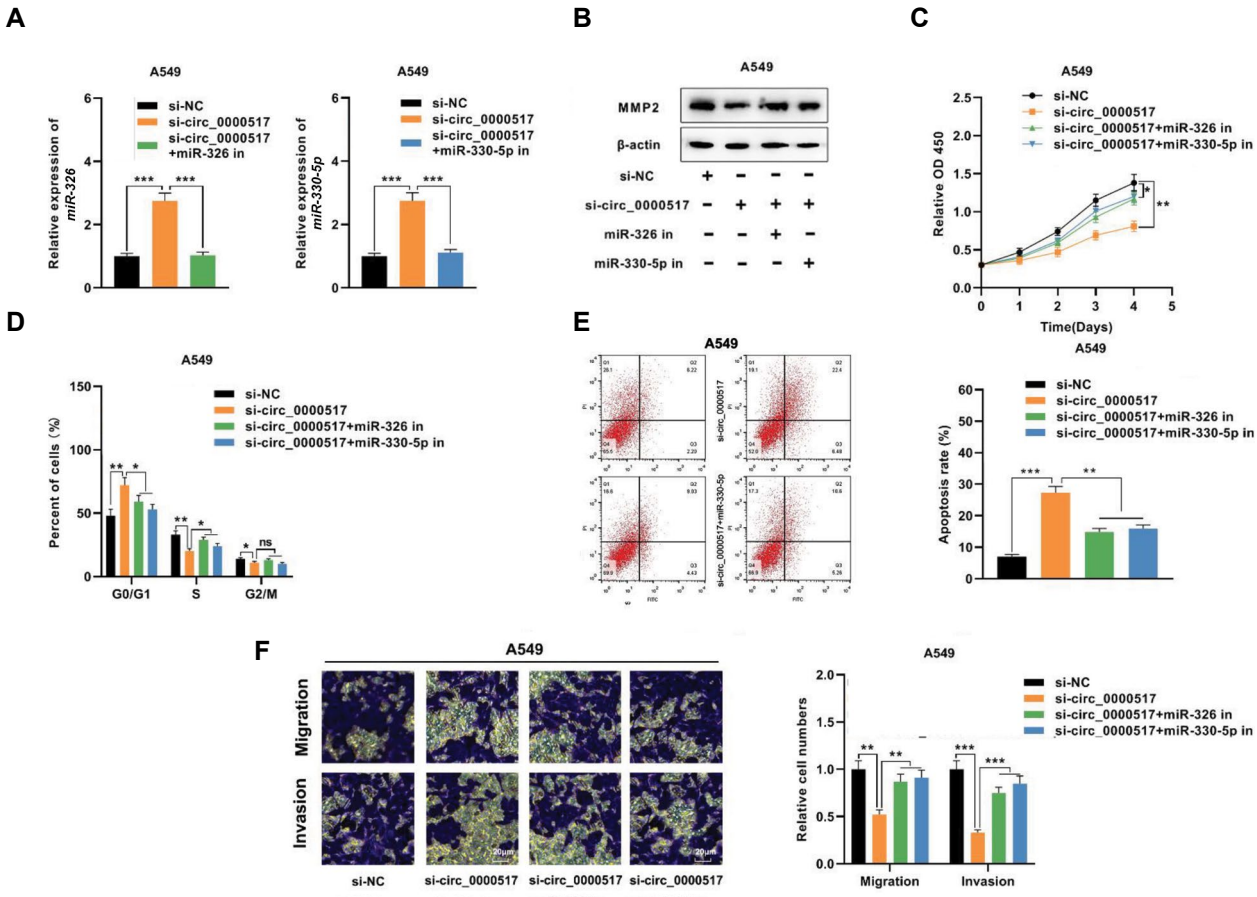

Fig.5: *Circ_0000517* facilitates NSCLC progression by acting on the miR-326/miR-330-5p-MMP2 axis. **A.** A549 cells with circ_0000517 knockdown were co-transfected with miR-326/miR-330-5p inhibitors or the negative control. qRT-PCR was employed to determine *miR-326/miR-330-5p* expression. **B.** Western blot was adopted to detect MMP2 protein expression in A549 cells co-transfected with circ_0000517 siRNA and miR-326/miR-330-5p inhibitors. **C.** CCK-8 assay was applied to detect the proliferation of A549 cells after their transfection. **D.** Flow cytometry was utilized to detect the cell cycle stage of A549 cells after the transfection. **E.** Flow cytometry was conducted to detect the apoptosis of A549 cells after their transfection. **F.** Transwell experiment was employed to detect the migration and invasion of A549 cells following transfection. *; P<0.05, **; P<0.01, ***; P<0.001, ns; Not significant, NSCLC; Non-small cell lung cancer, and qRT-PCR; Quantitative real-time polymerase chain reaction.

Discussion

NSCLC is one of the deadliest threats to human health (20). Despite the emergence of a variety of new treatment strategies for NSCLC, most patients still show poor prognosis due to metastasis and recurrence (21). In recent years, an increasing number of research demonstrates the importance of circRNAs in cancer biology (22, 23) and circRNAs have become a hotspot in cancer research. Aberrantly expressed circRNAs are reported to serve as biomarkers for the early diagnosis of several human cancers, such as gastric cancer, HCC, glioma, and prostate cancer (24, 25). Importantly, more and more studies reveal that circRNA is associated with NSCLC development. For instance, *circ_0001946* is down-regulated in NSCLC, and knocking it down enhances cancer cell proliferation, migration, and invasion, while restraining apoptosis (26). *Circ_0067934* expression, however, is up-regulated in NSCLC, and its overexpression is markedly linked to low survival, which can be an independent factor affecting the prognosis of NSCLC patients (27). Furthermore, *circ_0017247* is overexpressed in NSCLC, and knocking it down prevents cancer cell metastasis and epithelial-mesenchymal transition (28). In the current work, the analysis of GSE158695 revealed that *circ_0000517* was up-regulated in NSCLC tissue specimens. *Circ_0000517* is transcribed from the *RPPH1* gene on chromosome 14:20811404-20811492 (29). Reportedly, *circ_0000517* is remarkably up-regulated in HCC and is related to high tumor, nodes, and metastases (TNM) staging (13). We demonstrated that *circ_0000517* is also highly expressed in NSCLC tissues and cells in the present study. The upregulation of *circ_0000517* was closely associated with higher clinical stage, lymph node metastasis, and poor prognosis in NSCLC patients. Knockdown of *circ_0000517* blocked the proliferation, migration, and invasion of NSCLC cells, while enhancing apoptosis. These findings indicate that *circ_0000517* is an oncogenic factor in NSCLC.

Reportedly, circRNAs mainly work as miRNA sponges to adsorb miRNAs and modulate target genes' expression, thereby exerting either pro- or anti-cancer effects (30). *Circ_0000517* is reported to modulate the expression levels of IGF1R and SMAD6 via sponging *miR-326* in HCC (29, 31). Furthermore, *circ_0000517* interacts with *miR-1296-5p* to increase *Txndc5* expression, facilitating the proliferation of HCC cells and repressing cell cycle arrest and apoptosis (32). In this work, *circ_0000517* was found to target and inhibit *miR-326* and *miR-330-5p* expression in NSCLC. Both *miR-326* and *miR-330-5p* are reported to be under-expressed in NSCLC; *miR-326* and *miR-330-5p* overexpression impedes the proliferation and invasion of NSCLC cells and suppresses tumor growth (33-35). In this work, compensation assays indicated that *miR-326/miR-330-5p* down-regulation partially counteracted the inhibitory effects of *circ_0000517* depletion on NSCLC cells. These findings suggest that *circ_0000517* works as a ceRNA to exert an oncogenic effect in NSCLC by modulating *miR-326* and *miR-330-5p* expression.

MMP2 is a matrix metalloproteinase that belongs to a large family of zinc-dependent endopeptidases (36). Mounting research demonstrates that aberrant MMP2 expression in diverse cancers is linked to tumor aggressiveness. For instance, by mediating MMP2 expression and activity in melanoma cells, long non-coding RNA (lncRNA) *GAS5* represses the invasion of cancer cells (37). *MiR-29b* inhibits gastric cancer tumor growth and cell migration through negatively regulating MMP2 (38). ROCk2 enhances HCC invasion and metastasis by modifying MMP2 ubiquitination and degradation (39). Importantly, high *MMP2* expression in NSCLC tissues indicates poor prognosis of the patients, and it is also a crucial effector of many oncogenic pathways to promote the malignant phenotypes of NSCLC cells (40). In this work, we reported that MMP2 was negatively regulated by *miR-326/miR-330-5p* and positively regulated by *circ_0000517*. Our work provides a new explanation regarding the mechanism of MMP2 dysregulation in NSCLC.

Conclusion

Taken together, this work demonstrates that *circ_0000517* is up-regulated in NSCLC tissues and cells. *Circ_0000517* knockdown impedes NSCLC cell proliferation and metastasis and thus, enhances apoptosis. Mechanistically, *circ_0000517* is implicated in NSCLC development by acting on the miR-326/miR-330-5p-MMP2 axis. Nonetheless, this work is limited by *in vitro* experiments, and remains to be confirmed by future *in vivo* experiments in animal models.

Acknowledgements

There is no financial support and conflict of interest in this study.

Authors' Contribution

Q.T., T.H.; Conceived and designed the experiments. Q.T., C.L.; Performed the experiments. C.L., Y.Sh.; Analyzed the data. Q.T.; Y.Sh.; Wrote the manuscript. All authors read and approved the final version of the manuscript.

References

1. Siegel RL, Miller KD, Jemal A. Cancer statistics, 2019. CA Cancer J Clin. 2019; 69(1): 7-34.
2. Herbst RS, Morgensztern D, Boshoff C. The biology and management of non-small cell lung cancer. Nature. 2018; 553(7689): 446-454.
3. Fan TWM, Zhang X, Wang C, Yang Y, Kang WY, Arnold S, et al. Exosomal lipids for classifying early and late stage non-small cell lung cancer. Anal Chim Acta. 2018; 1037: 256-264.
4. Khanna P, Blais N, Gaudreau PO, Corrales-Rodriguez L. Immunotherapy comes of age in lung cancer. Clin Lung Cancer. 2017; 18(1): 13-22.
5. Mayne NR, Lin BK, Darling AJ, Raman V, Patel DC, Liou DZ, et al. Stereotactic body radiotherapy versus delayed surgery for early-stage non-small-cell lung cancer. Ann Surg. 2020: 272(6): 925-929.
6. Zhang P, Zhang XO, Jiang T, Cai L, Huang X, Liu Q, et al. Comprehensive identification of alternative back-splicing in human tissue transcriptomes. Nucleic Acids Res. 2020; 48(4): 1779-1789.
7. Sanger HL, Klotz G, Riesner D, Gross HJ, Kleinschmidt AK. Viroids

are single-stranded covalently closed circular RNA molecules existing as highly base-paired rod-like structures. Proc Natl Acad Sci USA. 1976; 73(11): 3852-3856.
8. Hsu MT, Coca-Prados M. Electron microscopic evidence for the circular form of RNA in the cytoplasm of eukaryotic cells. Nature. 1979; 280(5720): 339-340.
9. Yuan X, Yuan Y, He Z, Li D, Zeng B, Ni Q, et al. The regulatory functions of circular RNAs in digestive system cancers. Cancers (Basel). 2020; 12(3): 770.
10. Liu J, Li D, Luo H, Zhu X. Circular RNAs: the star molecules in cancer. Mol Aspects Med. 2019; 70: 141-152.
11. Liu Z, Zhou Y, Liang G, Ling Y, Tan W, Tan L, et al. Circular RNA hsa_circ_001783 regulates breast cancer progression via sponging miR-200c-3p. Cell Death Dis. 2019; 10(2): 55.
12. Bi J, Liu H, Cai Z, Dong W, Jiang N, Yang M, et al. Circ-BPTF promotes bladder cancer progression and recurrence through the miR-31-5p/RAB27A axis. Aging (Albany NY). 2018; 10(8): 1964-1976.
13. Wang X, Wang X, Li W, Zhang Q, Chen J, Chen T. Up-regulation of hsa_circ_0000517 predicts adverse prognosis of hepatocellular carcinoma. Front Oncol. 2019; 9: 1105.
14. Franco-Zorrilla JM, Valli A, Todesco M, Mateos I, Puga MI, Rubio-Somoza I, et al. Target mimicry provides a new mechanism for regulation of microRNA activity. Nat Genet. 2007; 39(8): 1033-1037.
15. Thomson DW, Dinger ME. Endogenous microRNA sponges: evidence and controversy. Nat Rev Genet. 2016; 17(5): 272-283.
16. Ma X, Liu C, Gao C, Li J, Zhuang J, Liu L, et al. circRNA-associated ceRNA network construction reveals the circRNAs involved in the progression and prognosis of breast cancer. J Cell Physiol. 2020; 235(4): 3973-3983.
17. Liu L, Wu SQ, Zhu X, Xu R, Ai K, Zhang L, et al. Analysis of ceRNA network identifies prognostic circRNA biomarkers in bladder cancer. Neoplasma. 2019; 66(5): 736-745.
18. Liu Y, Lu C, Zhou Y, Zhang Z, Sun L. Circular RNA hsa_circ_0008039 promotes breast cancer cell proliferation and migration by regulating miR-432-5p/E2F3 axis. Biochem Biophys Res Commun. 2018; 502(3): 358-363.
19. Wang YG, Wang T, Ding M, Xiang SH, Shi M, Zhai B. hsa_circ_0091570 acts as a ceRNA to suppress hepatocellular cancer progression by sponging hsa-miR-1307. Cancer Lett. 2019; 460: 128-138.
20. Bray F, Ferlay J, Soerjomataram I, Siegel RL, Torre LA, Jemal A. Global cancer statistics 2018: GLOBOCAN estimates of incidence and mortality worldwide for 36 cancers in 185 countries. CA Cancer J Clin. 2018; 68(6): 394-424.
21. Nanavaty P, Alvarez MS, Alberts WM. Lung cancer screening: advantages, controversies, and applications. Cancer Control. 2014; 21(1): 9-14.
22. Meng S, Zhou H, Feng Z, Xu Z, Tang Y, Li P, et al. CircRNA: functions and properties of a novel potential biomarker for cancer. Mol Cancer. 2017; 16(1): 94.
23. Verduci L, Strano S, Yarden Y, Blandino G. The circRNA-microRNA code: emerging implications for cancer diagnosis and treatment. Mol Oncol. 2019; 13(4): 669-680.
24. Kristensen LS, Hansen TB, Venø MT, Kjems J. Circular RNAs in cancer: opportunities and challenges in the field. Oncogene. 2018; 37(5): 555-565.
25. Patop IL, Kadener S. CircRNAs in cancer. Curr Opin Genet Dev. 2018; 48: 121-127.
26. Huang MS, Liu JY, Xia XB, Liu YZ, Li X, Yin JY, et al. Hsa_circ_0001946 inhibits lung cancer progression and mediates cisplatin sensitivity in non-small cell lung cancer via the nucleotide excision repair signaling pathway. Front Oncol. 2019; 9: 508.
27. Wang J, Li H. CircRNA circ_0067934 silencing inhibits the proliferation, migration and invasion of NSCLC cells and correlates with unfavorable prognosis in NSCLC. Eur Rev Med Pharmacol Sci. 2018; 22(10): 3053-3060.
28. Li CH, Wang YB, Chen KB. Circ_0017247 accelerates epithelial-mesenchymal transition in non-small cell lung cancer. Eur Rev Med Pharmacol Sci. 2019; 23(3 Suppl): 256-263.
29. He S, Guo Z, Kang Q, Wang X, Han X. Circular RNA hsa_circ_0000517 modulates hepatocellular carcinoma advancement via the miR-326/SMAD6 axis. Cancer Cell Int. 2020; 20: 360.
30. Han D, Li J, Wang H, Su X, Hou J, Gu Y, et al. Circular RNA circMTO1 acts as the sponge of microRNA-9 to suppress hepatocellular carcinoma progression. Hepatology. 2017; 66(4): 1151-1164.
31. He S, Yang J, Jiang S, Li Y, Han X. Circular RNA circ_0000517 regulates hepatocellular carcinoma development via miR-326/IGF1R axis. Cancer Cell Int. 2020; 20: 404.
32. Zang H, Li Y, Zhang X, Huang G. Circ_0000517 contributes to hepatocellular carcinoma progression by upregulating TXNDC5 via sponging miR-1296-5p. Cancer Manag Res. 2020; 12: 3457-3468.
33. Sun C, Huang C, Li S, Yang C, Xi Y, Wang L, et al. Hsa-miR-326 targets CCND1 and inhibits non-small cell lung cancer development. Oncotarget. 2016; 7(7): 8341-8359.
34. Wang Y, Xu R, Zhang D, Lu T, Yu W, Wo Y, et al. Circ-ZKSCAN1 regulates FAM83A expression and inactivates MAPK signaling by targeting miR-330-5p to promote non-small cell lung cancer progression. Transl Lung Cancer Res. 2019; 8(6): 862-875.
35. Cui LH, Xu HR, Yang W, Yu LJ. lncRNA PCAT6 promotes non-small cell lung cancer cell proliferation, migration and invasion through regulating miR-330-5p. Onco Targets Ther. 2018; 11: 7715-7724.
36. Hagemann C, Anacker J, Ernestus RI, Vince GH. A complete compilation of matrix metalloproteinase expression in human malignant gliomas. World J Clin Oncol. 2012; 3(5): 67-79.
37. Chen L, Yang H, Xiao Y, Tang X, Li Y, Han Q, et al. Lentiviral-mediated overexpression of long non-coding RNA GAS5 reduces invasion by mediating MMP2 expression and activity in human melanoma cells. Int J Oncol. 2016; 48(4): 1509-1518.
38. Wang T, Hou J, Jian S, Luo Q, Wei J, Li Z, et al. miR-29b negatively regulates MMP2 to impact gastric cancer development by suppressing gastric cancer cell migration and tumor growth. J Cancer. 2018; 9(20): 3776-3786.
39. Huang D, Du X, Yuan R, Chen L, Liu T, Wen C, et al. Rock2 promotes the invasion and metastasis of hepatocellular carcinoma by modifying MMP2 ubiquitination and degradation. Biochem Biophys Res Commun. 2014; 453(1): 49-56.
40. Zhang L, Li N, Yan HC, Jiang H, Fang XJ. Expression of novel CD44st and MMP2 in NSCLC tissues and their clinical significance. Oncol Res Treat. 2017; 40(4): 192-196.

Original Article

Radioprotective Effects of Combined Melatonin and Famotidine Treatment on Radiation Induced Apoptosis in Peripheral Blood Leukocytes of Breast Cancer Patients and Normal Individuals

Elham Samei, Ph.D.[1], Hossein Mozdarani, Ph.D.[2]*, Farhad Samiei, M.D.[3], Gholamreza Javadi, Ph.D.[1]

1. Department of Genetics, Science and Research Branch, Islamic Azad University, Tehran, Iran
2. Department of Medical Genetics, Faculty of Medical Sciences, Tarbiat Modares University, Tehran, Iran
3. Department of Radiotherapy, Cancer Institute, Tehran University of Medical Sciences, Tehran, Iran

**Corresponding Address: Department of Medical Genetics, Faculty of Medical Sciences, Tarbiat Modares University, Tehran, Iran*
Email: mozdarah@modares.ac.ir

Received: 03/January/2020, Accepted: 22/February/2020

Abstract

Objective: The aim of this study was to evaluate the effects of individual or combined use of two antioxidants, melatonin and famotidine on radiation induced apoptosis in leukocytes from breast cancer (BC) patients.

Materials and Methods: In this experimental study, the DPPH assay was used to determine the appropriate doses of melatonin and famotidine for treatment of BC and control leukocytes. The leukocytes were cultured in complete RPMI-1640 medium and treated with either agent for two hours. Cells were exposed to 4 Gy gamma rays generated from a Co-60 source at a dose rate of 0.85 Gy for 48 hours before harvesting. The cells were placed on slides and the neutral comet assay was performed. A total of 500 cells were stained with ethidium bromide and assessed for the amount of apoptosis under a fluorescent microscope x400 magnification.

Results: We observed significantly more apoptosis following radiation alone in the leukocytes from BC patients compared with normal individuals ($P<0.01$). Individual use of famotidine and melatonin induced very low frequencies of apoptosis that was not significantly different from the control ($P>0.05$). However, when combined with radiation, there was a decreased frequency of apoptosis in leukocytes of both normal and BC patients ($P<0.05$). The effect of famotidine was more pronounced than melatonin.

Conclusion: Melatonin, despite its potent antioxidant property, does not significantly affect radiation induced apoptosis in leukocytes derived from normal individuals; however, it has a moderately significant protective effect on in leukocytes derived from BC patients. Therefore, when used with radiation it might not intervene with the radiotherapy (RT) regimen of BC cancer patients. Famotidine is a good radioprotector for normal tissue. However, the efficacy of RT might be reduced with an accumulation of famotidine in tumour tissues.

Keywords: Antioxidants, Apoptosis, Breast Cancer, Ionizing Radiation, Leukocytes

Cell Journal(Yakhteh), Vol 23, No 5, October 2021, Pages: 562-567

Citation: Samei E, Mozdarani H, Samiei F, Javadi Gh. Radioprotective effects of combined melatonin and famotidine treatment on radiation induced apoptosis in peripheral blood leukocytes of breast cancer patients and normal individuals. Cell J. 2021; 23(5): 562-567. doi: 10.22074/cellj.2021.7378.

Introduction

Breast cancer (BC) is one of the most common cancers and leading causes of death in women. The prevalence of BC in Iran is increasing and affected people are relatively younger compared to other countries (1, 2). About 80% of patients with BC receive radiotherapy (RT) that involves the use of ionizing radiation (IR). IR leads to cellular and molecular damages via direct or indirect actions. Therefore, chromosomal aberrations, cell death, alterations in the oxidation status of cells and alterations in cellular haemostasis in tumours as well as normal tissues are expected after irradiation (3). Prominent effects of sparsely IR such as X-rays or gamma rays include the formation of free radicals that interact with nucleic acids and lead to DNA damage. IR produces a variety of damages in DNA. From these, double-strand breaks are most critical effects that lead to chromosomal aberrations and two different modes of cell death termed mitotic or clonogenic cell death and apoptosis (4). Patients with BC show various biological reactions to RT that range from mild to acute adverse effects and include skin erythema, fibrosis, immunologic complications, or secondary cancers (5, 6).

The results of studies have shown that about 40% of patients with BC are sensitive to radiation (7-9). Therefore, it is of utmost importance to reduce the radiation side effects for these patients. To date, different naturally occurring or synthetic agents have been used to countermeasure radiation side effects. From various available agents, antioxidants such as melatonin and famotidine are reported to effectively reduce radiation induced cellular damages in normal tissues.

The results of studies show that H2 receptor antagonists such as cimetidine and famotidine, which are usually used to treat peptic ulcers, can be potent hydroxyl radical scavengers (10, 11). The radioprotective effects of these agents on radiation induced chromosomal aberrations and micronuclei in mouse bone marrow cells and human peripheral blood lymphocytes have been reported (12-14). Famotidine was shown to reduce radiation induced apoptosis in normal lymphocytes (15).

Melatonin, an indolic compound, is secreted at night by the

pineal gland. Hardeland et al. (16) have published a review of the physiology and function of melatonin. Different studies have been performed to determine the oncostatic properties of melatonin against various tumours, including BC (17-19). Melatonin and its metabolites were found to be a direct free radical scavenger agent (20-22) that had the capability to stimulate the production of anti-oxidative enzymes and reduce the expression of pro-oxidative enzymes. Therefore, its use as a radioprotector and anti-cancer agent has been proposed (23). The anti-carcinogenic properties of melatonin and its anti-oxidative and free radical scavenging activity have been shown in different experimental models of carcinogenesis induced by oxidative damage inducing agents, which indicate the protective effects of melatonin (24-26).

The aim of this study was to evaluate the antiapoptotic effects of melatonin and famotidine alone or in combination on radiation induced apoptosis on lymphocytes of normal and BC individuals. BC patients have genomic instability (3); therefore, a different response to radiation in BC cells is expected compared to normal cells. To the best of our knowledge, there is no report about the combined treatment of famotidine and melatonin on radiation apoptosis induced in peripheral blood leukocytes of BC patients. Apoptosis was assessed by the neutral comet assay (single cell gel electrophoresis). The comet assay is reported to be a very reliable method for assessment of apoptosis induced by DNA damaging agents (15, 27, 28).

Materials and Methods

DPPH assay

In this experimental study, the DPPH assay, with 2, 2-diphenyl-1-picrylhydrazyl was used to evaluate the antioxidant properties of famotidine and melatonin in order to choose their optimum concentrations when combined with radiation. This method is an antioxidant assay based on electron-transfer that produces a violet solution in ethanol. This free radical, which is stable at room temperature, undergoes reduction in the presence of an antioxidant molecule and gives rise to a colourless ethanol solution. The DPPH assay was conducted according to standard procedure (29). The DPPH solution was prepared with 90% ethanol and we added various concentrations of melatonin and famotidine to this solution. After 30 minutes, the solution was read with an ELISA reader that had a 512 nm UV spectrum (BioTek, Taiwan). The percentage of absorbance was calculated using the following formula:

$$\text{Inhibition} = (\text{OD control} - \text{OD sample})/\text{OD control} \times 100\%$$

Blood sampling and drug treatment

The Ethical Committee at Natitional Institute for Medical Research Development (NIMAD, Tehran, Iran), approved this experimental study (IR.NIMAD.REC.1397.069). All participants gave written informed consent for study participation and completed a written questionnaire that asked information related to their life- styles. All non-smokers without viral infection, antibiotic consumption and X-ray at least one month prior to sample collection were included in the study. Table 1 lists the demographic information of the study participants. Venous blood samples were collected in heparinized vacutainers from 10 luminal A patients with BC whose age ranged between 23 and 66 years (mean: 37.4 ± 11) and 5 normal (control) individuals whose age ranged between 25 and 76 years (mean: 46 ± 13.9). Blood samples were divided into two parts: i. Not exposed to radiation-the control group that included untreated control, melatonin alone, famotidine alone, and combined melatonin-famotidine samples and ii. Exposed to gamma radiation, alone or in combination with famotidine and melatonin. Whole blood cultures were prepared by the addition of 0.1 ml blood to 0.4 ml RPMI-1640 medium (Gibco, BRL, UK) supplemented with antibiotics (penicillin 100 IU/ml and streptomycin 100 µg/ml, Sigma, USA), 10% L-glutamine (2 mM, Sigma, USA) and 15% foetal bovine serum (FBS, Gibco BRL, UK). Famotidine and melatonin powder (Chemodaru Pharmaceuticals, Iran) were dissolved in RPMI medium, then added to culture vessels two hours prior to irradiation at concentrations of 80 µg/ml (famotidine) and 800 µg/ml (melatonin).

Table 1: Study participants' demographic information

Normal control					**Mean age ± SD**					
# 5					**37.4 ± 11**					
Luminal A BC patients	**Age (Y)**	**Age at onset (Y)**	**R/L**	**Type**	**Grade**	**Stage**	**ER**	**PR**	**Her2**	**Ki67**
P1	47	46	R	D	2	1A	70	70	N	25
P2	47	46	L	D	2	2A	100	100	N	25
P3	45	44	R	L	2	2A	80	80	N	12.5
P4	26	26	R	D	2	3A	100	100	N	13.5
P5	76	75	L	D	2	2B	100	100	N	11.5
P6	42	41	L	D	1	2A	100	90	N	7.5
P7	42	41	R	D	1	2A	90	90	N	5
P8	44	43	R	D	1	2A	100	90	N	13.5
P9	45	44	R	D	1	1A	95	70	N	2
P10	46	45	R	D	2	1A	100	100	N	4.5
Mean ± SD	46 ± 11.58	45.1 ± 11.41					93.5 ± 10.01	89 ± 11.36		12 ± 7.54

BC; Breast cancer, P1-P10; Patient number, R/L; Right/left, ER; Oestrogen receptor, PR; Progesterone receptor, and SD; Standard deviation.

Irradiation

The culture vessels were irradiated with a therapeutic Co-60 gamma ray source (Theratrone, 780-C, Canada) at a dose of 4 Gy. The dose rate was 0.8 Gy/minute at a source to sample distance (SSD) of 80 cm. Irradiation was done at an ambient temperature (23 ± 2˚C). After irradiation, the cells were incubated at 37˚C for up to 48 hours.

Neutral comet assay

The neutral comet assay was used to assess apoptotic and non-apoptotic cells according to previously published protocols (15, 30) with minor modifications. Briefly, the previously incubated cells were centrifuged and the cell pellets were mixed with 0.75% low melting agarose (LMP, Fermentas, Germany) in phosphate-buffered saline (PBS) and immediately covered with a coverslip. The slides were kept at 4˚C for 15 minutes. After removal of the coverslips, the slides were transferred to lysis buffer that contained 2.5 M NaCl, 0.1 M EDTA, 10 mM Tris base, 1% N-lauryl sarcosine, 1% Triton X-100, and 10% dimethyl sulphoxide (DMSO, all from Merck, Germany) with a final pH of approximately 10. The slides were kept at 4˚C in the dark for 30 minutes, then washed with an electrophoresis buffer. After lysis, the slides were placed in a horizontal electrophoresis chamber that was filled with fresh electrophoresis buffer. Electrophoresis was conducted at 20 Volts and 100 mA. The slides were washed with distilled water for 5 minutes and then fixed in ethanol for 5 minutes at room temperature. The air-dried slides were stained with an ethidium bromide solution (20 µg/ml) and covered with coverslips. The number of apoptotic and non-apoptotic cells were scored using a fluorescent microscope (Nikon) equipped with an excitation filter (510-550 nm) and barrier filter (590 nm) at 400x magnification. Figure 1 shows typical normal and apoptotic cells analysed under the microscope. A total number of 500 cells were randomly assessed for each slide.

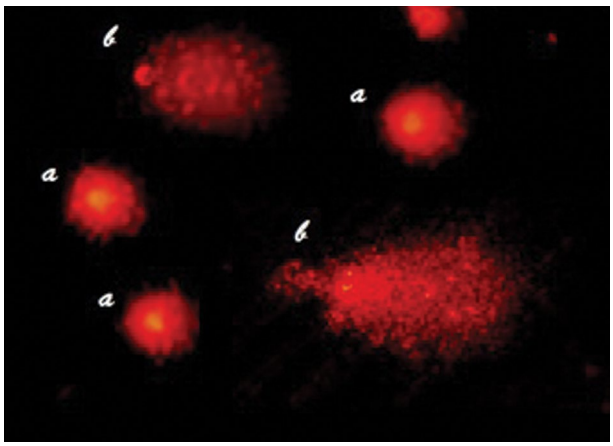

Fig.1: Typical photomicrographs of non-apoptotic and apoptotic neutral comet assay results. Apoptotic cells show a very small head and a fan-like tail. a; Non-apoptotic and b; Apoptotic (magnification: x400).

Statistical analysis

Data were analysed using SPSS software (version 18, SPSS Inc., USA). All data were first tested by using the Kolmogorov Smirnov test for normal distribution. Then, to compare the two groups, we used the Mann Whitney non-parametric test and analysis of variance (ANOVA) to compare more than two groups. $P<0.05$ were considered to be statistically significant. All figures were drawn with the use of GraphPad Prism software, version 4.0 (California Corporation, USA).

Results

DPPH assay

Famotidine

As seen in Figure 2**,** famotidine did not show any antioxidant capacity. The higher dose of famotidine was more effective. There was no significant difference between the 20 µg/ml and 40 µg/ml concentrations ($P>0.05$). However, there was a statistically significant difference between the other doses and the 80 µg/ml dose ($P<0.05$). Therefore, we used the 80 µg/ml dose for all of the radiation experiments.

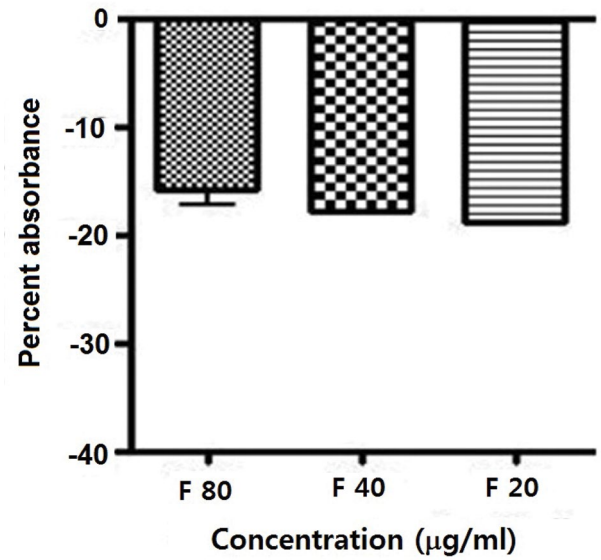

Fig.2: Percent absorbance of famotidine (F) as assayed with 2, 2-diphenyl-1-picrylhydrazyl (DPPH) and read by an ELISA reader with a 512 nm UV spectrum. Error bars show standard deviation (SD) of mean values from triplicate repeats.

Melatonin

Figure 3 shows the results of the DPPH assay for melatonin. There was a dose-dependent potent antioxidant capacity with melatonin. A significant difference existed between the 200 µg/ml dose and the 800 and 1200 µg/ml doses ($P<0.05$). However, the difference between the 800 and 1200 µg/ml concentrations was not statistically significant ($P>0.05$). Therefore, we used the 800 µg/ml dose for all of the radiation experiments.

Neutral comet assay

Normal individuals

Figure 4 shows the results of this assay. As seen,

irradiation of whole blood leukocytes with gamma rays induced a comparatively high percentage of apoptosis compared to the control non-irradiated samples (P<0.01). There were no significant differences between the drug treatments whether used alone or in combination with the control group (P>0.05). There was no significant difference between radiation alone and in combination with melatonin (P>0.05). However, there were significant differences between radiation and famotidine alone and between famotidine in combination with melatonin (P<0.05).

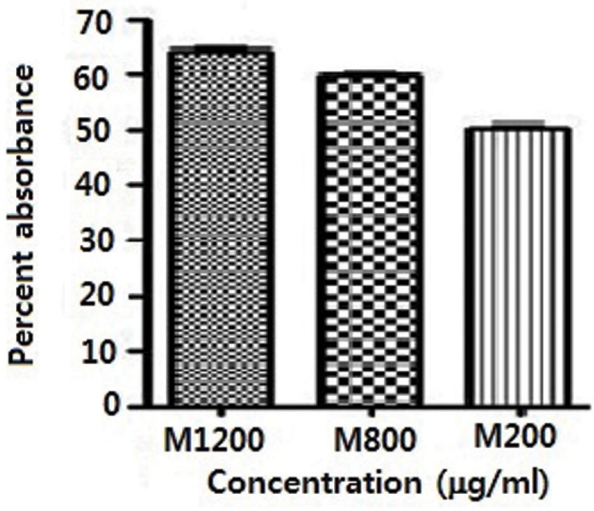

Fig.3: Percent absorbance of melatonin (M) as assayed with 2, 2-diphenyl-1-picrylhydrazyl (DPPH) and read by an ELISA reader with a 512 nm UV spectrum. Error bars show standard deviation (SD) of mean values from triplicate repeats.

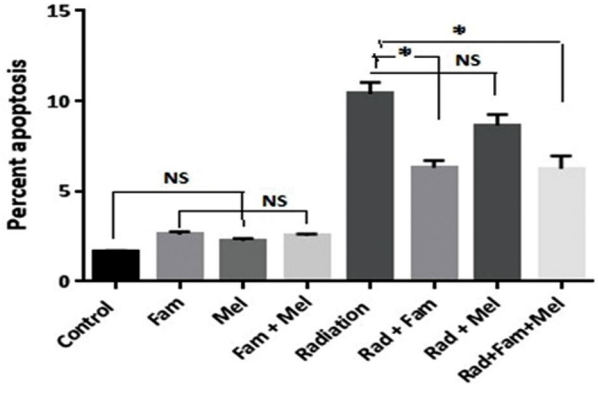

Fig.4: Treatment with famotidine (Fam) and melatonin (Mel), alone or in combination, prior to gamma irradiation of leukocytes from normal individuals. NS; Non-significant and *; P<0.01 error bars indicate standard error of mean (SEM).

Breast cancer patients

Figure 5 shows significant differences between the radiation and drug treatment groups (famotidine and melatonin), either alone or in combination (P<0.05). A higher background frequency of apoptosis was seen in the BC leukocytes (P<0.05). Radiation induced significantly higher frequency of apoptosis in leukocytes from BC patients compared to normal individuals (P<0.05).

A protective effect for radiation induced apoptosis was seen for both normal and BC leukocytes when radiation was combined with famotidine and famotidine plus melatonin (P<0.05). The results indicated no significant protective effect with melatonin combined with radiation in leukocytes from normal individuals (P>0.05); however, the effect was statistically significant for BC patients (P<0.05).

The comet assay results showed a significant increase in apoptosis following irradiation and significant decrease in the presence of combined melatonin and famotidine.

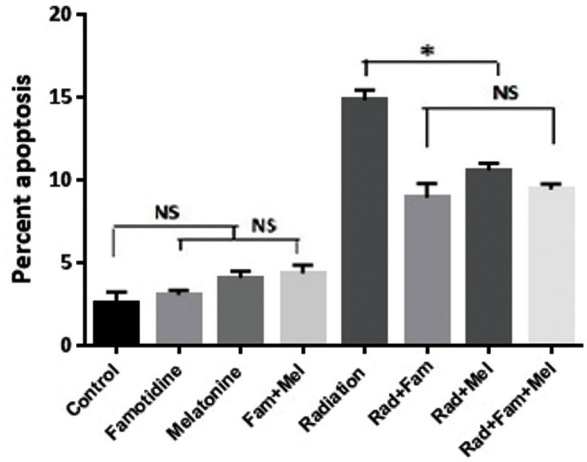

Fig.5: Treatment with famotidine and melatonin, alone or in combination, prior to gamma irradiation of leukocytes from breast cancer (BC) patients. NS; Non-significant, *; P<0.01 error bars indicate standard error of mean (SEM).

Discussion

RT is an efficient treatment modality for about 50% of patients with malignant breast tumours. The direct and indirect effects of IR potent inducers of DNA damage, chromosomal instability and cell death in tumour and normal tissues. Most patients can tolerate RT; however, some suffer from severe adverse effects. This variability in response may be caused by a genetic predisposition and inherent radiosensitivity in BC patients (3, 31). The cytotoxic reactions of normal tissues to IR limits the efficiency of RT. Unfortunately, an appropriate protocol to prevent or treat these side effects has not been developed. Therefore, the inherent radiosensitivity of normal cells might be considered a serious problem in management of RT for BC. The use of radioprotectors has been proposed to reduce normal tissue radiotoxicity. To date, no appropriate single radioprotector has been introduced for this purpose. The combined regimen of chemical or naturally occurring antioxidants might be useful for BC

patients. The application of famotidine and melatonin two hours prior to irradiation led to a significant reduction in the frequency of radiation induced apoptosis. A similar observation was made with leukocytes from BC patients, although there was a higher frequency of apoptosis. The combination of famotidine and melatonin was more effective than melatonin alone, but not as effective as famotidine alone. The DPPH assay results and results from other studies show that melatonin is potent antioxidant (32, 33). The radioprotective potential of melatonin is shown by different investigators using different end points such as protection of lymphocytes against gamma rays, reducing frequency of chromosomal aberration and micronuclei, and reducing radiation induced cytotoxicity in normal tissue (24-26, 34).

Melatonin might reduce DNA damage, because of its direct radical scavenging actions of free radicals induced by IR (35). Melatonin and most of its metabolites have the capability to scavenge free radicals and reactive nitrogen species (20). Moreover, melatonin stimulates the activities of antioxidant enzymes to remove ROS before damaging DNA and assists the mechanisms involved in DNA damage repair (36). Therefore, melatonin, as a potent antioxidant, exerts a radioprotective effect. Furthermore, besides being a potent antioxidant, melatonin is a potent inducer of apoptosis. It was shown that melatonin increased frequency of the programmed cell death induced by ROS generated by arsenic trioxide, activation of the p38/JNK pathways, and by upregulation of Redd1 expression in human BC cells (37).

The synergistic effect of melatonin has been shown with anti-cancer drugs, which led to effective anti-proliferative and pro-apoptotic activities in colon cancer cell lines by activating the cytochrome c/caspase signalling pathways (38). These observations might explain why the radioprotective effects of melatonin on normal lymphocytes did not significantly differ with radiation alone. Melatonin has been shown to enhance the radiosensitivity of cancer cellsthrough inhibition of proliferation, promotion of cell cycle arrest, and inhibition of proteins involved in DNA double-strand break repair (39).

Famotidine led to a considerable decrease in the frequency of gamma irradiation induced apoptosis. The results of previous studies showed the radioprotective potency of famotidine against gamma ray induced chromosomal and micronuclei induction (12, 14) as well as radiation induced apoptosis in normal cells (15). Ching et al. (10) previously reported that antagonists of the histamine H2 receptor such as cimetidine, famotidine and ranitidine are not only good inhibitors of histamine-stimulated gastric acid secretion, but also are potent radical scavengers. Although the antioxidant potency of famotidine has not been assessed as much as for melatonin, the reduction in frequency of radiation induced apoptosis by famotidine is much more considerable compared to melatonin. This observation is consistent with findings from other H2 receptor antagonists, cimetidine alone or in combination with famotidine, on gamma ray induced micronuclei in mouse bone marrow (13, 40). Famotidine is effective against radiation induced apoptosis via OH radical scavenging and an intracellular antioxidant mechanism (15). The combination of famotidine and melatonin used with radiation led to a protective effect that was similar to famotidine alone. The mechanism by which famotidine reduces radiation induced apoptosis is not clearly understood, but it may be due to its antioxidant properties and is not measurable by the DPPH assay.

Conclusion

The results imply that melatonin, despite its potent antioxidant property, does not significantly affect radiation induced apoptosis in leukocytes derived from normal individuals. However, a moderate significant protection is induced in leukocytes derived from BC patients. When used with radiation, it might not intervene with the RT regimen for BC cancer patients. Famotidine, on the other hand is a good radioprotector for normal tissue, but if it accumulates in tumour tissues, it might reduce the efficacy of RT.

Acknowledgements

The authors sincerely appreciate the contributions by all of the healthy volunteers and BC patients for their participation in this study. Research reported in this publication was partially supported by Elite Researcher Grant Committee under award number (958776) from the National Institutes for Medical Research Development (NIMAD), Tehran, Iran. There is no conflicts of interest in this study.

Authors' Contributions

E.S., H.M.: Participated in the study design, data collection and evaluation, drafting the manuscript, statistical analysis, data interpretation and conclusion. F.S.; Participated in patient evaluation, diagnosis and blood sampling. G.J.: Participated in data analysis and drafting the manuscript. All authors performed editing and approving the final version of this manuscript for submission, also approved the final draft.

References

1. Rafiemanesh H, Salehiniya H, Lotfi Z. Breast cancer in iranian woman: incidence by age group, morphology and trends. Asian Pac J Cancer Prev. 2016; 17(3): 1393-1397.
2. Akbari ME, Sayad S, Sayad S, Khayamzadeh M, Shojaee L, Shormeji Z, et al. Breast cancer status in Iran: statistical analysis of 3010 cases between 1998 and 2014. Int J Breast Cancer. 2017; 2017: 2481021.
3. Mozdarani H. Breast cancer and paradigm of genomic instability. Arch Breast Cancer. 2016; 3(4): 102-105.
4. Hall EJ, Giaccia AJ. Radiobiology for the radiologist. 8th ed. Wolters Kluwer; 2018.
5. Javadinia SA, Dehghani M, Ferns GA, Shahid Sales S, Avan A. Toxicity of adjuvant radiotherapy in patients with breast cancer: a review study. Rep Radiother Oncol. 2018; 5(1): e89328.
6. Clarke M, Collins R, Darby S, Davies C, Elphinstone P, Evans V, et al. Effects of radiotherapy and of differences in the extent of surgery for early breast cancer on local recurrence and 15-year survival: an overview of the randomised trials. Lancet. 2005; 366(9503):

2087-2106.
7. Shahidi M, Mozdarani H, Bryant PE. Radiation sensitivity of leukocytes from healthy individuals and breast cancer patients as measured by the alkaline and neutral comet assay. Cancer Lett. 2007; 257(2): 263-273.
8. Ryabchenko NM, Glavin OA, Shtefura VV, Anikushko MF. Chromosomal radiosensitivity in ukrainian breast cancer patients and healthy individuals. Exp Oncol. 2012; 34(2): 121-124.
9. Mozdarani H, Ziaee Mashhadi AH, Alimohammadi Z. G2 chromosomal radiosensitivity and background frequency of sister chromatid exchanges of peripheral blood lymphocytes of breast cancer patients. Int J Radiat Res. 2011; 9(3): 167-174.
10. Ching TL, Haenen GR, Bast A. Cimetidine and other H2 receptor antagonists as powerful hydroxyl radical scavengers. Chem Biol Interact.1993; 86(2): 119-127.
11. Lapenna D, DeGioia S, Mezzetti L. H_2-receptor antagonists are scavengers of oxygen radicals. Eur J Clin Invest. 1994; 24(7): 476-481.
12. Ghorbani M, Mozdarani H. In vitro radioprotective effects of histamine H2 receptor antagonists against gamma rays induced chromosomal aberrations in human lymphocytes. Iran J Radiat Res. 2003; 1(2): 99-104.
13. Mozdarani H, Gharbali A. Radioprotective effects of cimetidine in mouse bone marrow cells exposed to gamma-rays as assayed by the micronucleus test. Int J Radiat Biol. 1993; 64(2): 189-194.
14. Zangeneh M, Mozdarani H, Mahmoudzadeh A. Potent radioprotective effects of combined regimens of famotidine and vitamin C against radiation-induced micronuclei in mouse bone marrow erythrocytes. Radiat Environ Biophys. 2015; 54(2): 175-181.
15. Mozdarani H, Ghoraeian P. Modulation of gamma-ray-induced apoptosis in human peripheral blood leukocytes by famotidine and vitamin C. Mutat Res. 2008; 649(1-2): 71-78.
16. Hardeland R, Cardinali DP, Srinivasan V, Spence DW, Brown GM, Pandi-Perumal SR, et al. Melatonin-a pleiotropic, orchestrating regulator molecule. Prog Neurobiol. 2011; 93(3): 350-384.
17. Mediavilla MD, Sanchez-Barcelo EJ, Tan DX, Manchester L, Reiter RJ. Basic mechanisms involved in the anti-cancer effects of melatonin. Curr Med Chem. 2010; 17(36): 4462-4481.
18. Reiter RJ, Rosales-Corral SA, Tan DX, Acuna-Castroviejo D, Qin L, Yang SF, et al. Melatonin, a full service anti-cancer agent: inhibition of initiation, progression and metastasis. Int J Mol Sci. 2017; 18(4): 843.
19. Sanchez-Barcelo EJ, Mediavilla MD, Alonso-Gonzalez C, Reiter RJ. Melatonin uses in oncology: breast cancer prevention and reduction of the side effects of chemotherapy and radiation. Expert Opin Investig Drugs. 2012; 21(6): 819-831.
20. Galano A, Tan DX, Reiter RJ. Melatonin as a natural ally against oxidative stress: a physicochemical examination. J Pineal Res. 2011; 51(1): 1-16.
21. Rodriguez C, Mayo JC, Sainz RM, Antolín I, Herrera F, Martín V, et al. Regulation of antioxidant enzymes: a significant role for melatonin. J Pineal Res. 2004; 36(1): 1-9.
22. Huang CC, Lai CJ, Tsai MH, Wu YC, Chen KT, Jou MJ, et al. Effects of melatonin on the nitric oxide system and protein nitration in the hypobaric hypoxic rat hippocampus. BMC Neurosci. 2015; 16: 61.
23. Johnke RM, Sattler JA, Allison RR. Radioprotective agents for radiation therapy: future trends. Future Oncol. 2014; 10(15): 2345-2357.
24. Vijayalaxmi, Meltz ML, Reiter RJ, Herman TS, Kumar S. Melatonin and protection from whole body irradiation: survival studies in mice. Mutat Res. 1999; 425(1): 21-27.
25. Vijayalazmi, Meltz ML, Reiter RJ, Herman TS. Melatonin and protection from genetic damage in blood and bone marrow: whole-body radiation studies in mice. J Pineal Res. 1999; 27(4): 221-225.
26. Vijayalaxmi, Reiter RJ, Meltz ML. Melatonin protects human blood lymphocytes from radiation-induced chromosome damage. Mutat Res. 1995; 346(1): 23-31.
27. Choucroun P, Gillet D, Dorange G, Sawicki B, Dewitte JD. Comet assay and early apoptosis. Mutat Res. 2001; 478(1-2): 89-96.
28. Husseini GA, O'Neill KL, Pitt WG. The comet assay to determine the mode of cell death for the ultrasonic delivery of doxorubicin to human leukemia (HL-60 cells) from pluronic P105 micelles. Technol Cancer Res Treat. 2005; 4(6): 707-711.
29. Kedare SB, Singh RP. Genesis and development of DPPH method of antioxidant assay. J Food Sci Technol. 2011; 48(4): 412-422.
30. Liao W, McNutt MA, Zhu WG. The comet assay: a sensitive method for detecting DNA damage in individual cells. Methods. 2009; 48(1): 46-53.
31. Scott D, Barber JB, Spreadborough AR, Burrill W, Roberts SA. Increased chromosomal radiosensitivity in breast cancer patients: a comparison of two assays. Int J Radiat Biol. 1999; 75(1): 1-10.
32. Tan DX, Manchester LC, Esteban-Zubero E, Zhou Z, Reiter RJ. Melatonin as a potent and inducible endogenous antioxidant: synthesis and metabolism. Molecules. 2015; 20(10): 18886-18906.
33. Reiter RJ, Tan DX, Manchester LC, Tamura H. Melatonin defeats neurally-derived free radicals and reduces the associated neuromorphological and neurobehavioral damage. J Physiol Pharmacol. 2007; 58 Suppl 6: 5-22.
34. Vijayalaxmi, Reiter RJ, Tan DX, Herman TS, Thomas CR Jr. Melatonin as a radioprotective agent: a review. Int J Radiat Oncol Biol Phys. 2004; 59(3): 639-653.
35. Reiter RJ, Tan DX, Galano A. Melatonin reduces lipid peroxidation and membrane viscosity. Front Physiol. 2014; 5: 377.
36. Sliwinski T, Rozej W, Morawiec-Bajda A, Morawiec Z, Reiter R, Blasiak J. Protective action of melatonin oxidative DNA damage-chemical inactivation versus base-excision repair. Mutat Res. 2007; 634(1-2): 220-227.
37. Yuan L, Collins AR, Dai J, Dubocovich ML, Hill SM. MT(1) melatonin receptor overexpression enhances the growth suppressive effect of melatonin in human breast cancer cells. Mol Cell Endocrinol. 2002; 192(1-2): 147-156.
38. Wang J, Guo W, Chen W, Yu W, Tian Y, Fu L, et al. Melatonin potentiates the antiproliferative and pro-apoptotic effects of ursolic acid in colon cancer cells by modulating multiple signaling pathways. J Pineal Res. 2013; 54(4): 406-416.
39. Alonso-Gonzalez C, Gonzalez A, Martinez-Campa C, Gomez-Arozamena J, Cos S. Melatonin sensitizes human breast cancer cells to ionizing radiation by downregulating proteins involved in double-strand DNA break repair. J Pineal Res. 2015; 58(2): 189-197.
40. Naeeji A, Mozdarani H, Shabestani Monfared A, Faeghi F, Ahmadi AA, Gholami M, et al. Oral administration of vitamin C, cimetidine and famotidine on micronuclei induced by low dose radiation in mouse bone marrow cells. J Biomed Phys Eng. 2017; 7(2): 117-126.

Original Article

Human Endometrial Stromal/Stem Cells Inhibit Apoptosis in Cisplatin-Induced Acute Kidney Injury in Male Wistar Rats

Hadis Zeinali, Ph.D.[1], Mahnaz Azarnia, Ph.D.[1]*, Peyman Keyhanvar, M.D., Ph.D.[2, 3], Reza Moghadasali, Ph.D.[4], Somayeh Ebrahimi-Barough, Ph.D.[5]

1. Faculty of Biological Sciences, Kharazmi University, Tehran, Iran
2. Stem Cell Research Center, Tabriz University of Medical Sciences, Tabriz, Iran
3. Department of Medical Nanotechnology, School of Advanced Medical Sciences, Tabriz University of Medical Sciences, Tabriz, Iran
4. Department of Stem Cells and Developmental Biology, Cell Sciences Research Center, Royan Institute for Stem Cell Biology and Technology, ACECR, Tehran, Iran
5. Department of Tissue Engineering and Applied Cell Sciences, School of Advanced Technologies in Medicine, Tehran University of Medical Sciences, Tehran, Iran

Corresponding Address: P.O.Box: 15719-14911, Faculty of Biological Sciences, Kharazmi University, Tehran, Iran
Email: azarnia@khu.ac.ir

Received: 15/December/2019, Accepted: 12/February/2020

Abstract

Objective: Acute kidney injury (AKI) is referred to as sudden decline in the function of kidney. Human endometrial stromal/stem cells (hEnSCs) are mesenchymal stem cell (MSC)-like cells, which are suitable candidates for regenerative medicine purposes, yet the effect of hEnSCs on cisplatin-induced AKI has not been studied; therefore, the present study was conducted to investigate this gap in the literature.

Materials and Methods: In this experimental study, hEnSCs were obtained from endometrial biopsy using collagenase I and were then cultured in DMEM/F12 medium. A total of 48 male Wistar rats (150-200 g) were classified into four groups: intact -receiving no treatment, model -receiving 5 mg/kg of body weight cisplatin, as well as phosphate-buffered saline (PBS) and cell -receiving either PBS or hEnSCs for three hours after cisplatin injection, respectively. Biochemical parameters, pathologic scores, apoptosis assay, *Bcl-2* and *Tnf-α* expression were evaluated on day 5.

Results: On day 5 post-transplantation we observed that HEnSCs injection has led to a decrease in both blood urea nitrogen (BUN) and serum creatinine (SCr), compared to the model and PBS groups (0.82 ± 0.03 vs. 1.42 ± 0.06, 1.09 ± 0.05 mg/dl and 61.53 ± 3.07 vs. 116.60 ± 2.12, 112.00 ± 1.35 mg/dl, respectively). The highest levels of pathologic scores were observed in model and PBS groups, while hEnSCs transplantation resulted in a decrease in pathologic scores (149.10 ± 7.03, 141.50 ± 4.68 vs. 118 ± 2.16). HEnSCs significantly decreased the percentage of TUNEL-positive cells in the cell group compared with model and PBS groups (20.37 ±. 3.37 vs. 33.67 ± 1.79, 31.53 ± 1.05 in glomeruli and 15.10 ± 1.47 vs. 42.33 ± 1.72, 39.23 ± 1.61 in tubules). In addition, HEnSCs resulted in upregulation of *Bcl-2* and downregulation of *Tnf-α* in the cisplatin-induced AKI.

Conclusion: Our results showed that injection of hEnSCs may improve AKI through lowering the amount of apoptosis in renal cells.

Keywords: Acute Kidney Injury, Apoptosis, Cisplatin, Human Endometrial Stromal/Stem Cell

Cell Journal(Yakhteh), Vol 23, No 5, October 2021, Pages: 568-575

Citation: **Zeinali H, Azarnia M, Keyhanvar P, Moghadasali R, Ebrahimi-Barough S. Human endometrial stromal/stem cells inhibit apoptosis in cisplatin-induced acute kidney injury in male wistar rats. Cell J. 2021; 23(5): 568-575. doi: 10.22074/cellj.2021.7322.**

Introduction

Acute kidney injury (AKI) is defined as sudden decline in the function of kidneys for waste removal, which is due to renal tubular damage (1). Cell death, as well as functional and morphological changes, occur in sub-lethal damage caused by AKI (2). About 20% and 33% of hospitalized adults and children, respectively, suffer from AKI, and the mortality rate due to AKI in patients of surgical and medical intensive care units (ICU) is high. Consequently, AKI has attracted much attention among nephrologist and intensive care unit care providers (3, 4). Common treatments used in AKI include pharmacological therapy, dialysis, and renal replacement therapy, but each of these treatments still has certain limitations (5). Dialysis and replacement therapies have no significant effect on the high rate mortality caused by AKI. Dialysis is commonly associated with socioeconomic problems. With regards to replacement therapy, the lack of enough donors and the use of immunosuppressive drugs following kidney transplantation may cause issues for the recipients. Pharmacological therapy has been unsuccessful in terms of recovering lost cells. Therefore, new therapeutic strategies for AKI seem to be instantly required (6).

Among the common experimental models of AKI are toxic models, which are caused by nephrotoxins, such as cisplatin. Cisplatin-induced extensive injury is usually assessed on days 3-5 post-treatment, whereas earlier time points may lead to sub-lethal changes (2). Cisplatin or cis-diamminedichloroplatinum (II) is a chemotherapeutic drug, which contains platinum, carboplatin or oxaliplatin. Platinum in cisplatin compound binds to DNA and results in crosslinking that triggers apoptosis (7). Sodium

wasting, disturbance of magnesium reabsorption and water absorption are among other consequences of cisplatin therapy. Additionally, prevention of kidney injury is very important in cisplatin therapy (8, 9). Cisplatin-induced tubular dysfunction is due to apoptosis and necrosis. Tubular cell death, resulting from cisplatin, occurs via multiple signaling pathways and mechanisms that have been considered as potential targets for various clinical treatments (10-14). Two signaling pathways of apoptosis include intrinsic (mitochondrial) and extrinsic (death receptor) pathways. Apoptosis is initiated by the extrinsic signaling pathway, which begins with a cell death signal or death ligand docking on tumor necrosis factor (TNF) superfamily death receptors (15). The intrinsic pathway of apoptosis, on the other hand, is regulated by B-cell lymphoma-2 (Bcl-2) protein family, as the Bcl-2 family members play different roles in intrinsic death pathway. For instance, anti-apoptotic Bcl-2 proteins inhibit pro-apoptotic members of the family (BAX and BAK) and thereby inhibit apoptosis (15, 16).

Multiple studies have demonstrated enormous potentials for mesenchymal stem cells (MSCs) to repair the damaged tissues via infusion and paracrine signaling (17-19). Human endometrial stromal/stem cells (HEnSCs) are MSC-like cells obtained from the endometrium. HEnSCs can be isolated easily, expand rapidly, have no major technical and ethical issues, and have a high clonogenicity; and therefore, are suitable candidates for therapeutic and tissue engineering purposes (20, 21). The repair of soft tissue defects is a promising regenerative capacity of the hEnSCs (22). Transplanted EnSCs in the peri-infarct area increase cellular proliferation, but decrease apoptosis via AKT, ERK1/2, STAT3 activation and p38 inhibition (23). Pabla and Dong have found that cisplatin exerts its ultimate destructive effects on renal function through necrosis and apoptosis of renal cells (8). Therefore, apoptosis reduction in renal tissue is one of the principal mechanisms that is noteworthy in AKI treatment.

To provide an evidence for the effectiveness of hEnSC transplantation in AKI treatment, the present study was designed based on the hypothesis that administration of these cells can modulate the expression levels of *Bcl-2* and *Tnf-α* in the renal tissue from cisplatin-induced AKI rats. Such changes in transcriptional activities of *Bcl-2* and *Tnf-α* are related to apoptosis inhibition, which can result in the improvement of renal pathology and function in rats receiving cell transplants after cisplatin injection.

Materials and Methods

The experimental study was performed on 48 male Wistar rats (150-200 g). The animals were kept in plastic cages. They had unlimited access to water and food, and were weighed daily. Ethical principles were followed in accordance with Tabriz University of Medical Sciences guidelines (IR.TBZMED.VCR.REC.1397.049). AKI was induced using intraperitoneal (IP) injection of cisplatin (Mylan, France). Animal care was provided by animal house of Kharazmi University at 22.0 ± 2.0°C.

A total of 48 rats were randomly divided into four groups (12 each). Group I (intact group) received no treatment; group II (model group) received 5 mg/kg of body weight cisplatin (IP), which was used to induce AKI; group III (PBS group) received 200 µl of phosphate-buffered saline (PBS, Invitrogen, USA) in caudal vein 3 hours after cisplatin injection; and group IV (cell group) received about 1 million hEnSCs suspended in PBS (200 µl) in caudal vein 3 hours after cisplatin injection. The rats were anesthetized by IP injection of 80-100 mg/kg ketamine and 5-10 mg/kg xylazine. The rats were sacrificed on the 3rd and 5th day after cisplatin injection. After anesthesia, blood collection was performed from the heart and the kidneys were collected rapidly for subsequent analyses.

Isolation of human endometrial stromal/stem cells

The cell donor was an infertile woman who had referred to the hospital seeking treatment. A written informed consent form was obtained from her prior to the procedure. Endometrial biopsies for hEnSC isolation were obtained from the fundal region of the uterine cavity. First, endometrium was scraped from the myometrium and then washed in PBS. Mechanical minced tissue was digested using 1 mg/ml collagenase type I (Gibco, USA) and 25 mM 4-(2 hydroxyethyl)-1 piperazineethanesulfonic acid (HEPES) in Hank's balanced salt solution (HBSS, Merck, Germany) at 37ºC for 30-45 minutes. Glandular epithelial components were removed by means of cell strainers (70 and 40 µm, Merck, Germany). Cell suspension was centrifuged for cellular plaque deposition and plated in DMEM/F12 medium (Merck, Germany) supplemented with 10% fetal bovine serum (FBS), 1% antibiotic Pen/Strep (Merck, Germany). Medium change was performed every 2-3 days and cellular passage was carried out when cultures reached about 80-90% confluency. The 3rd to 5th passage cells were used for injection.

Flow cytometric analysis of human endometrial stromal/stem cells

After the 3rd passage, cells were characterized for expression of surface markers by flow cytometry (BD FACS Calibur, USA). Following hEnSCs fixation (2% paraformaldehyde in PBS, 4°C, 1 hour), cells were washed and incubated using the following PerCP- or phycoerythrin (PE)- or fluorescein-isothiocyanate (FITC)-conjugated antibodies (4°C, 1 hour): CD73-PerCP (5 µl, BD Pharmingen, USA), CD90-FITC (3 µl, Exbio, Czechia), CD105-PE (3 µl, Exbio, Czechia), CD146-PE (3 µl, BD Biosciences, USA), CD31-PE (3 µl, Immunostep, Spain) and CD34-PE (3 µl, Exbio, Czechia). CD31 and CD34 are endothelial and hematopoietic markers, respectively. Negative control was FITC-conjugated mouse IgG1. Data were analyzed using FlowJo™ v10.6.1 software.

Renal function

On days 3 and 5 after transplantation of cells, rats

were anesthetized and blood samples were collected from the rat hearts. After 30 minutes, blood samples were centrifuged (3000 rpm, 10 minutes) and upper layer or serum was isolated. Samples were stored at -20˚C until analysis. To access the renal function, we determined levels of blood urea nitrogen (BUN), serum creatinine (SCr), serum sodium (Na), and potassium (K) on days 3 and 5 after cellular therapy. Biochemical markers of the sera were measured using a Selectra Pro M (ELITechGroup, USA) and a starlyte electrolyte analyzer (Diamond Diagnostics Inc., USA).

Histopathological assay by hematoxylin and eosin staining

Histological examination of the kidneys was performed on day 5. Kidneys were washed twice with PBS, quickly fixed in 10% formalin solution (Merck, Germany), then processed and embedded in paraffin (Merck, Germany). Finally, 5-µm thick sections were obtained. Histological examination was performed using hematoxylin (Merck, Germany) and eosin (Merck, Germany) staining. The slides were observed under a light microscope (Zeiss, Germany). The presence of pathologic tubular damage (including apoptosis, necrosis, lumen dilation, debris in the lumen and nuclear fragmentation) was scored in 10 non-overlapping fields (100 tubules) for each kidney section by a researcher who was blind to the experimental groups. The score 0 represents no tubular damage, 1= tubular injury in no more than one third of the tubule cells, 2= one third to two thirds of the tubular cell injury, and 3= more than two thirds of the tubular injury. Finally, total pathologic score was obtained by adding all 100 scores. The maximum score was 300.

Immunohistochemical analysis

TUNEL assay was performed on paraffin-embedded tissues using the terminal deoxynucleotidyl transferase–mediated dUTP nick-end labeling (TUNEL) method (In Situ Cell Death Detection Kit, Roche, Germany) according to the manufacturer's instruction.

Paraffin sections (5-µm thick) of kidneys were rehydrated in a series of alcohol and water after deparaffinization with xylene. Then sections digested by proteinase K solution (10 minutes, 37˚C) were washed in PBS for 2 minutes, and after blocking (i.e. blocking endogenous peroxidase, 3% H_2O_2 for 30 minutes), were incubated with TdT enzyme solution (60 minutes, 37˚C). A stop/wash buffer (30 minutes, 37˚C) was used to terminate the reaction. The reaction was visualized using a 3, 3′-diaminobenzidine (DAB) chromogen (Pro Taqs, Cat#300155400) and tissue counterstaining was performed using hematoxylin. Sections were observed for TUNEL+ cells per high-power field (HPF) under a light microscope (Zeiss, Germany). For each kidney, 10 fields were selected randomly at 40x magnification, and the number of TUNEL-positive cells and the total number of cells in the glomeruli and tubules were counted using ImageJ software (LOCI, University of Wisconsin). The percentage of apoptotic cells was evaluated in a blind manner. Data were analyzed using GraphPad software.

Real-time polymerase chain reaction

The kidney samples were minced and RNA was extracted using a Maxcell extraction kit (Iran). Synthesis of cDNA was performed using First Strand cDNA synthesis kit (Maxcell, Iran). RNA/primer mixture (14 µl) including 1 µl random hexamer, 1 µl of 10 mM dNTP mix, total RNA (volume based on normalization calculations), and DEPC water (up to 14 µl), was incubated for 5 minutes at 65˚C and was then placed on ice immediately for 1 minute. Next, 1 µl Dia star (reverse transcriptase, RT), 1 µl of 8 mM DTT and 4 µl of 5X RT buffer were mixed to prepare reaction master mix. Reaction master mix was added to RNA/primer mixture and then placed in the thermal cycler as follows: 50˚C, 60 minutes, and 95˚C, 5 minutes. Real time-polymerase chain reaction (PCR) was carried to in duplicate. Reaction volume was 25 µl consisting Real Q Plus 2X Master Mix Green (Ampliqon, Denmark), 2 µl of primer mixture and 2 µl of cDNA under the following thermal cycling: 5 minutes at 50˚C, 5 minutes at 95˚C and 40 cycles of denaturation for 30 seconds and annealing/extension at 60-62˚C. Relative expression levels of *Bcl-2* and *Tnf-α* mRNA were calculated using the $2^{-\Delta\Delta CT}$ method. *Gapdh* gene was considered as internal control. Primer sequences are showed in Table 1.

Table 1: The primer sequences were used in the real-time polymerase chain reaction

No.	Gene symbol	Gene name	Primer sequences (5′-3′)	TM	GC%
1	*Bcl-2*	B-cell lymphoma 2	F: CTTTGAGTTCGGTGGGGTCA	59.35	55.00
			R: TCCACAGAGCGATGTTGTCC	59.35	55.00
2	*Tnf-α*	Tumor necrosis factor alpha	F: GGCAGGTTCTGTCCCTTTCAC	61.78	57.14
			R: TTCTGTGCTCATGGTGTCTTTTCT	59.30	41.67
3	*Gapdh*	Glyceraldehyde 3-phosphate dehydrogenase	F: CAAGTTCAACGGCACAGTCA	57.30	50.00
			R: CCCCATTTGATGTTAGCGGG	59.35	55.00

Statistical analysis

Data are shown as mean ± SEM. Data analyses were performed using GraphPad Prism 8.0.2 (GraphPad Software Inc., USA). We compared the differences among the groups using One-way analysis of variance (ANOVA) with Tukey test. Analyses of body weight between days 1 and 5 were done in each group using two-way ANOVA. Expression levels of mRNA were analyzed using the comparative Ct method. $P<0.05$ were considered as statistically significant.

Results

Human endometrial stromal/stem cells culture and characterization

Isolation of undifferentiated hEnSCs was easily performed due to their adherence to plastic flasks. The results of hEnSCs immunophenotyping at passage 3 are presented in histograms in Figures 1A and B. HEnSCs were positive for MSC markers, including CD73, CD90 and CD105, as well as for the marker of endometrial stem cell, CD146. Although they expressed high levels of these markers, they did not express CD31 and CD34, which are endothelial and hematopoietic progenitor cell markers, respectively (Fig.1A, B). HEnSCs were spindle-shaped and were relatively elongated (Fig.1C). These cells were cultured and reached 80-90% confluency before passage.

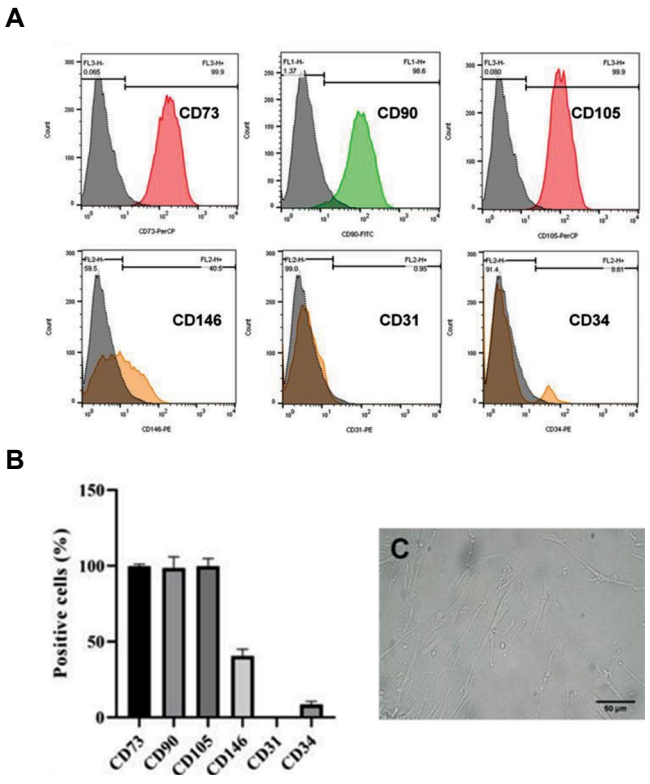

Fig.1: Flow cytometry and morphological feature of extracted hEnSCs after the 3rd passage. **A, B.** HEnSCs are positive for MSC markers and are negative for hematopoietic and endothelial markers. Data show the mean of positive cells (%) ± SEM. **C.** HEnSCs are spindle-shaped and relatively elongated cells (scale bar: 50 µm). hEnSCs; Human endometrial stromal/stem cells and MSC; Mesenchymal stem cell.

Changes of body weight

In the present study, all rats were weighed daily at the appointed time. Body weights were reduced until day 5 in all groups except for the intact group. Body weight for intact group was 150.00 ± 9.55 g and 172.90 ± 10.30 g on days 1 and 5, respectively. Cisplatin administration induced weight loss in model and PBS groups on day 5 as compared to day 1 (172.50 ± 8.99 g, and 186.8 0 ± 8.14 g, vs. 164.50 ± 5.57 g, and 172.00 ± 6.70 g, respectively). Interestingly, a lower body weight loss in cell-transplanted rats (177.50 ± 5.18 g on day 5, 182.00 ± 5.174 g on day 1) as compared to model and PBS groups, may indicate the therapeutic effects of hEnSCs on the disturbance of tubular concentration function (Fig.2A).

Biochemical analysis of renal function

Successful cisplatin-induced AKI was determined by measuring biochemical markers in blood samples obtained on days 3 and 5. The observed increase in biochemical markers indicated the development of AKI.

The BUN levels in all groups were almost similar on the 3rd day without a statistically significant difference. On day 5, the BUN levels in model and PBS groups were higher (116.60 ± 2.12 and 112.00 ± 1.35 mg/dl, respectively) as compared to those of the hEnSC-transplanted and intact rats (61.53 ± 3.07 and 24.04 ± 0.89 mg/dl, respectively) on day 5. The highest level of BUN was observed in the model group, but cell injection resulted in a significant decrease in BUN levels (Fig.2B).

The changes of SCr quantities were similar to those of BUN levels. SCr increased significantly in model, PBS, and hEnSC-transplanted groups as compared with the healthy intact animals (0.65 ± 0.02 mg/dl) on day 5. Also, a significant decrease ($P<0.05$) was observed in the SCr level in the group receiving hEnSCs compared to the model and PBS groups (0.82 ± 0.03 vs. 1.42 ± 0.06, 1.09 ± 0.05 mg/dl respectively) on day 5 (Fig.2B).

Serum Na and K levels on day 3 were similar among the groups (about 150 milliequivalent (meq)/l and 4.5 meq/l, respectively). On day 5, there were significant decreases ($P<0.05$) in the mean values of Na levels in the model, PBS and the cell groups (131.60 ± 1.61, 134.30 ± 2.37 and 143.00 ± 3.13 meq/l, respectively) as compared to that of the intact group (153.80 ± 2.92 meq/l), but the difference between PBS and the cell groups was not significant. Also, cell treatment resulted in the mild increase of Na level (Fig.2B). Moreover, on day 5, we observed a significant decrease ($P<0.05$) in the mean K levels in the model and PBS (3.87 ± 0.13 and 4.20 ± 0.19 meq/l, respectively) as compared to those of the intact and the cell groups (5.41 ± 0.23 and 5.00 ± 0.22 meq/l, respectively). In addition, the quantities of K in rats receiving hEnSCs were not significantly different compared with those of the intact group on day 5 (Fig.2B).

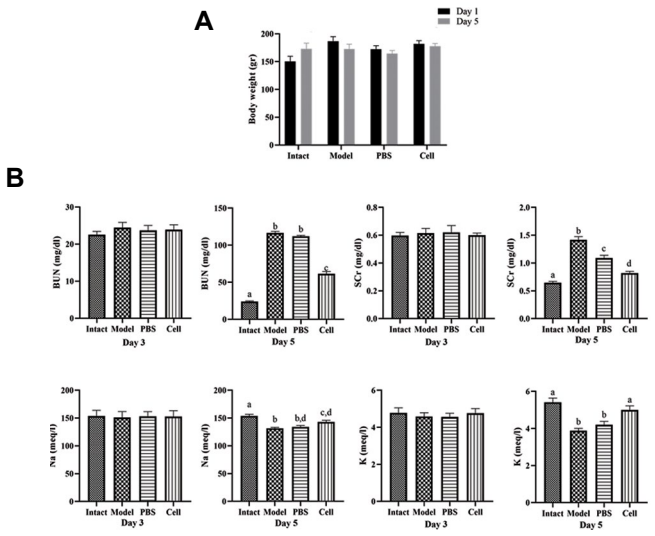

Fig.2: Body weight and serum biochemical changes after hEnSCs injections. All animals except for the intact group received cisplatin (5 mg/kg, IP) on day 1. After 3 hours, the cell group received 1×10^6 hEnSCs in 200 µl PBS. **A.** Mean body weights of the treated animals. **B.** The collected serum samples are from days 3 and 5 after cisplatin. Following hEnSCs injections the levels of BUN, SCr, ion Na, and K were analyzed as shown here. Each column presents mean ± SEM. a-d; Show significant differences between groups (P<0.05), hEnSCs; Human endometrial stromal/stem cells, IP; Intraperitoneal, PBS; Phosphate-buffered saline, BUN; Blood urea nitrogen, SCr; Serum creatinine, Na; Sodium, and K; Potassium.

Pathologic changes

Examination of renal sections was performed in the cortex and medulla regions on day 5 (Fig.3, original magnification:×40). Light microscopic analyses showed significant changes in the renal tissue on day 5 after cisplatin injection. Histological examination of the kidney tissues obtained from both model and PBS groups showed proximal and distal tubular injury with cell debris in the lumen, lumen dilation, regenerative changes in tubular cells, nuclear fragmentation, and apoptosis and necrosis of the epithelial cells (Fig.3C-F). On day 5 following hEnSC injection, a significant improvement was observed in renal glomeruli and tubules, thus the pathologic scores for tubular damage were 118.8 ± 2.15 for the cell group versus 149.1 ± 7.02 and 141.5 ± 4.68 for the model and PBS groups, respectively. Similar to the beneficial effects on the serum biomarkers associated with renal function, hEnSCs had a significant effect on renal pathology, as they improved the renal pathologic scores (Fig.3).

Evaluation of apoptosis in tubular epithelial cells and glomeruli after cell therapy

Apoptosis in paraffin embedded tissues was detected using TUNEL kit and data were analyzed via ImageJ Software. On day 5, the percentage of TUNEL-positive apoptotic cells in tubules and glomeruli increased significantly in both model and PBS groups in comparison to the intact group (Fig.4A-F) (33.67 ± 1.79, 31.53 ± 1.05 vs. 6.37 ± 1.05 in glomeruli and 42.33 ± 1.72, 39.23 ± 1.61 vs. 4.67 ± 1.17 in tubules). HEnSC-transplantation resulted in a marked reduction of apoptotic cells in the renal tissue (Fig.4G, H), suggesting an inhibitory effect of the hEnSCs on cisplatin-induced apoptosis. The results of the percentage of apoptotic cells in different groups are shown in histograms Figure 4 I and J.

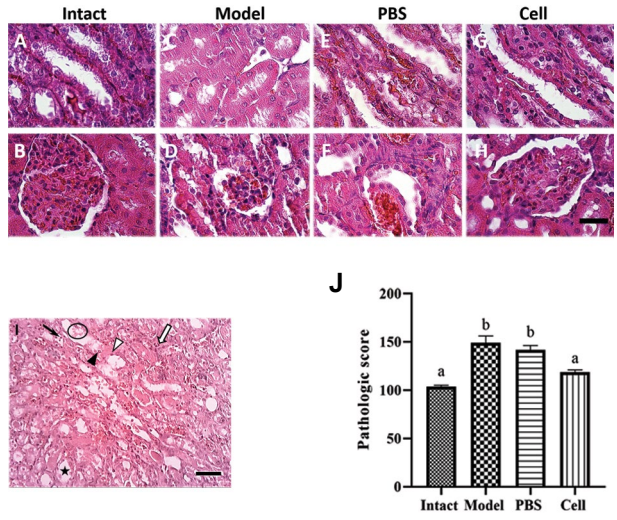

Fig.3: Pathologic analyses of kidneys after hEnSCs injection on day 5. **A-H.** HEnSCs injection led to significant reduction of pathologic injuries in renal tissue (original magnification: ×40, scale bar: 50 µm). **I.** Photomicrograph shows tubular injuries: cell debris in the lumen (circle), lumen dilation (star), regenerative change in tubular cells or flattening of the epithelium lining the tubules (white triangle), nuclear fragmentation (white arrow), apoptosis (black arrow) and necrosis (black triangle) (original magnification: ×10, scale bar: 100 µm). **J.** Histogram shows pathologic scores in different groups. a, b; Show significant differences between groups (P<0.05), hEnSCs; Human endometrial stromal/stem cells, and PBS; Phosphate-buffered saline.

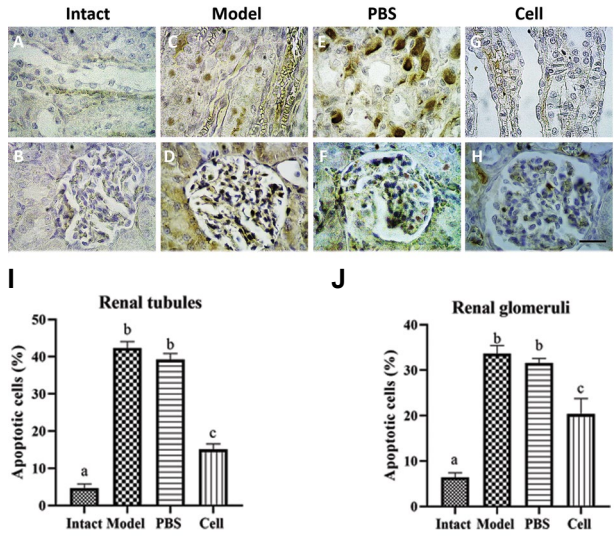

Fig.4: Results of TUNEL test after hEnSCs injection on day 5. **A, B.** Intact group, **C, D.** Model animals receiving the cisplatin, **E, F.** PBS group receiving PBS 3 hours after cisplatin injection, **G, H.** Cell group receiving hEnSCs 3 hours after cisplatin injection. TUNEL (+) cells were observed in tubules and glomeruli (original magnification: ×40, scale bar: 50 µm). **I, J.** Histograms showed the percentage of TUNEL (+) cells. Each column presents mean ± SEM. a-c; Show significant differences between groups (P<0.05), hEnSCs; Human endometrial stromal/stem cells, and PBS; Phosphate-buffered saline.

Effects of treatment with hEnSCs on renal mRNA expression of *Bcl-2* and *Tnf-α*

Investigation of direct effect of hEnSC treatment on renal production of *Bcl-2* and *Tnf-α* was done using real-time PCR. The expression levels of the mRNA for *Bcl-2* (anti-apoptotic and anti-inflammatory gene, intrinsic apoptotic pathway) and *Tnf-α* (pro-apoptotic and pro-inflammatory cytokine gene, extrinsic apoptotic pathway) changed after cisplatin and hEnSC injection in comparison to those of the intact group on day 5 (Fig.5). The mean *Bcl-2* levels in the intact, model, PBS and cell groups were 1.00 ± 0.28, 1.21 ± 0.12, 2.28 ± 0.22, and 15.74 ± 0.55, respectively. Model, PBS, and the cell groups showed a meaningful increase ($P<0.05$), when compared to the intact group, but the difference between the model and PBS groups was not significant. The mean *Tnf-α* levels were 1.00 ± 0.61, 2.35 ± 0.71, 3.16 ± 1.39, and 1.38 ± 0.39 in the intact, model, PBS, and cell groups respectively. Cisplatin treatment caused an increase in *Tnf-α* levels but hEnSCs transplantation lead to a decrease in *Tnf-α* level in the cell group. The difference between the experimental groups in terms of *Tnf-α* level was not significant.

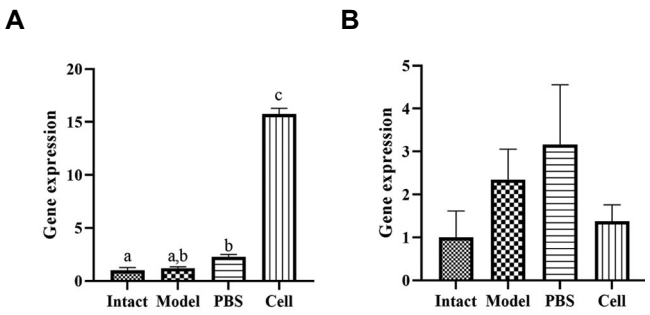

Fig.5: Changes of gene expression in renal tissue after hEnSC transplantation on day 5. **A.** *Bcl-2* and **B.** *Tnf-α* expression in intact, model, PBS and cell groups on day 5. Values are presented as mean ± SEM. a-c; Show significant differences between groups ($P<0.05$), hEnSC; Human endometrial stromal/stem cells, and PBS; Phosphate-buffered saline.

Discussion

The majority of stem cell therapy studies have focused on the use of bone marrow (BM)-MSCs. The useful effects of these cells on the function of kidneys have clearly been demonstrated in different AKI animal models by various groups (24).

To date, BM has been considered as the most ideal source of stem cells for transplantation in regenerative medicine; however, the disadvantages related to BM-MSC such as the invasive method of extraction, age-related decline of stemness and proliferative ability, the required anesthesia for the donors, etc. restrict its applications. Human endometrium also is considered as a source for stem cells. In 2010, about 430,000 inpatient hysterectomies were carried out in the US alone, demonstrating that it is a significant source of endometrial stem cells. Fortunately, hEnSCs exist in the superficial layers of this tissue, so these cells are accessible without impairment of endometrial function (25-27). In regenerative medicine, BM-MSCs are more suitable for hard tissue engineering, such as bone, whereas EnSCs are predicted to be more suitable candidates for soft tissue engineering including kidney (22).

Obtaining endometrial specimen does not require anesthesia or sedatives and causes minimal morbidity and pain. One of the clinical limitations of using MSCs is age-related proliferative ability, whereas, the proliferative capacity of hEnSCs is not impaired in the elderly (28). The effects of endometrial MSC-like or hEnSCs on renal function and apoptosis reduction in AKI has not been studied thoroughly so far. To investigate such effects, we injected hEnSCs after induction of AKI using a single dose of cisplatin. Subsequently, we determined the levels of serum biomarkers, renal pathology, and apoptotic cell percentage in renal tubules and glomeruli, as well as expression of *Bcl-2* and *Tnf-α* genes using real-time PCR.

The results of biochemical and histological analyses showed that 5 mg/kg body weight cisplatin successfully induces AKI, while hEnSCs infusion leads to the recovery of the AKI-associated signs. Following cell therapy, the levels of serum biomarkers were closer to those of the normal state and the pathologic score was reduced as well. Several reports in cisplatin-induced AKI model have shown that MSCs ameliorated the cisplatin effects on renal tissue (7, 19, 29), nonetheless, beneficial effects of MSCs on the recovery of cisplatin effects are still controversial (30).

It has previously been shown that cisplatin (5 mg/kg) results in the increase of urea, creatinine, K level, and significant changes in monkey renal tissue on day 4. These results demonstrated that intra-renal arterial injection of autologous BM-MSCs ameliorated the levels of urea and creatinine. BM-MSCs were not observed to have a significant influence on pathologic scores of kidneys, hyaline casts and fibrosis scores on days 4 and 28 after cisplatin injection (30). Similarly, we have shown that BUN, SCr and Na underwent changes, but the K level and the renal histologic scores improved after cell transplantation.

Sun et al. investigated therapeutic effects of human urine-derived stem cells (USCs) in cisplatin-induced AKI in a rat model. They induced AKI using IP injection of 5 mg/kg cisplatin and at 24 hours later injected 2×10^6 USCs/ 0.2 ml PBS via tail vein. One of the criteria to evaluate in their study was histological changes. Tubular damage score and the number of injured glomeruli decreased markedly after USC injection on day 4 (31). Our histopathologic results were similar to those of their study, because hEnSCs improved histological scores in our rat model of cisplatin-induced AKI significantly.

Ultimate damaging impact of cisplatin on the kidneys, results from apoptosis and necrosis of renal cells (8). Different stimuli including intracellular (reactive oxygen species [ROS]-induced mitochondrial damage) and extracellular (activation of death receptors) lead to cell death (32). Cisplatin induces renal cell apoptosis via p53-

mediated activations of caspase-2, 3, 8, while TNF-α synthesis by phosphorylation of p38 MAPK may be the basis of necrosis in tubular cells (33). Also, it has been shown that outer mitochondrial membrane damage and activation of apoptotic intrinsic pathway can be induced by cisplatin. Bcl-2 family plays a significant role in nephrotoxicity of cisplatin. Treatment by cisplatin results in the reduction of Bcl-2 and BAX ratio, upregulation of apoptotic genes, degradation or decrease of anti-apoptotic proteins, and increase of pro-apoptotic proteins and inflammatory mediators, such as TNF-α (34-38). Therefore, reduction of renal cell apoptosis is one of the important mechanisms to be considered in the treatment of AKI.

Human umbilical cord-derived MSCs (HUC-MSCs) reduce cell apoptosis and help repair tubular epithelial cells via upregulation of *Bcl-2* and *Bmp-7* (39). MSCs attenuate cisplatin-induced nephrotoxicity by modulating renal inflammation. MSCs significantly recover cisplatin-induced renal failure by apoptosis suppression in p53-dependent and paracrine manner (29, 40). These results, as reported in previous studies, support our findings. The present study demonstrated that the transplantation of hEnSCs result in upregulation of *Bcl-2* and downregulation of *Tnf-α*, which is consistent with apoptosis decrease and improvement of renal function. These findings suggest a relationship between the change in the intrinsic and extrinsic pathways of apoptosis and the infusion of hEnSCs. Administration of hEnSCs leads to a significant decrease of TUNEL-positive cells after the cisplatin injection. Our findings suggest that one of the important renoprotective effects of hEnSCs may depend on the inhibition or reduction of apoptosis.

Conclusion

Endometrium is a potential source of stromal/stem cells. These cells can be extracted without ethical and technical problems. In the present study, transplantation of hEnSCs changed the expression of *Bcl-2* and *Tnf-α* in renal tissue of animals with cisplatin-induced AKI. According to the findings of biochemical assays, renal pathology evaluation, and gene expression analyses, hEnSCs may be involved in apoptosis inhibition in kidneys and therefore in the improvement of their function in this model of AKI. Further research on changes of other biomarkers, such as cystatin c and NGAL, other pathological and functional aspects of the kidney, and also details of apoptotic pathways are necessary to confidently consider the clinical application of hEnSCs for the treatment of renal diseases.

Acknowledgements

There is no financial support and conflict of interest in this study.

Authors' Contributions

H.Z.; Performed experimental work, data collection and evaluation, and drafting the manuscript. M.A.; Supervised the process of experiments and manuscript, and undertakes correspondence. P.K.; Contributed substantially to the conception and design of the study. R.M.; Collaborate on data analysis and manuscript preparation. S.E.-B.; Performed cell isolation and supervision on cellular analyses. All authors read and approved the final manuscript

References

1. Thadhani R, Pascual M, Bonventre JV. Acute renal failure. N Engl J Med. 1996; 334(22): 1448-1460.
2. Heyman SN, Rosenberger C, Rosen S. Acute kidney injury: lessons from experimental models. Contrib Nephrol. 2011; 169: 286-296.
3. Susantitaphong P, Cruz DN, Cerda J, Abulfaraj M, Alqahtani F, Koulouridis I, et al. World incidence of AKI: a meta-analysis. Clin J Am Soc Nephrol. 2013; 8(9): 1482-1493.
4. Lassnigg A, Schmidlin D, Mouhieddine M, Bachmann LM, Druml W, Bauer P, et al. Minimal changes of serum creatinine predict prognosis in patients after cardiothoracic surgery: a prospective cohort study. J Am Soc Nephrol. 2004; 15(6): 1597-1605.
5. Li Q, Tian SF, Guo Y, Niu X, Hu B, Guo SC, et al. Transplantation of induced pluripotent stem cell-derived renal stem cells improved acute kidney injury. Cell Biosci. 2015; 5: 45.
6. Missoum A. Recent updates on mesenchymal stem cell based therapy for acute renal failure. Curr Urol. 2019; 13(4): 189-199.
7. Shalaby RH, Rashed LA, Ismaail AE, Madkour NK, Elwakeel SH. Hematopoietic stem cells derived from human umbilical cord ameliorate cisplatin-induced acute renal failure in rats. Am J Stem Cells. 2014; 3(2): 83-96.
8. Pabla N, Dong Z. Cisplatin nephrotoxicity: mechanisms and renoprotective strategies. Kidney Int. 2008; 73(9): 994-1007.
9. Perazella MA, Moeckel GW. Nephrotoxicity from chemotherapeutic agents: clinical manifestations, pathobiology, and prevention/therapy. Semin Nephrol. 2010; 30(6): 570-581.
10. Jiang M, Dong Z. Regulation and pathological role of p53 in cisplatin nephrotoxicity. J Pharmacol Exp Ther. 2008; 327(2): 300-307.
11. Clark JS, Faisal A, Baliga R, Nagamine Y, Arany I. Cisplatin induces apoptosis through the ERK-p66shc pathway in renal proximal tubule cells. Cancer Lett. 2010; 297(2): 165-170.
12. Ramesh G, Reeves WB. TNF alpha mediates chemokine and cytokine expression and renal injury in cisplatin nephrotoxicity. J Clin Invest. 2002; 110(6): 835-842.
13. Zhang B, Ramesh G, Norbury CC, Reeves WB. Cisplatin-induced nephrotoxicity is mediated by tumor necrosis factor-alpha produced by renal parenchymal cells. Kidney Int. 2007; 72(1): 37-44.
14. Zhuang S, Schnellmann RG. A death-promoting role for extracellular signal-regulated kinase. J Pharmacol Exp Ther. 2006; 319(3): 991-997.
15. Zaman S, Wang R, Gandhi V. Targeting the apoptosis pathway in hematologic malignancies. Leuk Lymphoma. 2014; 55(9): 1980-1992.
16. Lopez J, Tait SWG. Mitochondrial apoptosis: killing cancer using the enemy within. Br J Cancer. 2015; 112(6): 957-962.
17. Morigi M, Imberti B, Zoja C, Corna D, Tomasoni S, Abbate M, et al. Mesenchymal stem cells are renotropic, helping to repair the kidney and improve function in acute renal failure. J Am Soc Nephrol. 2004; 15(7): 1794-1804.
18. Morigi M, Rota C, Montemurro T, Montelatici E, Lo Cicero V, Imberti B, et al. Life-sparing effect of human cord blood-mesenchymal stem cells in experimental acute kidney injury. Stem Cells. 2010; 28(3): 513-522.
19. Peng X, Xu H, Zhou Y, Wang B, Yan Y, Zhang X, et al. Human umbilical cord mesenchymal stem cells attenuate cisplatin-induced acute and chronic renal injury. Exp Biol Med (Maywood). 2013; 238(8): 960-970.
20. Langstein HN, Robb GL. Reconstructive approaches in soft tissue sarcoma. Semin Surg Oncol. 1999; 17(1): 52-65.
21. Chan RWS, Schwab KE, Gargett CE. Clonogenicity of human endometrial epithelial and stromal cells. Biol Reprod. 2004; 70(6): 1738-1750.
22. Verdi J, Tan A, Shoae-Hassani A, Seifalian AM. Endometrial stem cells in regenerative medicine. J Biol Eng. 2014; 8: 20.
23. Jiang Z, Hu X, Yu H, Xu Y, Wang L, Chen H, et al. Human endometrial stem cells confer enhanced myocardial salvage and regen-

eration by paracrine mechanisms. J Cell Mol Med. 2013; 17(10): 1247-1260.
24. Barnes CJ, Distaso CT, Spitz KM, Verdun VA, Haramati A. Comparison of stem cell therapies for acute kidney injury. Am J Stem Cells. 2016; 5(1): 1-10.
25. Wright JD, Herzog TJ, Tsui J, Ananth CV, Lewin SN, Lu YS, et al. Nationwide trends in the performance of inpatient hysterectomy in the United States. Obstet Gynecol. 2013; 122(2 Pt 1): 233-241.
26. Götte M, Wolf M, Staebler A, Buchweitz O, Kelsch R, Sch AN, et al. Increased expression of the adult stem cell marker Musashi-1 in endometriosis and endometrial carcinoma. J Pathol. 2008; 215(3): 317-329.
27. Shoae Hassani A, Mortazavi-Tabatabaei SA, Sharif S, Seifalian AM, Azimi A, Samadikuchaksaraei A, et al. Differentiation of human endometrial stem cells into urothelial cells on a three-dimensional nanofibrous silk-collagen scaffold: an autologous cell resource for reconstruction of the urinary bladder wall. J Tissue Eng Regen Med. 2015; 9(11): 1268-1276.
28. Darzi S, Werkmeister JA, Deane JA, Gargett CE. Identification and characterization of human endometrial mesenchymal stem/stromal cells and their potential for cellular therapy. Stem Cells Transl Med. 2016; 5(9): 1127-1132.
29. Yao W, Hu Q, Ma Y, Xiong W, Wu T, Cao J, et al. Human adipose-derived mesenchymal stem cells repair cisplatin-induced acute kidney injury through antiapoptotic pathways. Exp Ther Med. 2015; 10(2): 468-476.
30. Moghadasali R, Azarnia M, Hajinasrollah M, Arghani H, Nassiri SM, Molazem M, et al. Intra-renal arterial injection of autologous bone marrow mesenchymal stromal cells ameliorates cisplatin-induced acute kidney injury in a rhesus Macaque mulatta monkey model. Cytotherapy. 2014; 16(6): 734-749.
31. Sun B, Luo X, Yang C, Liu P, Yang Y, Dong X, et al. Therapeutic effects of human urine-derived stem cells in a rat model of cisplatin-induced acute kidney injury in vivo and in vitro. Stem Cells Int. 2019; 2019: 1-13.
32. Holditch SJ, Brown CN, Lombardi AM, Nguyen KN, Edelstein CL. Recent advances in models, mechanisms, biomarkers, and interventions in cisplatin-induced acute kidney injury. Int J Mol Sci. 2019; 20(12): 3011.
33. Miller RP, Tadagavadi RK, Ramesh G, Reeves WB. Mechanisms of cisplatin nephrotoxicity. Toxins (Basel). 2010; 2(11): 2490-2518.
34. Sheikh-Hamad D, Cacini W, Buckley AR, Isaac J, Truong LD, Tsao CC, et al. Cellular and molecular studies on cisplatin-induced apoptotic cell death in rat kidney. Arch Toxicol. 2004; 78(3): 147-155.
35. Santos NAG, Bezerra CSC, Martins NM, Curti C, Bianchi MLP, Santos AC. Hydroxyl radical scavenger ameliorates cisplatin-induced nephrotoxicity by preventing oxidative stress, redox state unbalance, impairment of energetic metabolism and apoptosis in rat kidney mitochondria. Cancer Chemother Pharmacol. 2008; 61(1): 145-155.
36. Jiang M, Wei Q, Wang J, Du Q, Yu J, Zhang L, et al. Regulation of PUMA-alpha by p53 in cisplatin-induced renal cell apoptosis. Oncogene. 2006; 25(29): 4056-4066.
37. Mostafa RE, Dalia OS, Dina FM. Cisplatin-induced nephrotoxicity in rats: modulatory role of simvastatin and rosuvastatin against apoptosis and inflammation. J Appl Pharm Sci. 2018; 8(04): 043-050.
38. Kim S, Lee EB, Song IH, Kim YJ, Park H, Kim YW, et al. Effects of human adipose-derived stem cells in regenerating the damaged renal tubular epithelial cells in an animal model of cisplatin-induced Acute Kidney Injury. Child Kidney Dis. 2015; 19(2): 89-97.
39. Li F, Xiong F, Zhang Y, Li Y, Zhao H, Cho SC, et al. Therapeutic effects of human umbilical cord-derived mesenchymal stem cells against acute tubular necrosis quantified through measures of iNOS, BMP-7 and Bcl-2. Open J Regen Med. 2013; 2(02): 31-38.
40. Kim JH, Park DJ, Yun JC, Jung MH, Yeo HD, Kim HJ, et al. Human adipose tissue-derived mesenchymal stem cells protect kidneys from cisplatin nephrotoxicity in rats. Am J Physiol Renal Physiol. 2012; 302: F1141-F1150.

Original Article

Effects of Adipose-Derived Stem Cells and Platelet-Rich Plasma Exosomes on The Inductivity of Hair Dermal Papilla Cells

Mohammad Ali Nilforoushzadeh, M.D.[1], Nasser Aghdami, M.D., Ph.D.[2], Ehsan Taghiabadi, Ph.D.[1]*

1. Skin and Stem Cell Research Center, Tehran University of Medical Sciences, Tehran, Iran
2. Department of Regenerative Biomedicine, Cell Science Research Center, Royan Institute for Stem Cell Biology and Technology, ACECR, Tehran, Iran

Corresponding Address: P.O. Box: 16635-148, Skin and Stem Cell Research Center, Tehran University of Medical Science, Tehran, Iran
Email: ehsan.taghiabadi@gmail.com

Received: 29/December/2019, Accepted: 19/May/2020

Abstract

Objective: Hair loss is a prevalent medical problem in both men and women. Maintaining the hair inductivity potential of human dermal papilla cells (hDPCs) during cell culture is the main issue in hair follicle morphogenesis and regeneration. The present study was conducted to compare the effects of different concentrations of exosomes derived from human adipose stem cells (hASCs) and platelet-rich plasma (PRP) on the proliferation, migration and expression of alkaline pholphatase (ALP), versican, and smooth muscle alpha-actin (α-SMA) in human DPCs.

Materials and Methods: In this experimental study, hDPCs, human hair DPCs and outer root sheet cells (ORSCs) were separated from healthy hair samples. The protocol of exosome isolation from PRP and hASCs comprises serial low speed centrifugation and ultracentrifugation. The effects of different concentrations of exosomes (25, 50, 100 µg/ml) derived from hASCs and PRP on proliferation (MTS assay), migration (scratch test) and expression of ALP, versican and α-SMA (real time-polymerase chain reaction) in human DPCs were evaluated.

Results: The flow cytometry analysis of specific cytoplasmic markers showed expression of versican (77%) and α-SMA (60.8%) in DPCs and K15 (73.2%) in ORSCs. According to NanoSight Dynamic Light Scattering, we found the majority of ASCs and PRP-exosomes (ASC-Exo and PRP-Exo) to be 30-150 nm in size. For 100 µg/ml of ASCs-Exo, the expressions of ALP, versican and α-SMA proteins increased by a factor of 1.2, 2 and 3, respectively, compared to the control group. The findings of our experiments illustrated that 100 µg/ml of ASCs-Exo compared to the same concentration of PRP-Exo significantly promote DPC proliferation and migration in culture.

Conclusion: This study introduced the potential positive effect of ASC-Exo in increasing the proliferation and survival of DPCs, while maintaining their hair inductivity. Thus, ASCs-Exo possibly provide a new effective procedure for treatment of hair loss.

Keywords: Adipose Stem Cells, Exosome, Hair Inductivity, Hair Loss, Platelet-Rich Plasma

Cell Journal(Yakhteh), Vol 23, No 5, October 2021, Pages: 576-583

Citation: **Nilforoushzadeh MA, Aghdami N, Taghiabadi E. Effects of adipose-derived stem cells and platelet-rich plasma exosomes on the inductivity of hair dermal papilla cells. Cell J. 2021; 23(5): 576-583. doi: 10.22074/cellj.2021.7352.**

Introduction

Hair loss is a common complaint of both male and female patients seeking beneficial treatments for this problem, worldwide (1) . As a general feature in human, hair plays a key role in beauty, social acceptance and self-esteem, therefore, hair loss is considered a major psychological challenge. Patent-pending statistics have shown increases in the costs of repairing hair loss over the past decade. Currently, hair loss is commonly treated with herbal extracts, platelet-rich plasma (PRP), adipose-derived stem cells (ASCs), keratinocyte-conditioned media and hair transplantation, none of which have yielded entirely satisfactory outcomes (2). Recent advances in tissue engineering and regenerative medicine have resulted in promising hair-loss treatments. Different research groups have so far made great efforts to develop the hair organoid structure in laboratories (3).

Although many studies claim reconstructing the hair structure using murine stem cells and dermal papilla cells (DPCs), they have failed in human cells (4). The major causes preventing successful implementation of the results of animal models in human cells include the hair DPCs losing their trichogenic ability, an inadequate number of hair in people with severe hair loss and the lack of appropriate medical grade culture media (5, 6). As mesenchymal cells in hair follicles, the dermal papilla play the main role in regulating hair growth (7, 8). Preserving the potential hair inductivity of dermal sheath cells (DSCs) and DPCs in cell culture is the main factor in *in vitro* morphogenesis and regeneration of hair follicles (9). Using the currently available methods for cultivating human dermal papilla reduces the inductive capacity of the dermal papilla and the expression of specific dermal papilla biomarkers. Optimizing culture conditions for DPCs is therefore essential. The therapeutic capacity of different sources of exosomes, including mesenchymal stem cells (MSCs), has been recently assessed in regenerative medicine. Compared to other effective approaches in maintaining both *in vivo* and *in vitro* hair inductivity of DPCs, exosome-based treatments may be the most effective methods (10, 11). The advantages of using exosomes in experimental and clinical applications

in hair loss include inducing endogenous mechanisms, simple processing, long-term storage, and reduced risks associated with immune responses (12). Research suggests that exosomes can induce cell proliferation, migration and angiogenesis, and promote tissue repair (13), nevertheless, the effects of exosomes on the trichogenic ability of DPCs and hair regrowth are yet to be defined. The present study was conducted to evaluate the effects of ASC exosomes (ASC-Exo) as well as PRP exosomes (PRP-Exo) on proliferation and migration of DPCs and the expression of hair-inductive genes. ASC-Exo and PRP-Exo contain different growth factors that are effective in cell proliferation. ASCs are easily accessible from various fat sources and improve the outcome for the treatment of hair loss.

Material and Methods

Isolation and culture of normal dermal papilla cells and outer root sheath cells from human scalp

In this experimental study, after obtaining informed consent from the donors, healthy hair samples were transferred to the cell culture laboratory of the Skin and Stem Cell Research Center of Tehran University of Medical Sciences. The Institutional Review Board and Ethical Committee of Tehran University of Medical Sciences (Tehran, Iran) approved this study (IR.TUMS.VCR.REC.1395.624).

Human hair DPCs and ORSCs were isolated from healthy hair samples to investigate their potential for hair production. The cells were isolated and cultured as follows:

1. The hair samples were transferred to the laboratory in a Dulbecco's Modified Eagle's Medium (DMEM)/F-12 (1:1) (Thermo Fisher Scientific, USA) supplemented with 10% fetal bovine serum (FBS, Hyclone, USA)+ 50 µg/ml of penicillin/streptomycin+50 µg/ml GlutaMAX™ Supplement (Thermo Fisher, USA).

2. The hair samples were rinsed in the Hanks' Balanced Salt Solution (HBSS, Gibco, USA)+50 µg/ml of penicillin/streptomycin (Gibco, USA), 70% ethanol and HBSS+50 µg/ml of penicillin/streptomycin, respectively.

3. The hair samples were placed in 1.2 unit/ml of dispase II (Gibco, USA) at 4ºC for 16 hours.

4. Part of the hair, i.e. its lowest one-third, was rinsed as dermal papilla in collagenase I (0.1%) (Sigma, USA) at 37ºC for 4 hours.

5. Collagenase I (Sigma, USA) was inactivated with a medium containing 10% FBS and the cells were passed through a 70-µm mesh filter and were then centrifuged at 1500 rpm for 5 minutes.

6. Part of the hair, i.e. its upper two-thirds, was rinsed as ORSCs in trypsin-EDTA (0.05%) (Gibco, USA) at 37ºC for 20 minutes.

7. Trypsin/EDTA enzyme was inactivated with a medium containing 10% FBS and the cells were passed through a 70-µm mesh filter and were then centrifuged at 200 rpm for 5 minutes.

8. Epithelial cells were cultured for 14 days in 6 well plates (TPP-Germany) coated with matrigel (Sigma, USA), and containing DMEM/F12 and gold KGM kits (Lonza, USA) at 37ºC in a humidified incubator with 5% CO_2.

9. Dermal papilla cells were also cultivated in 6 well plates (TPP- Germany) with DMEM/F12 and +10% FBS+50 µg/ml penicillin/streptomycin+50 µg/ml Glutamax (Gibco, USA) at 37˚C in a humidified incubator with 5% CO_2. The cell culture medium was carefully changed every 3 days depending on the confluency of the cells.

Flow cytometry for identifying dermal papilla cells and outer root sheath cells

The DPCs and ORSCs were collected and incubated with primary antibodies against α-SMA (R&D-USA), K15 (Abcam, USA), and versican (Abcam, USA) at 4ºC for 15 hours, and then incubated with secondary goat anti-human-FITC (Abcam, USA) antibodies, goat anti human-FITC (Abcam, USA), After washing the collected cells with phosphate-buffered saline (PBS), the fluorescent cells were analyzed with flow cytometry (FC500; Beckman Coulter, Brea, CA, USA).

Characterization of dermal papilla and hair outer root keratinocytes using immunohistochemical test

Immunohistochemical staining was performed according to standard protocols. In brief, dermal papilla and hair keratinocytes were fixed in 4% paraformadehyde solution and permeabilized using Triton X-100 (MERK, Germany, 0.2%). After washing with PBS/Tween (PBST) 0.05% (Sigma, USA), the cells were incubated in primary antibodies, including anti-versican (Abcam, USA), anti-α-SMA (R&D, USA) and anti-K15 (Abcam, USA), overnight at 4ºC. After washing, dermal papilla and hair keratinocytes were incubated in secondary antibodies for one hour at 37ºC. Specific cell markers were ultimately checked with fluorescence microscope Olympus Model DP71. DAPI was also applied for nuclear staining.

Assessing alkaline phosphatase and toluidine blue staining in dermal papilla cells

The *in vitro* activity of alkaline pholphatase (ALP) in DPCs was investigated by culturing DPCs in 6 well plates and fixed in 4% paraformaldehyde solution and stained according to the ALP kit instructions (Sigma, USA). The extracellular matrix of human dermal papillae contains chondroitin 6-sulfate, heparan sulfate proteoglycans, laminin and type IV collagen. DPCs can be identified by determining the metachromatic features of these cells using toluidine blue staining. After fixation and washing with toluidine blue (Merck, Germany), the DPCs were stained and examined under a light microscope.

Isolating platelet-rich plasma from human cord blood

Approximately 200 ml of pooled human cord blood was collected in four 50 ml-conical tubes, containing 2×10^{11} total platelets on average. Pooled human cord blood was centrifuged at 300 g for 30 minutes at room temperature to obtain plasma. The plasma obtained from each tube was then transferred to a new 50 ml-conical tube and centrifuged at 200 g for 15 minutes. The PRP was ultimately stored at -80ºC for exosome isolation.

Collection of conditioned medium from human adipose stem cells

According to the isolation procedure discussed, passage 3 hASCs were obtained from the Royan Stem Cell Bank in Tehran, Iran and cultured for 48 hours in DMEM/F12 medium supplemented with 10% exosome-free FBS and 1% penicillin/streptomycin in a humidified incubator with 5% CO_2 at 37ºC before collecting the conditioned medium, which was then stored at -80ºC for exosome isolation.

Exosome isolation from platelet-rich plasma and human adipose stem cells

The protocol of exosome isolation from PRP involves serial low speed centrifugation and ultracentrifugation. The hASCs conditioned medium and PRP were centrifuged at 300 g for 10 minutes to remove the cells. The dead cells were also removed by centrifuging at 2,000 g for 10 minutes. The supernatant was transferred to a 15-ml conical tube, and centrifuged at 10,000 g to remove cell debris. In the next step, the supernatant was ultra-centrifuged at 100,000 g for 2 hours (BECKMAN COULTER, MODEL: Optima L-100XP, USA) to obtain exosomes containing proteins. The supernatant was again collected in a new tube and centrifuged at 100,000 g for 2 hours at 4ºC. The pellet containing exosomes (40 µg/200 ml) was diluted in 1×PBS and stored at -80ºC for future use.

Identifying the exosomes derived from human adipose stem cells and platelet-rich plasma

The concentrations of the exosomes derived from hASCs and PRP were specified using BCA protein assay kits (Thermo Fisher, USA). NanoSight LM10 (Nanosight) and Nanoparticle Tracking Analysis software version 2.2 were used to determine the particle size and distribution of the exosomes. Expressions of CD9, CD63, CD81, ITG101 and Calnexin proteins in the collected exosomes were analyzed using western blotting. The exosomes were morphologically characterized using a 100 kV-transmission electron microscopy (KYKYEM3200, Germany).

Western blotting

The extracted proteins in the exosomes derived from hASCs and PRP were isolated using a 10% sodium dodecyl sulfate PAGE (SDS-PAGE) gel, and then transferred to a nitrocellulose membrane. The blots were blocked with 5% skimmed milk, then washed three times with a TBST buffer, and incubated at 4ºC for 15 hours with primary antibodies such as (anti-CD81, 1:100; Thermo Fisher Scientific, Waltham, MA, USA), (anti-CD9, 1:100; Thermo Fisher Scientific, Waltham, MA, USA), (monoclonal anti-TSG101, 1:100; Thermo Fisher Scientific, Waltham, MA, USA) , (anti-CD63, 1:100; Thermo Fisher Scientific, Waltham, MA, USA) and (anti-calnexin, 1:100; Thermo Fisher Scientific, Waltham, MA, USA). In the next step, the blots were detected by their corresponding secondary antibodies. Biorad's ChemiDoc MP Imaging System was used for band detection.

Analyzing the exosomes derived from human adipose stem cells and platelet-rich plasma with NanoSight dynamic light scattering

The pellets of exosomes derived from hASCs and PRP were diluted in 100 µl of PBS, and the particle size and distribution of the exosomes were analyzed using NanoSight dynamic light scattering (632.8 nm laser) and BI 200SM Research Goniometer System (Brookhaven Instruments Corporation, Holtsville, NY, USA).

Internalization of exosomes by dermal papilla

Whether the ASCs-Exo and PRP-Exo can enter DPCs was investigated. The procedure of labeling human dermal papilla is as described below:

Centrifuging the ASCs-Exo was performed at 100,000 g for 60 minutes. Next, 200 µl of Diluent C of PKH26 kits (Sigma, USA) was added to the ASCs-Exo and PRP-Exo pellets. 200 µl of Diluent C was added to PBS^-.

Then 200 µl dye solution in Diluent C was prepared by adding 4 µl of the PKH26 Dye solution to 200 µl of a Diluent C in a conical tube and mixing well. 200 µl of the ASCs-Exo and PRP-Exo (0.2 µg/µl) solution were added to 200 µl of the dye solution followed by performing pipette mixing. The ASCs-Exo and PRP-Exo solution and the dye solution were incubated for 5 minutes. The staining procedure was stopped by adding an equal volume of 1% bovine serum albumin (BSA) for 1 minute. Centrifuging The ASCs-Exo was centrifuged at 100,000 g for 60 minutes and was suspended in 200 µl of PBS^-. The uptake of both ASCs-Exo and PRP-Exo was analyzed by dermal papilla with fluorescence microscopy.

Cell scratch assay

Human hair DPCs were seeded into 6-well plates with a density of 3×10^5 per well of 6-well plates. Two days later, the plates were scratched with the tip of a 100 µl-sterile pipette. The serum-free cell culture medium containing 0, 25, 50 and 100 µg/ml of hASCs-Exo and PRP-Exo were added. Photos were taken from the scratched area and analyzed with ImageJ, and the width of the area was measured at time points of 0, 12 and 24 hours.

Cell proliferation assay-MTS test

In this experimental study we analyzed the effects

of exosomes on cell proliferation using the MTS assay. DPCs were cultured (10^4 cells/well) in 96-well plates for 72 hours at 37ºC with different groups of exosomes. MTS assessments were performed using conditioned medium and the MTS solution (Promega, USA) at a 5:1 ratio. Absorbance was measured at 490 nm for each experimental group using an ELISA reader (Thermo, USA).

Scanning electron microscopy of human adipose stem cells and platelet-rich plasma-exosomes

The pellet of the exosomes derived from hASCs and PRP were suspended in 0.2-1 ml of DPBS. The samples were fixed for 12 hours in a 2.5% paraformaldehyde solution and a 0.1 M sodium phosphate buffer pH=7.2. One drop (5 µl) of the exosome suspension was added to clean slides, which were immersed in 1% osmium tetroxide for 1 hour, dehydrated in ethanol and distilled water, and then were dried under a ventilation hood. The samples were coated with gold in a sputter coater (Hitachi, Japan) before being examined through SEM (KYKYEM3200, Germany) with an accelerating voltage of 24 kV. The SEM images were analyzed in ImageJ to evaluate the exosomes' size.

Real-time polymerase chain reaction

Total RNA was extracted from cultivated dermal papilla with ASCs-Exo and PRP-Exo, using RNeasy Mini kits (Qiagen, Germany), and then reversed transcribed into complementary DNA (cDNA). Appropriate primers were designed for PCR as shown below:

Versican-
F: 5′TGAGCATGACTTCCGTTGGACTGA3′
R: 5′CCACTGGCCATTCTCATGCCAAAT3′

α-SMA-
F: 5′GTTTGAGACCTTCAATGTCCC3′
R: 5′CGATCTCACGCTCAGCAGTGA3′

ALP-
F: 5′CAACAGGGTAGATTTCTCTTGG3′
R: 5′GGTCAGATCCAGAATGTTCC3′

Statistical analysis

In vitro assays were performed three times to better validate the experimental data. All the data were displayed as mean ± standard deviation (SD) using a one-way test by Minitab® 16.1.0 statistical software (Minitab Inc., State College, PA, USA). P values of less than or equal to 0.05 (one star), 0.01 (two stars), 0.005 (three stars) and 0.0001 (four stars) were considered as statistically significant.

Results

Characterization of cultivated dermal papilla cells and outer root sheet cells

As shown in figure 1Aa, the cultivated hDPCs grow in a spindle-shape with a sunflower morphology. The results of the ALP staining of the cultured hDPCs suggest these cells are able to induce hair growth (Fig.1Ab). Toluidine blue staining shows the potential for producing the extracellular matrix of hDPCs (Fig.1Ac). The results of immunostaining of the hDPCs showed the expression of α-SMA (Fig.1Ad-Af) and secondary antibody control in hDPC (Fig.1Ag-Ai), versican (green) and nuclei were stained with DAPI (blue, Fig.1Ak-Am) and secondary antibody control in hDPC (Fig.1An-Ap). The flow cytometry of the specific cytoplasmic markers of the DPCs showed expression of α-SMA (60.8%, Fig.1B) and versican (77%, Fig.1C).

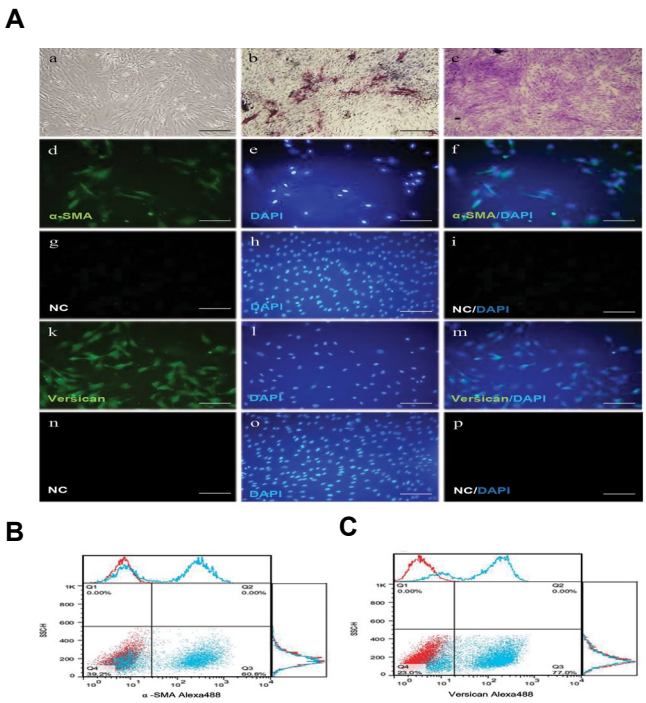

Fig.1: The morphology and cell profile markers of human dermal papilla cells (hDPCs). **A.** The morphology and cell profile markers of hDPC. **Aa.** hDPC showed a typical spindle-like morphology of fibroblast cell. **Ab.** Alkaline phosphatase activity (red) showed in hDPC passage two into a conventional culture medium. **Ac.** Dermal papilla colony tested strongly positive for toluidine blue staining (red). **Ad.** Immunofluorescent Imaging data was presented as α-SMA expression after culture (green). **Ae.** Nuclei were stained with DAPI (blue) and **Af.** Pseudo colored merged image. **Ag-Ai.** Secondary antibody control in hDPC. As a negative control, staining was performed without primary antibody, showing non-specific staining by the secondary antibody (Alexa Fluor 488 goat anti-mouse, (control). **Ak.** Immunofluorescent Imaging data was presented as versican expression after culture (green). **Al.** Nuclei were stained with DAPI (blue) and **Am.** Pseudo colored merged image. **An-Ap.** Secondary antibody control in hDPC. As a negative control, staining was performed without primary antibody, showing non-specific staining by the secondary antibody (Alexa Fluor 488 goat anti-rabbit, (control). Flow data are presented as dot plot and histograms from the specific markers (blue) overlaid with control (red) from hDPC. The dot plot and histogram flow cytometry analysis illustrated that hDPC were positive for **B.** α-SMA and **C.** Versican (scale bars: 200 µm, n=3).

The morphology of cultivated polygonal-shaped ORSCs is shown in Figure 2Aa. The results of the immunostaining of the ORSCs showed the expression of K15 (green) with nuclei stained with DAPI (blue, Fig.2Ab-Ad) and the secondary antibody control in hDPC (Fig.2Ae-Ag). The

flow cytometry of the specific cytoplasmic markers of the ORSCs showed K15 (73.2%, Fig.2B).

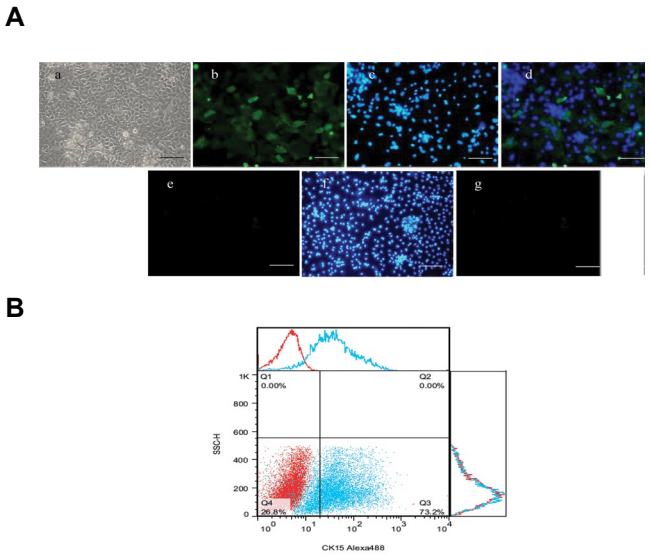

Fig.2: The morphology and cell profile markers of outer root sheet cells (ORSCs). **A.** The morphology and cell profile markers of ORSCs. **Aa.** ORSCs showed a typical morphology of polygonal-shaped structures. **Ab.** Immunofluorescent imaging data was presented as K15 expression after culture (green). **Ac.** Nuclei were stained with DAPI (blue) and **Ad.** Pseudo colored merged image. **Ae-g.** Secondary antibody control in human dermal papilla cells (hDPCs). As a negative control, staining was performed without primary antibody, showing non-specific staining by the secondary antibody [Alexa Fluor 488 Goat anti-mouse (control)]. **B.** Flow data is presented as histograms from specific markers (blue) overlaid with control (red) from ORSCs. The histograms of flow cytometry analysis illustrated that ORSCs were positive for K15 (scale bars: 200 µm, n=3).

Characterization of human adipose stem cells and platelet-rich plasma - exosomes

The morphology of the exosomes was analyzed using electron microscopy after their isolation from the supernatants of human ASCs and cord blood PRP. According to the SEM results (Fig.3A, B), the round-shaped ASCs-Exo and PRP-Exo were 50-150 nm in diameter. The distribution and concentration of the exosomes were evaluated using NanoSight analysis. According to NanoSight Dynamic Light Scattering (Fig.3C, D), we found the majority of ASCs and PRP-Exo to be 30-150 nm in size. A few exosomal markers such as CD9, CD63, CD81, ITG101 and Calnexin were detected using western blotting (Fig.3E, F). The results of exosome characterization suggested the appropriate purity of specific exosomes.

Internalization of exosomes by human dermal papilla

Previous research suggests that exosomes can enter different types of cells. The entrance of human ASCs and cord blood PRP exosomes into human DPCs was therefore examined. According to Figure 3G, the uptake of human ASCs and cord blood PRP exosomes by DPCs were evaluated using fluorescence microscopy. The results illustrated that exosomes can enter the DPCs cytoplasm and be localized in the perinuclear area.

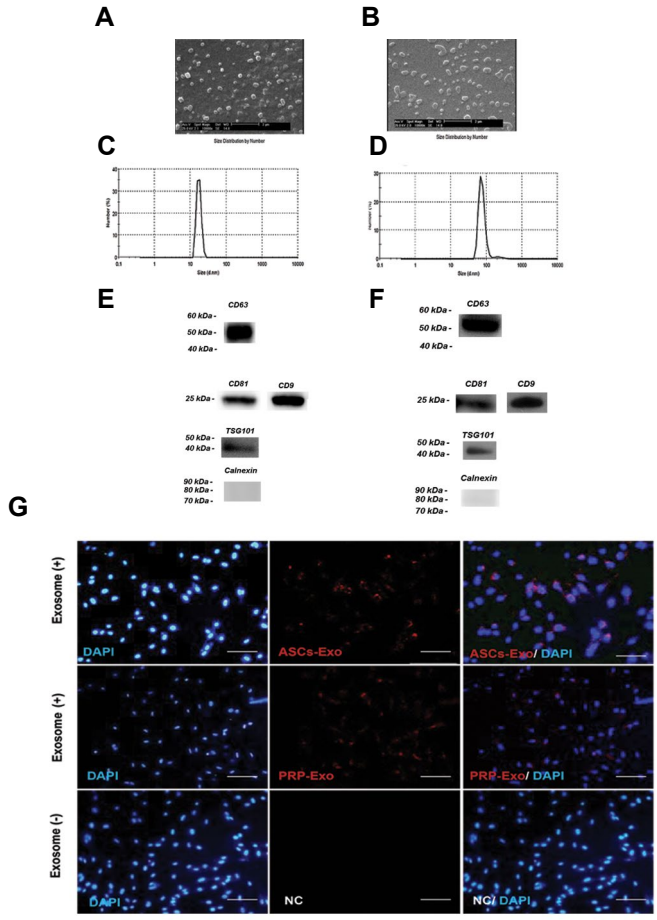

Fig.3: Characterization of exosomes derived from ADSc and PRP. **A, B.** SEM evaluation of exosomes (scale bars: 2 µm). **C, D.** Nanoparticle evaluation of ASC-Exo and PRP-Exo. The mean diameter of ASC-Exo and PRP-Exo were 167 and 147 nm. **E, F.** Immunoblotting for CD63, CD81, CD9, TSG101 and Calnexin in exosomes. **G.** Internalization of exosomes by human dermal papilla: confirmation of the uptake of exosomes in hDPC. The PKH26 (red) kit (20 µg/mL) were applied to stain ASC-Exo or PRP-Exo and incubated with hDPC for 24 hours (scale bars: 200 µm). PBS was used as negative control (NC). Nuclei were stained with DAPI (blue) for counterstaining (n=3). ADSc; Adipose-derived stem cells, PRP; Platelet-rich plasma, ASC; Adipose stromal cell exosome, hDPC; Human dermal papilla cell, and PBS; Phosphate-buffered saline.

ASCs-Exos and PRP-Exos induced dermal papilla migration, proliferation, and *in vitro* ALP activity

According to previous research, it is suggested that exosomes can promote the migration of DPCs. The results of the scratch closure test revealed ASCs-Exo group with concentration 100 µg/ml significantly increased migration of DPCs compared to experimental groups at 12- and 24-hour time points [Alexa Fluor 488 Goat anti-mouse (control)].

The MTS assay was used to evaluate the cell proliferation of DPCs at different concentrations of exosomes after 3 days (Fig.5). Investigating the metabolic activity of different sources of exosome through a two-dimensional culture of hDPCs showed a significant increase in 100µg/ml of ASCs-Exo (Fig.5A) compared to PRP-Exo (Fig.5B).

ASC-Exo induce *ALP, versican* and *α-SMA* expression in the cultured DPCs

According to (Fig.6), culturing the DPCs with ASC-Exo

significantly increased the expression of *ALP, versican* and *α-SMA* compared to a co-culture with PRP-Exo. For 100 µg/ml of ASC-Exo, the expressions of ALP, versican and α-SMA proteins were respectively increased by a factor of 1.2, 2 and 3 compared to in the control group, suggesting the effectiveness of ASC-Exo in maintaining the trichogenic ability of DPCs. Although these results suggest that taking an exosome approach to the culture of DPCs can effectively maintain the trichogenic ability of these cells, further studies are required to obtain a clinically applicable protocol.

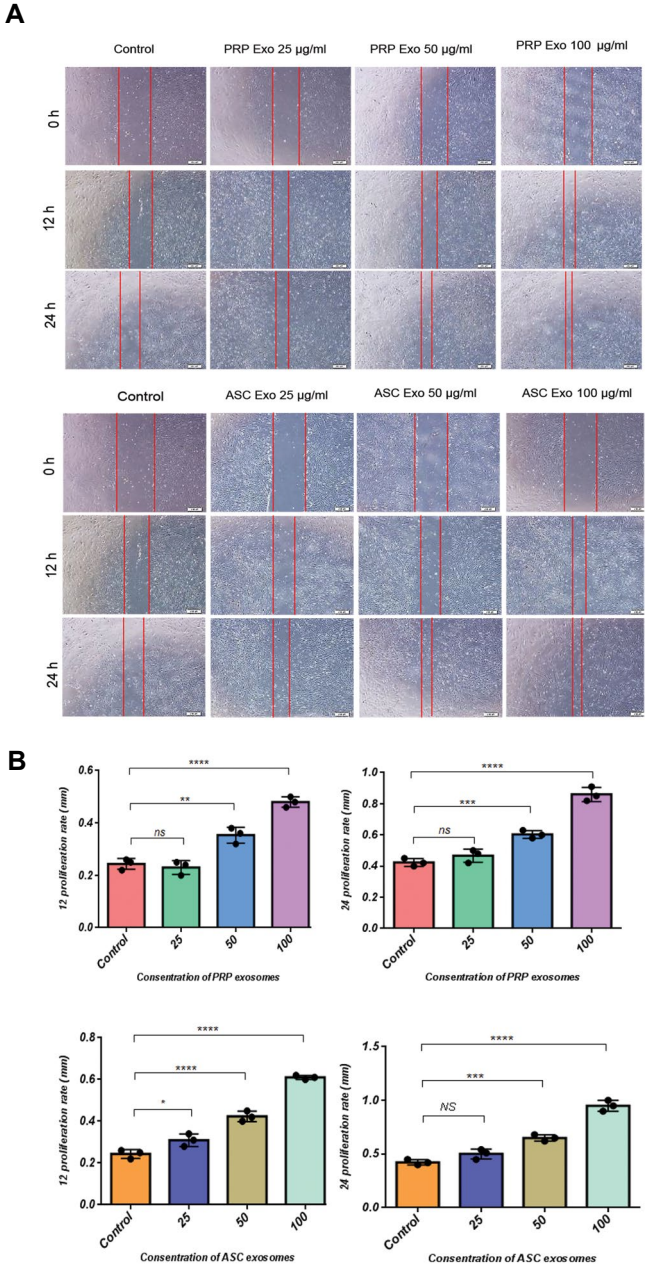

Fig.4: Scratch assay of human dermal papilla cells treated with different concentrations of ASCs and PRP exosomes. Relative wound area changes by different concentrations of **A.** ASCs exosomes and PRP exosomes treatment. ASCs-Exo or PRP-Exo were co-incubated with hDPC (left) and the scratch area at designated study points was normalized against that obtained at 0 hour. The cells cultured with serum (10%) were applied as control group. **B.** Light microscopy images of scratch assay of hDPC were manually delineated to ImageJ software analysis (scale bars: 200 µm, n=3). NS; Not significant, *; P<0.05, **; P<0.01, ***; P<0.005, ****; P<0.0001, ASCs; Adipose stromal cell exosome, PRP; Platelet-rich plasma, and hDPCs; Human dermal papilla cell.

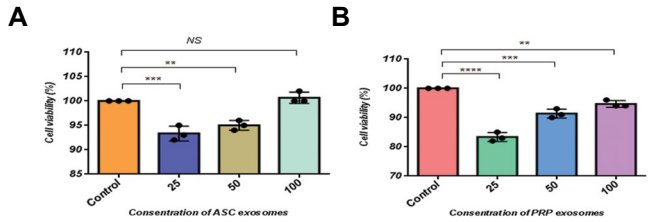

Fig.5: Cell proliferation and cell viability by MTS assay. Human DPC were plated into 96-well plates for 24 hours with or without different concentrations (25, 50, 100 mg/mL) of **A.** ASC-Exo and **B.** PRP-Exo. NS; Not significant, **; P<0.01, ***; P<0.005, ****; P<0.0001 (n=3), DPC; Dermal papilla cell, ASC; Adipose stromal cell exosome, and PRP; Platelet-rich plasma.

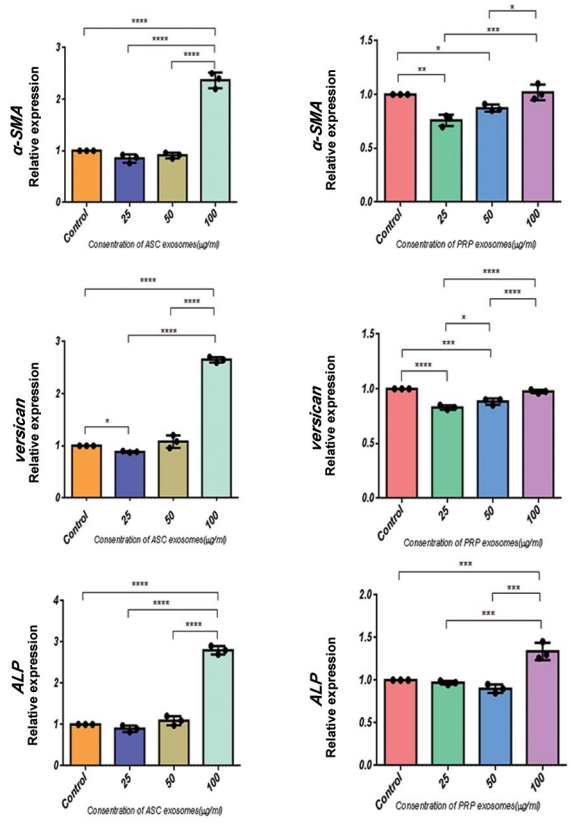

Fig.6: Comparison of the *α-SMA, versican* and *ALP* mRNA expressions following different concentrations of ASCs and PRP exosome treatments. Different experimental groups such as 100, 50 and 25 µg/mL of ASC-Exo or PRP-Exo were incubated with hDPC for 48 hours respectively. The qRT-PCR analysis and the expression of each gene of exosome-treated hDPC was normalized against the expression of cultivated cells with serum (10%), which were used as the control group. All data are expressed as mean ± standard deviation (SD) from three replicates. *; P<0.05, **; P<0.01, ***; P<0.005, and ****; P<0.0001 (n=3).

Discussion

DPCs play a key role in regulating the behavior of epithelial cells in terms of morphogenesis and function in hair follicles (14, 15). Hair growth can be maintained and new hair formation may be induced by DPC singling and growth factors (16, 17). Transplanting a combination of DPCs and keratinocytes in nude mice was found to induce hair follicle formation. Losing the hair follicle inductivity

after several passages in tissue culture and limited hair follicle sampling were, however, the major obstacles in transplantation of DPCs (18-20). Therefore, we examined the possibility of a new method to maintain hair follicle inductivity of dermal papilla cells in a 2D cell culture condition. Our result indicated that a combination of ASC secretory growth factors in DP cell culture maintain hair follicle inductivity after several passages compared to conventional methods.

Recent studies suggest that paracrine mechanisms such as conditioned medium and exosomes play a major role in cell-based therapies (21). ADSC-derived secretory growth factors, such as keratinocyte growth factor, vascular endothelial growth factor (VEGF), platelet-derived growth factor (PDGF) and hepatocyte growth factor are effective in hair regeneration. The paracrine mechanism of an ADSC-conditioned medium was shown to be improved by hypoxia (22). In addition, PRP contains different growth factors, such as PDGF, transforming growth factor β (TGF-β), VEGF, epidermal growth factor (EGF), insulin-like growth factor (IGF) and fibroblast growth factor (FGF), which have been applied to treat androgenic alopecia and chronic wounds (23, 24). Despite the promising results of using stem cell-derived conditioned media (CM) in treating different diseases, the short half-life of cytokines and growth factors present in CM is a disadvantage for regenerative therapy (25).

In the field of dermatology, exosomes have been found to have an effective role in wound healing, preventing scarring and inducing hair growth. Exosomes can therefore provide more efficient and safer treatments compared to CM and stem cell therapy (26, 27). Different components of exosomes, such as RNAs, miRNAs and proteins mediate cell-cell communication and function. Protection from degradation is a specific advantage of exosomal therapeutic applications compared to CM (21). The other advantages include long term shelf life, long-range of intracellular communications, simple storage and lower risks of immune system reactions following treatment (28). The results of previous studies have shown that activation of Erk and Akt signaling pathways along with PRP-Exo induce cell angiogenesis (29). PRP-Exo can increase the proliferation and migration of endothelial cells and fibroblasts in chronic wounds (30). Therefore, in this study two groups of exosomes were used to evaluate the maintenance of thricogenic ability of dermal papilla in a 2D cell culture condition. Our results revealed that the culture of human DPCs with ASC-Exo exhibited significantly increased migration, proliferation and hair inductivity compared to other experimental groups. In the hair cycle, MSC exosomes can stimulate the progression of the hair follicle telogen phase to the anagen phase (31, 32). A previous study has found activation of Wnt/β-catenin signaling by umbilical cord MSC-derived exosomes in a site of wound healing (33). Other recent findings have shown that DPC exosomes can delay the conversion the hair anagen phase to the catagen phase through activation of β-catenin and Shh signaling pathways (32).

Thus, our results are consistent with the other reports (25, 31, 32) that exosomes maintain *in vitro* hair inductivity of dermal papilla cells. The results of our study demonstrated that when 100 μg/ml ASCs-Exo was compared to the same concentration of PRP-Exo, the former significantly promoted DP proliferation and migration, as well as expression of ALP, versican and α-SMA proteins. Thus, ASCs-Exo provide a novel effective approach for the treatment of hair loss. Although the mechanism of exosomes is still unclear, we recommend the exact mechanism of exosomes to investigate this issue due to their rich combination of different RNAs, growth factors and proteins which are dependent on the function of adipose derived mesenchymal cells.

Conclusion

We successfully applied exosomes as a new method to support hair inductivity of human DPCs and to improve the outcome of hair loss treatment. Using a different strategy for the maintenance of hair inductive capacity of dermal papilla cells may provide an appropriate method for discovering new therapeutic goals for hair regeneration. Further studies should not only aim to use a different strategy with different compounds and adjuvants but also expand the existing knowledge on the maintenance of dermal papilla hair inductivity.

Acknowledgments

The authors would like to thank the Skin and Stem Cell Research Center and Royan Institute for financially supporting this project. This research was a Ph.D. student thesis from Tehran University of Medical Science. There is no conflict of interest in this article.

Authors' Contributions

E.T.; Participated in study design, data collection and evaluation, drafting and statistical analysis. M.A.N.; Performed hair follicle collection. M.A.N., N.A.; Contributed extensively in interpretation of the data and the conclusion. E.T., N.A.; Conducted molecular experiments and RT-qPCR analysis. All authors performed editing and approving the final version of this manuscript for submission, also approved the final draft.

References

1. Wolff H, Fischer TW, Blume-Peytavi U. The diagnosis and treatment of hair and scalp diseases. Dtsch Arztebl Int. 2016; 113(21): 377-386.
2. Fukuoka H, Narita K, Suga H. Hair regeneration therapy: application of adipose-derived stem cells. Curr Stem Cell Res Ther. 2017; 12(7): 531-534.
3. Lehmann R, Lee CM, Shugart EC, Benedetti M, Charo RA, Gartner Z, et al. Human organoids: a new dimension in cell biology. Mol Biol Cell. 2019; 30(10): 1129-1137.
4. Ohyama M. Use of human intra-tissue stem/progenitor cells and induced pluripotent stem cells for hair follicle regeneration. Inflamm Regen. 2019; 39: 4.
5. Choi BY. Hair-growth potential of ginseng and its major metabolites: a review on its molecular mechanisms. Int J Mol Sci. 2018; 19(9): 2703.
6. Orasan MS, Roman II, Coneac A, Muresan A, Orasan RI. Hair loss

and regeneration performed on animal models. Clujul Med. 2016; 89(3): 327-334.
7. Driskell RR, Clavel C, Rendl M, Watt FM. Hair follicle dermal papilla cells at a glance. J Cell Sci. 2011; 124(Pt 8): 1179-1182.
8. Morgan BA. The dermal papilla: an instructive niche for epithelial stem and progenitor cells in development and regeneration of the hair follicle. Cold Spring Harb Perspect Med. 2014; 4(7): a015180.
9. Kalabusheva E, Terskikh V, Vorotelyak E. Hair germ model in vitro via human postnatal keratinocyte-dermal papilla interactions: impact of hyaluronic acid. Stem Cells Int. 2017; 2017: 9271869.
10. Galieva LR, James V, Mukhamedshina YO, Rizvanov AA. Therapeutic potential of extracellular vesicles for the treatment of nerve disorders. Front Neurosci. 2019; 13: 163.
11. Phinney DG,Pittenger MF. Concise review: MSC-derived exosomes for cell-free therapy. Stem Cells. 2017; 35(4): 851-858.
12. Mansoor H, Ong HS, Riau AK, Stanzel TP, Mehta JS,Yam GHF. Current trends and future perspective of mesenchymal stem cells and exosomes in corneal diseases. Int J Mol Sci. 2019; 20(12): 2853.
13. Ferreira AdF,Gomes DA. Stem cell extracellular vesicles in skin repair. Bioengineering (Basel). 2018; 6(1): 4.
14. Yang CC, Cotsarelis G. Review of hair follicle dermal cells. J Dermatol Sci. 2010; 57(1): 2-11.
15. Zhu N, Huang K, Liu Y, Zhang H, Lin E, Zeng Y, et al. miR-195-5p regulates hair follicle inductivity of dermal papilla cells by suppressing Wnt/beta-catenin activation. Biomed Res Int. 2018; 2018: 4924356.
16. Alonso MR, Anesini C. Clinical evidence of increase in hair growth and decrease in hair loss without adverse reactions promoted by the commercial lotion ECOHAIR(R). Skin Pharmacol Physiol. 2017; 30(1): 46-54.
17. Gentile P, Garcovich S. Advances in regenerative stem cell therapy in androgenic alopecia and hair loss: Wnt pathway, growth-factor, and mesenchymal stem cell signaling impact analysis on cell growth and hair follicle development. Cells. 2019; 8(5): 466.
18. Abaci HE, Coffman A, Doucet Y, Chen J, Jackow J, Wang E, et al. Tissue engineering of human hair follicles using a biomimetic developmental approach. Nat Commun. 2018; 9(1): 5301.
19. Nilforoushzadeh M, Rahimi Jameh E, Jaffary F, Abolhasani E, Keshtmand G, Zarkob H, et al. Hair follicle generation by injections of adult human follicular epithelial and dermal papilla cells into nude mice. Cell J. 2017; 19(2): 259-268.
20. Qiao J, Zawadzka A, Philips E, Turetsky A, Batchelor S, Peacock J, et al. Hair follicle neogenesis induced by cultured human scalp dermal papilla cells. Regen Med. 2009; 4(5): 667-676.
21. Vizoso FJ, Eiro N, Cid S, Schneider J, Perez-Fernandez R. Mesenchymal Stem cell secretome: toward cell-free therapeutic strategies in regenerative medicine. Int J Mol Sci. 2017; 18(9): 1852.
22. Park BS, Kim WS, Choi JS, Kim HK, Won JH, Ohkubo F, et al. Hair growth stimulated by conditioned medium of adipose-derived stem cells is enhanced by hypoxia: evidence of increased growth factor secretion. Biomed Res. 2010; 31(1): 27-34.
23. Pavlovic V, Ciric M, Jovanovic V, Stojanovic P. Platelet rich plasma: a short overview of certain bioactive components. Open Med (Wars). 2016; 11(1): 242-247.
24. Taniguchi Y, Yoshioka T, Sugaya H, Gosho M, Aoto K, Kanamori A, et al. Growth factor levels in leukocyte-poor platelet-rich plasma and correlations with donor age, gender, and platelets in the Japanese population. J Exp Orthop. 2019; 6(1): 4.
25. Pawitan JA. Prospect of stem cell conditioned medium in regenerative medicine. Biomed Res Int. 2014; 2014: 965849.
26. Ojeh N, Pastar I, Tomic-Canic M, Stojadinovic O. Stem cells in skin regeneration, wound healing, and their clinical applications. Int J Mol Sci. 2015; 16(10): 25476-25501.
27. Wang X, Jiao Y, Pan Y, Zhang L, Gong H, Qi Y, et al. Fetal dermal mesenchymal stem cell-derived exosomes accelerate cutaneous wound healing by activating notch signaling. Stem Cells Int. 2019; 2019: 2402916.
28. Wang J, Sun X, Zhao J, Yang Y, Cai X, Xu J, et al. Exosomes: a novel strategy for treatment and prevention of diseases. Front Pharmacol. 2017; 8: 300.
29. Ferreira JR, Teixeira GQ, Santos SG, Barbosa MA, Almeida-Porada G, Goncalves RM. Mesenchymal stromal cell secretome: influencing therapeutic potential by cellular pre-conditioning. Front Immunol. 2018; 9: 2837.
30. Guo SC, Tao SC, Yin WJ, Qi X, Yuan T, Zhang CQ. Exosomes derived from platelet-rich plasma promote the re-epithelization of chronic cutaneous wounds via activation of YAP in a diabetic rat model. Theranostics. 2017; 7(1): 81-96.
31. Carrasco E, Soto-Heredero G, Mittelbrunn M. The role of extracellular vesicles in cutaneous remodeling and hair follicle dynamics. Int J Mol Sci. 2019; 20(11): 2758.
32. Yan H, Gao Y, Ding Q, Liu J, Li Y, Jin M, et al. Exosomal micro rnas derived from dermal papilla cells mediate hair follicle stem cell proliferation and differentiation. Int J Biol Sci. 2019; 15(7): 1368-1382.
33. Yin S, Ji C, Wu P, Jin C, Qian H. Human umbilical cord mesenchymal stem cells and exosomes: bioactive ways of tissue injury repair. Am J Transl Res. 2019; 11(3): 1230-1240.

Original Article

Lysophosphatidic Acid Alters The Expression of Apoptosis Related Genes and miR-22 in Cultured and Autotransplanted Ovaries

Maryam Dehghan, Ph.D.[1], Shirin Shahbazi, Ph.D.[2], Mojdeh Salehnia, Ph.D.[1]*

1. Department of Anatomy, Faculty of Medical Sciences, Tarbiat Modares University, Tehran, Iran
2. Department of Medical Genetics, Faculty of Medical Sciences, Tarbiat Modares University, Tehran, Iran

Corresponding Address: P.O.Box: 14115-111, Department of Anatomy, Faculty of Medical Sciences, Tarbiat Modares University, Tehran, Iran
Email: salehnim@modares.ac.ir

Received: 02/December/2019, Accepted: 07/April/2020

Abstract

Objective: The aim of this study was to evaluate the effect of lysophosphatidic acid (LPA) on the follicular development, incidence of cell death, and expressions of apoptosis related genes and miR-22 in transplanted ovaries.

Materials and Methods: In this experimental study, three-week-old mice ovaries were cultured for 24 hours in the presence and absence of LPA, and we assessed cell survival and normal follicular rates in some of the cultured ovaries. The remaining cultured ovaries were autotransplanted in the presence and absence of LPA as four experimental groups (LPA^-/LPA^-, LPA^-/LPA^+, LPA^+/LPA^-, LPA^+/LPA^+). The follicular development, immunohistochemistry for BAX, and expressions of genes related to apoptosis and miR-22 by real time reverse transcription polymerase chain reaction (RT-PCR) were studied at the first oestrous cycles in the recovered ovaries. Sera 17-β-oestradiol (E2) and progesterone (P4) levels were also assessed.

Results: Both cell survival and normal follicular rates were significantly higher in cultured ovaries in the presence of LPA after 24 hours ($P<0.05$). There was an increase in follicular development in comparison with the intact control group in the four transplanted groups ($P<0.05$). The LPA^+/LPA^- group had significantly higher follicular development, a decline in BAX positive cells, and a decrease in pro-apoptotic gene expressions in parallel with enhanced expression of anti-apoptotic and miR-22 genes and higher levels of hormones compared with the non-treated and intact control groups ($P<0.05$).

Conclusion: LPA, as a survival factor, improves follicular development in transplanted ovaries by providing a balance between the anti- and pro-apoptotic genes in association with an increase in miR-22 expression.

Keywords: Apoptosis, Autotransplantation, BAX Protein, Lysophosphatidic Acid, Ovarian Follicle

Cell Journal(Yakhteh), Vol 23, No 5, October 2021, Pages: 584-592

Citation: **Dehghan M, Shahbazi Sh, Salehnia M. Lysophosphatidic acid alters the expression of apoptosis related genes and miR-22 in cultured and autotransplanted ovaries. Cell J. 2021; 23(5): 584-592. doi: 10.22074/cellj.2021.7303.**

Introduction

The follicular apoptosis was tack placed in grafted ovaries and it reduced the number of follicles within the transplanted tissue. The ovarian apoptosis is mediated by two main internal and external pathways that are involved by some regulatory proteins such as BAX, BAD as pro-apoptotic and BCL2, as an anti-apoptotic protein (1).

MicroRNAs are small non-coding RNAs that regulate gene expressions and inhibit messenger RNA translation. They have an important role in controlling apoptosis in several cell types (2-10).

Among the microRNAs, *miR-22* plays an essential role in apoptosis inhibition in several cell types; however, its involvement in regulation of ovarian follicular apoptosis is not well-known (8-16). Real-time reverse transcription polymerase chain reaction (RT-PCR) assessment of *miR-22* expression in healthy and atretic follicles showed that its expression decreased during mouse follicular atresia. In addition, it was suggested that *miR-22* suppressed mouse granulosa cell apoptosis and decreased *Bax* expression in these cells *in vitro* (12).

Apoptosis could be induced by physical conditions such as oxidative stress after transplantation of ovarian tissues (17). Therefore, more attention has been focused on the use of antioxidants, growth factors, and anti-apoptotic factors to improve the quality of ovarian grafts (18-20). Lysophosphatidic acid (LPA) is a small molecule (430-480 Da) that has been detected in several tissues and biological fluids such as serum, follicular fluid, and plasma. LPA is produced from the phospholipids of the cellular membrane by two enzymes, autotaxin and phospholipase A. Ovarian cells, endometrial cells, mast cells, erythrocytes and neurons produce LPA and it has physiological as well as pathological functions in these cells (21). LPA regulates anti-apoptotic, differentiation and proliferation processes via its G protein-coupled receptors (LPA1-6) on granulosa cells (22-24). LPA has been shown to enhance oocyte maturation and follicular development in bovine, mouse and human (25-31). Abedpour et al. (29, 31) reported that supplementation of mouse ovary culture media with LPA for seven days enhanced the developmental rate of follicles and LPA acted as an anti-cell death factor. A similar effect was reported by Boruszewska et al. (25), when they added LPA to bovine oocyte maturation media. Despite the increased interest in

improving ovarian follicle survival after transplantation, to the best of our knowledge no report has assessed the effects of LPA treatment on the improvements in follicular development during the pre-transplantation period (*in vitro* culture) and transplantation of mouse ovaries. The aim of this study was to clarify several aspects of LPA supplementation, as an anti-apoptotic factor, during *in vitro* culture and transplantation of mouse ovaries. We investigated the following: i. Cell survival and normal follicular development at the morphological level, ii. The incidence of BAX positive cells by immunohistochemistry and the expressions of apoptosis related genes (*Bax*, *Bad,* and *Bcl2*), and iii. The level of *miR-22*, as an inhibitory factor of apoptosis, in transplanted ovaries in response to LPA treatment.

Materials and Methods

All materials were obtained from Sigma-Aldrich (Dusseldorf, Germany) unless otherwise indicated.

Animals

The Ethics Committee for Animal Research at Tarbiat Modares University (IR.TMU.REC.1395.530) approved this experimental study. Three-week-old female NMRI mice (n=114) comprised the experimental group and six-week-old adult female NMRI mice (n=14) were the control group. The mice were kept under controlled conditions (20-24˚C, 12/12 hour light: dark cycle, and 40-50% humidity) at the animal house of Tarbiat Modares University, Tehran, Iran.

Ovary removal

The animals (n=114) were anesthetized with intraperitoneal injections of ketamine (50 mg/kg) and xylazine (5 mg/kg). The right ovary of each mouse was removed through a dorsal horizontal incision and then cultured *in vitro*. The left ovary was left intact.

In vitro culture of ovarian tissues

The right ovaries (n=114) were individually cultured on inserts (Millicell-CM, 0.4-μm pore size, Millipore Corp, Billerica, MA, US) at 37˚C and 5% CO_2 for 24 hours in the presence (n=57) and absence (n=57) of LPA. The culture media consisted of 300 μl α-MEM medium supplemented with 5% foetal bovine serum; 1% insulin, transferrin, and selenium (Invitrogen, UK), and 100 mIU/ml recombinant follicle stimulating hormone (Serono, Switzerland). The treated group had 20 μM LPA (INstruchemie, The Netherlands) added to the culture medium (31).

The cultured ovaries were observed under an inverted microscope and some of the cultured ovaries were considered for assessment of ovarian cell survival using Calcein AM (n=6 for the LPA-treated group and n=6 for the non-treated group) and for morphological analysis with haematoxyline and eosin (n=5 for the LPA-treated group and n=5 for the non-treated group). The other cultured ovaries were encapsulated with sodium alginate and then transplanted under kidney capsule (n=45 for the LPA-treated group and n=45 for the non-treated group).

Assessment of ovarian cell survival after *in vitro* culture

We evaluated and compared the survival rate of ovarian cells 24 hours after the *in vitro* culture in the presence and absence of LPA. The cultured ovaries (n=6 per group) were incubated with 3 mg/ml collagenase type I at 37˚C, washed with phosphate-buffered saline (PBS), and passed through a filter that had a pore size of 40 μm. The collected cells were stained with double fluorescent labelling dyes with Calcein AM and ethidium homodimer according to a live/dead viability kit (Live/Dead Viability/Cytotoxicity Kit, Molecular Probes, Life Technologies, Germany). Briefly, the cells were washed with PBS and incubated in 1.6 μM Calcein AM and 5.5 μM EthD-1 for 30-45 minutes at 37˚C in the dark. Then, they were placed on slides and covered by a coverslip and observed under a fluorescent microscope. The cells were reported as viable (stained green) or nonviable (stained red). Photographs (n=5) of each sample were prepared and imported into ImageJ software, then the mean percent of viable and nonviable cells were counted per 1000 μm^2 in each sample.

Encapsulation of *in vitro* cultured ovaries in sodium alginate

The cultured ovaries were encapsulated in sodium alginate (n=92); briefly, the ovaries were individually immersed into 5 μl droplets of sodium alginate at a concentration of 0.5% (w/v) in PBS (with or without LPA) at room temperature and then they were gently transferred into a cross-linking solution (50 mM $CaCl_2$ and 140 mM NaCl) for two minutes (31). In the LPA-treated group, 20 μM LPA was added to the sodium alginate solution. Finally, the encapsulated ovaries from both groups were individually autotransplanted under kidney capsules as follows.

Ovarian transplantation into the kidney capsule

The ovaries were divided into the following four experimental groups:

Experimental group A: The right ovaries (n=14) were removed, cultured for 24 hours, encapsulated in sodium alginate without any supplementation, and subsequently autotransplanted into the right kidney capsule (LPA^-/LPA^-).

Experimental group B: The right ovaries (n=5) were removed and cultured without LPA for 24 hours, then encapsulated in sodium alginate with LPA and autotransplanted under the right kidney capsule (LPA^-/LPA^+).

Experimental group C: The right ovaries (n=14) were removed and cultured in medium that contained LPA for 24 hours, encapsulated in sodium alginate without any supplementation, and subsequently autotransplanted into

the right kidney capsule (LPA^+/LPA^-).

Experimental group D: The right ovaries (n=5) were removed and cultured in medium supplemented with LPA for 24 hours, encapsulated in sodium alginate that contained LPA, and autotransplanted into the right kidney capsule (LPA^+/LPA^+).

The left ovaries of the mice were intact in all of the experimental groups.

Prior to transplantation, the mice from the four experimental groups were anesthetised with i.p. injections of ketamine (50 mg/kg) and xylazine (5 mg/kg). A dorsal horizontal incision was generated and the right kidney capsule was exposed. The cultured encapsulated ovary was inserted under the kidney capsule through a tiny hole by using watchmaker's forceps. The body wall and skin incision were closed and the mice were kept under aseptic conditions until the healed ovaries were collected.

Vaginal cytology

Three weeks after the ovaries were transplanted, the stages of the mice oestrous cycles were confirmed daily by vaginal cytology under a light microscope at 400x magnification. The stages of the oestrous cycle were identified as prooestrus, oestrus, metoestrus, or dioestrus by the presence or absence of nucleated epithelial cells, cornified epithelial cells, and leukocytes.

Hormonal assay

We evaluated the endocrine function of the ovaries in the experimental groups with lower (group A) and higher (group C) follicular developmental rates. For this analysis and prior to collection of the ovaries, we obtained blood samples by cardiac puncture with a needle from the heart without thoracotomy in mice. Then, the sera separated and keep at -20˚C until hormonal analysis (n=3 for each group). The concentrations of 17-β-estradiol (E2) and progesterone (P4) were measured using a microplate enzyme immunoassay kit (Biotest AG, Germany) that had a sensitivity of 6.5 pg/mL. The sera of six-week-old mice, as the intact control group (n=3), were collected and analysed in the same manner as the experimental groups.

Recovery of transplanted ovaries

The animals were sacrificed by cervical dislocation during the prooestrus phase of the first oestrous cycle. The transplanted ovaries were recovered and collected, first for the morphological study, then for immunohistochemical and molecular analyses for apoptosis and *miR-22* expression.

Histological evaluation

For morphological analysis, the ovaries cultured *in vitro* (for 24 hours) in the presence and absence of LPA and recovered tissue at first oestrus cycles (5 ovaries in each group) were fixed in Bouin's solution for 8 hours. They were embedded in paraffin wax, serially sectioned at 5 µm and mounted on slides with 5th intervals and stained with haematoxylin and eosin method. The same procedure was done for ovaries obtained from six-week-old mice during the prooestrus phase, as the intact control group (n=5).

The tissue sections were studied under a light microscope in order to determine the normal and degenerated follicles at different developmental stages. The ovarian follicles were classified as primordial (oocytes surrounded by single layer of squamous pregranulosa cells), primary (surrounded by single layer of cuboidal granulosa cells), preantral (two or more layers of cuboidal granulosa cells), and antral follicles with the antrum cavity (31). In order to avoid counting follicles more than once, we only counted follicles that were in the sections with visible oocyte nuclei.

Immunohistochemistry

Another set of tissue sections from the experimental group that had lower (group A) and higher (group C) follicular developmental rates were placed on coated slides and used for the immunohistochemical studies. The tissue sections from each sample of the recovered and control ovaries (n=3 ovaries in each group) were randomly deparaffinised, rehydrated in descending ethanol solutions, and finally washed in PBS. Antigen retrieval was performed by boiling the tissue slides in 10 mM citrate buffer (10 mM, pH=6) in a microwave oven for 10 minutes at 700 W. Then, they were cooled at room temperature and washed in PBS. The sections were immersed in 0.3% Triton X100 for 30 minutes then washed in PBS, blocked with goat serum (30 minutes) and incubated overnight at 4˚C in a humid chamber with the primary antibody, anti-BAX polyclonal antibody, (Elabscience Biotechnology Co, Wuhan, China; 1:100). The tissue sections were washed, incubated with polyclonal goat anti-rabbit antibody (Elabscience Biotechnology Co, Wuhan, China; 1:20) conjugated with FITC for 30 minutes, and washed in PBS. Then, the tissue slides were evaluated under a fluorescent microscope at ×400 magnification. Photographs of each section were prepared and imported into ImageJ software. Then, we counted the number of BAX positive cells per 1000 μm^2 of ovarian tissue in three sections from each sample.

RNA extraction

Experimental groups A and C and the intact control group were considered for molecular analysis (n=6 per group). Total RNA was extracted using TRIzol reagent according to the manufacturer's instructions in the RNeasy Mini Kit (Qiagen, Germany). Briefly, the ovaries were individually homogenized in 0.5 ml of TRIzol reagent, then 0.2 ml of chloroform was added per one ml of TRIzol and the samples were centrifuged at 12000 g for 10 minutes. The upper colourless aqueous phase was transferred to a fresh 1.5 ml microtube and 500 µl of 100% isopropanol (Sigma-Aldrich, Germany) was added, then the samples were centrifuged at 12000 g for 10 minutes followed by the addition of 1.5 ml 70% ethanol

per one ml of TRIzol reagent to the samples. The RNA concentration was determined with a spectrophotometer (Eppendorf, Germany).

cDNA synthesis

cDNA was synthesized with a cDNA synthesis kit (Thermo Fisher Scientific, Germany) according to the manufacturer's instructions. Oligo (dT) was used for cDNA synthesis and the reverse transcriptase reaction was incubated at 65˚C for 5 minutes and at 42˚C for 60 minutes. In order to evaluate *miR-22* gene expression, cDNA was synthesized using a commercial cDNA synthesis kit (Thermo Fisher Scientific, Germany). Stem loop was used for cDNA synthesis and the reverse transcriptase reaction was incubated at 16˚C for 30 minutes and at 42˚C for 60 minutes. After inactivation of the reverse transcriptase enzyme at 70˚C for 5 minutes, the product was stored at -20˚C until real-time RT-PCR assessment.

Real-time reverse transcription polymerase chain reaction

Primer-BLAST tool in NCBI was used to design primers for the apoptosis related genes that included *Bax*, *Bcl2,* and *Bad* and the housekeeping gene, *β-actin*, and for *miR-22* and its housekeeping gene (*U6*) (Table S1, See supplementary Online Information at www.celljournal.org). Real-time RT-PCR was performed using a QuantiTect SYBR Green RT-PCR Kit (Qiagen, Germany). The thermal program of real-time RT-PCR was set with the following parameters: initial holding stage for 5 minutes at 95˚C; 40 cycles with cycling stages of 15 seconds at 95˚C, 58˚C for 30 seconds, and 72˚C for 15 seconds; and a melting curve stage at 95˚C for 15 seconds, 60˚C for 1 minute, and 95˚C for 15 seconds. After completing the PCR run, the melting curve was analysed using the amplicon.

Statistical analysis

All experiments were conducted with a minimum of three replicates. Statistical analysis was performed using SPSS software (SPSS Inc., Chicago, USA). Values are written as mean ± SD. One-way ANOVA and the post hoc Tukey test were used to compare differences in follicular count, BAX positive cells, mRNA expression, and hormone levels. A $P<0.05$ was considered to be statistically significant.

Results

Morphology of cultured ovaries under an inverted microscope

Figure 1A, B shows the morphological characteristics of the cultured ovaries in the presence and absence of LPA under an inverted microscope. The follicles grew within the cortical parts of the ovaries and the antral follicles had a spherical shape with large, clear antral cavities.

The survival rate of cultured ovarian cells

Figure 1C, D shows images of a Calcein AM stained cell suspension obtained from the ovaries cultured *in vitro* for 24 hours in the presence and absence of LPA. The images in the figure show that the viable cells stained green whereas nonviable cells stained red. A significantly greater ($P<0.05$) mean percentage of cells survived in the LPA-treated group (90.17 ± 5.06%) compared to the non-treated group (76.08 ± 4.01%, Fig.1E).

Morphological analysis of *in vitro* cultured ovaries

Representative light microscopy photograph of sections from the *in vitro* cultured ovaries that were stained with haematoxyline and eosin after 24 hours are shown in Figure 1F-G. Follicles at different developmental stages had normal structures in both of the studied groups.

From the 482 total follicles counted in the non-treated group, 99.21 ± 0.06% had normal morphology and out of the 534 total follicles in the LPA-treated group, 99.69 ± 0.07% had normal morphology. This rate was significantly higher in the LPA-treated group in comparison with the non-treated group ($P<0.05$). There was no significant difference between these groups in terms of percentages of follicles at the different developmental stages (Table 1).

Morphological analysis in recovered transplanted ovaries at the first oestrous cycle

The morphology of transplanted ovaries sections in four experimental groups and the intact control group at the proestrus phase is shown in Figure 1J-M. Follicles from both study groups, which are grown at different developmental stages, are visible in this figure. The total number of follicles counted were 539 in the intact control group. The total number of counted follicles in the experimental groups were 415 (group A), 489 (group B), 525 (group C), and 529 (group D).

Table 1: The percentages of normal follicles at different developmental stages in cultured mouse ovaries

Group	Total no. F	Normal F.	Degenerated F.	Primordial F.	Primary F.	Preantral F.
LPA^-	482	478 (99.21 ± 0.06)	4 (0.79 ± 0.06)	239 (49.91 ± 1.18)	112 (23.50 ± 0.56)	127 (26.59 ± 0.65)
LPA^+	534	532 (99.69 ± 0.07)[a]	2 (0.31 ± 0.07)[a]	262 (49.22 ± 1.16)	126 (23.72 ± 0.56)	144 (27.06 ± 0.63)

Data are presented as n (mean ± SD%). The percentages of follicles at different developmental stages in all studied groups were calculated according to the normal follicles. These assessments were done in five repeats in the studied groups. LPA^-; Untreated, LPA^+; Treated with LPA, LPA; Lysophosphatidic acid, F; Follicles, and [a]; Significant differences with the LPA^- group ($P<0.05$).

There was no significant difference in terms of the mean percentages of normal follicles between the intact control group (99.76 ± 0.07%) and experimental groups C (99.68 ± 0.08%) and D (99.70 ± 0.08%) (Table 2, P>0.05). The mean percentages of primordial and primary follicles significantly decreased and the preantral and antral follicles increased in all four experimental groups in comparison with the intact control group (P<0.05). Among the experimental groups, the lowest percentage of primordial follicles and the highest percentage of antral follicles were seen in experimental group C (P<0.05).

Immunohistochemistry for BAX

Figure 2A-C shows photomicrographs related to the immunohistochemistry of the recovered ovarian sections in experimental groups A and C, and the intact control ovaries. The number of BAX positive cells (green colour, Fig.2) was significantly higher in experimental group A (3.20 ± 0.18 per 1000 μm^2) in comparison with the intact control (1.11 ± 0.11 per 1000 μm^2) and experimental group C (1.37 ± 0.11 per 1000 μm^2, P<0.05).

Real-time reverse transcription polymerase chain reaction

Figure 3 shows the relative expression ratios of the apoptosis related genes to *β-actin*. In the intact control group, the expression ratios were 5.128 ± 0.55 for *Bax,* 0.615 ± 0.04 for *Bad* and 1.116 ± 0.08 for *Bcl2*. In experimental group A, they were 10.99 ± 1.14 (*Bax*), 1.376 ± 0.06 (*Bad*), and 0.747 ± 0.20 (*Bcl2*) and for experimental group C, the expression ratios were 6.239 ± 0.60 (*Bax*), 0.702 ± 0.02 (*Bad*), and 0.980 ± 0.06 (*Bcl2*). There were significant differences between experimental group A and the two other groups in terms of the gene expressions (P<0.05).

The relative expression ratio of *miR-22* to *U6* in the intact control group was 3.702 ± 0.24, in experimental group A it was 1.804 ± 0.12 and in experimental group C it was 3.323 ± 0.20. There was a higher expression ratio of *miR22* in experimental group C in comparison with the two other groups (P<0.05, Fig.4).

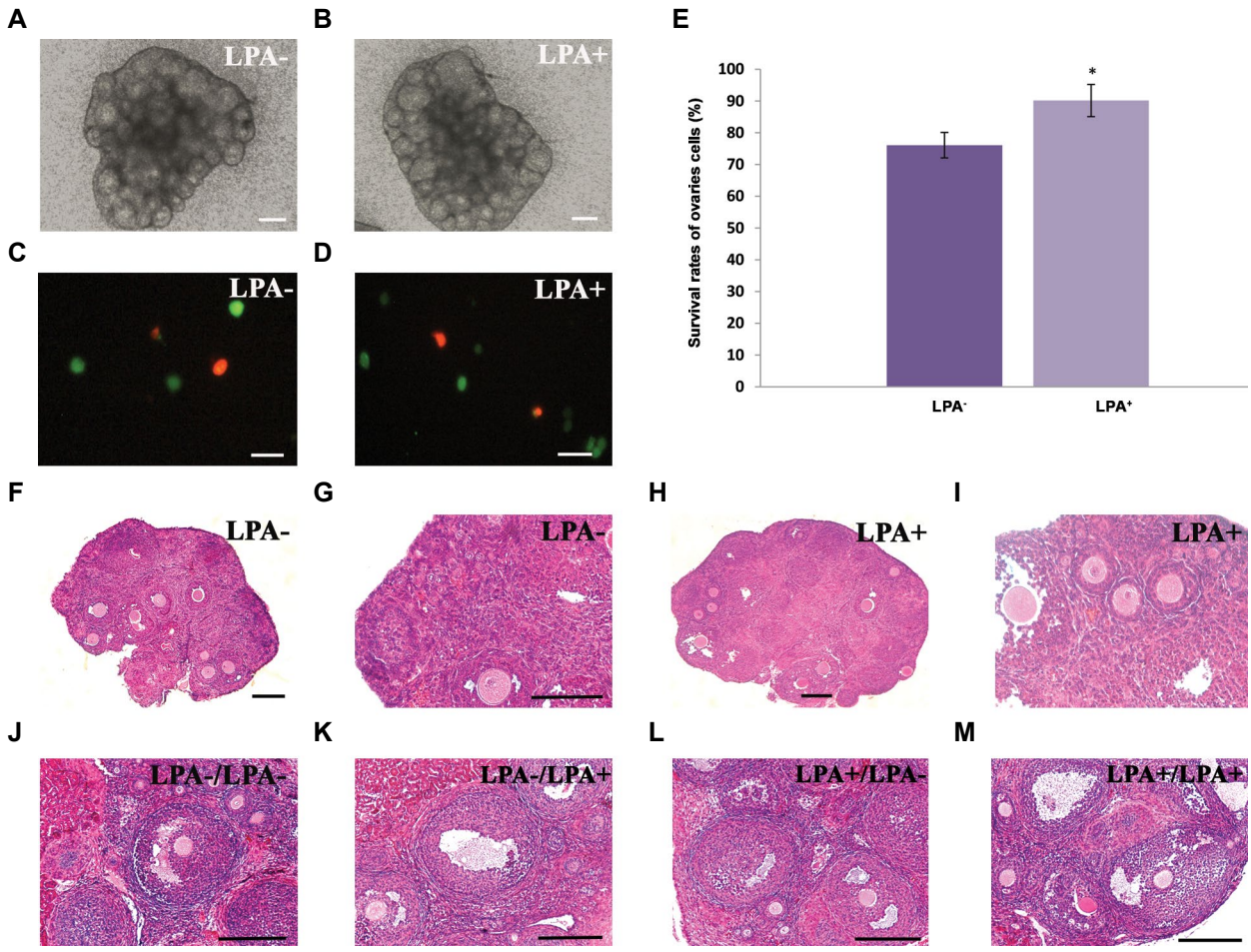

Fig.1: Phase contrast micrograph of cultured ovaries in the studied groups. **A.** Cultured without any supplementation for 24 hours (LPA^-) and **B.** Cultured in the presence of LPA for 24 hours (LPA^+). **C.** Representative fluorescence microscopy images of isolated cells derived from cultured ovaries that were stained with Calcein AM in the absence of LPA and **D.** The LPA-treated group. The viable cells stained green and the nonviable cells stained red. **E.** Comparison of the survival rates of ovarian isolated cells in the studied groups. *; Significant difference with other group (P<0.05). **F, G.** Light microscopic observation of haematoxylin and eosin stained tissue sections of the ovaries cultured for 24 hours in LPA^- group and **H, I.** In LPA^+ group. Representative photographs of transplanted ovarian sections in the experimental groups are shown in the last row. **J.** Experimental group A (LPA-/LPA-). **K.** Experimental group B (LPA^-/LPA^+). **L.** Experimental group C (LPA^+/LPA^-). **M.** Experimental group C (LPA^+/LPA^+). These assessments were done in five repeats in the studied groups. LPA; Lysophosphatidic acid (scale bar: A, B: 300 µm, C, D: 50 µm, F, H, G, I, J, K, L, M: 100 µm).

Table 2: The percentages of normal follicles at different developmental stages in the first oestrous cycle

Group	Total no. F.	Normal F.	Primordial F.	Primary F.	Preantral F.	Antral F.
Intact control (Six-week-old ovaries)	539	538 (99.76 ± 0.07)	280 (52.04 ± 0.60)	118 (21.93 ± 0.68)	117 (21.74 ± 0.63)	23 (4.29 ± 0.61)
Exp. A (LPA^-/LPA^-)	415	412 (99.27 ± 0.05)^{a}	113 (27.38 ± 0.74)^{a}	75 (18.17 ± 0.58)^{a}	145 (35.24 ± 0.77)^{a}	79 (19.21 ± 0.59)^{a}
Exp. B (LPA^-/LPA^+)	489	487 (99.51 ± 0.08)^{ab}	70 (14.33 ± 0.75)^{ab}	58 (11.89 ± 0.63)^{ab}	256 (52.65 ± 1.15)^{ab}	103 (21.13 ± 0.56)^{ab}
Exp. C (LPA^+/LPA^-)	525	523 (99.68 ± 0.08)^{b}	53 (10.09 ± 0.72)^{ab}	43 (8.24 ± 0.61)^{ab}	289 (55.27 ± 0.74)^{ab}	138 (26.40 ± 0.61)^{ab}
Exp. D (LPA^+/LPA^+)	529	527 (99.70 ± 0.08)^{bc}	70 (13.34 ± 0.80)^{abcd}	50 (9.44 ± 0.63)^{abcd}	284 (53.88 ± 0.88)^{abcd}	123 (23.34 ± 0.55)^{abcd}

Data are presented as n (mean ± SD%). The percentages of follicles at different developmental stages in all studied groups were calculated according to the normal follicles. These assessments were done in five repeats in the studied groups. LPA^-; Untreated, LPA^+; Treated with LPA, LPA; Lysophosphatidic acid, F; Follicles, [a]; Significant differences with intact control group (P<0.05), [b]; Significant differences with the LPA^-/LPA^- group (P<0.05), [c]; Significant differences with the LPA^-/LPA^+ group (P<0.05), and [d]; Significant differences with the LPA^+/LPA^- group (P<0.05).

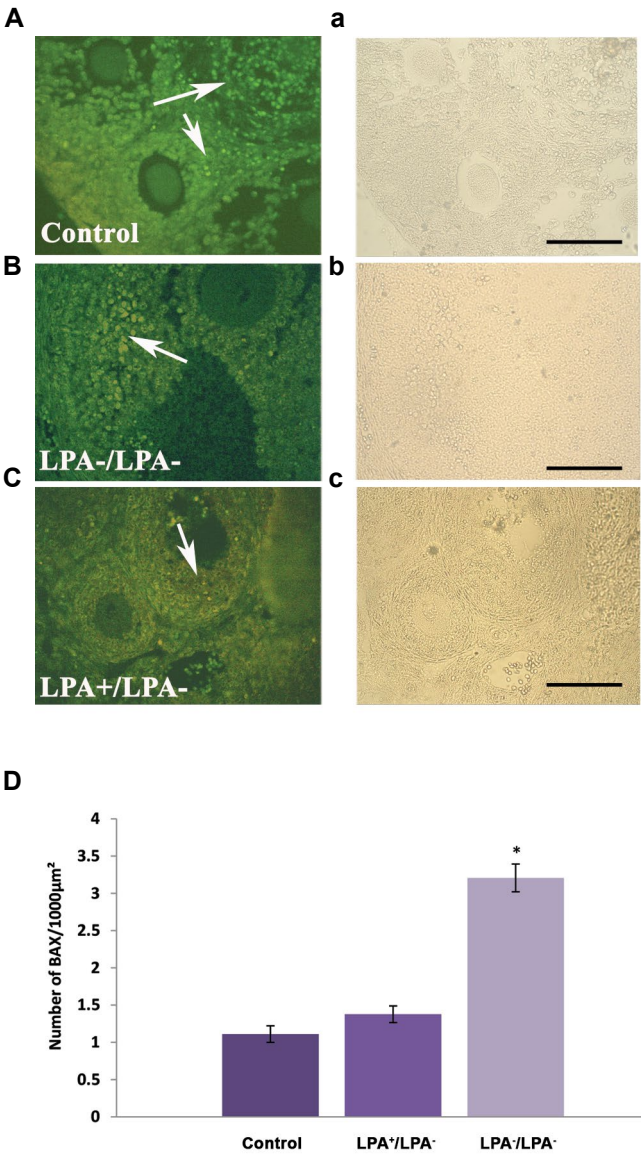

Fig.2: Photomicrographs of transplanted mouse ovarian sections immunostained for BAX antibody and observed under fluorescent microscopy (first column) and by phase contrast microscopy (second column). **A., a.** Intact control group, **B., b.** Experimental group A (LPA^-/LPA^-), **C., c.** Experimental group C (LPA^+/LPA^-). Green colour shows the positive cell reaction (white arrow) for the BAX antibody, and **D.** A comparison of the number of BAX positive cells/1000 µm² in the studied groups. *; Significant difference with the other groups (P<0.05). The immunocytochemistry analysis was repeated three times. LPA; Lysophosphatidic acid (scale bar: 100 µm).

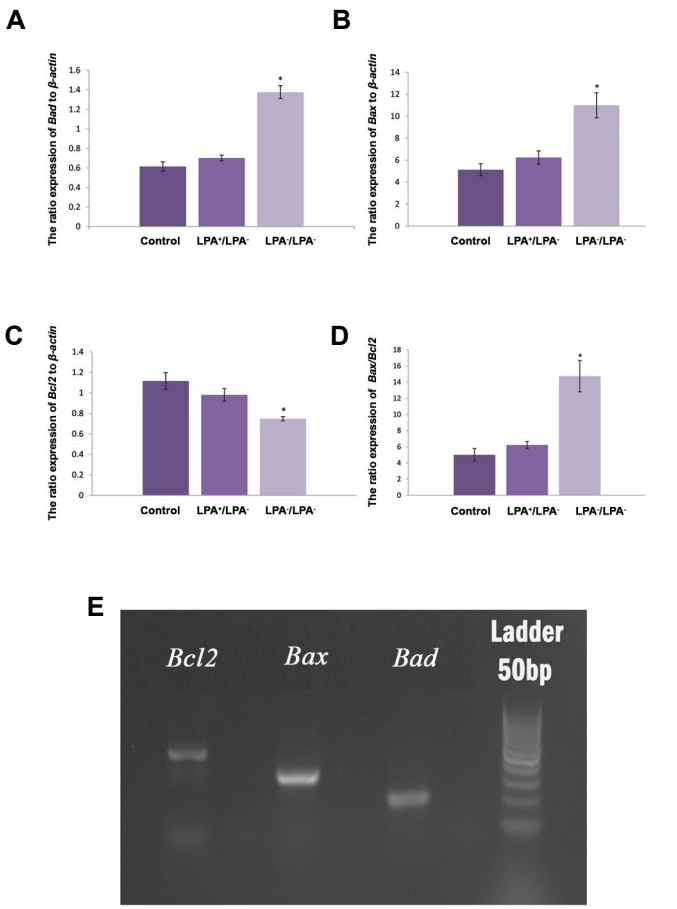

Fig.3: The relative expression ratio of pro- and anti-apoptotic genes to *β-actin* in studied groups. The comparison of gene expression in transplanted mouse ovaries in experimental groups A (LPA^-/LPA^-) and C (LPA^+/LPA^-), and the intact control group are shown in parts **A.** *Bad*, **B.** *Bax*, **C.** *Bcl2*, and **D.** *Bax/Bcl2*. **E.** Agarose gel electrophoresis of the PCR products of the genes related to apoptosis. Lane 1; *Bad*, Lane 2; *Bax*, Lane 3; *Bcl2*, and Lane 4; 50 bp ladder. These assessments were done in three repeats in the studied groups. LPA; Lysophosphatidic acid and *; Significant difference with the other groups (P<0.05), and PCR; Polymerase chain reaction.

17-β-estradiol and progesterone levels

The concentrations of E2 and P4 in sera of the intact control and experimental groups A and C are presented and compared in Table S2 (See supplementary Online Information at www.celljournal.org). Experimental group

C had significantly higher levels of E2 and P4 compared to the intact control and experimental group A (P<0.05).

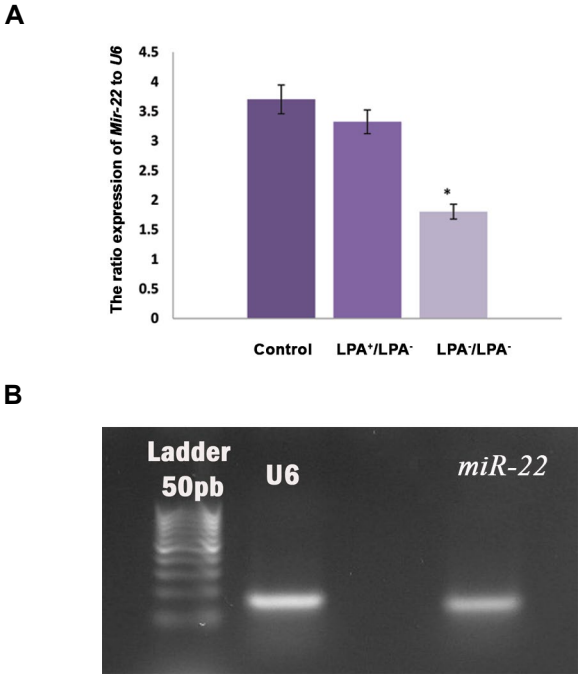

Fig.4: The relative expression ratio of the *miR-22* gene to U6 in studied groups. **A.** The comparison of gene expression in transplanted mouse ovaries in experimental groups A (LPA^-/LPA^-) and C (LPA^+/LPA^-), and the intact control group. **B.** Agarose gel electrophoresis of the PCR product of the *miR-22* gene. Lane 1; 50 bp ladder, Lane 2; U6, and Lane 3; *miR-22*. These assessments were done in three repeats in the studied groups. LPA; Lysophosphatidic acid, *; Significant difference with the other groups (P<0.05), and PCR; Polymerase chain reaction.

Discussion

In this study, in order to improve the quality of the transplanted ovaries, we first examined the effects of LPA supplementation during an *in vitro* culture and tissue transplantation. The results showed that the rate of follicular development in the LPA-treated groups were significantly higher than the non-treated and intact control groups. Follicular development is related to growth and proliferation of follicular cells and to maturation of these cells and oocytes. A possible relation to these results is that LPA might act as a growth factor to stimulate the proliferation of follicular granulosa and theca cells; therefore, the expansion of follicular cells could shift the growth of primordial and primary follicles to the preantral and antral stages. The action of LPA is mediated directly by binding to its receptors on follicular cells (21, 23). Expressions of LPA receptors were detected in mouse and bovine ovaries (28, 29). Similarly, the *in vitro* expansion of bovine cumulus cells was also demonstrated in response to LPA (25). Sinderewicz et al. (28) postulated that LPA enhanced the growth and development of bovine follicles via expression of LPA receptors and autotaxin genes. On the other hand, binding of LPA to its surface receptors could increase the expression of LPA receptor genes and, in turn, have a positive feedback on the effects of LPA. In this regard, our group has recently reported significant enhancement in the expression of LPAR1-4 receptor genes after LPA was added to the culture media of mouse ovarian tissues (29).

LPA may also act as a maturation factor. This effect of LPA on oocyte maturation was shown in several studies (25-32). Komatsu et al. (32) suggested that LPA treatment promoted the nuclear maturation of mouse oocytes during IVM through lowering intra-oocyte cAMP levels. Jo et al. (30) demonstrated that addition of LPA to culture media, especially at 30 μM, improved oocyte maturation, fertilization and blastocyst formation in mice. These researchers also reported that LPA stimulated phospholipase C through the G protein on the surface of cumulus cells and activated mitogen-activated protein (MAP) kinase pathways. Addition of LPA to culture media appears to increase oocyte mRNA amount that is considered as a quality markers of oocyte. Also LPA enhances oocyte maturation rates by stimulating the expression of developmental competence-related factors (25, 33). Zhang et al. (27) showed that LPA promoted meiotic progression of porcine oocytes from the germinal vesicle to metaphase II by stimulating the expression of cyclin B1, a marker of cytoplasmic maturation, by activation of the MAP kinase pathway. In addition, it was suggested that LPA might indirectly interact with other factors that stimulate and regulate follicular development. However, this suggestion should be confirmed by more analysis.

However, we also observed significant enhancement in the amount of E2 and P4 in the LPA-treated group. This result revealed that LPA positively influenced the function of granulosa and theca cells by production of high concentrations of steroid hormones. Similarly, Boruszewska et al. (34) demonstrated that LPA stimulated the synthesis of E2 in bovine granulosa cells by converting the androgens to E2 via cytochrome P450 aromatase in granulosa cells. It has been suggested that LPA participates in ovarian follicle growth and differentiation by stimulation of E2 production, which may occur via an increase in the expression of follicle stimulating hormone receptor. LPA may be involved in autocrine and/or paracrine signalling between oocyte and cumulus cells during follicular development (23).

We compared the follicular proportions at different developmental stages at the first oestrus cycle in all transplanted groups to the intact control group. Our results showed the percentage of large antral follicles in all grafted ovaries was significantly higher than the intact control group. This phenomenon showed rapid development and early discharge of ovarian reserve in the experimental groups, especially in experimental group C (LPA^+/LPA^-), which could affect longevity of the transplanted tissue. Possibly, in the transplanted groups, an immediate lack of negative feedback after grafting could facilitate the production of gonadotropin releasing hormone (GnRH), follicle-stimulating hormone (FSH), and luteinizing hormone (LH), which improved follicle growth in the grafted ovaries. This suggestion correlated with premature follicular discharge observed in the

transplanted groups in comparison with the intact control group.

Despite follicular loss after ovarian transplantation in terms of ischemia, we noted that the integrity of the tissue was well-preserved in the LPA-treated groups, which was shown by the high survival rate observed with Calcein AM staining, a high percent of normal follicles, and low incidence of BAX positive cells in the LPA-treated group. These observations suggest that LPA acts as a survival factor during *in vitro* culture and encapsulation of tissue within sodium alginate. Hu et al. (35) have reported that LPA is a survival and growth factor, which prevents spontaneous apoptosis through LPA receptor activation of the anti-apoptotic protein AKT/PKB. McLaughlin et al. (36) have indicated that the Akt pathway promotes cell survival by inhibiting pro-apoptotic proteins such as BAD, BAX, forkhead, and p53 and by activating pro-survival proteins such as BCL2. A similar effect of LPA is well-known in other cell types and the results of these studies show that LPA, via its receptors, leads to cell responses that include protection from apoptosis (22-24). At the molecular level, our results confirmed that LPA supplementation of culture media had a positive effect on the decline in transcription levels of pro-apoptotic (*Bax* and *Bad*) genes and an increase in anti-apoptotic (*Bcl2*) gene expression. The *Bax/Bcl2* ratio was lower in ovaries cultured in the presence of LPA compared to the non-treated group. The ratio of *Bcl2* to *Bax* may be an indicator of the tendency of ovarian cells and follicles toward survival or apoptosis (1). BAX, BAD and BCL2 are regulatory proteins that control the mitochondrial pathway of apoptosis; therefore, follicular development competence in the LPA-treated group might be enhanced through modulation of these apoptotic related gene expressions. This conclusion agreed with the findings reported in other cell types or oocytes (26, 33). In these studies, LPA played a role in cell survival by preventing apoptosis through activation of the anti-apoptotic protein or by alterations in the anti-apoptotic and pro-apoptotic balance, which resulted in a significantly lower *Bcl2/Bax* ratio (33). Zhou et al. (37) reported that the anti-apoptotic effects of LPA involve inhibition of caspase and *Bax*, and the activation of *Bcl2*. Treatment of porcine embryos with LPA resulted in increased expression of the anti-apoptotic *Bcl2* gene and decreased expression of the pro-apoptotic *Bax* and *caspase 3* genes (27). Torres et al. (38) showed that addition of LPA to the culture media of bovine embryos reduced *Bax* expression.

In present study, for the first time, we investigated the expression of *miR-22* in correlation with apoptotic related genes and follicular development in cultured and transplanted ovaries. Our results revealed that the higher expression of *miR-22* was associated with a decline in the incidence of BAX positive cells and pro-apoptotic gene expressions in the LPA-treated group. The results of several studies revealed that *miR-22* played an essential role in regulation of apoptosis in different cell types (12-14). Overexpression of *miR-22* inhibited cardiac myocyte apoptosis (39) and had a neuroprotective effect through reduction in caspase activation (40). *miR-22* might have a similar effect on other cell types, including ovarian cells and follicles. Xiong et al. demonstrated that *miR-22* expression decreased during mouse follicular atresia and they suggested that *miR-22* suppressed mouse granulosa cell apoptosis *in vitro* (12). Lv et al. (14) reported that *miR-22* regulated cell proliferation and inhibited cell apoptosis by targeting the *eIF4EBP3* gene in human cervical squamous carcinoma cells. *miR-22* decreased BAX expression in granulosa cells by targeting the silent mating-type information regulation 2 homologue 1 (*SIRT1*) gene (12).

Conclusion

LPA, as a survival factor, improves follicular development in transplanted ovaries by providing a balance between anti-apoptotic and pro-apoptotic genes in association with an increase in *miR-22* expression.

Acknowledgments

This work was financially supported by Tarbiat Modares University of Medical Sciences and the Iranian National Science Foundation. The authors have no conflicts of interest. We express our appreciation to Mr. Pour Bayranvand for his technical assistance.

Authors' contributions

M.D.; Performed the experiments, analysed the data and contributed to writing the manuscript. Sh.Sh.; Contributed to molecular study and gene expression analyses. M.S.; Supervised the study and contributed to design of study, data collection, analysis, and writing the manuscript. All authors read and approved the final manuscript.

References

1. Hussein MR. Apoptosis in the ovary: molecular mechanisms. Hum Reprod Update. 2005; 11(2): 162-78.
2. Tesfaye D, Gebremedhn S, Salilew-Wondim D, Hailay T, Hoelker M, Grosse-Brinkhaus C, et al. MicroRNAs: tiny molecules with a significant role in mammalian follicular and oocyte development. Reproduction. 2018; 155(3): R121-R135.
3. Li Q, Du X, Liu L, Pan Z, Cao S, Li Q. MiR-126* is a novel functional target of transcription factor SMAD4 in ovarian granulosa cells. Gene. 2019; 711: 143953.
4. Zhu W, Yang M, Shang J, Xu Y, Wang Y, Tao Q, et al. MiR-222 inhibits apoptosis in porcine follicular granulosa cells by targeting the THBS1 gene. Anim Sci J. 2019; 90(6): 719-727.
5. Zhang J, Xu Y, Liu H, Pan Z. MicroRNAs in ovarian follicular atresia and granulosa cell apoptosis. Reprod Biol Endocrinol. 2019; 17(1): 9.
6. Li Q, Du X, Pan Z, Zhang L, Li Q. The transcription factor SMAD4 and miR-10b contribute to E2 release and cell apoptosis in ovarian granulosa cells by targeting CYP19A1. Mol Cell Endocrinol. 2018; 476: 84-95.
7. Yao W, Pan Z, Du X, Zhang J, Li Q. miR-181b-induced SMAD7 down regulation controls granulosa cell apoptosis through TGF-β signaling by interacting with the TGFBR1 promoter. J Cell Physiol. 2018; 233(9): 6807-6821.
8. An X, Song Y, Hou J, Zhang Y, Chen K, Ma H, et al. Chi-miR-4110 promotes granulosa cell apoptosis by targeting Sma- and Mad-related protein 2 (Smad2) in the caprine ovary. PLoS One. 2017; 12(7): e0181162.
9. Xu L, Sun H, Zhang M, Jiang Y, Zhang C, Zhou J, et al. MicroRNA-145 protects follicular granulosa cells against oxidative stress-

induced apoptosis by targeting Krüppel-like factor 4. Mol Cell Endocrinol. 2017; 452: 138-147.
10. Worku T, Rehman ZU, Talpur HS, Bhattarai D, Ullah F, Malobi N, et al. MicroRNAs: new insight in modulating follicular atresia: a review. Int J Mol Sci. 2017; 18(2): 333.
11. Chen Z, Qi Y, Gao C. Cardiac myocyte-protective effect of microRNA-22 during ischemia and reperfusion through disrupting the caveolin-3/eNOS signaling. Int J Clin Exp Pathol. 2015; 8(5): 4614-4626.
12. Xiong F, Hu L, Zhang Y, Xiao X, Xiao J. miR-22 inhibits mouse ovarian granulosa cell apoptosis by targeting SIRT1. Biol Open. 2016; 5(3): 367-371.
13. Li Y, Gu Y, Tang N, Liu Y, Zhao Z. miR-22-Notch signaling pathway is involved in the regulation of the apoptosis and autophagy in human ovarian cancer cells. Biol Pharm Bull. 2018; 41(8): 1237-1242.
14. Lv KT, Liu Z, Feng J, Zhao W, Hao T, Ding WY, et al. MiR-22-3p Regulates cell proliferation and inhibits cell apoptosis through targeting the eIF4EBP3 gene in human cervical squamous carcinoma cells. Int J Med Sci. 2018; 15(2): 142-152.
15. Nie M, Yu S, Peng S, Fang Y, Wang H, Yang X. miR-23a and miR-27a promote human granulosa cell apoptosis by targeting SMAD5. Biol Reprod. 2015; 93(4): 98.
16. Wang C, Li D, Zhang S, Xing Y, Gao Y, Wu J. MicroRNA-125a-5p induces mouse granulosa cell apoptosis by targeting signal transducer and activator of transcription 3. Menopause. 2016; 23(1): 100-107.
17. Yang H, Lee HH, Lee HC, Ko DS, Kim SS. Assessment of vascular endothelial growth factor expression and apoptosis in the ovarian graft: can exogenous gonadotropin promote angiogenesis after ovarian transplantation? Fertil Steril. 2008; 90 Suppl 4: 1550-1558.
18. Kolusari A, Okyay AG, Koçkaya EA. The effect of erythropoietin in preventing ischemia–reperfusion injury in ovarian tissue transplantation. Reprod Sci. 2018; 25(3): 406-413.
19. Kang BJ, Wang Y, Zhang L, Li SW. Basic fibroblast growth factor improved angiogenesis of vitrified human ovarian tissues after in vitro culture and xenotransplantation. Cryo Letters. 2017; 38(3): 194-201.
20. Fransolet M, Noël L, Henry L, Labied S, Blacher S, Nisolle M, et al. Evaluation of Z-VAD-FMK as an anti-apoptotic drug to prevent granulosa cell apoptosis and follicular death after human ovarian tissue transplantation. J Assist Reprod Genet. 2019; 36(2): 349-359.
21. Wocławek-Potocka I, Rawińska P, Kowalczyk-Zieba I, Boruszewska D, Sinderewicz E, Waśniewski T, et al. Lysophosphatidic acid (LPA) signaling in human and ruminant reproductive tract. Mediators Inflamm. 2014; 2014: 649702.
22. Sinderewicz E, Grycmacher K, Boruszewska D, Kowalczyk-Zięba I, Staszkiewicz J, Ślężak T, et al. Expression of factors involved in apoptosis and cell survival is correlated with enzymes synthesizing lysophosphatidic acid and its receptors in granulosa cells originating from different types of bovine ovarian follicles. Reprod Biol Endocrinol. 2017; 15(1): 72.
23. Choi JW, Herr DR, Noguchi K, Yung YC, Lee CW, Mutoh T, et al. LPA receptors: subtypes and biological actions. Annu Rev Pharmacol Toxicol. 2010; 50: 157-186
24. Yung YC, Stoddard NC, Chun J. LPA receptor signaling: pharmacology, physiology, and pathophysiology. J Lipid Res. 2014; 55(7): 1192-1214.
25. Boruszewska D, Sinderewicz E, Kowalczyk-Zieba I, Grycmacher K, Woclawek-Potocka I. The effect of lysophosphatidic acid during in vitro maturation of bovine cumulus–oocyte complexes: cumulus expansion, glucose metabolism and expression of genes involved in the ovulatory cascade, oocyte and blastocyst competence. Reprod Biol Endocrinol. 2015; 13: 44.
26. Hwang SU, Kim KJ, Kim E, Yoon JD, Park KM, Jin M, et al. Lysophosphatidic acid increases in vitro maturation efficiency via uPA-uPAR signaling pathway in cumulus cells. Theriogenology. 2018; 113: 197-207.
27. Zhang JY, Jiang Y, Lin T, Kang JW, Lee JE, Jin DI. Lysophosphatidic acid improves porcine oocyte maturation and embryo development in vitro. Mol Reprod Dev. 2015; 82(1): 66-77.
28. Sinderewicz E, Grycmacher K, Boruszewska D, Kowalczyk-Zięba I, Staszkiewicz-Chodor J, Łukaszuk K, et al. Expression of genes for enzymes synthesizing lysophosphatidic acid, its receptors and follicle developmental factors derived from the cumulus-oocyte complex is dependent on the ovarian follicle type in cows. Anim Reprod Sci. 2018; 192: 242-250.
29. Abedpour N, Salehnia M, Ghorbanmehr N. Effect of lysophosphatidic acid on the follicular development and the expression of lysophosphatidic acid receptor genes during in vitro culture of mouse ovary. Vet Res Forum. 2018; 9(1): 59-66.
30. Jo JW, Jee BC, Suh CS, Kim SH. Addition of lysophosphatidic acid to mouse oocyte maturation media can enhance fertilization and developmental competence. Hum Reprod. 2013; 29(2): 234-241.
31. Abedpour N, Salehnia M, Ghorbanmehr N. The effects of lysophosphatidic acid on the incidence of cell death in cultured vitrified and non-nitrified mouse ovarian tissue: Separation of necrosis and apoptosis border. Cell J. 2018; 20(3): 403-411.
32. Komatsu J, Yamano S, Kuwahara A, Tokumura A, Irahara M. The signaling pathways linking to lysophosphatidic acid-promoted meiotic maturation in mice. Life Sci. 2006; 79(5): 506-511.
33. Boruszewska D, Torres AC, Kowalczyk-Zieba I, Diniz P, Batista M, Lopes-da-Costa L, et al. The effect of lysophosphatidic acid during in vitro maturation of bovine oocytes: embryonic development and mRNA abundances of genes involved in apoptosis and oocyte competence. Mediators Inflamm. 2014; 2014: 670670.
34. Boruszewska D, Sinderewicz E, Kowalczyk-Zieba I, Skarzynski DJ, Woclawek-Potocka I. Influence of lysophosphatidic acid on estradiol production and follicle stimulating hormone action in bovine granulosa cells. Reprod Biol. 2013; 13(4): 344-347.
35. Hu X, Haney N, Kropp D, Kabore AF, Johnston JB, Gibson SB. Lysophosphatidic acid (LPA) protects primary chronic lymphocytic leukemia cells from apoptosis through LPA receptor activation of the anti-apoptotic protein AKT/PKB. J Biol Chem. 2005; 280(10): 9498-9508.
36. McLaughlin M, Kinnell HL, Anderson RA, Telfer EE. Inhibition of phosphatase and tensin homologue (PTEN) in human ovary in vitro results in increased activation of primordial follicles but compromises development of growing follicles. Mol Hum Reprod. 2014; 20(8): 736-744.
37. Zhou T, Du L, Chen C, Han C, Li X, Qin A, et al. Lysophosphatidic acid induces ligamentum flavum hypertrophy through the LPAR1/Akt pathway. Cell Physiol Biochem. 2018; 45(4): 1472-1486.
38. Torres AC, Boruszewska D, Batista M, Kowalczyk-Zieba I, Diniz P, Sinderewicz E, et al. Lysophosphatidic acid signaling in late cleavage and blastocyst stage bovine embryos. Mediators Inflamm. 2014; 2014: 678968.
39. Cong BH, Zhu XY, Ni X. The roles of microRNA-22 in myocardial infarction. Sheng Li Xue Bao. 2017; 69(5): 571-578.
40. Ma J, Shui S, Han X, Guo D, Li T, Yan L. microRNA-22 attenuates neuronal cell apoptosis in a cell model of traumatic brain injury. Am J Tran Res. 2016; 8(4): 1895-1902.

Case Report

Pre-Implantation Genetic Testing for Monogenic Disorders (PGT-M) in A Family with A Novel Mutation in *DPAGT1* Gene

Zahra Tabatabaei, M.Sc.[1#], Khadijeh Karbalaie, Ph.D.[2#], Parham Habibzadeh, M.D.[1], Mohammad Ali Farazi Fard, M.Sc.[1], Mohammad Ali Faghihi, M.D., Ph.D.[1, 3], Mohammad-Hossein Nasr Esfahani, Ph.D.[2, 4*]

1. Persian BayanGene Research and Training Center, Shiraz University of Medical Sciences, Shiraz, Iran
2. Department of Animal Biotechnology, Cell Science Research Center, Royan Institute for Biotechnology, ACECR, Isfahan, Iran
3. Center for Therapeutic Innovation, Department of Psychiatry and Behavioral Sciences, University of Miami Miller School of Medicine, Miami, USA
4. Isfahan Fertility and Infertility Center, Isfahan, Iran

#These authors contributed equally to this work.

Corresponding Address: P.O.Box: 8165131378, Department of Animal Biotechnology, Cell Science Research Center, Royan Institute for Biotechnology, ACECR, Isfahan, Iran
Email: mh.nasr-esfahani@royaninstitute.org

Received: 25/December/2019, Accepted: 07/March/2020

Abstract

Congenital disorders of glycosylation (CDG) are a heterogeneous group of systemic disorders characterized by defects in glycosylation of lipids and proteins. One of the rare subtypes of CDG is CDG-Ij (MIM # 608093), which is caused by pathogenic mutations in *DPAGT1*, a gene encoding UDP-N-acetylglucosaminedolichyl-phosphate N-acetylglucosaminephosphotransferase enzyme. This enzyme catalyzes the first step of oligosaccharide synthesis in glycoprotein biosynthesis pathway. Preimplantation genetic testing for monogenic disorders (PGT-M) is a diagnostic technique that can reveal the genetic profile of embryos before implantation phase of *in vitro* fertilization (IVF). Currently, this approach is performed using next generation sequencing (NGS) technology. Herein, with the help of whole-exome and Sanger sequencing, we detected a novel missense mutation (NM_001382, c.1217 A>G) in *DPAGT1* gene in two families with consanguineous marriage. Using different online bioinformatics tools including MutationTaster, I-Mutant v2.0, T- Coffee, and CADD v1.0, this mutation was predicted pathogen. Finally, after performing PGT-M followed by successful pregnancy, a normal child was born in one of these families. In conclusion, we identified a novel pathogenic mutation in *DPAGT1* in a family with multiple members affected by CDG, which extends the range of pathogenic variants associated with CDG and therefore facilitates early detection of the disease.

Keywords: Congenital Disorders of Glycosylation, Genetic Testing, *In Vitro* Fertilization, Next Generation Sequencing

Cell Journal(Yakhteh), Vol 23, No 5, October 2021, Pages: 593-597

Citation: **Tabatabaei Z, Karbalaie Kh, Habibzadeh P, Farazi Fard MA, Faghihi MA, Nasr Esfahani MH. Pre-implantation genetic testing for monogenic disorders (PGT-M) in a family with a novel mutation in DPAGT1 gene. Cell J. 2021; 23(5): 593-597. doi: 10.22074/cellj.2021.7335.**

Introduction

Lipid or protein glycosylation defects result in a heterogeneous group of neurometabolic disorders that are collectively called "congenital disorders of glycosylation" (CDG) (1). N-glycosylation and O-glycosylation are the two major types of glycosylation. Defective N-glycosylation results in type I and II CDG (2, 3). These two conditions are differentiated based on the underlying pathophysiology; the former is mainly due to glycan biosynthesis errors, while the latter results from errors in processing of the produced glycan. DPAGT1-CDG (CDG-Ij, MIM # 608093) is a rare autosomal recessive disorder caused by pathogenic mutations in *DPAGT1*, encoding UDP_ N- acetylglucosamine- dolichyl-phosphate N- acetylglucosaminephosphotransferarse (GPT), the enzyme taking part in dolichol-linked oligosaccharide pathway (4, 5). The DPAGT1-CDG-Ij disease is characterized by failure to thrive and feeding difficulties that become evident soon after the birth. Moreover, neurological signs, including tremor, clonus, and muscle fasciculation may soon be seen. Neurological abnormalities, including: psychomotor retardation, seizures, mental retardation, hyperexcitabilty, ataxia, and progressive microcephaly may appear. In addition, liver dysfunction in these individuals can lead to coagulopathy and hypoproteinemia. Some individuals with CDG have facial anomalies, inverted nipples, and subcutaneous fat pads (6-9).

Over the last four decades, assisted reproductive technologies (ART), including *in vitro* fertilization (IVF) and intra-cytoplasmic sperm insemination (ICSI), have led to the birth of over five million children (10). Recent advances in this field have brought hope for couples who have had children afflicted with different genetic disorders. In the past, preimplantation genetic testing for monogenic disorders (PGT-M) was performed using fluorescent in situ hybridization (FISH) and comparative genomic hybridization (CGH) for screening embryos with aneuploidy or chromosomal rearrangement. However, recently more comprehensive and advanced genetic diagnostic techniques such as whole-exome sequencing

(WES) have supplanted the aforementioned techniques.

To date, there are only a few reports of patients with CDG due to pathogenic mutations in *DPAGT1*. Identification of various mutations responsible for the development of the disease bolsters diagnostic precision and subsequently paves the way for better genetic counseling and PGT-M. In this study, we report on a family with multiple individuals affected by CDG due to a novel mutation in *DPAGT1* gene and subsequently present the outcome of the PGT-M based on the identified variant for one of these couples.

Cases report

All couples provided written informed consent for clinical and molecular studies. The Ethics Committee of the Persian BayanGene Research and Training Center approved the protocol (PBG- 06122016- 5708). As illustrated in Figure 1, our participants are couples from a big family.

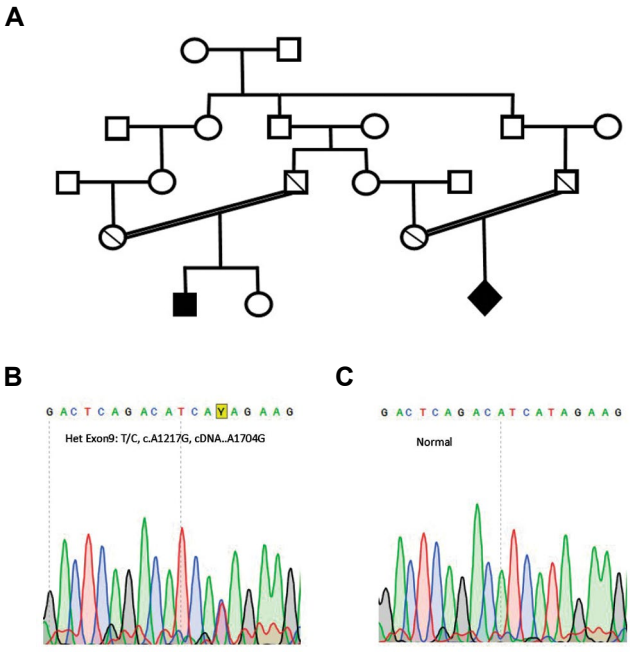

Fig.1: Family pedigree and sequencing chromatograms of two families. **A.** Pedigree and kinship relationship of the apparently normal couples. The first couple (left side) had a deceased 4-month boy (proband) and requested PDG for their second pregnancy. The second couple (right side) had an aborted embryo. **B.** Sequencing chromatograms of both couples show heterozygous mutation for the identified variant. **C.** The normal sequencing chromatogram of the unaffected girl embryo which was homozygous for the wild type variant.

The proband was a product of consanguineous marriage who was born with low Apgar scores. He was subsequently admitted to neonatal intensive care unit (NICU). He had severe hyperexcitability, hypotonia and swallowing difficulty. A thorough laboratory investigation including chromosomal analysis and metabolic evaluation was performed. However, no abnormality was identified. Brain computed tomography (CT) revealed no structural abnormalities. Electroencephalography and echocardiography were normal. The patient was discharged from the hospital. However, he was readmitted after a week due to severe respiratory distress. Clinical and imaging evaluations were in favor of aspiration pneumonia. The patient was subsequently intubated and placed on mechanical ventilation. Broad-spectrum antibiotics were started. However, his clinical condition deteriorated and he subsequently died at the age of four months. The parents of the affected individual and another couple in the family with an aborted fetus were subsequently referred for genetic counselling.

Genomic DNA was isolated from blood samples of both couples and the aborted fetus using QIAamp DNA Mini kit (Qiagen, Germany). The optical density of the extracted DNA was examined at 260 nm and 280 nm using the Nanodrop Analyzer (ND-1000) spectrophotometer (Thermo Fisher Scientific, USA).

The extracted DNA was used for WES using Illumina HiSeq2000 platform, by a standard Illumina protocol for pair-end 99-nucleotide sequencing. Sequencing was performed to sequence close to 100 million reads. The results of WES were aligned using BWA aligner tool (11). Consequently, the variants were identified and annotated via GATK (12) and ANNOVAR (13) software programs. A novel homozygous missense mutation in exon 9 of DPAGT1 gene (NM_001382: c.A1217G:p.Y406C) was identified in the aborted fetus. Sanger sequencing was subsequently used to study the identified mutation in other family members. The following primers were used to amplify the exon 9 of DPAGT1 gene and the flanking intronic sequences:

F: 5′-CTGAAATGTGAGTGTGGATAAC-3′
R: 5′-CCATACATGAGAGAAACCTC-3′

Results of sequencing were analyzed using 4-peaks software, which confirmed that both couples were heterozygous and that the aborted fetus was homozygous for the identified mutation (Fig.1). The detected mutation was analyzed with MutationTaster, a mutation predictor software for deep-sequencing (14), and I-Mutant v2.0, for the prediction of the protein stability upon mutations (15). Both of these softwares are free web-based applications. Furthermore, the amino acid sequence of GPT in different species was aligned with T-Coffee, a multiple sequence alignment software (16). This mutation was also analyzed using published Combined Annotation Dependent Depletion software (CADD v1.0), a web-based application that scores any possible human single-nucleotide variant (SNV) (17). Analysis using MutationTaster, blastn and blastp showed that the amino acid under investigation was conserved in all available sequences of mammalian species (Table 1). The reliability index (RI) of this protein was found to decrease upon tyrosine substitution, measured by protein sequence analysis with I-Mutant v2.0. In addition, this software indicated that substitution of this amino acid with any other amino acids caused a decrement in RI (Table 2A). Sequence alignment of this protein with T-Coffee showed that this amino acid was conserved (Table 2A). This mutation had a raw score of 3.96 and a Phred-like score (C-score) of 20.3 when analyzed with the CADD program as a single-nucleotide variation (SNV).

Table 1: The evolutionary conservation for *DPAGT1* in other species at the amino acid level based on MutationTaster analysis. These homologus sequences were aligned with the corresponding human *DPAGT1* sequence using **A.** Blastp and **B.** Blastn respectively

Species	Match	Gene	NT	Alignment
A				
Human			406	F S I R Y Q L V R L F **Y** D V
Mutated	Not conserved		406	F S I R Y Q L V R L F C D V
Chimpanzee	All identical	ENSPTRG00000004370	406	F S I R Y Q L V R L F **Y** D V
Mmulatta	All identical	ENSMMUG0000014872	406	F S I R Y Q L V R L F **Y** D V
Fcatus	All identical	ENSFCAG00000001163	406	F S I R Y Q L V R L F **Y** D V
Mmusculus	All identical	ENSMUSG00000032123	408	F S I R Y Q L V R L F **Y** D V
Ggallus	All identical	ENSGALG00000000285	407	F S I R Y Q L V R L F **Y** D V
Trubripes	All identical	ENSTRUG0000001661	414	F S I R Y Q L V R L F **Y** D V
Drerio	All identical	ENSDARG00000061061	404	F S I R Y Q L V R L F **Y** D V
Dmelanogaster	All identical	FBgn0032477	406	F S I R Y Q L V R L F **Y**
Celegans	All identical	Y60A3A.14	410	F S I R Y Q L V R L F **Y** D V
Xtropical	All identical	ENSXETG00000021574	406	F S I R Y Q L V R L F **Y** D V
B				
Human		11324	11324	T C G A C T CT T C T **A** T G A T G T C T G A G T
Mutated	Not conserved	11324	11324	t c g a c t c t t c t g t g a t g t c t g a g
Ptroglodytes	All identical	7050	7050	t c g a c t c t t c t **a** t g a t g t c t g a g
Mmulatta	All identical	13780	13780	t c g a c t c t t c t **a** t g a t g t c t g a g
Fcatus	All identical	6806	6806	t c g a c t c t t c t **a** c
Mmusculus	All identical	8268	8268	t c g a c t c t t c t **a** t g a t g t c t g a g
Ggallus	No alignment	n/ a	n/ a	
Trubripes	No alignment	n/ a	n/ a	
Drerio	No alignment	n/ a	n/ a	
Dmelanogaster	No alignment	n/ a	n/ a	
Celegans	No alignment	n/ a	n/ a	
Xtropical	No alignment	n/ a	n/ a	

NT; Amino acid position and n/a; Not available.

Table 2: Sequence alignment of GPT protein. **A.** The measured level of protein stability, the change value of free energy (DDG) and the RI of GPT protein upon every single-point mutation in tyrosine position at 25˚C and neutral environment using I-Mutant v2.0. **B.** Multiple sequence alignment of GPT protein with T-Coffee showed that tyrosine 406 (Y) was a highly conserved residue during the evolution across the Mamalia class

A

Position	WT	NEW	DDG	Stability	RI	pH	T
406	Y	C	-0.02	Decrease	5	7	25
406	Y	G	-3.58	Decrease	9	7	25
406	Y	H	-1.67	Decrease	8	7	25
406	Y	I	-0.30	Decrease	4	7	25
406	Y	L	-0.26	Decrease	5	7	25
406	Y	M	-0.51	Decrease	5	7	25
406	Y	T	-0.88	Decrease	7	7	25
406	Y	P	-1.26	Decrease	3	7	25
406	Y	S	-1.64	Decrease	8	7	25
406	Y	A	-1.94	Decrease	9	7	25
406	Y	V	0.16	Decrease	2	7	25
406	Y	K	-0.26	Decrease	5	7	25

B

Species	Protein	Alignment
Homo sapiens	NP_001373.2	T L L L L L L Q I L G S A I T F S I R Y O L V R L F **Y** D V
Mus musculus	NP_031901.2	T L L L L L L Q V L S S A A T F S I R Y Q L V R L F **Y** D V
Rattus norvegicus	NP_955420.1	T L F L L L L Q V L S S A V T F S I R Y Q L V R L F **Y** D V
Danio rerio	NP_001082880.1	T A I M L L M Q V L G S A V A F G I R Y H L V R L F **Y** D V
Cricetulus griseus	NP_001230970.1	T L L L L L L Q I L S S A V T F S I R Y Q L V R L F **Y** D V
Macaca mulatta	NP_001244785.1	T L L L L L L Q I L G S A F T F S I R Y Q L V R L F **Y** D V
		* : : * * : * : * . * * : * . * * * : * * * * * * * *

WT; Amino acid in wild type protein, NEW; n\New amino acid after mutation, DDG; DG (new protein)-DG (wild type) in kcal/mol, DDG <0; Decrease stability, DDG >0; Increase stability, RI; Reliability index, pH; -log [H+], T; Temperature (°C), *; Identical amino acids, and :; Just identical amino acids.

Following verification of heterozygous mutation in the couple, they were referred to Isfahan Fertility and Infertility Center, Iran. Upon their request, intracytoplasmic sperm injection (ICSI) was carried out based on routine method performed in the center (18). Using the gonadotropin-releasing hormone (GnRH) agonist protocol, hyper ovulation was induced. In this aim 150 IU of Cinal-F (CinnaGene, Iran) and 75 Menogon (Ferring, Germany) were used. Monitoring was carried out with using vaginal ultrasound. Cetrotide (Merck-Serono, Germany) was administered when the size of the dominant follicle was 13 mm. Ovulation induction was induced with 10,000 IU of human chorionic gonadotropin (hCG, Ferring, Germany). Thirty-six hours post-hCG, the ovum was picked up and three mature meiosis 2 (MII) oocytes were obtained. ICSI was carried out according to the standard protocol. On day 3, two embryos in 8-16-cell stage were found suitable for blastomere biopsy. Each blastomere was washed in phosphate buffered saline without calcium and magnesium (PBS) and transferred to polymerase chain reaction (PCR) tube for DNA amplification using REPLI-g Single Cell kit (Qiagen, Germany). PCR was subsequently performed on the amplification products of the exon 9 of the *DPAGT1* gene. Sanger sequencing was then performed on the PCR products to determine the genotype of the embryos using 3130xl Genetic Analyzer (Applied Biosystems, USA). Based on the results of the Sanger sequencing, two blastomeres were found unaffected and one of them was transferred which resulted in the birth of a healthy girl.

Discussion

Glycosylated proteins play an important role in many biological pathways including cell signaling, protein stability and immune defense (19). In this study, we identified a novel pathogenic missense mutation in *DPAGT1* gene leading to congenital disorder of glycosylation

(CDG) in a family. The pathogenic nature of the identified variant was supported by the absence of this variant in our local database and other publicly available genetic databases. In addition, highly conserved nature of the amino acid affected by this mutation, and extensive analysis of other individuals in the family, reinforced the pathogenic nature of the detected variant. Furthermore, PGT-M based on the identified variant resulted in a normal healthy child.

All patients affected by CDG, but those who suffered from CDG-Ib, had similar clinical presentations with substantial variation in severity (20). Compared with previous reports, the patient reported in this study had the most severe clinical features, presenting with serious problems at birth that led to death by the age of four months. Pathogenic mutations in *DPAGT1* are also known to cause limb-girdle congenital myasthenic syndrome with tubular aggregates, highlighting the importance of N-glycosylation of proteins in maintaining the function of the neuromuscular junction (21). Since the patient in this report did not undergo a thorough clinical evaluation, this disorder could not be ruled out in this patient.

The rate of consanguineous marriage in any society depends on a wide range of social, religious, and demographic factors (22, 23). With a mean rate of 38.6%, in some community, Iran is one of the countries with the highest rates of consanguineous marriage (24). Therefore, autosomal-recessive disorders pose a major issue to this society. This underscores the importance of causative genetic variants identification in these disorders and subsequently, taking advantage of PGT-M techniques to prevent the transfer of deleterious variants to the next generation.

Conclusion

We identified a novel pathogenic mutation in *DPAGT1* gene based on bioinformatics analysis and genome sequencing. Subsequently, based on couples' request, PGT-M was performed, which resulted in the birth of a healthy girl.

Acknowledgements

The authors would like to thank the family members for participating in this study. There is no financial support and conflict of interest in this study.

Authors' Contributions

M.A.F., M.-H.N.E.; Conception and design of the manuscript. Z.T., Kh.K., P.H., M.A.F.F.; Data acquisition, data analysis, and interpretation. Kh.K.; Manuscript drafting. P.H., Z.T., M.A.F, M.-H.N.E.; Revising the manuscript for critically important intellectual content. All authors read and approved the final manuscript.

References

1. Péanne R, de Lonlay P, Foulquier F, Kornak U, Lefeber DJ, Morava E, et al. Congenital disorders of glycosylation (CDG): quo vadis? Eur J Med Genet. 2018; 61(11): 643-663.
2. Jaeken J. Congenital disorders of glycosylation. Ann N Y Acad Sci. 2010; 1214(1): 190-198.
3. Ng BG, Freeze HH. Perspectives on glycosylation and its congenital disorders. Trends Genet. 2018; 34(6): 466-476.
4. Bretthauer RK. Structure, expression, and regulation of UDP-GlcNAc: dolichol phosphate GlcNAc-1-phosphate transferase (DPAGT1). Curr Drug Targets. 2009; 10(6): 477-482.
5. Würde AE, Reunert J, Rust S, Hertzberg C, Haverkämper S, Nürnberg G, et al. Congenital disorder of glycosylation type Ij (CDG-Ij, DPAGT1-CDG): extending the clinical and molecular spectrum of a rare disease. Mol Genet Metab. 2012; 105(4): 634-641.
6. Jaeken J, Lefeber D, Matthijs G. Clinical utility gene card for: DPAGT1 defective congenital disorder of glycosylation. Eur J Hum Genet. 2015; 23(12).
7. Timal S, Hoischen A, Lehle L, Adamowicz M, Huijben K, Sykut-Cegielska J, et al. Gene identification in the congenital disorders of glycosylation type I by whole-exome sequencing. Hum Mol Genet. 2012; 21(19): 4151-4161.
8. Wu X, Rush JS, Karaoglu D, Krasnewich D, Lubinsky MS, Waechter CJ, et al. Deficiency of UDP-GlcNAc: dolichol phosphate N-acetylglucosamine-1 phosphate transferase (DPAGT1) causes a novel congenital disorder of glycosylation type Ij. Hum Mutat. 2003; 22(2): 144-150.
9. Yuste-Checa P, Vega AI, Martín-Higueras C, Medrano C, Gámez A, Desviat LR, et al. DPAGT1-CDG: functional analysis of disease-causing pathogenic mutations and role of endoplasmic reticulum stress. PLoS One. 2017; 12(6): e0179456.
10. Kissin DM, Jamieson DJ, Barfield WD. Monitoring health outcomes of assisted reproductive technology. N Eng J Med. 2014; 371(1): 91-93.
11. Li H, Durbin R. Fast and accurate short read alignment with Burrows-Wheeler transform. Bioinformatics. 2009; 25(14): 1754-1760.
12. Wang K, Li M, Hakonarson H. ANNOVAR: functional annotation of genetic variants from high-throughput sequencing data. Nucleic Acids Res. 2010; 38(16): e164-e164.
13. McKenna A, Hanna M, Banks E, Sivachenko A, Cibulskis K, Kernytsky A, et al. The genome analysis toolkit: a mapreduce framework for analyzing next-generation DNA sequencing data. Genome Res. 2010; 20(9): 1297-1303.
14. Schwarz JM, Cooper DN, Schuelke M, Seelow D. MutationTaster2: mutation prediction for the deep-sequencing age. Nat Methods. 2014; 11(4): 361-362.
15. Capriotti E, Fariselli P, Casadio R. I-Mutant2. 0: predicting stability changes upon mutation from the protein sequence or structure. Nucleic Acids Res. 2005; 33(Web Server issue): W306-W310.
16. Notredame C, Higgins DG, Heringa J. T-coffee: a novel method for fast and accurate multiple sequence alignment. J Mol Biol. 2000; 302(1): 205-217.
17. Kircher M, Witten DM, Jain P, O'Roak BJ, Cooper GM, Shendure J. A general framework for estimating the relative pathogenicity of human genetic variants. Nat Genet. 2014; 46(3): 310-315.
18. Nasr-Esfahani MH, Tavalaee M, Deemeh MR, Arbabian M, Parrington J. Can assessment of total acrosin activity help predict failed or low fertilization rate ICSI for implementation of artificial oocyte activation? The Open Andrology Journal. 2010; 2(1): 19-26.
19. Wolfe LA, Krasnewich D. Congenital disorders of glycosylation and intellectual disability. Dev Disabil Res Rev. 2013; 17(3): 211-225.
20. Freeze H H. Update and perspectives on congenital disorders of glycosylation. Glycobiology. 2001; 11(12): 129R-143R.
21. Belaya K, Finlayson S, Slater CR, Cossins J, Liu WW, Maxwell S, et al. Mutations in DPAGT1 cause a limb-girdle congenital myasthenic syndrome with tubular aggregates. Am J Hum Genet. 2012; 91(1): 193-201.
22. Bittles AH, Black ML. Consanguinity, human evolution, and complex diseases. Proc Natl Acad Sci USA. 2010; 107 Suppl 1: 1779-1786.
23. Jurdi R, Saxena PC. The prevalence and correlates of consanguineous marriages in Yemen: similarities and contrasts with other Arab countries. J Biosoc Sci. 2003; 35(1): 1-13.
24. Saadat M. Consanguineous marriages in Iranian folktales. Community Genet. 2007; 10(1): 38-40.

Case Report

Digenic Mutations in Junctional Epidermolysis Bullosa in An Iranian Family

Kourosh Riahi, M.D.[1], Farideh Ghanbari Mardasi, Ph.D.[2]*, Farah Talebi, M.Sc.[3], Farzad Jasemi, M.D.[4], Javad Mohammadi Asl, Ph.D.[5]

1. Department of Pediatrics, Faculty of Medicine, Ahvaz Jundishapur University of Medical Sciences, Ahvaz, Iran
2. Department of Medical Genetics, School of Medicine, Tehran University of Medical Sciences, Tehran, Iran
3. Department of Genetic, Faculty of Science, Shahid Chamran University of Ahvaz, Ahvaz, Iran
4. Department of Internal Medicine, Faculty of Medicine, Ahvaz Jundishapur University of Medical Sciences, Ahvaz, Iran
5. Department of Medical Genetics, Faculty of Medicine, Ahvaz Jundishapur University of Medical Sciences, Ahvaz, Iran

**Corresponding Address: P.O.Box: 64941-15333, Department of Medical Genetics, School of Medicine, Tehran University of Medical Sciences, Tehran, Iran*
Email: ghanbari246@gmail.com

Received: 11/October/2019, Accepted: 11/May/2020

Abstract

In this study, we describe one Iranian patient who was diagnosed with Epidermolysis Bullosa (EB) because of mutations in three candidate genes, including 3 mutations. Two missense mutations in the *LAMA3* (D3134H) and *LAMB3* (Y339H) genes and also, a synonymous mutation in the *ITGB4* (H422H) gene were identified that leads to the Junctional-EB-Herlitz (JEB-Herlitz) clinical phenotype. The patient had a heterozygous *LAMA3* mutation combined with a heterozygous mutation in *LAMB3*. Our results propose that these mutations produce novel protein-coding transcripts which explain the JEB-Herlitz phenotype in the patient. Interestingly, this is the first report indicating that a digenic inheritance in the *LAMA3* and *LAMB3* which is responsible for JEB-Herlitz. Also, this is the first digenic inheritance recognized in the JEB-Herlitz family. This study provides a new way to clarify the molecular mechanisms of *LAMA3* and *LAMB3* genes in JEB-Herlitz.

Keywords: *ITGB4*, Junctional Epidermolysis Bullosa Herlitz, *LAMA3, LAMB3*, Sequence Analysis

Cell Journal(Yakhteh), Vol 23, No 5, October 2021, Pages: 598-602

Citation: Riahi K, Ghanbari Mardasi F, Talebi F, Jasemi F, Mohammadi Asl J. Digenic mutations in junctional epidermolysis bullosa in an Iranian family. Cell J. 2021; 23(5): 598-602. doi: 10.22074/cellj.2021.7208.

Introduction

Epidermolysis Bullosa (EB) is the name used to define a heterogeneous group of inherited mechanobullous disorders that has been subdivided into three categories [EB simplex (EBS), dystrophic EB (DEB) and junctional EB (JEB)] based on the ultrastructural level of skin cleavage and immunofluorescence detection of cutaneous antigens (1-3). There are two major JEB subtypes, *JEB*-Herlitz (generalized), and JEB-non-Herlitz (localized) and each is typified by blister formation within the lamina lucida. JEB Herlitz is an autosomal recessive and severe form of EB that leads to the premature demise of the affected patients within a few months after birth. Many mutations in one of the 3 genes *LAMA3*, *LAMB3*, and *LAMC2* encode the a3, b3, and g2 subunit polypeptides of laminin 5 underlie this disease (4). In the present study, we performed next-generation sequencing (NGS) to identify the genetic mutations leading to JEB-Herlitz in an Iranian pedigree.

Case report

A 7-year-old Iranian girl, first child of consanguineous Iranian parents, was presented to our genetic counseling center because of widespread congenital skin blistering (JEB-Helitz) (Fig.1A). She had generalized blisters and erosions on her whole body, some dystrophic fingernails and toenails, with subungual hyperkeratosis and thickening of the nail plate. Hair involvement was limited to eyebrow alopecia. She did not have oral lesions. Also, in her unaffected parent, there was no previous family history of genetic diseases (Fig.1B).

After obtaining informed consent, genomic DNA was extracted from peripheral leukocytes of the patient, her parent, and 200 healthy controls by using the standard salting-out method (5). The study was performed in accordance with the Declaration of Helsinki and based on the guidelines of the Ethics Committee of Iran's Ministry of Health and Medical. Sequence analysis was carried out by using a custom-designed (user-defined) NimbleGen chip capturing of 9 EB related genes followed by Next Generation Sequencing (NGS, BGI-Clinical Laboratories, Shenzhen, China). After NGS sequencing, the sequence reads were mapped to the reference human genomic DNA (UCSC/hg19) using the Burrows-Wheeler Alignment software (BWA v.0.7.10). Then, the subsequent variant was called with the Genome Analysis Toolkit (GATK) software versions 4 (https://software.broadinstitute.org/gatk/, GATK-3.5) (6) to assemble the consensus sequence and detect single nucleotide polymorphisms (SNPs) and indels in target regions. Moreover, detected rare variants [minor allele frequency (MAF), 1%] in the affected girl were compared with database of SNP (dbSNP) (7) and 1000 genomes databases (8). Predicting candidate variants effect on protein structure and phylogenetic conservation, bioinformatics tools

like PolyPhen-2 (9), SIFT (10) were used. And, the variant pathogenicity risk was estimated by CADD score (11).

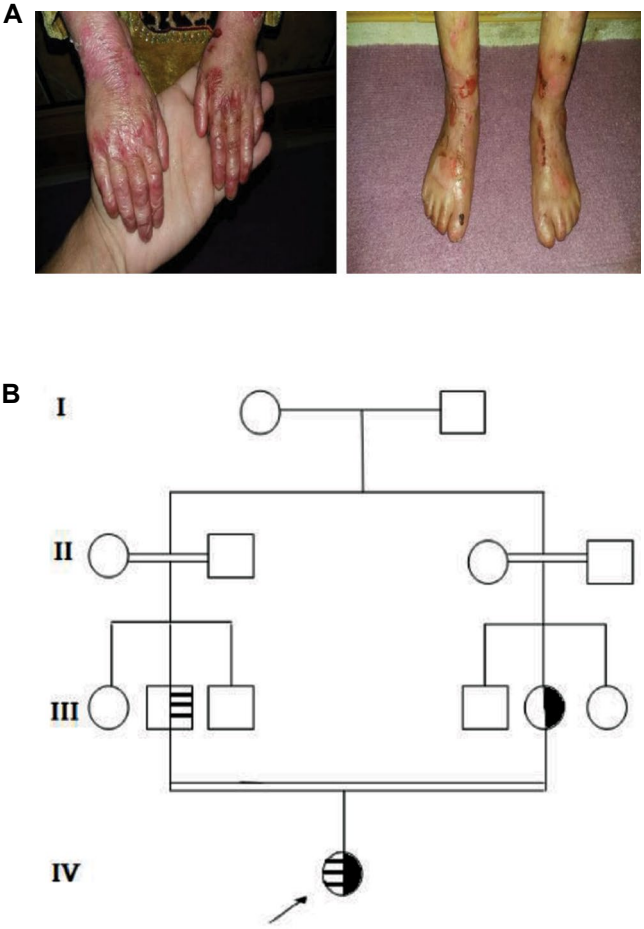

Fig.1: Clinical features and pedigree. **A.** Severe and widespread blistering in patient IV-1. **B.** Autosomal recessive inheritance pedigree. Areas with black color indicate maternal *LAMA3* mutations. ◑; Horizontal stripes and ▤; Paternal *LAMB3* mutations.

Then, direct Sanger sequencing was carried out with ABI3130 sequencer (Applied Biosystems, Foster City, CA, USA) to confirm potential causative variants in the patient. Primer sequences for pathogenic variants in the *LAMA3*, *LAMB3* and *ITGB4* genes (NM_198129, NM_000228 and NM_000213, respectively) were previously reported (12). Parent were examined for co-segregation analysis of the variants with the phenotype.

Targeted exon capturing and NGS of 9 known EB related genes was performed in our patient. Among these genes, we detected 3 variants in the *LAMA3*, *LAMB3* and *ITGB4* genes in the patient which was absent in 200 healthy controls. Also, these variants were not previously reported in the same Iranian patients. Direct sequencing of the *LAMA3*, *LAMB3*, and *ITGB4* genes confirmed that the patient and her mother were heterozygous for c.9641 G>A mutation in exon 71 of the *LAMA3* gene (Fig.2A). This mutation (p. D3134H) affected a highly conserved amino acid residue (Fig.2B). Moreover, the patient and her father were found to carry a heterozygous c.1405 T > C in exon 9 of the *LAMB3* gene (p.Y339H) (Fig.2A, B). The patient also carried the c.1430 C>T mutation in a heterozygous state in the *ITGB4* gene (p.H422H) (Fig.2A).

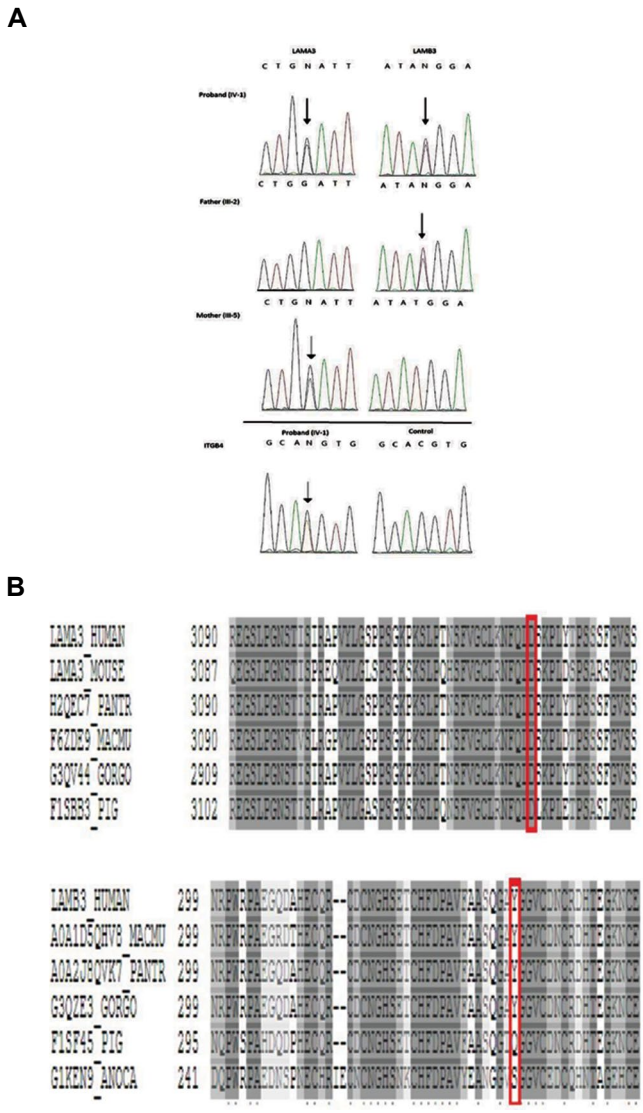

Fig.2: Digenic mutations in an Iranian family with Junctional Epidermolysis Bullosa (JEB). **A.** The result of DNA sequencing of the patient, father and mother. Patient: sequence analysis reveal a heterozygous G>C transversion at cDNA position 9641 of the *LAMA3* gene resulting in p.D3134H substitution, a heterozygous T>C transition at cDNA position 1405 of the *LAMB3* gene resulting in p.Y339H substitution and a heterozygous C>T transition at cDNA position 1266 of the *ITGB4* gene resulting in silent substitution p.H422H in the patient. Father: the father has p.Y339H substitution in the *LAMB3* gene. Mother: the mother has p.D3134H substitution in the *LAMA3* gene. (The p.D3134H, p.Y339H and p.H422H are marked with an arrow). **B.** Conservation analysis. Protein alignments show conservation of the amino acid sequence of *LAMA3* p.D3134H variant and *LAMB3 p.*Y339H variant between species around the mutation sites that marked with vertical line (red).

The segregate analysis confirmed these pathogenic mutations co-segregates with the disease phenotype in the patient. The family exhibited a typical autosomal recessive inheritance pattern of JEB-Herlitz (Fig.1B). Bioinformatics analysis was done by PolyPhen, SIFT and CADD (Table 1) and indicated that the p. D3134H and p. Y339H mutations together probably cause *LAMA3* and *LAMB3* dysfunction leading to the JEB-Herlitzclinical phenotype.

Table 1: *Various i*n silico bioinformatics tools have been developed that predict the mutations

Gene	Prediction software		
	SIFT score	**PolyPhen score**	**CAAD score**
LAMA3	0.00 (Deleterious)	0. 9 (Probably damaging)	23 (Likely benign)
LAMB3	0.8 (Tolerated)	0.0 (Benign)	12 (Likely benign)

Discussion

In this study, NGS was applied to identify the causative genes defects associated with EB in an Iranian pedigree. The index patient was a double-heterozygous carrier for two missense mutations in the *LAMA3* and *LAMB3* genes. So far, researchers reported eighteen missense mutations in the *LAMA3* gene based on the HGMD database (13). Our first identified mutation, (p. D3134H), in the patient and her mother, was in the laminin G-like 4 (LG-4) domain of *LAMA3* protein C-terminal that leads to loss negatively charged side chains and replaced by a positively charged residue. The second identified mutation in the proband and her father, c.1405T>C, was a heterozygous mutation in the laminin epidermal growth factor-like 2 (EGF-like 2) domain of the LAMB3 protein. Although, these mutations have previously been reported, this is the first report of mutations of *LAMA3* and *LAMB3* genes in an Iranian EB patient. Following evidences prove that these mutations can lead to EB: i. Next generation sequencing only identified these mutations to be the main cause of EB in the patient. ii. Direct Sanger sequencing proved the mutations in the proband and also, based on recognizing heterozygote mutations in her parents, the pattern of inheritance must be an autosomal recessive and digenic. iii. Using predicting online tools such as SIFT, polyphen, CADD , these variants will be damaging and tolerated (p.D3134H and p.Y339H, respectively). iv. The amino acids comparative alignment of LAMA3 and LAMB3 proteins across all Kingdoms showed that p. D3134 of *LAMA3* gene is highly conserved during evolution. v. Also, a substitution Asp3134His in *LAMA3* gene and a substitution Tyr339His in *LAMB3* gene can create major problems in the LAMA3 and LAMB3 proteins. Thus, these mutations in *LAMA3* and *LAMB3* genes are pathogenic in our patient with EB.

According to simplified Schäffer definition, the most part of cases in digenic diseases are categorized into two classes (14). The first class represents true digenic (TD) instances: variants at both loci are essential for disease and, variants at one of the two loci lead to no phenotype (15). The second class we will refer to as the composite (CO) class as it consists of diverse possibilities: A composite case in digenic diseases can refer to mendelizing variants plus modifiers, when a driver variant is essential for the phenotype but rare variants in a second gene, generally correlated to the same pathway, may change the phenotype (16).

All involved variants impact, the genes allelic condition, the gene ability of enduring loss of function (LOF) variants, and also, the involved genes correlation are likely to identify the digenic effect. Several common properties of digenic combinations are characteristic for the two classes, and somehow reflect the underlying biological mechanisms. The digenic effect is often strongly influenced by the impact of the variants implicated as well as their zygosity (17).

The digenic inheritance in genes has been reported in some human phenotypes, for example, retinitis pigmentosa (18, 19), non-syndromic hereditary deafness, Wardenburg syndrome type 2, Bardet-Biedl syndrome, autosomal recessive ocular albinism, JEB and EBS (20, 21). Previously, digenic inheritance has been described in a case with severe nonlethal JEB (JEB- non-Herlitz), in which one mutation in the *LAMB3* gene and two mutations in the type XVII collagen gene were identified (22). The collagen XVII and Laminin-5, two functionally related proteins, abnormal expression led to the primary hemidesmosome structure and the basement membrane separation of the epidermis, with severe skin blistering as the clinical appearance. Also, digenic inheritance was reported in three previous cases with EBS in which mutations occur in *KRT5* and *KRT14* genes (Table 2) (23-25).

The fact that the p.D3134H (in *LAMA3*) and p.T339H (in *LAMB3*) mutations reported in present study affects an extremely conserved residue, supports a positive pathogenic role for these genes in causing the disease phenotype. Therefore, these results propose that digenic inheritance was directly involved in modifying/causing the clinical phenotype in this patient.

As a rare disease, this is the first report that indicated a JEB-Herlitz responsible digenic inheritance of *LAMA3* and *LAMB3*. Also, this is the first digenic inheritance recognized in an Iranian JEB-Herlitz family.

Table 2: Previous studies on the digenic inheritance in EB

Origin t	Type of EB	Genes	Pathogenic variant	Protein effect	Type of mutation	Method
German	JEB	*COL17A1*	c. T2669G	L855X	Missense	candidate gene sequencing
			c. C3781T	R1226X	Missense	
		LAMB3	**c.** C1903T	R635X	Missense	candidate gene sequencing
Jewish Ashkenazi	EBS	*KRT5*	c. T548C	p.I183T	Missense	candidate gene sequencing
		KRT14	c. G1163A	p.R388H	Missense	candidate gene sequencing
Australian	EBS	*KRT5*	c.464T>C	p. Leu155Pro	Missense	candidate gene sequencing
		KRT14	c.881T>C	p. Met294Thr	Missense	candidate gene sequencing
Polish	EBS	*KRT5*	c.1412G>A	p.Arg471His	Missense	candidate gene sequencing
		KRT14	c.815T>C	p.Met272Thr	Missense	candidate gene sequencing
Iranian	JEB-Herlitz	*LAMA3*	c. G9641C	p. D3134H	Missense	candidate gene sequencing
		LAMB3	c. T1405C	p.Y339H	Missense	candidate gene sequencing

EB; Epidermolysis Bullosa, JEB; Junctional-EB, and EBS; EB simplex.

Conclusion

We emphasize that one mutation detection in one gene is not sufficient for determining the molecular basis of JEB-Herlitz in a given family. Moreover, we present evidence implicating digenic inheritance in identifying a clinical phenotype in JEB-Herlitz, proposing that full sequencing of all JEB-Herlitzrelated genes may develop the quality of genetic counseling and prenatal diagnosis of affected individuals in this clinically heterogeneous disease.

Acknowledgments

The authors thank the Milad Genetic Counseling Center for their financially support. Also, the authors would like to thank the family members for their kind participation, cooperation and support throughout the period of this study. There is no conflict of interest in this study.

Authors' Contributions

F.T.; Conception and design. J.M.A., F.Gh.M.; All experimental work, data and statistical analysis, and data interpretation. K.R., F.J.; Clinical investigation and sample collection. F.Gh.M.; Drafted and revision the manuscript. All authors read and approved the final manuscript.

References

1. Sawamura D, Nakano H, Matsuzaki Y. Overview of epidermolysis bullosa. J Dermatol. 2010; 37(3): 214-219.
2. Uitto J, Richard G. Progress in epidermolysis bullosa: from eponyms to molecular genetic classification. Clin Dermatol. 2005; 23(1): 33-40
3. Lanschützer C, Laimer M, Pohla-Gubo G, Nischler E, Eady RA, Klausegger A, et al. Life with epidermolysis bullosa (EB). Etiology, diagnosis, multidisciplinary care and therapy. In: Fine JD, Hintner H, editors. New York: Springer-Verlag Wien; 2009; 338.
4. Ghohestani RF, Li K, Rousselle P, Uitto J. Molecular organization of the cutaneous basement membrane zone. Clin Dermatol. 2001; 19(5): 551-562.
5. Intong LR, Murrell DF. Inherited epidermolysis bullosa: new diagnostic criteria and classification. Clin Dermatol. 2012; 30(1): 70-77.
6. McKenna A, Hanna M, Banks E, Sivachenko A, Cibulskis K, Kernytsky A, et al. The genome analysis toolkit: a mapReduce framework for analyzing next-generation DNA sequencing data. Genome Res. 2010; 20(9): 1297-1303.
7. Smigielski EM, Sirotkin K, Ward M, Sherry ST. dbSNP: a database of single nucleotide polymorphisms. Nucleic Acids Res. 2000; 28(1): 352-355.
8. Clarke L, Zheng-Bradley X, Smith R, Kulesha E, Xiao C, Toneva I, et al. The 1000 Genomes Project: data management and community access. Nat Methods. 2012; 9(5): 459-462.
9. Adzhubei IA, Schmidt S, Peshkin L, Ramensky VE, Gerasimova A, Bork P, et al. A method and server for predicting damaging missense mutations. Nat Methods. 2010; 7(4): 248-249.
10. Kumar P, Henikoff S, Ng PC. Predicting the effects of coding non-synonymous variants on protein function using the SIFT algorithm. Nat Protoc. 2009; 4(7): 1073-1081.
11. Rentzsch P, Witten D, Cooper GM, Shendure J, Kircher M. CADD: predicting the deleteriousness of variants throughout the human genome. Nucleic Acids Res. 2019; 47(D1): D886-D894.
12. Pulkkinen L, McGrath JA, Christiano AM, Uitto J. Detection of sequence variants in the gene encoding the beta 3 chain of laminin 5 (LAMB3). Hum Mutat. 1995; 6(1): 77-84.

13. Stenson PD, Ball EV, Mort M, Phillips AD, Shiel JA, Thomas NST, et al. Human gene mutation database (HGMD): 2003 update. Hum Mutat. 2003; 21(6): 577-581.
14. Schaffer AA. Digenic inheritance in medical genetics. J Med Genet. 2013; 50(10): 641-652.
15. Posey JE, Harel T, Liu P, Rosenfeld JA, James RA, Coban Akdemir ZH, et al. Resolution of disease phenotypes resulting from multilocus genomic variation. New Engl J Med. 2017; 376(1): 21-31.
16. Gonzaga-Jauregui C, Harel T, Gambin T, Kousi M, Griffin LB, Francescatto L, et al. Exome sequence analysis suggests that genetic burden contributes to phenotypic variability and complex neuropathy. Cell Rep. 2015; 12(7): 1169-1183.
17. Gazzo A, Raimondi D, Daneels D, Moreau Y, Smits G, Van Dooren S, et al. Understanding mutational effects in digenic diseases. Nucleic Acids Res. 2017; 45(15): e140.
18. Zhang H, Labouesse M. The making of hemidesmosome structures in vivo. Dev Dyn. 2010; 239(5): 1465-1476.
19. Titeux M, Pendaries V, Tonasso L, Décha A, Bodemer C, Hovnanian A. A frequent functional SNP in the MMP1 promoter is associated with higher disease severity in recessive dystrophic epidermolysis bullosa. Hum Mutat. 2008; 29(2): 267-276.
20. Kajiwara K, Berson EL, Dryja TP. Digenic retinitis pigmentosa due to mutations at the unlinked peripherin/RDS and ROM1 loci. Science. 1994; 264(5165): 1604-1608.
21. Dryja TP, Hahn LB, Kajiwara K, Berson EL. Dominant and digenic mutations in the peripherin/RDS and ROM1 genes in retinitis pigmentosa. Invest Ophthalmol Vis Sci. 1997; 38(10): 1972-1982.
22. Badano JL, Katsanis N. Beyond mendel: an evolving view of human genetic disease transmission. Nat Rev Genet. 2002; 3(10): 779-789.
23. Morell R, Spritz RA, Ho L, Pierpont J, Guo W, Friedman TB, et al. Apparent digenic inheritance of Waardenburg syndrome type 2 (WS2) and autosomal recessive ocular albinism (AROA). Hum Mol Genet. 1997; 6(5): 659-664.
24. Floeth M, Bruckner-Tuderman L. Digenic junctional epidermolysis bullosa: mutations in COL17A1 and LAMB3 genes. Am J Hum Genet. 1999; 65(6): 1530-1537.
25. Padalon-Brauch G, Ben Amitai D, Vodo D, Harel A, Sarig O, Sprecher E, et al. Digenic inheritance in epidermolysis bullosa simplex. J Invest Dermatol. 2012; 132(12): 2852-2854.